AD A033782

ARO-13067.1-A-C

THE UNIVERSITY OF NORTH CAROLINA
AT
CHAPEL HILL
27514

MATERIALS RESEARCH CENTER
PHILLIPS HALL

FINAL REPORT

ARPA Order: No. 3005
Program Code: No. 61101E
University of North Carolina - Chapel Hill
Start: 1 June 1975
Stop: 30 September 1976
Award: $110,000 obligated

Grant: No. DAHC 04-75-G-0144
P.I.: Charles S. Smith, 919-933-3018
Project Scientist: Charles S. Smith
Title: Fuel Cells and Solid Electrolytes
Date: 30 October 1976
Period: 1 June 1975 - 30 September 1976

Sponsored by
Defense Advanced Research Projects Agency
ARPA Order No. 3005

Approved for public release;
distribution unlimited

DDC
DEC 28 1976

DISCLAIMER NOTICE

THIS DOCUMENT IS THE BEST QUALITY AVAILABLE.

COPY FURNISHED CONTAINED A SIGNIFICANT NUMBER OF PAGES WHICH DO NOT REPRODUCE LEGIBLY.

SECURITY CLASSIFICATION OF THIS PAGE (When Data Entered)

REPORT DOCUMENTATION PAGE

READ INSTRUCTIONS BEFORE COMPLETING FORM

1. REPORT NUMBER: Proposal No. 13067	2. GOVT ACCESSION NO.: --
3. RECIPIENT'S CATALOG NUMBER: (9) --	
4. TITLE (and Subtitle): (6) FINAL REPORT Fuel Cells and Solid Electrolytes.	5. TYPE OF REPORT & PERIOD COVERED: Final Report. 1 June 1975 - 30 Sept 1976.
	6. PERFORMING ORG. REPORT NUMBER: -
7. AUTHOR(s): (10) 1. Thomas J. Meyer, 2. Royce W. Murray, 3. Sang-il Choi, 4. Thomas L. Isenhour	8. CONTRACT OR GRANT NUMBER(s): (15) DAHC 04-75-G-0144, ARPA Order-3005
9. PERFORMING ORGANIZATION NAME AND ADDRESS: University of North Carolina, Materials Research Center, Phillips Hall, Chapel Hill, N.C. 27514	10. PROGRAM ELEMENT, PROJECT, TASK AREA & WORK UNIT NUMBERS: ARPA Order No. 3005, Program Element Code 61101E
11. CONTROLLING OFFICE NAME AND ADDRESS: Materials Science Office, Defense Advanced Research Projects Agency, 1400 Wilson Boulevard Arlington, Va. 22209	12. REPORT DATE: 30 October 1976
	13. NUMBER OF PAGES: 141
14. MONITORING AGENCY NAME & ADDRESS (if different from Controlling Office): U. S. ARMY Research Office, P. O. Box 12211, Research Triangle Park, North Carolina 27709 (12) 139p.	15. SECURITY CLASS. (of this report): Unclassified
	15a. DECLASSIFICATION/DOWNGRADING SCHEDULE: --

16. DISTRIBUTION STATEMENT (of this Report)

Approved for public release; distribution unlimited.

(18) ARO (19) 13067.1-A-C

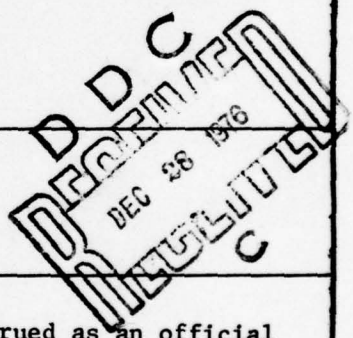

17. DISTRIBUTION STATEMENT (of the abstract entered in Block 20, if different from Report)

Same.

18. SUPPLEMENTARY NOTES

The findings in this report are not to be construed as an official Dept. of Army position unless so designated by other authorized documents.

19. KEY WORDS (Continue on reverse side if necessary and identify by block number)

Fuel cells, homogeneous catalysic, electrocatalysis, surface composition, x-ray photoelectron spectroscopy, solid electrolytes, beta-alumina, machine decisions, failure analysis

20. ABSTRACT (Continue on reverse side if necessary and identify by block number)

This report recounts results on four diverse topics

1. Homogeneous catalysis of Net Electrochemical Reactions as Applied to Fuel Cells.
2. Electrocatalysis: Application of X-ray Photoelectron Spectroscopy to Surface Composition of Electrode Materials
3. Theoretical Investigation of Solid Electrolytes
4. Application of Machine Decisions to Failure Analysis.

DD FORM 1 JAN 73 1473 EDITION OF 1 NOV 65 IS OBSOLETE

SECURITY CLASSIFICATION OF THIS PAGE (When Data Entered)

403020

FUEL CELLS AND SOLID ELECTROLYTES

Introduction

This document is the Final Report of research at the University of North Carolina, administered by the Materials Research Center, monitored by the ARMY Research Office and funded by the Advanced Research Projects Agency as detailed in the proceding 1473 form.

The report comprises results on four projects which are some what diverse and which are reported individually by the authors as listed below.

1. Electrocatalysis: Application of X-ray Photoelectron Spectroscopy to Surface Composition of Electrode Materials
   R. W. Murray
2. The Catalysis of Organic Oxidation Processes. Fuel Cells.
   T. J. Meyer
3. Superionic Conductors (Solid Electrolytes): Theoretical Study
   Sang-il Choi
4. Applications of Pattern Recognition in Chemistry
   T. L. Isenhour

Because four projects are covered, the report is constructed around the *important* publications, reprints and preprints, which have directly resulted from the work. For each project, these reproduced publications are preceded by a short overview, together with recommendations, which is intended to provide cohesion as well as a meaningful abstract.

Some of the projects had been supported by ARPA under a previous grant for varying periods of time. This format of report then essentially covers *the entire period* of ARPA support; this period of time is indicated explicitly by each author.

Charles S. Smith
Director, Materials
Research Center

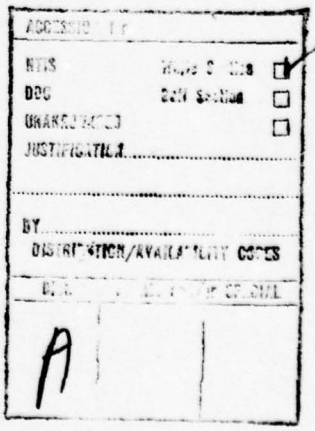

ELECTROCATALYSIS: APPLICATION OF X-RAY PHOTOELECTRON SPECTROSCOPY TO SURFACE COMPOSITION OF ELECTRODE MATERIALS

R. W. Murray

Final Technical Report

1 June 1974 - 30 September 1976

Personnel:

C. Michael Elliott, Research Assistant, received Ph.D., December 1975; P. R. Moses, Research Associate; John Lennox, Research Associate; Larry Wier, Research Assistant.

The support provided to the Principal Investigator during the above period provided the basis for initiating a new area of electrochemical research, now known as CHEMICALLY MODIFIED ELECTRODES. The goals of the research are illustrated schematically as follows.

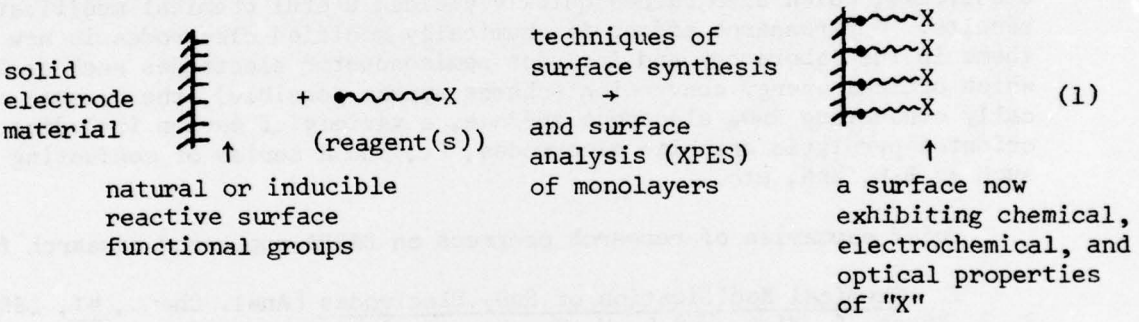

By this reaction, it is possible to transform the normally poorly predictable solid electrode surface into a surface with chemically predictable, and selected, properties. Development of the surface synthetic capability implied by Reaction 1 likewise implies availability of a large variety of new and novel electrochemical surfaces. Chemical modification of the surfaces of conducting materials useful as electrochemical electrodes had never been previously accomplished using covalent binding, chemically predictive reactions.

If the reagent (X) is electroactive, secondly,

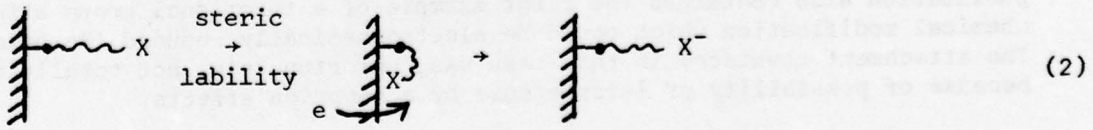

In Reaction 2, we have the opportunity to observe the electrochemistry of an immobilized reactant, with the connotations therein of the study of details of the steric requirements for electron transfer, effect of electrostatics on charge transfer events, required distances over which charge transfer can occur, and other fundamentally important features of electrochemical reactions. Study of Reaction 2 comprises a completely virgin area of electrochemistry. Lastly, if the species X^- is chosen to exhibit chemically labile charge transfer

exchange with a solution substrate (S) which is itself not normally reduced rapidly at the electrode surface then

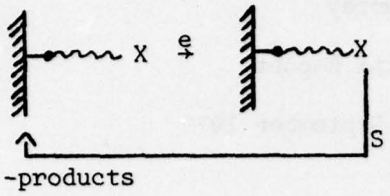

(3)

Reaction 3 comprises a totally new concept of electrocatalysis and does so in a manner which allows a chemically predictive approach to design of an electrode surface to accomplish a particular electrocatalysis.

Our research has thus far successfully demonstrated examples of Reactions 1 and 2. Our initial efforts, with DARPA support, focused on highly doped SnO_2 electrodes. Success in chemical modification of this electrode material came rather quickly. The direction of an existing NSF grant was reoriented to carry forward the SnO_2 work, and the DARPA effort was shifted to focus on carbon electrodes, which also rather quickly yielded useful chemical modification results. Our research effort in chemically modified electrodes is now a major theme in the laboratory and includes semiconductor electrodes such as TiO_2 (for which optical energy conversion schemes appear possible), the unusual electronically conducting RuO_x electrode surface, a variety of carbon including highly oriented pyrolytic graphite electrodes, Pt, and a series of conducting ceramics such as B_4C, ZrN, etc.

Brief summaries of research progress on DARPA-supported research follow:

1. Chemical Modification of SnO_2 Electrodes [Anal. Chem., 47, 1882 (1975); P. R. Moses, L. Wier, and R. W. Murray, reprints attached]. In this report, we demonstrate that commercially available organosilanes can be used to chemically modify SnO_2 electrode surfaces, incorporating on these surfaces synthetically useful functional groups, such as amine and pyridyl. This report, the first on chemically modified electrodes from our laboratory and the second (by a few months) in the literature, has attracted some attention.

2. Chemically Modified Carbon Electrodes [Anal. Chem., 48, 1247 (1976), C. M. Elliott and R. W. Murray, reprints attached]. This subsequent, parallel study on carbon electrodes demonstrated that similar chemical modification chemistry with organosilanes was possible on graphite and glassy carbon. This publication also contained the first example of a functional group attached via chemical modification which could be electrochemically reduced (Reaction 2). The attachment chemistry in this case was, unfortunately, not totally unambiguous because of possibility of interference by adsorption effects.

3. Chemically Modified Electrodes. IV. Evidence for Formation of Monolayers of Bonded Organosilane Reagents [submitted to J. Electroanal. Chem., D. F. Untereker, J. C. Lennox, L. M. Wier, P. R. Moses and R. W. Murray, preprint attached]. Of vital importance in attachment of organosilane reagents to electrode surfaces via Reaction 1 is maintenance of monolayer stereochemistry. The possibility of forming polymeric silicones on the electrode surface thus required careful examination. An extensive set of measurements has now demonstrated our surface synthetic capability of forming monolayers of bonded organosilane reagents.

4. Chemically Modified Electrodes. III. SnO_2 and TiO_2 Electrodes Bearing an Electroactive Reagent [submitted to J. Amer. Chem. Soc., P. R. Moses and R. W. Murray, preprint attached]. This particular research was not DARPA-supported, but is included here because it comprises our initial, unambiguous demonstration of Reaction 2, one of the primary objectives of the initial DARPA project. The manuscript demonstrates that methylpyridinium bonded to SnO_2 and TiO_2 electrodes can be reduced by charge transfer from the electrode. The immobilized methylpyridinium yields an electrochemical wave at the same potential as unbonded (solution) methylpyridinium ion. The electrochemical result was confirmed by observations of the electrode surface by XPES. The methylpyridinium examples comprise two of five clear cut instances of Reaction 2 which we now have in hand. The other three examples of Reaction 2 are, unlike the methylpyridinium example, chemically reversible and put us in a position to begin examination of electrocatalytic situations in Reaction 3.

5. Studies of Chemical Reactivity of Organosilane-Bonded Amine and Pyridyl Functions on Carbon Electrodes. On SnO_2 and TiO_2 electrodes, we have determined that organosilane-immobilized amine and pyridyl functional groups exhibit their normal chemical reactivity. That is, immobilized amine groups undergo reactions with acid chlorides to form amide bonds. This is a convenient route to further attachment of other chemical reagents to these electrode materials. In an attempt to carry out the same reaction chemistry on carbon electrodes, a series of experiments spanning several months, disappointingly revealed that on carbon the amine and pyridyl functionalities are not reliably reactive toward other normal reagent materials. It appears that the paths open to further synthetic modification of organosilane-modified carbon electrodes on SnO_2, TiO_2 , and other electrodes are not available to us on carbon electrodes. We are now employing a different approach to chemical modification of carbon electrodes which focuses on the following chemical reaction

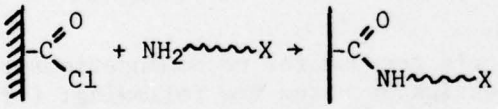

(4)

This reaction appears to be much better behaved and we are again making progress in devising chemically modified carbon electrodes, using the edge planes of highly oriented pyrolytic graphite.

6. pK_b of Immobilized Amines. During our studies of amine functionalities bound to carbon electrodes via organosilane chemistry, we did determine by XPES that these amine groups to a substantial extent can be protonated by acids and subsequently deprotonated by bases. We carried out a series of experiments in which an amine-bearing carbon electrode was exposed to solutions of various pH (buffered), the electrode surfaces removed from the solution and air-blown dry, and the relative proportions of N and NH^+ determined from the N 1s XPES band intensities. We observed in a plot versus pH a break in the ratio N/NH^+ which occurs at pH values expected from the amine group pK_b values. We in effect "titrate" the amine surface and detect the titration by XPES. Such a detection of a surface chemical equilibrium by XPES spectroscopy has not been accomplished previously. This work is in the house-cleaning stage and will be written up for publication.

7. Chemical Modification of SnO_2 with $RuCl_3$ Solutions. In a somewhat different approach to chemical modification of SnO_2 electrodes, we observe that contact of these electrodes with solutions of $RuCl_3$ results in incorporation of considerable quantitites of Ru. The quantity of material bound to the surface is somewhat more reproducible, and more stable, if the SnO_2 electrode has been pre-treated with an amine-bearing organosilane. There is evidence that in the course of the attachment reaction the amine group becomes one of the ligands bound to the Ru metal center. XPES results suggest that 1-2 Cl ligands remain on each Ru, and that the remaining 3-4 ligand sites of Ru are either SnO_2 lattice oxygens or coordinated water. Depth-profile experiments using XPES demonstrate that a substantial layer of Ru exists at the electrode surface, but that a considerable amount of Ru also penetrates the SnO_2 lattice by as much as 50 Å. Electrochemical experiments on the Ru/modified SnO_2 electrodes show a chemically reversible charge transfer wave centered about 0 volts in aqueous solution of neutral pH. Study of this surface redox process indicates that the electrochemical reaction is a $Ru^{2+,3+}$ couple, and that the Ru involved in this wave is that bound to the SnO_2 surface. At more anodic potentials, approximately +0.9 volt, a charge transfer wave is observed which appears to be an oxidation either of both surface and sub-surface Ru to Ru^{4+}. This conversion is irreversible and the $Ru^{2+,3+}$ couple is no longer evident.

Our primary interest in this particular type of chemically modified electrode stems from the fact that mixtures of Sn and Ru oxides are employed in making the so-called "dimensionally stable anodes" (DSA^R) which are presently of great commercial importance in the chlor-alkali industry. Electrodes which contain these metals and exhibit the electrochemical properties we have observed have not been reported. Our results may be useful in understanding the catalytic activity of the commercial electrodes. End of Report.

Further Work:

In response to the DARPA Director's request for recommendations to the DOD for further work, this Principal Investigator notes the following: (i) It is our intention to continue our research in chemically modified electrodes as we believe we have opened up a new area of electrochemistry of clear fundamental importance and which may very well have substantial industrial importance as well. We are aware of now at least four other research groups now working in this area and have experienced interest and inquiries for information from others. The idea of tailor-making electrode surfaces is clearly appealing. (ii) The second comment that the Principal Investigator would make to the DOD concerns the manner in which support for this research was terminated. The termination decision, made during the second year of support, apparently did not include consideration of the scientific merit of the work, but was based on an arbitrary new perception of the "mission" of the DARPA agency. Good basic research cannot be turned on and off like a faucet or a construction contract. It is regrettable that the DOD bureaucracy sometimes does not seem to realize this. The Principal Investigator is appreciative of the Director of Materials Sciences' efforts to assist the research through passing along information about its need for support to other agencies. Some replacement of the lost funds has been secured.

Chemically Modified Tin Oxide Electrode

P. R. Moses, L. Wier, and R. W. Murray

Kenan Laboratories of Chemistry, University of North Carolina, Chapel Hill, N.C. 27514

Surface synthetic procedures are described whereby, via silane chemistry, amine, pyridyl, and ethylenediamine ligands can be attached to SnO_2 electrodes. The surface reactions and confirmatory chemical tests involving amine protonation and metal coordination are followed by X-ray photoelectron spectroscopy (ESCA). The modified electrodes retain electrochemical activity toward solution reactants.

Chemical modifications transforming heterogeneous, unpredictive surfaces into chemically predictive ones is an area of research gradually percolating into diverse fields. Separation scientists have for several years chemically modified solid supports to improve chromatographic column performance. Such "bonded phase" work has depended on organosilane reactions with the surfaces of silica or alumina particles (*1, 2*). In another separations application, glass wool surfaces have been derivatized with dithiocarbamate ligands, scavenging trace metals for X-ray photoelectron spectroscopy (ESCA) measurement (*3*). Acid–base dye indicators attached (*4*) to silica surfaces create "solid indicators". Homogeneous catalysts such as rhodium diphenylphosphine complexes have been attached to silica, again using organosilane chemistry, to provide heterogeneous hydroformylation catalysts (*5, 6*).

Electrochemistry is a field where chemically predictive surfaces are at a premium. As yet no stable covalently bonded electrode surfaces have been described. An important step in this direction was taken by Lane and Hubbard (*7*), who described the strong chemisorption of electroactive allyl compounds on Pt electrodes.

We report here surface synthetic techniques by which several ligands (amine, pyridine, and ethylenediamine) can be covalently bonded to the surfaces of tin oxide electrodes. Preparation of these surface ligand sites is a first step toward surface-bound metal complex redox centers, among several applications. The surface bonding depends on reactions of organosilane reagents with hydroxyl groups on the tin oxide surfaces. Reacted surfaces were examined by electron spectroscopy as one means of demonstrating successful surface synthesis. The electrochemical viability of the derivatized tin oxide electrodes was demonstrated by electrochemical reactions of model electrochemical couples (ferrocyanide, *o*-tolidine).

EXPERIMENTAL

The tin oxide electrodes were obtained as antimony-doped, transparent films on glass from PPG Industries, Pittsburgh, Pa. Four-point probe measurements indicated a film resistivity of ca. 5 ohms square^{-1}. Interference patterns were used to estimate film thickness at 6×10^{-5} cm. Specimens for surface modification and ESCA or electrochemical examination were prepared from 12 × 12 × ⅛ inch stock by either cutting the glass into ½-inch squares under a flowing stream of water using a diamond saw or by epoxying a 4 × 4 inch plate onto a plate of uncoated glass and drilling ¼-inch disks (for ESCA) with a 5/16-inch diamond drill. The epoxy is removed by pyrolysis at 450 °C. Freshly cut specimens were either extracted with heptane overnight to remove surface grease and then heated at 450 °C in air for several hours, or treated with hot concentrated HCl for several hours followed by copious washing with distilled water and then alcohol. Surface acidification does not seem to be an essential prerequisite for reactivity of tin oxide surfaces toward silanes, as no gross differences in reactivity were discerned for the two pretreatment procedures. Minor differences undoubtedly exist.

The organosilanes are commercially available, from Petrarch Systems, PCR Chemical Company, or Silar Chemical Company. They were used without further purification, employing serum cap and syringe techniques to protect the reagents and reacting solutions from moisture. Reactions of trichlorosilanes and triethoxysilanes were selected to emphasize high surface yields. Specific reagents include aminopropyltriethoxysilane, 3-(2-aminoethylamino)propyltrimethoxysilane (Dow Corning Z-6020 Silane), 3-dichloropropyltrichlorosilane (Dow Corning Z-6010 Silane), and β-trichlorosilyl-2-ethylpyridine.

Silanization reactions were carried out in dry deaerated benzene or xylene. Electrode specimens were reacted under 50 ml of a ca. 10% solution of refluxing silane, under nitrogen, for several hours with trichlorosilanes to several days with triethoxysilanes. Minimum reaction times actually required were not investigated. After reaction, the solution was decanted and the specimens were washed under nitrogen with several portions of fresh solvent. With the ethylenediamine reagent, washing was with water and then alcohol.

All organosilanes are liquids except the pyridine reagent, which is solid and less reactive than most. After refluxing overnight with this reagent, electrode specimens were especially carefully washed with hot solvent and then alcohol to remove the last traces of unreacted silane from the electrode surface.

Electron spectroscopy proved invaluable in following the surface synthesis. ESCA spectra were obtained with a DuPont Model 650B spectrometer with Mg anode. Under optimum conditions a ¼-inch gold disk yields a $4f_{5/2}$ peak intensity of 400,000 counts/sec with FWHM of 1.2 eV. The pumping system consists of a cryogenic forepump with titanium ion main pump; typical operating vacuum is 1×10^{-7} Torr. At this pressure, and using specimens necessarily exposed to laboratory atmosphere, a contamination C 1s peak of ca. 30,000 counts/sec appears on all samples. Our experience in this and other ESCA-electrochemical studies shows that alterations occur in the contamination carbon film during spectrometer X-ray exposure, and an adherent, insulating film often forms which adversely affects subsequent electrochemical use. Accordingly, electrochemical data were always obtained prior to ESCA examination, or on separate specimens. No examples of electrochemical destruction of the organosilicon layer were encountered except where extensive scans of potential beyond the background limits were involved.

As the tin oxide electrode films were deposited on an insulating substrate, ESCA charging shifts of several eV were common. The C 1s contamination peak was employed as a reference peak and was assigned a value of 285.0 eV (*8, 9*). All binding energies reported are referenced to this value.

Electrochemical experiments on tin oxide were carried out in miniature Lucite cells of design similar to that employed by Kuwana and associates (*10*), using a peripheral copper ring for electrical contact and an O-ring seal. The geometrical area of the electrode exposed to the cylindrical solution cavity is determined by the sealing O-ring; this area is 0.031 cm^2 for one cell and 0.079 cm^2 for another. The auxiliary electrode was a Pt wire coil; potentials are referenced to an SCE of design after Adams (*11*). Electrochemical instrumentation was conventional. No *iR* compensation was employed. The cyclic voltammetric experiment is used here as the principal electrode-characterizing technique.

RESULTS AND DISCUSSION

Schematically the reaction of an organosilane with a surface hydroxyl group is representable as

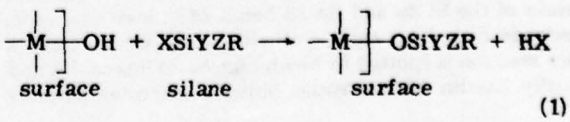

(1)

Reprinted from ANALYTICAL CHEMISTRY, Vol. 47, Page 1882, October 1975
Copyright 1975 by the American Chemical Society and reprinted by permission of the copyright owner

Table I. Summary ESCA Data for SnO_2 Electrodes[a]

Electrode	Sn $3d_{5/2}$	Si 2p[b]	N 1s	NH^+ 1s	Cl $2p_{3/2}$[c]	d, Å[d]
Unreacted	487.7 ± 0.3	102.4 ± 0.2	400.5 ± 0.2		199.3	
	(114 ± 33)	(0.51 ± 0.23)	(0.96 ± 0.26)		(0.31)	
SnO_2/PrCl	487.7 ± 0.2	102.3 ± 0.2			200.2	9.1
	(50.1 ± 24)	(3.6 ± 0.4)			(25 ± 0.3)	
SnO_2/$PrNH_2$	487.5	102.4	400.3 ± 0.1	401.9 ± 0.1		5.1
	(72 ± 40)	3.9	(Sh)	(4.4 ± 2)		
SnO_2/en	487.4 ± 0.2	102.2 ± 0.2	399.3 ± 0.3	400.6 ± 0.2		10.6
	(43.5 ± 39)	(3.3 ± 2.0)	(2.8 ± 0.9)	(3.0 ± 0.4)		
SnO_2/Py	487.3 ± 0.2	102.4 ± 0.2	399.4 ± 0.4	401.8 ± 0.3		~1
	(105.0 ± 40)	(5.0 ± 1.7)	(3.7 ± 1.3)			

[a] Binding energies in eV; intensities (kilocounts sec^{-1}). [b] Center of unresolved Si $2p_{1/2}$, Si $2p_{3/2}$ doublet. [c] Cl $2p_{1/2}$ is a partially resolved shoulder on this band. [d] Calculated from Equation 2 using λ = 11 Å.

In the case M equals Si (e.g., silica surface), the Si–O–Si bond is known to be very stable to acids and bases as well as thermally stable to as high as 300 °C (*1*). Where M equals Sn, the modified surface chemical stability does not equal that of silica, but is nonetheless quite good. Treatment of tin oxide electrodes derivatized with, for example, aminopropyltriethoxysilane (designated SnO_2/$PrNH_2$ electrodes) with room temperature 1*M* mineral acid is without effect. Hot concentrated HCl, however, within 2–3 hours has hydrolyzed approximately 50% of the surface groups. More immediate hydrolysis is observed by soaking in 0.1*M* NaOH.

It is known from chromatographic (*1*) and other studies that the order of reactivity of halosilanes with silica is $X_3SiR > X_2SiR_2 > XSiR_3$. This relationship was also observed with SnO_2 surfaces in a series of reactions where X ≡ Cl and R ≡ methyl. The Si 2p ESCA band was most intense for SnO_2 treated with Cl_3SiCH_3, and least for $ClSi(CH_3)_3$. The $ClSi(CH_3)_3$, although less reactive, did produce Si 2p bands well above background silicon.

Organosilanes with more than one reactive group have the potential of binding to more than one surface site. A trichlorosilane does not, however, necessarily bind to three surface sites. Boucher et al. (*5*), for instance, demonstrated during the immobilization of diphenylphosphine groups on silica that the trichlorosilane reagent claimed slightly less than two sites per silane. The fate of the remaining silane reactive group is of some importance. The formation of linear siloxane polymers bound to silica surfaces at only a few sites has been claimed by Aue and Hastings (*12, 13*) in connection with chromatographic bonded phases. Polymer formation can occur if a dichloro or trichlorosilane forms one >Sn–O–Si< surface link, and then a second Si–Cl bond becomes hydrolyzed by water, forming >Sn–O–Si(OH)<. If this occurs in the presence of unreacted solution chlorosilane, a polymer chain can be initiated at the Si(OH) site. Organosilane polymerization is thought to be more severe for smaller, more reactive silanes, such as trichloromethylsilane (*14*). It can be avoided altogether by the use of monochlorosilanes.

We employed X_3SiR silanes to emphasize high surface coverages at this phase of our surface modification research, and also because most suitable ligand-bearing commercial organosilanes are of this category. We have attempted to minimize the possibilities for polymer formation by utilizing dry solvents, by carefully and thoroughly washing excess silane from the tin oxide specimens with fresh aprotic solvent before exposing the specimens to moisture or other hydrolyzing substances, and by ESCA checks of the Si 2p and Sn 3d bands of at least one SnO_2 electrode disk from each synthetic batch. Occasionally a poor reaction is spotted in which high Si 2p intensities and usually low Sn 3d intensities indicate extensive polymer formation. Suitable functioning of a tin oxide specimen as an electrode serves as an additional criterion of at least minimal polymer formation, and electrochemical data were taken for each chemically modified surface described below.

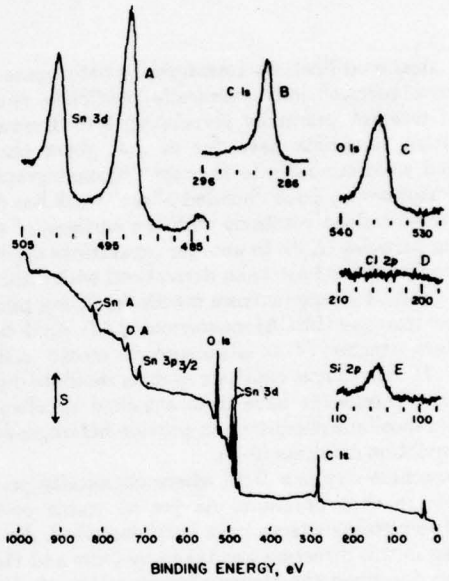

Figure 1. ESCA spectra of unreacted SnO_2 electrode

Lower curve, survey scan, *S* (sensitivity) = 40,960 counts/sec, 4 scans averaged; Curve *A*, Sn $3d_{5/2}$, $3d_{3/2}$, doublet at *S* = 81,920 counts/sec, one scan; Curve *B*, C 1s at *S* = 20,480 counts/sec, one scan; Curve *C*, O 1s at *S* = 20,480 counts/sec, one scan; Curve *D*, Cl 2p at *S* = 10,240 counts/sec, 8 scans averaged; Curve *E*, unresolved Si $2p_{3/2}$, $2p_{1/2}$ doublet, *S* = 10,240 counts/sec, 8 scans averaged

Unreacted SnO_2 Electrodes. Unreacted SnO_2 specimens were characterized by ESCA preparatory to study of chemically modified ones. A survey ESCA spectrum of unreacted SnO_2 is shown in Figure 1, and data are summarized in Table I. The spectrum contains strong bands for O 1s at 532 eV, oxygen Auger at 750 eV, Sn $3p_{3/2}$ at 715 eV, Sn $3d_{3/2}$ at 497 eV, Sn $3d_{5/2}$ at 487 eV, and C 1s at 285 eV (reference peak). A small N 1s peak of about 300 counts/sec is present on unreacted electrodes which have not been first heated to ca. 450 °C for several hours. The binding energy for this peak, 400.5 eV, suggests it is a reduced form (e.g., not nitrate), either adsorbed dinitrogen or atmospheric amine impurities (*15*).

Unreacted SnO_2 specimens also exhibit a minute Si 2p band. This band is reduced only about 10% by masking the cut edge of the SnO_2–silica disk. It is reduced 10–20% by thorough washing of the SnO_2 surface with a 0.1*M* NaOH solution. Our initial interpretation of the residual signal

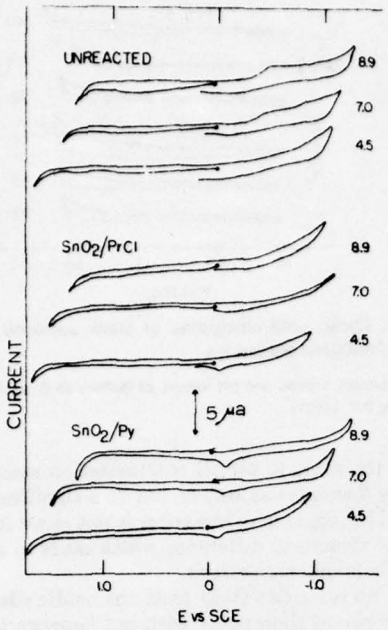

Figure 2. Cyclic voltammograms of blank solutions on unreacted SnO_2, Si O_2/PrCl, and SnO_2/Py electrodes

Numbers beside curves are pH values of phosphate buffers. 50 mV/sec. Dots represent sweep origin

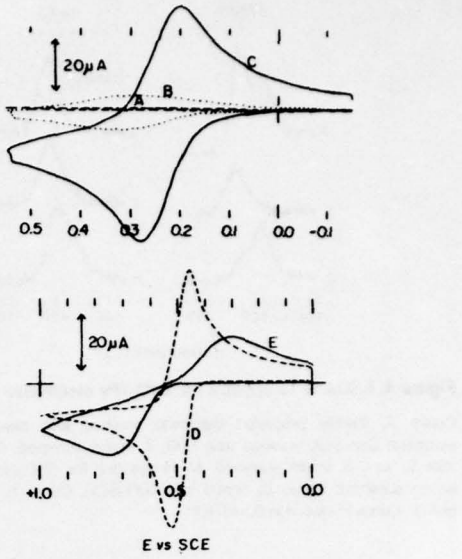

Figure 3. Cyclic voltammograms in 0.1*M* KCl, 0.5*M* glycine, pH 2.4, 100 mV/sec

Curve *A*, blank solution, unreacted SnO_2; Curve *B*, blank solution, SnO_2/en; Curve *C*, 2m*M* $Fe(CN)_6^{4-}$, SnO_2/en. Cyclic voltammograms in 0.1*M* KCl, pH 2.3, 2m*M* *o*-tolidine, 50 mV/sec. Curve *D*, unreacted SnO_2; Curve *E*, SnO_2/en; blank solution scans indistinguishable from zero on this current scale

Table II. Cyclic Voltammetric Data[a] for SnO_2/Py and SnO_2/PrCl

V, mV/sec	E_p^a	E_p^c	ΔE_p	$i_p^a/ac\ V^{1/2}$	i_p^c/i_p^a
1m*M* ferrocyanide, 0.1*M* KCl, 0.5*M* glycine, pH 2.4					
Unreacted SnO_2					
5	0.268	0.214	0.054	10.7×10^2	0.91
10	0.270	0.212	0.058	10.6×10^2	1.00
50	0.279	0.205	0.074	11.1×10^2	1.00
100	0.289	0.197	0.092	11.1×10^2	1.00
2m*M* ferrocyanide, 0.1*M* KCl, 0.5*M* glycine, pH 2.4					
SnO_2/Py					
5	0.270	0.216	0.054	9.6×10^2	0.99
10	0.274	0.214	0.060	8.8×10^2	1.00
50	0.282	0.205	0.077	9.9×10^2	0.99
100	0.293	0.197	0.096	10.4×10^2	0.97
1m*M* ferrocyanide, 0.1*M* KCl, 0.5*M* glycine, pH 2.4					
SnO_2/PrCl					
10	0.294	0.176	0.118	7.1×10^2	1.00
20	0.290	0.176	0.114	7.5×10^2	0.80
40	0.294	0.167	0.127	7.1×10^2	0.95
100	0.305	0.167	0.138	6.1×10^2	0.93

[a] Current constant $i_p/ac\ V^{1/2}$ in A $sec^{1/2}$ cm/$volt^{1/2}$ mole. *E* vs. SCE. Electrode area = 0.031 cm^2.

was in terms of pinholes which penetrate the SnO_2 film to expose the underlying silica. Pinholes in SnO_2–silica obtained from Corning have been observed in scanning electron micrographs (*16*). Using a comparison to the Si 2p band intensity (14,200 counts/sec) on a clean soft glass disk, the pinhole interpretation leads to ~3% of the total SnO_2 area being penetrated. We subsequently have determined that argon sputtering of ~30 Å of SnO_2 surface completely eliminates the Si 2p signal on unreacted SnO_2 disks. This result indicates that the source of the Si signal is more likely a surface species deposited during or after the film preparation. The pinhole interpretation would require sputtering-induced topological changes which are probably unlikely.

As an incidental illustration of the detection of adsorption on SnO_2 by ESCA, we soaked several unreacted SnO_2 specimens in $Cu(NO_3)_2$ solutions using either water or acetone as solvent, and following with extensive rinsing. A fairly intense copper spectrum with bands at Cu $2p_{1/2}$ 954.6 eV and Cu $2p_{3/2}$ 934.7 eV resulted. Other metal cations, such as Pb^{2+} and Fe^{3+}, also strongly adsorb on SnO_2 (*17*). A spectrum of crystalline $Cu(NO_3)_2$ exhibits the Cu 2p bands at 957.0 and 937.0 eV plus the multiplet satellites associated with the Cu(II) state (*18*). These satellites are very weak in the SnO_2-adsorbed copper spectrum, and the 2p binding energies of the adsorbed copper are more typical of the Cu(I) or Cu(0) states than Cu(II) (*18*). While the apparent reduction of the copper might occur concurrently with its adsorption onto SnO_2, it is more probable that the adsorbed Cu(II) is thermally reduced to Cu(I) during the ESCA X-ray irradiation. Thermal reduction of CuO to Cu_2O has been observed (*19*) and we have seen prominent Cu(I) bands in spectra of small amounts of $Cu(NO_3)_2$ deposited on metal surfaces.

Cyclic voltammetry experiments on blank aqueous solutions (Figure 2) and solutions of model electrochemical reactants (Figure 3) gave results on unreacted PPG SnO_2 generally similar to literature reports (*20*, *21*). Blank voltammograms do not depend particularly on solution pH except for the background potential limits. The cathodic and anodic limits (as defined at an arbitrary 5-μA level) move in the expected directions with pH change, the cathodic limit moving 60 mV/pH unit, the anodic limit moving at a lower pace. Cyclic voltammetric data for $Fe(CN)_6^{4-}$ in Table II show diffusion control and reversibility; resistance effects increase ΔE_p slightly over the reversible value at the higher sweep rates.

SnO_2/PrCl Electrodes. Tin oxide electrodes were reacted with 3-chloropropyltrichlorosilane as an example of

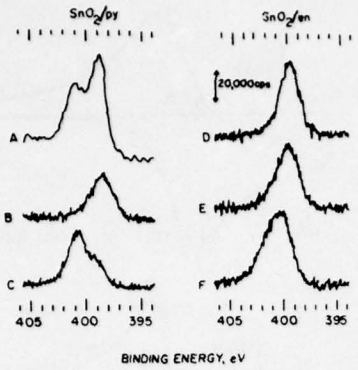

Figure 4. ESCA N 1s spectra for SnO_2/Py electrodes

Curve *A*, freshly prepared electrode washed with benzene, 32 scans summed; Curve *B*, washed with H_2O, 8 scans summed; Curve *C*, washed with 0.1*M* I, 8 scans summed. N 1s spectra for SnO_2/en electrodes, 15 scans summed: Curve *D*, rinsed in 0.1*M* NaOH; Curve *E*, rinsed in pH 6.9 buffer; Curve *F*, rinsed in 0.1*M* HCl

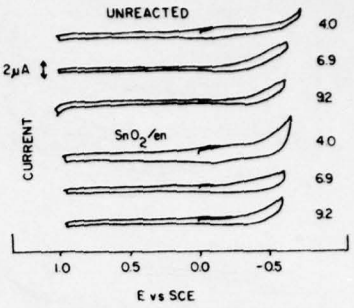

Figure 5. Cyclic voltammograms of blank solutions on unreacted SnO_2 and SnO_2/en electrodes

Numbers beside curves are pH values of buffers (4.0, acid phthalate; 6.9, phosphate; 9.2, borax)

an "inert" grouping. The 3-chloropropyltrichlorosilane reagent is quite reactive, fuming vigorously in moist air. ESCA data summarized in Table I show silicon (unresolved Si $2p_{3/2}$ and Si $2p_{1/2}$) and chlorine (Cl $2p_{/32}$) bands appear after reaction, and the Sn 3d doublet diminishes in intensity as a consequence of the overlaying molecular film. The binding energy for Sn 3d electrons is insufficiently altered by the –Sn–O–Si– bonds to be resolved from lattice tin; we see no change in the Sn 3d binding energy for this or any other modified surface. Likewise, Si 2p binding energies are unchanged throughout the series of modified surfaces.

The intensity of the Sn 3d bands varies substantially from specimen to specimen (Table I). The average diminution of the Sn 3d band (from unreacted SnO_2) can be used to estimate the surface coverage achieved by the silanization reaction, using the relation

$$I_{Sn}/I_{Sn,\,unreacted} = \exp[-d/\lambda] \qquad (2)$$

where d is the silane film depth and λ is the escape depth (Å) of Sn 3d photoelectrons through the surface film. (No electron escape angle correction is needed since $\theta = 90°$.) Taking $\lambda \sim 11$ Å for 487 eV Sn 3d electrons, which have 767 eV kinetic energy (*22*), $d \sim 9$ Å for the SnO_2/PrCl electrode film. Assuming unity density, this depth translates to 6×10^{-10} mole/cm^2, roughly monolayer coverage. The assumptions involved in this estimate are crude, particularly that of λ. Escape depth of photoelectrons through organics may well be several times larger than those in metals (*23, 24*), and so d values given in Table I may be low.

Blank solution cyclic voltammograms (Figure 2) at SnO_2/PrCl electrodes are not particularly distinguished from those on unreacted electrodes except for generally smaller charging currents, as would be expected from replacement of surface –SnOH groups with the neutral silane moiety. Cyclic voltammograms of $Fe(CN)_6^{4-}$ are likewise well-formed and undistinguished, except that ΔE_p (Table II) indicates lowered reversibility on the SnO_2/PrCl electrode. The derivatized surface is completely accessible to electrochemical reactant in a diffusional sense, but the effective (microscopic) electrode area must nonetheless be lowered by the attachment of the silane groups. The smaller microscopic area means higher current *density*, increased charge transfer rate limitations, and mild irreversibility.

SnO_2/Py Electrode. ESCA data for electrodes treated with β-trichlorosilyl-2-ethylpyridine are summarized in Table I. Bands for Si 2p and N 1s appear at intensities roughly the same as for other silanization reactions. Sn 3d intensity decreases as before, but to a significantly smaller extent. The meaning of the latter is not clear; it may reflect a surface structural difference which leads to a different λ for the Sn 3d photoelectrons.

When an electrode fresh from the acidic silanization reaction is rinsed thoroughly with hot benzene and its N 1s band observed, the N 1s appears as a doublet of approximately equal peaks. Rinsing with 0.1*M* HCl largely eliminates the lower binding energy peak; rinsing with base or distilled water does the reverse. These effects, illustrated in Figure 4, clearly are due to protonation of the pyridyl nitrogen. Electrodes treated with 3-aminopropyltriethoxysilane (SnO_2/$PrNH_2$) exhibit similar behavior on acid–base treatment (Table I). The shift in binding energy, 1.5 eV, between N 1s and NH^+ 1s agrees with earlier observations of protonation effects (*23, 25*). The absolute N 1s binding energies for the surface-bound pyridines and amines are roughly 1.5 eV higher than those reported for free bases (*23*).

The reactivity of SnO_2/Py as a ligand surface was further demonstrated by soaking the electrode in a dilute, neutral $Cr(NO_3)_2$ solution obtained by passing degassed 0.1*M* $Cr(NO_3)_3$ through a Jones reductor. Oxygen was passed through the solution for several minutes to reoxidize the Cr^{2+}. This procedure was repeated three more times, each reaction being followed by a copious (water) rinsing of the SnO_2/Py electrodes and removal of an electrode specimen for ESCA examination. After each of the first three steps, the Cr 2p band (575 eV) increased, with no increase recorded on the fourth reaction cycle. Concurrently, the N 1s band broadened toward higher binding energy, indicating overlap of two closely spaced peaks. No Cr 2p bands were observed on similarly treated unreacted SnO_2 or on SnO_2/Py electrodes soaked in unreduced $Cr(NO_3)_3$ solution.

Cyclic voltammograms of blank solutions (Figure 2) and of $Fe(CN)_6^{4-}$ (Table II) on SnO_2/Py show only minor differences from unreacted SnO_2 electrodes.

SnO_2/en Electrodes. A comparison of ESCA data for unreacted SnO_2 and that for SnO_2 reacted with 3-(2-aminoethylamino)propyltrimethoxysilane shows diminution of the Sn 3d band and appearance of Si 2p and N 1s bands. Protonation studies gave results analogous to those above. Exposure of a given specimen (or a series of SnO_2/en specimens) to continually higher pH solutions enhances the lower binding energy N 1s band at the expense of the higher (Figure 4). The total shift observed with pH was ~1.5 eV. We are unable at present to discern whether both amine nitrogens become protonated.

Electrochemical experiments on SnO_2/en in buffered blanks at various pH illustrate the double layer-modifying

Table III. Cyclic Voltammetric Data[a] for SnO_2/en Electrodes

2m*M* ferrocyanide, 0.1m*M* KCl, 0.5*M* glycine, pH 2.4

	Unreacted SnO_2					SnO_2/en				
V, mV/sec	E_p^a	E_p^c	ΔE_p	$i_p^a/ac\ V^{1/2}$	i_p^c/i_p^a	E_p^a	E_p^c	ΔE_p	$i_p^a/ac\ V^{1/2}$	i_p^c/i_p^a
50	0.266	0.205	0.061	9.49×10^2	0.97	0.271	0.205	0.066	8.87×10^2	0.81
100	0.268	0.202	0.066	9.36×10^2	0.99	0.276	0.200	0.076	8.91×10^2	0.86
300	0.278	0.185	0.093	9.73×10^2	0.95	0.291	0.185	0.106	9.11×10^2	0.83
500	0.288	0.180	0.108	9.66×10^2	0.92	0.300	0.175	0.125	9.13×10^2	0.82
				2m*M* *o*-tolidine, 0.1*M* KCl, pH 2.3						
	Unreacted SnO_2					SnO_2/en				
50	0.517	0.460	0.057	1.53×10^3	0.91	0.628	0.360	0.268	8.83×10^2	0.70
100	0.526	0.449	0.077	1.52×10^3	0.82	0.657	0.342	0.315	8.36×10^2	0.63
300	0.549	0.432	0.117	1.44×10^3	0.79	0.690	0.332	0.358	7.62×10^2	0.57
500	0.581	0.405	0.176	1.34×10^3	0.76	0.717	0.320	0.397	7.33×10^2	0.49

[a] Current constant $i_p/ac\ V^{1/2}$ in A $sec^{1/2}$ cm/volt$^{1/2}$ mole. Electrode area = 0.079 cm^2. *E* vs. SCE.

result of derivatization with a neutral base. In a pH 9.2 buffer, the level of charging current, which reflects the double layer capacitance, for unreacted SnO_2 and SnO_2/en electrodes is indistinguishable. When the pH is lowered, on the other hand, to pH 4, where the amine becomes protonated, the capacitance current for the SnO_2/en electrode is significantly enhanced (Figure 5). The effect is that of an electrode positive of its point of zero charge, on which a cation is strongly adsorbed.

The charge given the SnO_2/en electrode surface by protonation is also apparently reflected in electrochemical behavior of a cationic reactant, *o*-tolidine. Figure 3 and Table III compare cyclic voltammograms for this reactant on unreacted SnO_2 and on SnO_2/en. It is apparent that the *o*-tolidine reaction on the latter is much less reversible than on unreacted SnO_2 surfaces. The cyclic voltammetric behavior of the anionic $Fe(CN)_6^{4-}$ reactant, on the other hand, is very nearly the same on unreacted SnO_2 and on SnO_2/en. An adsorption wave, traced to the glycine buffer component and peculiar to the SnO_2/en electrode, is probably the source of the lower quality i_p^c/i_p^a data for $Fe(CN)_6^{4-}$ on that electrode.

General Comments. The results demonstrate that SnO_2 surfaces exhibit a reactivity toward organosilanes quite analogous to that of silica surfaces. Further, in the absence of double layer complications, silanization of the SnO_2 surface does not adversely affect its usefulness as an electrode. We anticipate that organosilanes will provide a versatile route to many varieties of modified SnO_2.

As we noted in the introduction, preparation of surface sites is only the first step in attaining electrochemically useful chemically modified electrodes. We will report on further attachments of redox centers in a future communication. A variety of factors connected with the –Sn–O–Si– surface linkages are also evident objects of continued study. With respect to the structure of the bonded layer, the questions of chain formation and the number of Sn–O–Si bonds formed per silicon center will require synthesis and investigations of $XSiR_3$ and X_2SiR_2 reagents. The role of SnO_2 surface water in the silanization process has probably been oversimplified here, and metal ion adsorption on SnO_2 as opposed to coordination by attached surface ligands requires discriminating tests. Finally, the response of the double layer parameters to chemical events like amine protonation invites probing of the chemical events through this medium. The pK_b of a surface amine is potential dependent (7) and on a positively charged electrode is probably, for instance, substantially larger than the "ordinary", unattached amine.

LITERATURE CITED

(1) E. Grushka, Ed., "Bonded Stationary Phases in Chromatography", Ann Arbor Science Pub., Ann Arbor, Mich., 1974.
(2) H. H. Weetall, *Science*, **166**, 615 (1969).
(3) D. M. Hercules, L. E. Cox, S. Onisick, G. D. Nichols, and J. C. Carver, *Anal. Chem.*, **45**, 1973 (1973).
(4) G. Bruce Harper, *Anal. Chem.*, **47**, 348 (1975).
(5) A. A. Oswald, L. L. Murrel, and L. J. Boucher, Abstracts Div. Petroleum Chem., 168th National Meeting of the American Chemical Society, Los Angeles, Calif., 1974.
(6) K. G. Allum, R. D. Hancock, I. V. Howell, S. McKenzie, R. C. Pitkethly, and P. J. Robinson, *J. Organomet. Chem.*, **87**, 203 (1975).
(7) R. F. Lane and A. T. Hubbard, *J. Phys. Chem.*, **77**, 1401, 1411 (1973).
(8) G. Johansson, J. Hedman, A. Berndtsson, M. Klasson, and R. Nilsson, *J. Electron Spectrosc. Relat. Phenom.*, **2**, 295 (1973).
(9) J. C. Carver, R. C. Gray, and D. M. Hercules, *J. Am. Chem. Soc.*, **96**, 6851 (1974).
(10) T. Kuwana and N. Winograd, "Spectroelectrochemistry" in "Electroanalytical Chemistry", Volume 7, A. J. Bard, Ed., Dekker, 1974.
(11) R. N. Adams, "Electrochemistry at Solid Electrodes", Dekker, New York, N.Y., 1969.
(12) W. A. Aue and C. R. Hastings, *J. Chromatogr.*, **42**, 319 (1969).
(13) W. A. Aue, C. R. Hastings, J. M. Augl, M. K. Norr, and J. V. Larsen, *J. Chromatogr.*, **58**, 295 (1971).
(14) I. V. Borisenko, A. V. Kiselev, R. S. Petrova, V. K. Chuikina, and K. D. Shcherbakova, *Russ. J. Phys. Chem.*, **39**, 1436 (1965).
(15) J. B. Sorrell and R. Rowan, *Anal. Chem.*, **42**, 1712 (1970).
(16) T. Kuwana, Ohio State University, private communication, 1975.
(17) H. A. Laitinen, University of Florida, private communication, 1975.
(18) P. E. Larson, *J. Electron Spectrosc. Rel. Phenom.*, **4**, 213 (1974).
(19) A. Rosencwaig and G. K. Wertheim, *J. Electron Spectrosc. Rel. Phenom.*, **1**, 493 (1973).
(20) J. W. Strojek and T. Kuwana, *J. Electroanal. Chem.*, **16**, 471 (1968).
(21) D. Elliot, D. L. Zellmer, and H. A. Laitinen, *J. Electrochem. Soc.*, **117**, 1343 (1970).
(22) P. W. Palmberg, *Anal. Chem.*, **45**, 549A (1973).
(23) K. Siegbahn et al., "ESCA, Atomic, Molecular, and Solid State Structure Studied by Means of Electron Spectroscopy", Almquist and Wiksells, Uppsala, 1967.
(24) B. L. Henke, *J. Phys. (Paris)*, **C4**, 115 (1971).
(25) L. E. Cox, J. J. Jack, and D. M. Hercules, *J. Am. Chem. Soc.*, **94**, 6575 (1972).

RECEIVED for review May 14, 1975. Accepted July 3, 1975. This research has been facilitated by the U.N.C. Materials Research Center under Defense Advanced Research Projects Agency Grant DAHC-157369, and by National Science Foundation Grant GP-38633X.

PRECEDING PAGE BLANK-NOT FILMED

Reprinted from ANALYTICAL CHEMISTRY, Vol. 48, Page 1247, July 1976
Copyright 1976 by the American Chemical Society and reprinted by permission of the copyright owner

Chemically Modified Carbon Electrodes

C. Michael Elliott[1] and Royce W. Murray*

Kenan Laboratories of Chemistry, University of North Carolina, Chapel Hill, N.C. 27514

Organosilane chemistry is employed to prepare chemically modified glassy carbon and graphite electrodes with surface bound amine, ethylenediamine, pyridine, and alkyl chloride groups. Electrode binding is detected by x-ray photoelectron spectroscopy (ESCA) as are chemical properties of the functional groups such as protonation, Cu(II) coordination, and amidization reactions. The modified electrodes retain electrochemical activity toward solution reactants and are themselves electrochemically stable. In other experiments, dinitrophenylhydrazine is bound to carbon surfaces based on a reaction with carbon surface quinone groupings. These carbons exhibit chemically irreversible electrochemical activity attributable to the bound dinitrophenylhydrazine.

A recent report (*1*) from this laboratory described how, via organosilane chemistry, a variety of functional groupings could be covalently attached to the surfaces of SnO_2 electrodes. Formation of the SnOSi surface ether bonds, which were electrochemically stable, was detected by x-ray photoelectron spectroscopy (ESCA). The surface-bound functional groupings (amine, ethylenediamine, pyridine, alkyl chloride) exhibited normal chemical properties where tested. The SnO_2 electrode surface was thus transformed into new electrode surfaces which possess *predictable* chemical properties. In the interest of expanding the application of organosilane chemistry to electrode materials, we have examined the reactions of organosilanes with the surfaces of two types of carbon, glassy carbon and spectroscopic graphite rod. The results of this study form the basis of this report. In a recent report, Miller and co-workers (*2*) described a chiral carbon electrode modified via different chemistry. We see this line of research as eventually leading to a wide array of chemically modified electrode surfaces with useful analytical, chemical, catalytic, and optical properties.

An extensive and recently reviewed (*3, 4*) body of literature on surface oxides and other functional groupings of carbon has been developed over the past several decades. The subject remains complex, the surface function types and population being governed by both source and previous history (thermal, chemical) of the carbon specimens. The graphite structure of carbon is known, consisting of stacked, fused-ring aromatic-like sheets (basal planes) (*5*). From single crystal graphite experiments showing (*6, 7*) that oxidation occurs almost exclusively at the exposed basal plane edges, it is expected that the predominance of graphitic carbon surface functions are to be found at such edges. The spectroscopic graphite rods used in this study are compacted microcrystalline graphite, and so a more or less uniformly random distribution of exposed basal plane edges and surface functions can be expected on the rod surfaces.

Three widely proposed and supposed carbon surface functions are phenolic (–OH), carboxylic acid, and quinone. These groups are present on carbon surfaces which have been exposed to chemical oxidants or to air during heating to between 200–400 °C. The particular evidences for the presence of the phenolic function includes detections on carbon powders of characteristic chemical reactions (*3, 8–10*) and appropriate pK values (*8, 11–13*). We have been unable to find reports characterizing the reaction of the carbon phenolic –OH with an organosilane to form a COSi surface ether, but it was on the supposition that such reaction would occur that this study was begun. Additionally, we suppose that such carboxylic groups as are present will also react with organosilane to form COSi surface esters.

Relatively little information is available on the surface chemistry of the other form of carbon used in this study—glassy or vitreous carbon. This material has been described as thin, tangled ribbons of graphite-like sheets which may be cross-linked to some extent (*14*). Glassy carbon should then have a substantial exposure of effective basal plane edges and possess surface functionalities similar to graphitic carbon. This supposition has been confirmed in the present study. Glassy carbon as an electrode material is nonporous and has good electrochemical characteristics.

Following the earlier used (*1*) approach to characterization of chemically modified SnO_2, the organosilane-reacted carbons were examined by ESCA spectroscopy after reaction and to test for appropriate chemical properties of the functional groupings borne by the organosilane reagent. The chemically modified carbon electrodes were also shown to continue to exhibit electrochemical reactivity toward conventional solution redox reagents (ferrocyanide, *o*-tolidine).

This report additionally contains data based on the quinone functionality of carbon surfaces. The presumption of surface quinone groupings is based on measurements of electrochemical (*15–18*) and chemical (*12, 16*) reducibility, infrared spectra (*3, 8, 19–21*) and characteristic quinone reactions (*9, 11, 12*). Organic *p*-quinones react (*22*) with arylhydrazines to form hydrazone-*p*-hydroxy-azo tautomeric pairs. Accord-

[1] Current address, Department of Chemistry, Stanford University, Calif.

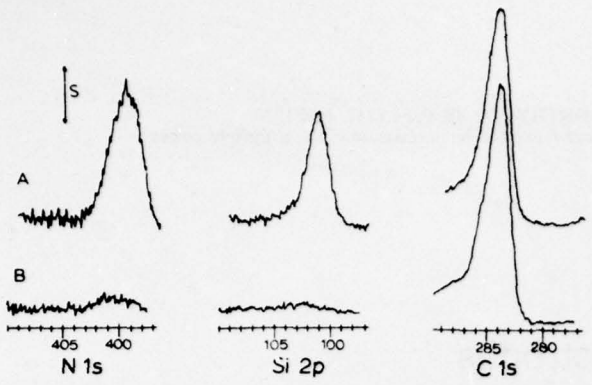

Figure 1. ESCA spectra for N 1s, Si 2p, and C 1s on glassy carbon reacted with γ-aminopropyltriethoxy silane (Curves A). Curves B are unmodified glassy carbon blanks. S = 1.71 kcounts/s for N and Si, 17.1 for C

ingly, preliminary experiments were conducted to test the reactivity of carbon surfaces toward arylhydrazines. The surface reaction products were characterized by ESCA spectroscopy and by their electrochemical reactivity. Studebaker (*9*) previously reacted 2,4-dinitrophenylhydrazine with carbon, supposing that the reaction was with surface aldehyde and ketone-like carbonyls. He apparently was unaware of the reactivity of arylhydrazines toward quinones.

EXPERIMENTAL

Preparation of Carbon Samples. Glassy carbon obtained from Gallard-Schlesinger Chemical Corp. (V10-50 vitreous carbon) as 2.7–3 mm × 150 mm rods was cut into 4-mm lengths with a carbide glass saw. One end of each specimen was surfaced to a mirror finish by SiC paper polishing followed by successively finer diamond paste down to 1 μm on a polishing wheel (*23*). After a specimen had been used in a surface modification reaction, the polished end of the glassy carbon could be readily resurfaced with 1-μm diamond paste. After polishing, glassy carbon specimens were washed of polishing compound with a succession of water, ethanol, and hot benzene followed by oven drying for 1 h at 60 °C. ESCA examination of pristine, polished-but-unreacted, and reacted-resurfaced glassy carbon surfaces showed no or only minor N, Cl, Si, or Cu peaks.

The spectroscopic graphite rod was Varian 4.5-mm diameter and of a grade used locally for spark source mass spectroscopy. Samples were prepared by breaking into 1-cm lengths, facing one end with a clean lathe bit, and polishing to a shiny finish by rubbing on bond paper. The porosity of the graphite prevented effective resurfacing after a surface modification experiment, and these specimens were ordinarily discarded after a single use. Graphite could be reacted directly after polishing without additional treatment.

Mounting of Carbon Samples. For ESCA experiments, the sample mounting device ideally should introduce no additional materials into the photoelectron-sampled region and should retain good electrical contact with the sample to minimize charging effects. The glassy carbon and graphite samples were mounted in a brass cup whose perimeter was fitted with a removable, shielding Teflon cap. The Teflon cap produced no interfering peaks except for C 1s and was removed during observation of the carbon sample's C 1s spectrum.

A demountable sample holder was devised for electrochemical observations of glassy carbon specimens, since it was desired that subsequent ESCA experiments and/or resurfacing be possible. This holder consisted of a Teflon cylinder which accommodated the flush insertion, under light pressure, of the glassy carbon rod. A hexane soluble sealant prevented intrusion of solution between Teflon and carbon. No contact of this sealant with the end of the carbon rod exposed to the solution was allowed. Graphite specimens were mounted for electrochemistry by shrinking Teflon tubing around the carbon rod and an end-to-end glass tube, with electrical contact made with a Hg bubble. The surplus Teflon was trimmed flush with the carbon surface using a razor blade.

Electrochemical backgrounds for porous graphite rod are poor unless the pores are filled with some inert material. Classical wax impregnation procedures are not possible in these circumstances. It was found that a 30-min soaking in *n*-decane (followed by drawing off of excess liquid by capillary action into a tissue corner) before placing in the electrochemical solution produced a suitable pore-filling effect without unduly perturbing the electrochemical properties of the carbon. When employing solvents in which *n*-decane is slightly soluble (such as acetonitrile), the solvent is first saturated with *n*-decane.

Organosilanes and Reaction Conditions. The organosilanes employed were trimethylchlorosilane (TMCS), 3-(2-aminoethylamino)propyltrimethoxysilane (en-silane), 3-chloropropyltrichlorosilane (PrCl-silane), γ-aminopropyltriethoxysilane ($PrNH_2$-silane) all from P.C.R. Chemical Co., and β-trichlorosilyl-2-ethylpyridine (Py-silane) from Petrarch Systems.

Reactions of $PrNH_2$-, en-, and PrCl-silanes with carbon surfaces were carried out using 1–2% solutions of the reagent in refluxing benzene under N_2 for ~12 h. The solution is decanted and the samples are shaken vigorously with five 50-ml portions of absolute ethanol, sitting in the last wash for 30 min, and then air dried. Graphite specimens were extracted in the last wash in a Soxhlet with the ethanol for several hours and oven dried for 1 h at 60 °C. In all circumstances, care was taken to exclude atmospheric moisture until the glassy carbon or graphite specimens had been completely washed of silane reagent. Except for absolute ethanol, all organic solvents are dried over Linde 4A sieves.

The Py-silane is a solid, and usually benzene solutions of this reagent exhibited small amounts of suspended insoluble polymer. To avoid contact of this solid with the carbon samples, the dry reagent solid was placed in a coarse fritted glass extraction thimble in a Soxhlet apparatus and the distilling benzene solution, in which the carbon specimens are placed, allowed to extract nonhydrolyzed reagent from the solid, carrying it down into the flask upon emptying of the Soxhlet.

Arylhydrazines and Reaction Conditions. The reagent employed was 2,4-dinitrophenylhydrazine (DNPH) (Baker). Carbon specimens were reacted in a refluxing 1% solution of the reagent in absolute ethanol containing 1% concentrated HCl for ~12 h. The reacted specimens were washed with ethanol/HCl and extracted in a Soxhlet for 12 h with absolute ethanol, then air dried.

Equipment. Electrochemical equipment for cyclic voltammetry was conventional as was the electrochemical cell. ESCA spectra were obtained with a DuPont 650B spectrometer with Mg anode. All binding energies (B.E.) are referenced to the carbon samples' C 1s peak at 284.0 eV (*24*). As with SnO_2, x-ray exposure affects subsequent electrochemical experiments adversely, and these were always conducted prior to ESCA examination.

RESULTS AND DISCUSSION

Reactions of Organosilanes with Carbon Surfaces. The reaction of an organosilane with a carbon surface phenolic group can be represented as

$$-\underset{\text{surface}}{\overset{|}{\underset{|}{C}}}-OH + XSiX_2R \rightarrow -\underset{\text{surface}}{\overset{|}{\underset{|}{C}}}-OSiX_2R + HX \qquad (1)$$

silane

In the present study "R" is PrCl, $PrNH_2$, en, or Py, and so the detection of a surface reaction by ESCA spectroscopy can be based on the appearance of Cl 2p or N 1s bands as well as those from Si 2p. Both graphite and glassy carbon surfaces react readily with these organosilanes without necessity of thermal or chemical pre-oxidation. Examples of the distinct Si 2p and N 1s bands observed on glassy carbon are shown in Figure 1. The graphite and glassy carbon specimens prior to reaction show only C 1s and O 1s bands. The C 1s band is not noticeably affected by surface reaction.

A compilation of binding energy and intensity data for reacted carbon surfaces is given in Table I. Comparison of the glassy carbon $PrNH_2$, en, and Py data with analogous data for these organosilanes bound to SnO_2 surfaces (*1*) reveals that the N 1s binding energies are about the same on carbon and on SnO_2 surfaces. This is qualitatively expected since the nitrogen base site is, ostensibly, not involved in surface binding and is "free" in both cases. The Si 2p binding energy in the COSi and SnOSi ethers on the other hand is 0.6–0.9 eV lower in the case of the carbon-bonded organosilane.

Table I. Summary ESCA Data for Modified Carbon Electrodes

Sample	Binding energy in eV vs C 1s at 284.0 (No. of samples) Band intensity in kcounts/s N 1s	NH^+ 1s	Si 2p	Cu $2p_{3/2}$
Glassy C/en	399.1 ± 0.2 (4)	400.1 (1)[a]	101.3 (1)	934.3 (1)
	3.52 ± 1.15		1.88	
Graphite C/en	399.9 ± 0.2 (2)		101.6 (1)	933.7 (1)
	6.21 ± 0.62			
Glassy C/$PrNH_2$	400.2 ± 0.5 (5)	401.5 (1)	101.7 ± 0.5 (4)	
	2.30 ± 0.45		2.39 ± 0.20	
Glassy C/Py	399.8 ± 0.4 (11)	401.1 (1)	101.8 ± 0.3 (8)	
	2.95 ± 0.99		2.58 ± 0.42	
Glassy C/8-hydroxyquinoline[b]	400.6 (1)			934.0 (1)
Glassy C/Figure 4[c]	399.5 ± 0.7 (2)		101.8 (1)	933.7 (1)
Glassy C/DNPH[d]	400.0 (1)			
	3.00			
	405.7 (1)			
	1.97			
Glassy C/reduced DNPH	400.2 (1)			
Graphite/DNPH	400.2 ± 0.1 (2)			
	2.28 ± 0.15			
	405.9 ± 0.2 (2)			
	2.05 ± 0.10			

[a] All NH^+ 1s bands poorly resolved and binding energies are estimates. [b] From Figure 4, Curve B. [c] From Figure 4, Curve A. [d] DNPH is dinitrophenylhydrazine.

The reproducibility of binding energies derived from different surface preparations is (except for C/$PrNH_2$ electrodes) about the same for carbon and SnO_2.

The carbon surface Si 2p bands for the $PrNH_2$-, en-, and Py-silanes are ~1.8× lower in intensity than those for SnO_2 (*1*). Direct comparison of these intensities is not straightforward, however, because of the difference in sample areas and heterogeneity in spectrometer surface sensitivity over the sample area (intensity is not simply proportional to sample area) (*25*). Qualitatively, the compared intensities suggest the same general level of organosilane surface coverage on the two electrode materials.

The N 1s/Si 2p band intensity ratios for chemically modified glassy carbons in Table I reflect the differing relative populations of nitrogen and silicon in the various organosilanes. The N 1s/Si 2p ratios for C/$PrNH_2$ and C/Py electrodes are 1.0 and 1.1, respectively, and that for C/en is 1.9.

The X_3SiR organosilane has of course the potential for binding to more than one surface site. The extent to which this occurs depends on the surface –OH population plus surface geometrical requirements, and reactions which compete with the surface –OH functions for the reactive XSi– (principally water hydrolysis). Geometrical estimates using tabular bond lengths (graphite C–C, 1.4 Å; C–O, 1.4 Å; silane Si–O, 1.5 Å) and a graphitic basal plane spacing of 3.4 Å (*26*) suggest that formation of two COSi bonds to a single organosilane molecule can occur with little if any strain on crystalline graphite. Formation of three surface ether bonds is possible but involves moderately strained COSi bonds.

In attempting to prepare a surface with a monolayer or less of covalently attached organosilane, with known spatial relation between electrode surface and functional groups of the organosilane, avoidance of chemically attached, deposited, or adsorbed, organosilane *polymer* is important and desirable. Formation of solution polymer components is minimized by use of scrupulously dry reaction conditions. Formation of surface-attached polymer chains is avoided by thorough washing of excess organosilane from the reacted carbon surface before any exposure to atmospheric moisture. Further, we have checked for physical polymer deposition by subjecting both smooth and roughened Teflon and Kel-F samples to organosilane reaction conditions. ESCA N 1s and Si 2p signals from the surfaces of these samples were <5% of those observed on chemically modified carbon. Also, Grushka (*27*) reported that adsorbed or deposited organosilane polymer could be removed from chromatographic silica surfaces by several hours' boiling in toluene. Neither boiling in toluene nor 1% HCl in ethanol overnight decreased the N 1s or Si 2p ESCA intensities by more than a few percent for glassy carbon reacted with $PrNH_2$- or Py-silane. Next, hydrolysis and polymer formation should not occur with a monofunctional organosilane such as trimethylchlorosilane. Binding of this reagent to glassy carbon was established by ESCA Si 2p bands. The reagent is much less reactive and longer and more forcing reaction conditions were required. Lastly, the intensity of the N 1s and Si 2p ESCA peaks for organosilane-reacted carbon is fairly reproducible from reaction to reaction.

Conditions for the organosilane reactions with carbon electrodes are similar to those employed for SnO_2 (*1*). We have since determined for SnO_2 electrodes (*28*) that sealed tube reaction with neat organosilane at 90 °C is an alternative procedure for modification of these surfaces. When the sealed tube procedure is applied to carbon, on the other hand, apparent severe polymer formation was encountered. Properties of glassy carbon surfaces modified by sealed tube reaction with neat organosilane at ~100 °C overnight include: (i) N 1s and Si 2p binding energies are normal but intensities are quite variable and 2–4× larger. (ii) The organosilane functional groups do not undergo the expected (vide infra) chemical reactions, such as protonation of basic nitrogen by acid washing, reaction of C/$PrNH_2$ with an acid chloride (*p*-nitrobenzoyl chloride), and scavenging of Cu^{2+} by C/en. (iii) Si 2p ESCA intensities are not appreciably reduced by overnight reflux in 10 M KOH in ethanol, a condition which ordinarily hydrolyzes the COSi surface ether. (iv) Brief polishing with 1-μm diamond dust, sufficient to completely resurface "normal"

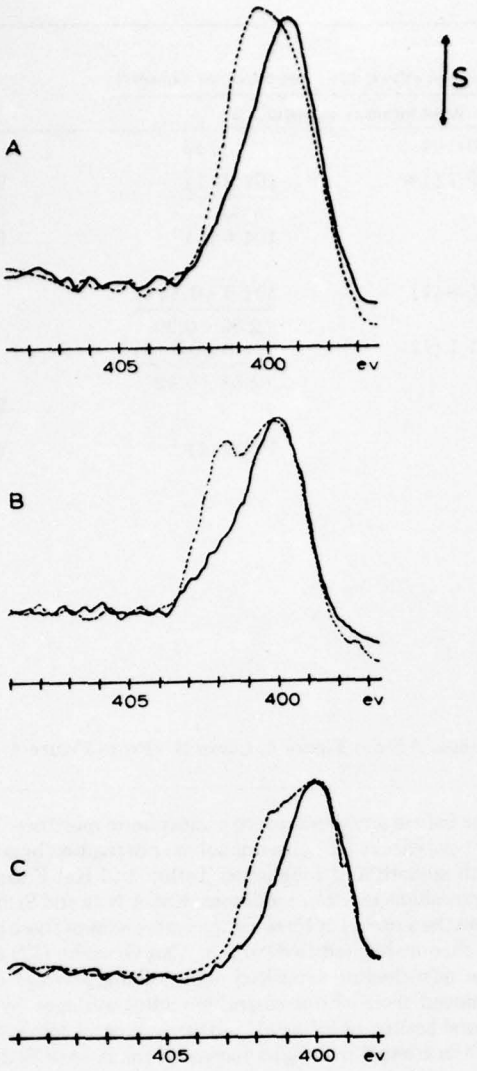

Figure 2. ESCA spectra of N 1s region showing protonation of surface bases for organosilanes bound to glassy carbon. Spectra digitally smoothed. Liquids removed by blowing dry with pure compressed air. In each case (- - -) has been dipped in concentrated HCl and (—) has been dipped in Na_2CO_3 solution and rinsed with water

Curve A: C/en, S = 1.024 kcounts/s. Curve B: C/Py, S = 0.819 kcounts/s. Curve C: C/$PrNH_2$, S = 1.024 kcounts/s

silanized glassy carbon, reduces Si 2p ESCA intensity to only ~0.5× that of the normal silane monolayer. Apparently the organosilane has not only polymerized but also has permeated the upper layers of the poorly porous glassy carbon surface.

Chemical Properties of Surface Bonded Organosilanes. An important question, of course, is the extent to which chemically modified electrode surfaces exhibit the chemical properties of the attached reagents. As part of a continuing study of chemical properties of chemically modified surfaces, we have examined, in a preliminary fashion, the acid–base, metal coordination, and organic-reaction behavior of carbon-bound organosilanes.

The $PrNH_2$-, en-, and Py-silanes when bound to SnO_2 surfaces (*1*) exhibit, after acid or base washing, N 1s ESCA spectra consistent with the basic character of these functions. Similar results were obtained in acid washing-ESCA experiments on the modified carbon surfaces. Acid-washed specimens exhibit N 1s bands or shoulders ~1.3 eV higher than specimens deprotonated by rinsing with water. Representative

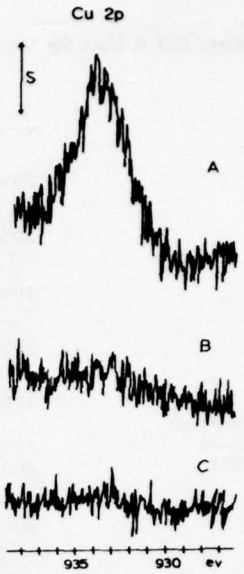

Figure 3. ESCA spectra of Cu $2p_{3/2}$ region for glassy carbons dipped in 10^{-4} M $Cu(NO_3)_2$ in acetone and extracted overnight in 0.4 mM HNO_3 in ethanol. S = 1.37 kcounts/s. Unsmoothed spectra

Curve A: C/en; Curve B: C/$PrNH_2$; Curve C: unmodified glassy carbon

N 1s spectra are shown in Figure 2 and data for free and protonated nitrogen are found in Table I. The increase in binding energy of N 1s upon protonation agrees with the ~1.5 eV shift reported earlier for free bases (*29, 30*). In no case after acid washing does protonation seem to be entirely complete (free nitrogen band absent). This may be a reflection of the so-called ESCA "transfer problem" and not representative of the actual acid–base equilibrium for a carbon surface in contact with the acid solution. Some preliminary results suggest the proportion of NH^+ was increased when less-volatile H_2SO_4 was used as the rinse acid.

The metal ion-binding properties of unreacted glassy carbon and glassy carbon modified with $PrNH_2$- and en-silanes were tested by brief exposure to aqueous 0.1 mM $Cu(NO_3)_2$ followed by overnight extraction with slightly acidic (~0.4 mM HNO_3) ethanol. The extraction was sufficient to remove any Cu^{2+} adsorbed on the unreacted carbon, as shown in Figure 3. (Unreacted glassy carbon and graphite readily adsorb traces of metal ions easily detected by ESCA.) Likewise, little if any Cu^{2+} was retained by the C/$PrNH_2$ surface. Glassy carbon modified by the en-silane, however, shows (Figure 3) an easily detectable Cu $2p_{3/2}$ band. The difference in the $PrNH_2$- and en-silanes probably reflects the chelating properties of the latter. An ethanol solution of the en-silane forms a blue-purple complex upon addition of $Cu(NO_3)_2$, but this color could not, of course, be visually seen on the carbon surface. Binding of Cu^{2+} to a C/en surface was also detected when using graphite rod samples.

A third chemical test for glassy C/$PrNH_2$ was amidization. Weetall et al. (*31*) have shown that glass surfaces modified with $PrNH_2$-silane can be amidized using *p*-nitrobenzoyl chloride. Reduction of the nitro function (with dithionite), formation of a diazonium salt, and reaction with 8-hydroxyquinoline resulted in apparent binding of the latter ligand to the glass surface. This set of reactions was applied to glassy C/$PrNH_2$ surfaces. The resulting carbon 8-hydroxyquinoline surfaces readily scavenged Cu^{2+} from acetone solutions (Curve B, Figure 4). An unreacted glassy carbon blank, Curve D, is a control experiment as is Curve C which followed the same procedure as Curve B except omitting formation of the diazonium salt. A small Cu^{2+} band results, showing that the

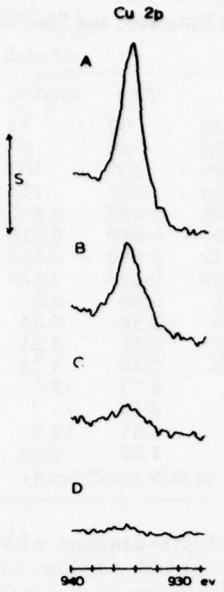

Figure 4. ESCA spectra of Cu $2p_{3/2}$ region for glassy carbons dipped in 10^{-4} M $Cu(NO_3)_2$ in acetone and rinsed with acetone. S = 3.41 kcounts/s. Smoothed spectra

Curve A: C/$PrNH_2$ "diazotized" and "coupled" directly to 8-hydroxyquinoline. See text. Curve B: C/$PrNH_2$ amidized, reduced, diazotized, and coupled to 8-hydroxyquinoline as in text. Curve C: C/$PrNH_2$ same as Curve B except not diazotized. Curve D: Unmodified glassy carbon

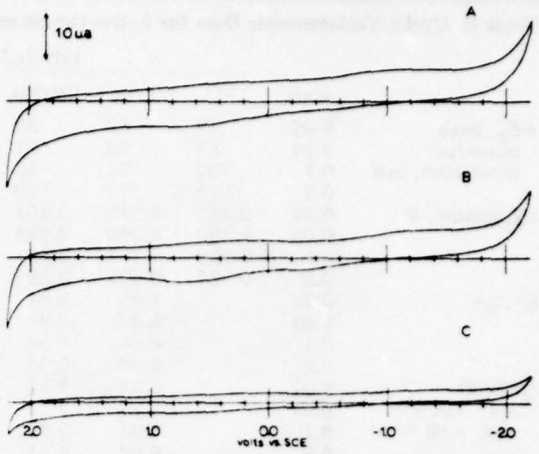

Figure 5. Cyclic voltammetry background scans for glassy carbon/en (Curve A), glassy carbon/$PrNH_2$ (Curve B), and unmodified glassy carbon (Curve C) in aqueous 0.1 M KCl–0.5 M glycine, pH 2.3, v = 0.2 V/s

carbon surface probably adsorbs some 8-hydroxyquinoline which retains copper coordinating properties. A fourth experiment was also done in which, inadvertently, reaction of C/$PrNH_2$ directly with nitrous acid followed by "coupling" to 8-hydroxyquinoline was attempted. In view of the instability of alkyldiazonium, it was surprising that the resulting surface showed considerable affinity for Cu^{2+} (Curve A). This experiment was repeated for verification. The chemistry of this surface is not understood.

In all of the preceding experiments in which Cu^{2+} was coordinated to modified carbon surfaces, the observed binding energy (Table I) for Cu $2p_{3/2}$ is less than that for Cu(II) (*32*). The apparent reduction of surface coordinated copper observed on SnO_2 electrodes (*1*) occurs also on carbon.

Electrochemistry on Carbon Modified by Organosilane Reactions. A major facet of our interest in modified carbon surfaces is ultimately their electrochemical properties. A plan, for example, to utilize the organosilane functional groups to assemble electrochemically active centers on the modified carbon surface is most reasonable if the modified surface is itself electrochemically stable and, furthermore, allows access of simple, "free" redox substances to the carbon electrode for electron transfer interaction. Accordingly, as with chemically modified SnO_2 (*1*), we have used modified glassy carbon as a cyclic voltammetric working electrode in blank supporting electrolyte solutions and in aqueous solutions of the model reactants ferrocyanide and *o*-tolidine.

Background supporting electrolyte scans of unmodified glassy carbon in aqueous 0.1 M KCl–0.5 M glycine buffer (pH 2.3) show reasonably featureless i–E behavior between +2.0 and −2.0 volts vs. SCE. Reproducibility of the level of background charging current from electrode to electrode was only fair (factor of 3× variation) and an occasional electrode exhibited much larger charging current. Background charging currents were consistently larger than an earlier report on glassy carbon (*23*). The background on unmodified carbon is compared in Figure 5 to that typical of glassy C/$PrNH_2$ and C/en. The level of charging current appears to be enhanced for both modified carbons. A similar enhancement of background charging current was observed for en-modified SnO_2 electrodes in acidic solution (*1*). If it is assumed that the $PrNH_2$ and en bases are protonated or partially protonated at pH 2.3, the effect is understood in terms of the capacitance of a surface with fixed positive sites in contact with an ionic solution.

In an attempt to explore the charging current effect further, the pH dependence of ac current for a 20 mV ac potential excitation at constant dc potential was examined. A significant increase in ac current, especially for the modified carbons, was observed at pH >2. The results were not acceptable for a quantitative study, however, as i_{ac} –pH profiles were poorly reproducible and showed aging effects even with unmodified carbon.

Cyclic voltammetric oxidations of ferrocyanide and *o*-tolidine were examined in aqueous 0.1 M KCl–0.5 M glycine on unmodified glassy carbon and on C/$PrNH_2$, C/en, C/PrCl, and C/Py. In all cases, the cyclic voltammograms were of normal shape. A data summary is given in Table II.

Considering first the current data of Table II, the oxidation waves are reasonably proportional to $v^{1/2}$ in all instances (e.g. ordinary diffusion control prevails). The chemical reversibility parameter, $i_p{}^c/i_p{}^a$, for ferrocyanide is close to unity; that for *o*-tolidine is low throughout by ~10% apparently because of a systematic measurement error. With the exception of the C/PrCl electrode, all of the chemically modified glassy carbon surfaces appear to be freely accessible to the two model electroreactants. This means there is appreciable unmodified carbon exposed, or that the reactants freely interpenetrate the organosilane layer, or that the electron transfer distance exceeds the layer thickness. To distinguish between these will be important but not possible at present.

For the C/PrCl surface, a 50% reduced value of $i_p{}^a/ACv^{1/2}$ is found. While this is partially attributable to the charge transfer irreversibility discussed below, it also indicates partial blocking of the available electrode surface probably because of some polymer formation during reaction of the glassy carbon surface with the very water sensitive 3-chloropropyltrichlorosilane. To affect the apparent electrode area by formation of islands of polymer, their dimensions must be comparable to the diffusion layer thickness (~10 μm) attained in these experiments.

While the chemical modification of the glassy carbon does not (except for C/PrCl) seem to significantly degrade the accessibility of its surface to a reactant, the organosilane layers do have an apparent small influence on charge transfer rate

Table II. Cyclic Voltammetric Data for Ferrocyanide and *o*-Tolidine Oxidation at Untreated and Modified Glassy Carbon[a]

		$Fe(CN)_6^{4-}$					*o*-Tolidine				
	v, v/s	C	C/en	$C/PrNH_2$	C/PrCl	C/Py	C	C/en	$C/PrNH_2$	C/PrCl	C/Py
ΔE_p, peak potential separation, mW	0.02	79	63	80	155	65	75	90	74	94	80
	0.04	87	68	84	211	68	75	98	87	97	82
	0.1	103	71	95	263	77	96	107	103	105	89
	0.2	112	79	100	293	80	99	123	114	113	96
E_p, anodic, V	0.02	0.287	0.285	0.291	0.345	0.287	0.509	0.513	0.503	0.513	0.511
	0.04	0.290	0.290	0.295	0.385	0.290	0.509	0.518	0.510	0.517	0.511
	0.1	0.298	0.293	0.301	0.420	0.297	0.522	0.520	0.518	0.523	0.515
	0.2	0.307	0.301	0.303	0.438	0.300	0.522	0.530	0.530	0.529	0.520
i_p^c/i_p^a	0.02		1.08	0.94	1.02	1.01	0.91	0.85	0.90	0.90	0.91
	0.04		0.98	0.97	0.93	1.04	0.90	0.86	0.84	0.88	0.89
	0.1		0.96	1.03	0.89	1.04	0.88	0.81	0.81	0.84	0.91
	0.2		0.96	0.96	0.79	1.10	0.88	0.83	0.75	0.79	0.86
$i_p^a/acv^{1/2}$, $A \cdot s^{1/2}\ cm/V^{1/2}$ mol, $\times 10^{-3}$	0.02		6.34	7.36	3.76	7.36	11.2	8.73	12.1	9.81	13.6
	0.04		6.77	7.11	3.38	7.11	11.2	8.49	11.2	9.64	12.7
	0.1		6.95	6.37	2.94	7.49	11.6	8.51	10.3	9.63	12.6
	0.2		6.90	6.51	3.18	6.62	10.6	7.98	9.46	9.57	12.7

[a] Aqueous 0.1 M KCl, 0.5 M glycine, pH 2.3, area = 0.059 cm^2, C^b = 2.0 mm, *E* vs SCE (NaCl, satd)

as reflected in the cyclic voltammetric peak potential separation ΔE_p (Table II). Ferrocyanide oxidation is pseudo-reversible on unmodified glassy carbon. The oxidation's reversibility is slightly *increased* on C/en and C/Py, and decreased on C/PrCl. These effects are thought to reflect the influence of positive surface sites on reaction of an anion, in the case of the former, and to reflect the presence of surface polymer in the case of the latter. The oxidation of *o*-tolidine is similarly pseudo-reversible on unmodified glassy carbon. On C/en, the *o*-tolidine oxidation is less reversible (positive surface–positive reactant); this was observed (*1*) on SnO_2/en but to a more extreme degree.

All of the electrochemical effects observed above are consistent in kind (if not degree) with those observed and discussed for chemically modified SnO_2 (*1*). Further, the overall results of the study of the organosilane reactions with carbon surfaces lead us to expect that these reactions will provide versatile routes to preparing new types of carbon electrodes. The organosilane reactivity toward carbon, and the results of chemical tests on the modified carbon surfaces, in general parallel the observations (*1*) on SnO_2, and we predict that future observations on one electrode material can be reasonably transposed to expectations of behavior of the other.

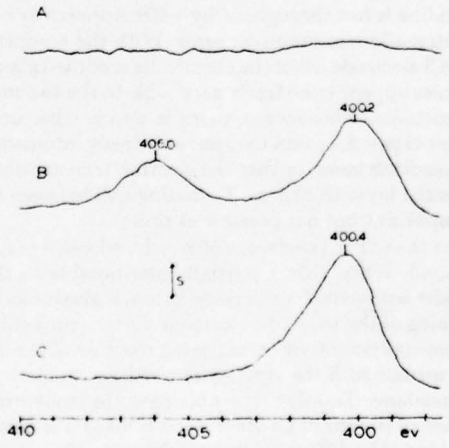

Figure 6. ESCA spectra of N 1s region for graphite rods. S = 0.546 kcount/s

Curve A: unmodified graphite. Curve B: C/DNPH, see text. Curve C: C/DNPH (different specimen) after electrochemically cycling between +2.0 and −2.0 volt vs. SCE in 1 M $NaClO_4$ in acetonitrile.

Reactions of Arylhydrazines with Carbon Surfaces. Arylhydrazines react with *p*-quinones (*22*) to form a tautomeric mixture of hydrazone and *p*-hydroxyazo compounds. Using dinitrophenylhydrazine as an example

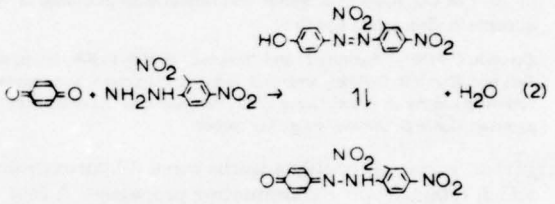

With addition of another mole of arylhydrazine, the reaction can proceed to form the bishydrazone. On a quinone-bearing carbon surface, the reaction could yield an azo-linkage:

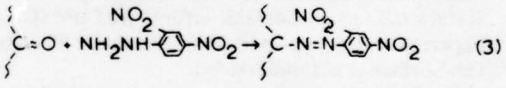

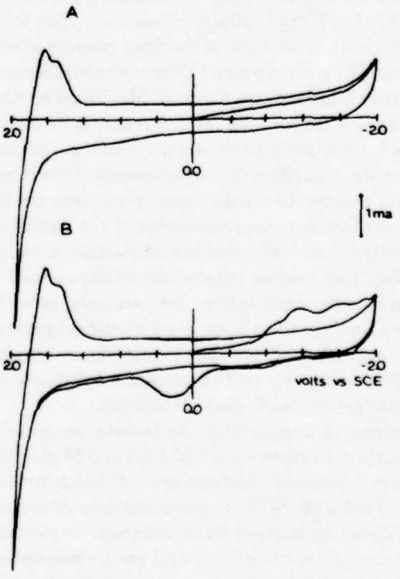

Figure 7. Cyclic voltammorgrams of unmodified graphite rod (Curve A) and graphite C/DNPH (Curve B) in 0.1 M $NaClO_4$ in acetonitrile. v = 0.1 V/s. Electrodes are *n*-decane impregnated. Electrode of Curve B used for Curve C in Figure 6

Both graphite rod and glassy carbon specimens were subjected to reaction with dinitrophenylhydrazine (DNPH) as described in the Experimental section. For both materials ESCA examination indicated the presence of surface DNPH. Figure 6 compares a blank graphite sample with a reacted one. Results for glassy carbon are essentially the same. Two somewhat broad N 1s bands are found on the modified carbons. The band at 400.2 eV is assigned to the azo nitrogens; that at 405.9 eV to the nitro functions. The nitro band intensity is expected to equal that for the azo nitrogens, but is less. Reduction in the ESCA spectrometer has been reported (29) for other nitroaromatics. In a separate experiment, the DNPH-reacted graphite was extracted with acidic ethanol for 72 h. Observation of an undiminished pair of N 1s bands demonstrates that the DNPH is chemically bonded to the carbon surface.

The bonded DNPH was determined to be electrochemically reactive on both graphite rod and glassy carbon. Figure 7 displays a cyclic voltammogram for graphite/DNPH in 1 M $NaClO_4$ in acetonitrile saturated with *n*-decane. A series of ill-defined cathodic waves commences at about −0.8 V, followed by several small anodic waves and one large peak at +0.22 V. Subsequent scans produce an *i*–*E* pattern indistinguishable from that on an unmodified graphite electrode. (Use of tetraethylammonium perchlorate supporting electrolyte produced the same result.) The electrochemical behavior is chemically irreversible.

The irreversibly reduced graphite specimen of Figure 7 was examined by ESCA as shown by Curve C, Figure 6. The nitro N 1s band disappears and the lower binding energy N 1s band grows in intensity. Plainly the surface electrochemistry involves, at least in part, reduction of both nitro functions.

The approximate potential at which nitro reduction occurs was established in a series of experiments on glassy carbon/DNPH. The cyclic voltammetry of glassy carbon/DNPH is even more poorly defined than that of graphite/DNPH in Figure 7. The bound DNPH reduction wave on glassy carbon commences at ~−0.7 V and is quite featureless, being a low, very broad wave just above background current level. The nitro reduction in glassy carbon/DNPH is nonetheless readily seen in ESCA experiments. Figure 8 shows in Curves B and A, a "before" and "after" like that of Figure 6. Also shown in a series of glassy carbon/DNPH electrodes which were potentiostated in acetonitrile for 3 min, briefly rinsed, and the N 1s ESCA determined. There is some scatter attendant to the use of a different electrode specimen for each potential. It is nonetheless evident that the (higher binding energy) nitro N 1s band diminishes significantly in intensity at ~−0.8 V vs. SCE. A band of intermediate (~401.5 eV) binding energy appears in this particular series of spectra. This band may represent a reduction product, but more likely is residual Et_4N^+ from the supporting electrolyte which was not completely removed in the brief electrode rinsing used.

The solution electrochemistry of adducts like those of reaction 2 has apparently not been previously studied. Complex redox behavior is anticipated given the presence of three electroactive functions (hydrazone, azo, and nitro) and the existence of bishydrazone as well as monohydrazone derivatives. Adducts of *p*-benzoquinone and 9,10-anthraquinone with DNPH were prepared, but not purified, and survey cyclic voltammetry performed on glassy carbon working electrodes (unmodified) in acetonitrile. A rich pattern of cathodic waves (≥3 waves) is found for the *p*-benzoquinone derivative commencing at about −0.6 V. None of this electrochemistry has been interpreted and data are not presented here. It is instructive, however, that the range of potentials over which "model" compounds and DNPH-modified carbons exhibit electroactivity are roughly the same.

These data can be interpreted in two ways. In one, the

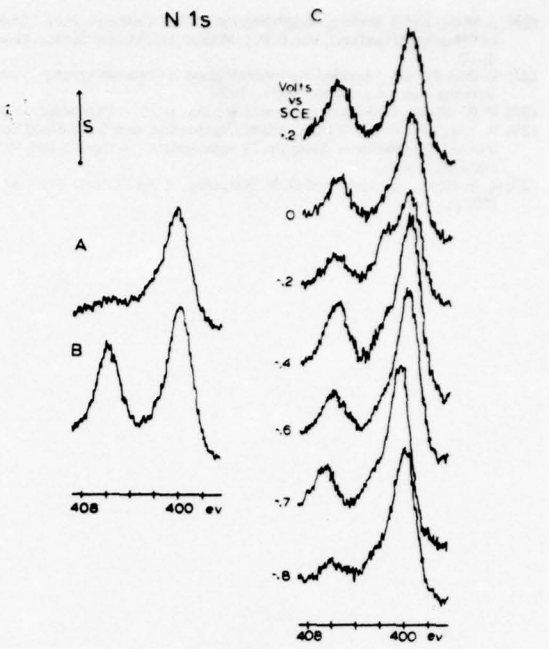

Figure 8. ESCA spectra of N 1s region for glassy carbon/DNPH. S = 1.64 kcounts/s. Electrochemistry done in 0.1 M tetraethylammonium perchlorate in acetonitrile

Curve A: C/DNPH cycled between 0 and −1.2 V. Curve B: C/DNPH (no electrochemistry done). Curve C: C/DNPH, a series of samples potentiostated at indicated potential for 3 min

DNPH is attached to the carbon surface by the quinone bonding mechanism of reaction 3. In the other, it is supposed that the DNPH is bonded to carbon by a mechanism *not* involving surface quinone functionality. The data do not allow unequivocal distinction between these interpretations, and it may well be that both processes occur. Certainly if quinones are present on carbon at all, reaction 3 is a reasonable chemical expectation, and the carbon surface affinity for aromatic substances is known in general to be quite high.

LITERATURE CITED

(1) P. R. Moses, L. Wier, and R. W. Murray, *Anal. Chem.*, **47**, 1882 (1975).
(2) B. F. Watkins, J. R. Behling, E. Kariv, and L. L. Miller, *J. Am. Chem. Soc.*, **97**, 3549 (1975).
(3) J. S. Mattson and H. B. Mark, Jr., "Activated Carbon", Marcel Dekker, New York, 1971.
(4) B. R. Puri, Surface Complexes on Carbon, from "Chemistry and Physics of Carbon", Vol. 6, P. L. Walker, Jr., Ed., Marcel Dekker, New York, 1970.
(5) V. Hofmann and F. Sinkel, *Z. Anorg. Chem.*, **245**, 7 (1940).
(6) G. R. Hennig, "Proceedings of the 5th Conference on Carbon", Vol. I, Pergamon Press, New York, 1962, p 143.
(7) G. R. Hennig, *J. Chim. Phys.*, **58**, 12 (1961).
(8) V. A. Garten, D. E. Weiss, and J. B. Willis, *Aust. J. Chem.*, **10**, 295 (1957).
(9) M. L. Studebaker, E. W. D. Huffman, A. C. Wolfe, and L. G. Nabors, *Ind. Eng. Chem.*, **48**, 162 (1956).
(10) B. R. Puri, *Carbon*, **4**, 391 (1966).
(11) H. P. Boehm, *Adv. Catal.*, **16**, 179 (1964).
(12) H. P. Boehm, E. Diehl, W. Heck, and R. Sappok, *Angew. Chem., Int. Ed. Engl.*, **3**, 669 (1964).
(13) D. S. Villars, *J. Am. Chem. Soc.*, **69**, 214 (1947).
(14) G. M. Jenkins and K. Kawamura, *Nature (London)*, **231**, 175 (1971).
(15) I. F. Jones and R. C. Kaye, *J. Electroanal. Chem. Interfacial Electrochem.*, **20**, 213 (1969).
(16) J. V. Hallum and H. V. Drushel, *J. Phys. Chem.*, **62**, 110, 1502 (1958).
(17) K. F. Blurton, *Electrochim. Acta*, **18**, 869 (1973).
(18) B. D. Epstein, E. Dalle-Molle, and J. S. Mattson, *Carbon*, **9**, 609 (1971).
(19) J. S. Mattson, H. B. Mark, Jr., and W. J. Weber, Jr., *Anal. Chem.*, **41**, 355 (1969).
(20) J. S. Mattson and H. B. Mark, Jr., *J. Colloid Interface Sci.*, **31**, 131 (1969).
(21) J. S. Mattson, L. Lee, H. B. Mark, Jr., and W. J. Weber, Jr., *J. Colloid Interface Sci.*, **33**, 284 (1970).
(22) W. Barsihe, *Ann.*, **357**, 171 (1907).
(23) R. E. Panzer and P. J. Elving, *J. Electrochem. Soc.*, **199**, 864 (1972).
(24) S. Hogstrom and S. E. Karlsson, *Ark. Fys.*, **26**, 451 (1964).
(25) D. Untereker, University of North Carolina, 1975, unpublished results.

(26) J. Maire and J. Mering, Graphitization of Soft Carbons, from "Chemistry and Physics of Carbon", Vol. 6, P. L. Walker, Ed., Marcel Dekker, New York, 1970.
(27) E. Grushka, Ed., "Bonded Stationary Phases in Chromatography", Ann Arbor Science Pub., Ann Arbor, Mich., 1974.
(28) P. R. Moses, University of North Carolina, 1975, unpublished results.
(29) K. Siegbahn et al., "ESCA, Atomic, Molecular, and Solid State Structure Studied by Means of Electron Spectroscopy", Almquist and Wiksells, Uppsala, 1967.
(30) L. E. Cox, J. J. Jack, and D. M. Hercules, *J. Am. Chem. Soc.*, **94**, 6575 (1972).
(31) K. F. Sugawara, H. H. Weetall, and G. D. Schucker, *Anal. Chem.*, **46**, 489 (1974).
(32) P. E. Larson, *J. Electron Spectrosc. Relat. Phenom.* **4**, 213 (1974).

RECEIVED for review February 17, 1976. Accepted April 5, 1976. This research has been facilitated by National Science Foundation Grant GP-38633X and by U.N.C. Materials Research Center under Defense Advanced Research Projects Agency Grant DAHC-15-73-G-0009.

Used copy
4/76 RWM

PRIVILEGED DOCUMENT
FOR REVIEW PURPOSES ONLY

61472
org

JUN 18 1976

JOURNAL OF THE AMERICAN
CHEMICAL SOCIETY

"Chemically Modified Electrodes. III. SnO_2 and TiO_2 Electrodes Bearing an Electroactive Reagent"

P. R. Moses and Royce W. Murray, Kenan Laboratories of Chemistry, University of North Carolina, Chapel Hill, North Carolina 27514

Abstract

The electroactive moiety methylpyridinium is covalently bonded to the surfaces of SnO_2 and TiO_2 film electrodes by means of organosilane chemistry. The immobilized methylpyridinium yields a surface wave at a potential similar to solution methylpyridinium. Synthesis of the immobilized methylpyridinium and its electroactivity are supported by ESCA data.

Chemically Modified Electrodes. III. SnO_2 and TiO_2 Electrodes Bearing an Electroactive Reagent.

Sir:

In an emerging new approach to electrochemistry, the surfaces of carbon[1,2] and tin oxide[3,4] electrodes have been chemically modified with several covalently attached reagents. The electrode surfaces exhibit the reagents' properties, such as inducing chirality in electrochemical processes[1] and surface base protonation equilibria[2,3]. We report here the first examples of chemically modified electrode surfaces which bear a covalently anchored[5] electroactive reagent. Such chemically modified electrodes present opportunities for fundamentally new approaches to the study of electrochemical reactions and to the tailoring of electrode surfaces for specific electrocatalytic properties.

The electrode materials employed are Sb-doped SnO_2 films (~5000 Å, 5 Ω square) on glass[3], and TiO_2 films (est. 1000 Å) on titanium prepared by anodization (15% H_2SO_4, 20% NaH_2PO_4, 50 v.) of polished titanium[7,8] followed by heating in 10% H_2 (in N_2, 400°C) for several hours.[9] The surfaces of both electrodes were reacted with β-trichlorosilyl(2-ethyl)-pyridine in benzene under anhydrous conditions[10] and then with refluxing neat CH_3I. The surface molecule sought is

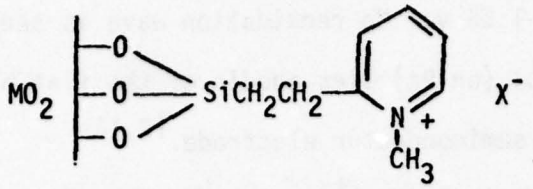

I

The silanization of SnO_2 electrodes has been demonstrated[3]; chemical modification of TiO_2 electrode surfaces has not been previously reported. We will refer to the chemically modified electrodes I as $TiO_2/Py(CH_3)^+$ and $SnO_2/Py(CH_3)^+$.

Fig 1

Figure 1 shows N 1s ESCA spectra of various TiO_2 electrodes. Following silanization (Curve B), pyridine N 1s appears at 400.0 e.v. Methylation (Curve D) produces a new band with binding energy (401.5 e.v.) quite close to that of N 1s in authentic methylpyridinium iodide (Curve C). An analogous set of ESCA N 1s spectra are obtained for SnO_2 electrodes. The methylation reaction is not quantitative on either electrode (~50% on TiO_2, ~70% on SnO_2). ESCA spectra of the surface counterion X^- after exposure of the electrode to solutions of various anions (I^-, Br^-, Cl^-, ClO_4^-, BF_4^-) show that X^- is readily exchangeable. The ESCA results are consistent with the expectations of I above, except that the actual number of MOSi bonds is undetermined.

Fig 2

Alkylpyridinium ions are electroreducible[12] but have not been studied in CH_3CN solvent. The initial (one electron) reduction product is thought to undergo dimerization. Figure 2 illustrates cyclic voltammograms in CH_3CN of free $Py(CH_3)^+$ and of the surface molecule I. On a Pt electrode (Curve A) free $Py(CH_3)^+$ shows an irreversible current peak -1.32 v. vs. S.C.E. and shows a re-oxidation wave at -0.15 v. Exhaustive reduction (coulometric $n \simeq 1$) of free $Py(CH_3)^+$ enhances the -0.15 v. wave; reoxidation of the product solution, presumably the mentioned dimer, regenerates ~80% of the original cation wave. On an unmodified

TiO_2 film electrode (Curve B), the irreversible free $Py(CH_3)^+$ wave appears at -1.56 v. No reoxidation wave is seen, unsurprisingly, since its potential (on Pt) lies anodic of the flat band potential of the *n*-type TiO_2 semiconductor electrode.[13,14]

A fresh $TiO_2/Py(CH_3)^+$ electrode exhibits an irreversible reduction wave (Curve C, Figure 2) at a potential (-1.35 ±0.04 v.) close to free $Py(CH_3)^+$ on Pt. An immediate repeat scan yields a current envelope (Curve D) identical to a background scan[15] on an unmodified TiO_2 electrode. Potentiostatting a reduced $TiO_2/Py(CH_3)^+$ electrode at 0.0 v. for a few minutes, however, regenerates reproducibly ~30% of the original surface wave as seen on the cathodic sweep, Curve E. These results indicate that on TiO_2 the surface species I is indeed electroreducible, and that its reduction product remains bound to the electrode and can be reoxidized. ESCA data support this view. Curve E of Figure 1 shows that the 401.5 e.v. quaternary nitrogen band is substantially eliminated on a $TiO_2/Py(CH_3)^+$ electrode reduced at -1.8 v. Curve F shows a $TiO_2/Py(CH_3)^+$ electrode first reduced, then reoxidized at 0.0 v.; the pyridinium N 1s band returns to an extent consistent with the electrochemistry. That the reoxidizable surface species is actually the 4,4' dimer of I is consistent with (but not proven by) these data. Given its rectifying properties,[13,14] the observed reoxidation reaction at TiO_2 may be somewhat unusual. We note, however, that the TiO_2 films used may be too thin for development of a full semiconductor space charge, that the reoxidation rate is quite slow, and that chemical modification as used here could introduce new surface states.

$SnO_2/Py(CH_3)^+$ electrodes also exhibit a cathodic wave (Curve F) ascribable to reduction of I. In this case, 3-4 repeat scans are required before the current falls to a steady background (Curve G). The $SnO_2/Py(CH_3)^+$ reduction peak is ~0.010 v. negative of that for free $Py(CH_3)^+$ (Curve H) on unmodified SnO_2. The ESCA N 1s spectrum of reduced $SnO_2/Py(CH_3)^+$ confirms reduction of the quaternary nitrogen; the X^- counterion spectrum also disappears. Although oxidations are observed on these heavily doped SnO_2 electrodes,[3] we have not observed reoxidation of a reduced $SnO_2Py(CH_3)^+$ electrode to regenerate the cathodic peak of Curve F.

The surface population Γ of $MO_2/Py(CH_3)^+$ centers is estimable from the charge passed in the cyclic voltammograms for their electrochemical reduction. The estimate is complicated somewhat by the broad background current enhancement[16] which is observed on both electrodes and which vanishes after a reduction cycle. On $TiO_2/Py(CH_3)^+$ assuming $\underline{n} = 1$, $\Gamma = 2.0 \pm 0.2 \times 10^{-9}$ mole/cm^2 and 2.6×10^{-10} mole/cm^2 (average of 5 electrodes) based respectively on inclusion of, and correction for, this background. The corrected analysis on $SnO_2/Py(CH_3)^+$ is 0.8×10^{-10} mole/cm^2. The corrected analysis is quite compatible with a molecular model estimate (~4×10^{-10} moles/cm^2) of monolayer coverage of $Py(CH_3)^+$ on the MO_2 surfaces. Surface roughness (factor < 2X estimated by microscopic examination) and unmethylated surface pyridine are partially self-cancelling factors not included in this coverage estimate.

Electroreactivity of I requires a steric "floppiness" of the electroactive center allowing a close approach to the electrode, as the connecting chain is electronically insulating. Neighbor-neighbor steric interferences could thus interfere with the electron transfer event. That I is shown in fact to be electroactive, on two electrode materials,

demonstrates that the strategy of immobilizing electron transfer sites on electrodes using flexible yet insulating molecular architecture can be successful. Other examples of electrochemically active chemically modified electrodes, and a more detailed analysis of the $MO_2/Py(R)^+$ electrodes, are subjects of continuing investigations.

P. R. Moses, Royce W. Murray*
Kenan Laboratories of Chemistry
University of North Carolina
Chapel Hill, North Carolina 27514

RECEIVED JUN 18 1976

Acknowledgement

This research has been facilitated by National Science Foundation Grants MPS-73-08758 and MPS-75-07863. The authors are indebted to Professor A. J. Bard for stimulating lectures given as Senior Visitor, U.N.C., March 1976 and to Professor T. J. Meyer for helpful discussions. Presented in part at the First Chemical Congress, Mexico City, December 1975.

References and Notes

1. B. F. Watkins, J. R. Behling, E. Kariv, and L. L. Miller, J. Amer. Chem. Soc., 97, 3549 (1975).

2. C. M. Elliott and R. W. Murray, Anal. Chem., 48, 1247 (1976).

3. P. R. Moses, L. Wier and R. W. Murray, Anal. Chem., 47, 1882 (1975).

4. N. R. Armstrong, A. W. C. Lin, M. Fujihira, and T. Kuwana, Anal. Chem., 48, 741 (1976).

5. As opposed to the already illustrated circumstance of chemisorbed electroactive species.[6]

6. R. F. Lane and R. T. Hubbard, J. Phys. Chem., 77, 1401, 1411 (1973).

7. K. L. Hardee and A. J. Bard, J. Electrochem. Soc., 122, 739 (1975).

8. A. Fujishima, K. Kohayahawa and K. Honda, J. Electrochem. Soc., 122, 1487 (1975).

9. M. S. Wrighton, D. S. Ginley, P. T. Wolczanski, A. B. Ellis, D. L. Morse, and A. Linz, Proc. Nat. Acad. Sci., 72, 1518 (1975).

10. Details of the reactions and the importance of anhydrous conditions in avoiding polymer formation are discussed elsewhere.[11]

11. D. F. Untereker, J. C. Lennox, L. M. Wier, P. R. Moses, and R. W. Murray, submitted.

12. M. Naarova' and J. Volke, Collection Czechoslov. Chem. Commun., 38, 2670 (1973); ibid., 37, 3371 (1972); M. S. Spritzer, J. M. Costa and P. S. Elving, Anal. Chem., 37, 211 (1965).

13. S. M. Frank and A. J. Bard, J. Amer. Chem. Soc., 97, 7427 (1975).

14. H. Gerisher in "Physical Chemistry: An Advanced Treatise," Vol. 9A, H. Eyring, D. Henderson, W. Jost, Eds., Academic Press, N.Y., 1970.

15. The unusual shape of this background is due to the high sweep rate and current sensitivity plus the electrode's semiconductor properties.

16. This background current is absent on some specimens and has been observed on modified electrodes bearing other electroactive groups.

Figure 1. ESCA N 1s spectra of chemically modified TiO_2 electrodes. B. E. referenced to C1s at 285 e.v. Curve A is blank TiO_2.

Figure 2. Cyclic voltammograms in 0.2M Et_4NClO_4/CH_3CN. Curves A,B(0.1 v/sec) and H(0.05 v/sec) are free $Py(CH_3)^+$ on unmodified electrodes. Curves C-E (0.50 v/sec) and F,G(0.050 v/sec) are $MO_2/Py(CH_3)^+$.

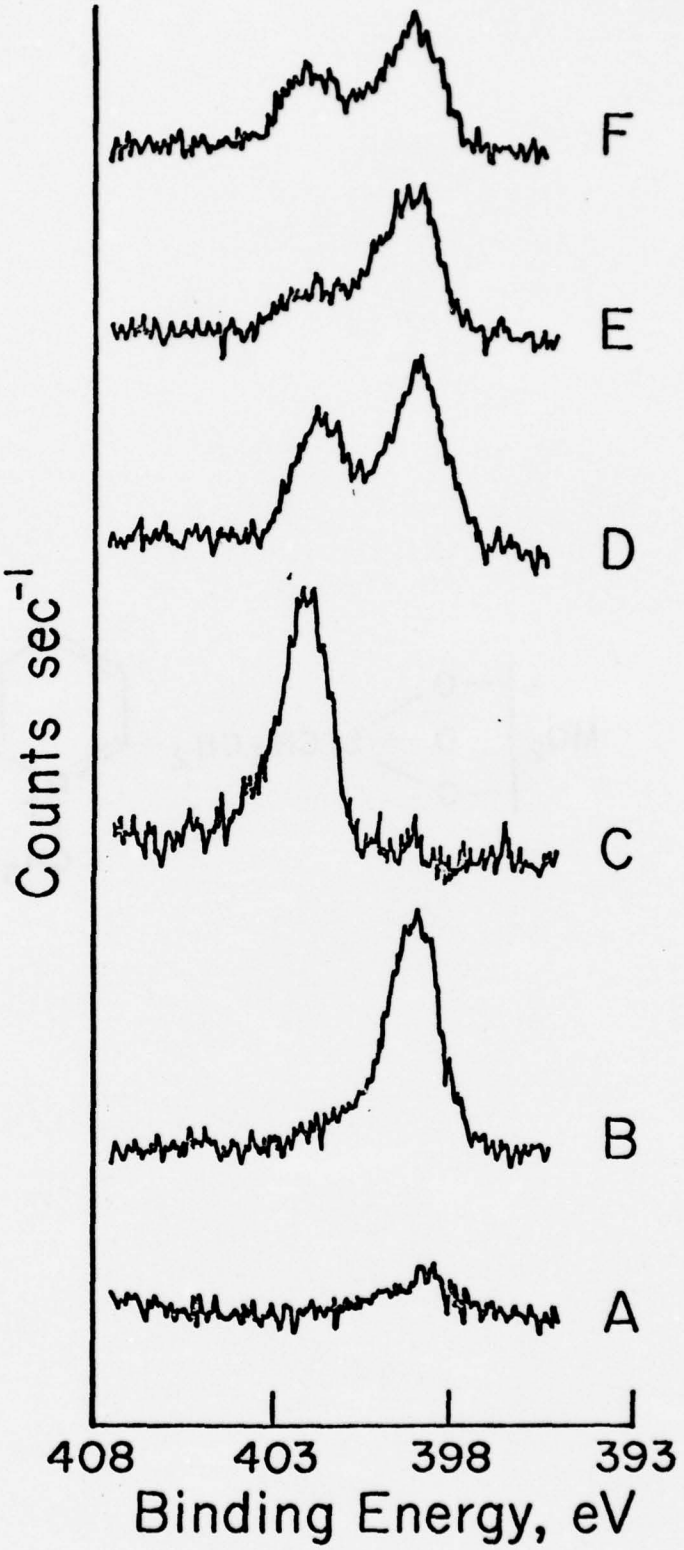
F
E
D
C
B
A
Counts sec⁻¹
408
403
398
393
Binding Energy, eV

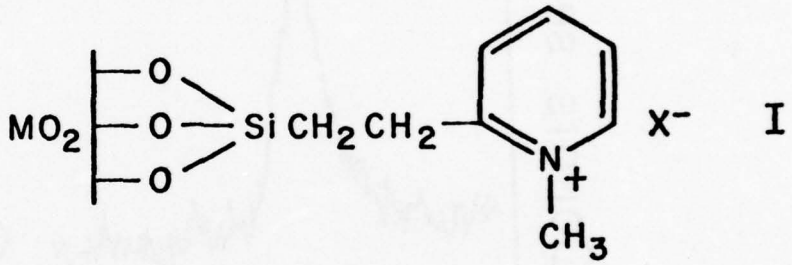

I

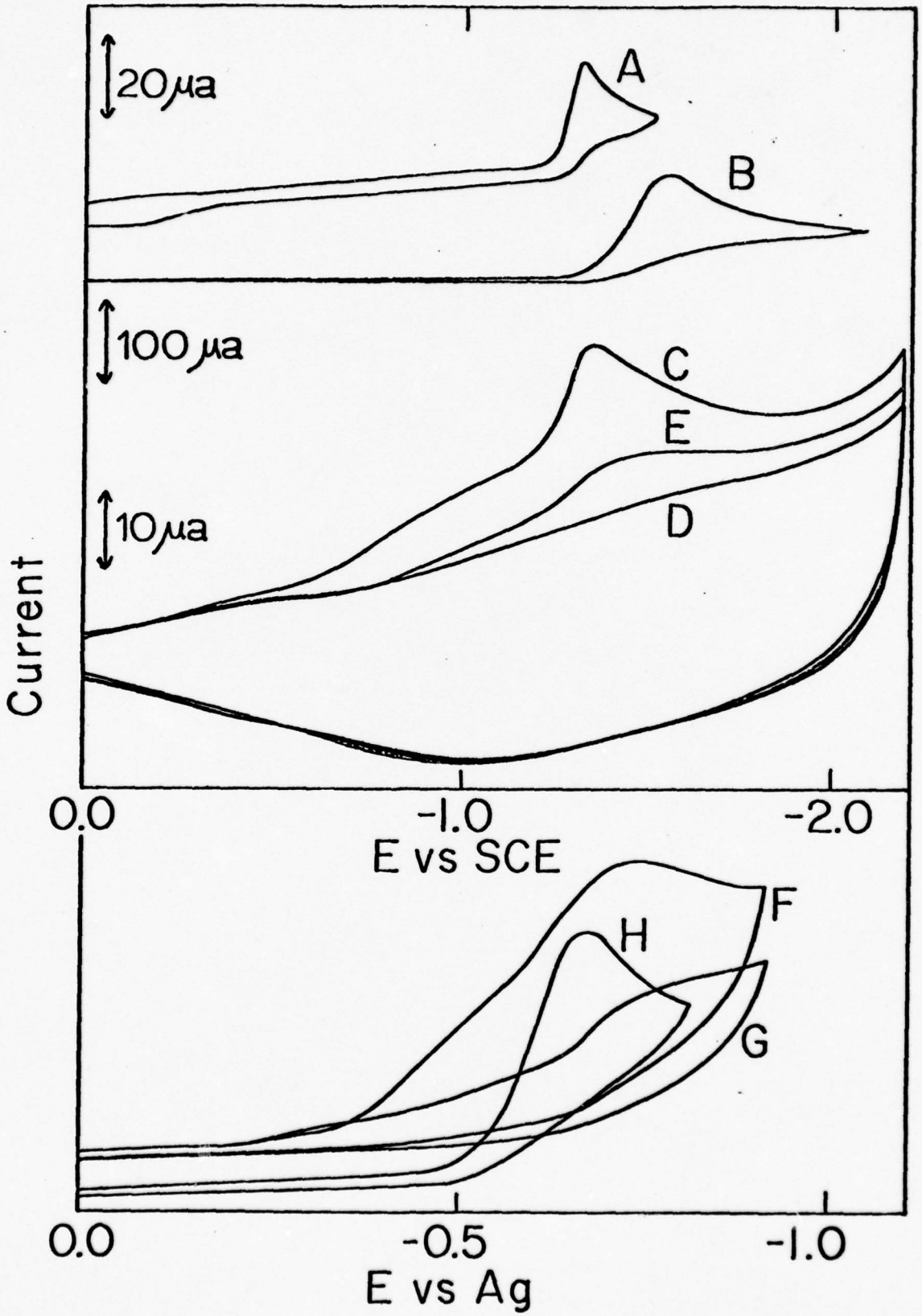
20μa
A
B
100μa
C
E
10μa
D
Current
0.0
-1.0
-2.0
E vs SCE
F
H
G
0.0
-0.5
-1.0
E vs Ag

CHEMICALLY MODIFIED ELECTRODES. IV. EVIDENCE FOR FORMATION OF MONOLAYERS OF BONDED ORGANOSILANE REAGENTS

D. F. Untereker[1], John C. Lennox, L. M. Wier,
P. R. Moses and Royce W. Murray

Kenan Laboratories of Chemistry
University of North Carolina
Chapel Hill, N.C. 27514

ABSTRACT

Organosilane reagents have been used under anhydrous reaction conditions to chemically modify the surfaces of SnO_2, TiO_2 and glassy carbon electrodes, and soft glass. Measurements of thickness of the resultant chemically bonded organosilane layers by ESCA intensity comparisons, and of mole/cm^2 coverage by electrochemical and optical experiments, are compatible with considering the bonded layers as primarily monomolecular as opposed to a multilayer surface polymer. As part of the study, the escape depth of Si 2p photoelectrons in an organosilane matrix was measured and compared to a theoretical prediction.

1. Present address: Medtronic, Inc., Minneapolis, Minnesota.

CHEMICALLY MODIFIED ELECTRODES. IV. EVIDENCE FOR FORMATION OF MONOLAYERS OF BONDED ORGANOSILANE REAGENTS

D. F. Untereker[1], John C. Lennox, L. M. Wier,
P. R. Moses and Royce W. Murray

Kenan Laboratories of Chemistry
University of North Carolina
Chapel Hill, N.C. 27514

1. Present address: Medtronic, Inc., Minneapolis, Minnesota.

1. INTRODUCTION

The kinetics and mechanism of electrochemical reactions are frequently determined by the surface properties of the electrode material. Thus, the notion of chemically modifying electrode surfaces, by binding of selected chemical reagents, to synthesize new surfaces with predictive and perhaps useful properties, is appealing. Over the past year, covalent binding of chemical reagents to the surfaces of carbon [1-3], SnO_2 [4-9], and TiO_2 [9] electrodes has been described. One binding method is based on reaction of organosilane reagents with surface -OH groups. Assuming a three bond linkage, the surface modification reaction is represented as

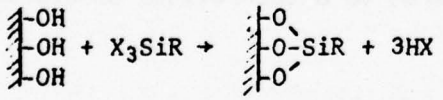

(1)

where X is chloride or alkoxyl and R is a carbon chain which can bear functionalities such as amine or pyridyl and which can be subsequently synthetically modified so as to incorporate an electrochemically reactive grouping into the surface bound reagent. The electrochemical reduction of thus prepared immobilized methylpyridinium has been observed [9].

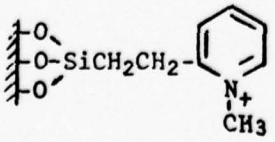

(2)

It is well known that the presence of moisture produces hydrolytic side reactions during the use of organosilane reagents for surface silanizations. Hydrolysis of an $XSiR_3$ reagent is of no consequence to the surface coverage obtained, but partial hydrolysis of a polyfunctional X_3SiR (or X_2SiR_2) reagent, either before or after formation of a surface bond, can lead to surface-bonded polymer structures such as

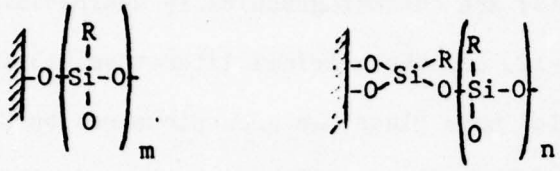

(3)

Electron transfer between an electrode and an immobilized redox group such as (2) is a novel electrochemical situation. Our working model for electron transfer presumes a necessary close approach of the redox group to the electrode (via flexing of the connecting chain). To investigate this model, and to use immobilized redox groups for electrocatalytic purposes, a monolayer form of surface bonding such as (1) is desirable, and polymer structures such as (3) are to be avoided. Accordingly, we have adopted the experimental procedure of conducting the surface silanization reaction under anhydrous conditions in order to attempt to limit the surface coverage to a monolayer.

This report presents and compares data on electrode surface coverage in reaction (1) as measured in a variety of ways on the different electrode materials. The objective is to assess the extent to which we are able to constrain reaction (1) to monolayer or submonolayer coverages. The data are drawn from three categories: (i) determination of thickness of the chemically bound layer via X-ray photoelectron spectral (ESCA) band intensities, (ii) determination of mole/cm^2 coverage from Faradaic charges for electrochemical reactions and from optical absorbances of bound chromophores, and (iii) effects attendant to reaction conditions. The substrate electrode surfaces include SnO_2 films on glass, TiO_2 films on Ti, and

glassy (vitreous) carbon. Some data are also given for flat soft glass surfaces.

Extensive literature exists on reactions of X_2SiR_2 and X_3SiR organosilanes with surfaces, primarily silica-based, through interests in "bonded phases" for liquid and gas chromatography and in enzyme immobilization. However, in most of these applications of organosilane reagents, surface polymerization is deliberately invoked by the addition of moisture, since the chemical and physical stability of structures such as (3) are chromatographically desirable. This is made clear in recent reviews [10-12] and the original literature [13-19]. In enzyme immobilization on controlled pore glass, an area pioneered by Weetall and coworkers, silanization procedures using X_3SiR reagents were initially conducted in organic solvents [20, 21], and the surface product was referred to as polymeric [21]. More recent procedures conduct these reactions in aqueous media [22-24], where polymerization seems more certain. Longer-wearing surfaces result [22]. Aqueous media were also used in recent silanizations of fiberglass [25] and silica gel [26] for trace metal scavenging studies.

Thus, prior uses of X_3SiR and X_2SiR_2 surface silanizations have not been concerned with avoiding surface polymer formation. Moreover, the experiments conducted and reported to characterize these silanized surfaces were not especially geared to determine the extent of monolayer and polymer formation. The extent of constraint of reaction (1) to monolayer coverage can be viewed as an unresolved question, and we regarded particular attention to this question as essential to our studies of systems such as (2).

2. EXPERIMENTAL

2.1 *Organosilane Surface Reactions*

The SnO_2 [4], TiO_2 [9], glassy carbon [3], and glass [27] surfaces were prepared for reaction as previously described. Careful attention was paid throughout to maintaining anhydrous conditions during both the organosilane reaction with the surface and the thorough washing of excess reagent from the

surface. The reaction procedures fall into the following general categories: Method A. Electrode specimens are reacted in 2-10% organosilane solutions in refluxing benzene or xylene under N_2 for a few hours up to overnight. Excess reagent is removed with a dry benzene wash. Method B. The specimen is reacted with neat organosilane in a sealed tube at 90°C for 12 hours, and subsequently washed with dry benzene. Method C. The specimen is reacted under a 1-5% organosilane solution in benzene at room temperature for 15 minutes, then washed with benzene. This experiment is ordinarily conducted in a glove box (Vacuum Atmospheres). Method D. The specimen is reacted in a 1% organosilane solution in benzene at 6°C under Ar for ~10 seconds and then washed with methanol.

The organosilane reagents employed are γ-aminopropyltriethoxysilane ($PrNH_2$ silane), 3-(2-aminoethylamino)propyltrimethoxysilane (en silane), and β-trichlorosilyl-2-ethylpyridine (Py silane).

SnO_2 Electrodes. Method A was employed for all organosilanes in our earlier surface modification work [4]. Method B has also been found to be satisfactory for SnO_2. However, we have found that these harsh reaction conditions are unnecessary as the SnO_2 surfaces in fact react very rapidly. Method C is currently used for the Py silane, and either C or D for the en and $PrNH_2$ silanes.

TiO_2 Electrodes. Method C is used for the Py and en silanes.

Glassy Carbon Electrodes. Method A was previously employed [3] and still is preferred for glassy carbon. The benzene solvent is dried by distillation from sodium and stored over molecular sieves. The reaction is conducted for 4 hours in 2-5% organosilane solutions. Use of the specially dried solvent appears to promote more stably bound surfaces. Method B has been observed [3] to be unsatisfactory for carbon.

Glass. Gold Seal microscope slide glass was silanized via Method B. Method A gave erratic results. (A suitable procedure is dependent upon the type of glass

as the milder Method C is satisfactory for the borosilicate Corning Code 7740 glass).

2.2 *ESCA*

We employ ESCA as a routine tool to detect surface modification reactions. The operating characteristics of our instrument (DuPont 650B electron spectrometer) have been reported [4]. Band intensities are reported here as peak areas, integrated using a planimeter and a linear baseline extrapolation under the peak wings. Because the electrode specimens are necessarily exposed during their synthesis to the laboratory atmosphere, a carbon C 1s contaminant peak is ubiquitous, but we find that its magnitude in a typical series of prepared specimens is fairly constant.

3. RESULTS AND DISCUSSION

3.1 *Sn $3d_{5/2}$ and Ti $2p_{3/2}$ ESCA Intensities on Chemically Modified SnO_2 and TiO_2*

Bonding of an organosilane layer to an electrode causes a diminution of the native photoelectron intensities of the electrode elements due to electron interactions with organosilane. The appropriate relation is [28]

$$I/I_{unreacted} = \exp(-d/\lambda) \qquad (4)$$

where d is the organosilane layer thickness and λ is the escape depth of the electrode element photoelectron through it. We previously determined [4] an average $I/I_{unreacted}$ = 0.38 for a collection of SnO_2 electrodes modified with en silane by Method A, which gives $d/\lambda = 0.96$. The band used was Sn $3d_{5/2}$ (photoelectron kinetic energy 766 e.v.), and estimating λ = 11 Å from a "universal" escape depth plot [29], d ≈ 11 Å was calculated for the organosilane layer.

Penn [30, 31] has since presented theory allowing calculation of λ values in free-electron-like materials. For photoelectrons of kinetic energy KE

$$\lambda_{KE} = KE/a[\ln(KE + b)] \qquad (5)$$

where a and b are calculable constants which depend most sensitively on the valence electron concentration (n_e) of the material and to a lesser extent on the scattering contributions of core electrons. The form of equation (5) applies to all materials but the accuracy of the calculations of a and b applied to non-free-electron-like materials is unassessed [31]. Application of Penn's theory to scattering of Sn $3d_{5/2}$ photoelectrons by a bonded en silane layer ($n_e = 2.5 \times 10^{23}$ cm^{-3}) gives $\lambda = 16.0$ Å. Using this revised λ value, $d \simeq 15$ Å for the earlier en silane data. Both values of d compare well with the model-estimated 10 Å thickness of a bonded monomolecular en silane layer.

We have also conducted new measurements of $I/I_{unreacted}$ for Sn $3d_{5/2}$ bands on SnO_2 electrodes modified with the en silane using Method D for reaction times ranging from 5 seconds to 6 minutes. In several experimental series using these very mild reaction conditions, the scatter in band intensities (~10%) was much less than in the previous data [4], and $I/I_{unreacted}$ averaged about 0.80 from which $d \simeq 4$ Å using $\lambda_{766} = 16$ Å. These very stable chemically modified electrode surfaces may be covered at sub-monolayer levels and clearly are free of extensive surface polymer formation. In a sputtering experiment with 1.5 Kev Ar^+ ions, the N 1s band of the en silane completely disappears in ~15 seconds.

Our experimental studies with chemically modified TiO_2 electrodes are less extensive than with SnO_2, but the available data follow the same pattern in that the Ti $2p_{3/2}$ band intensity is attenuated by the organosilane surface reaction. For TiO_2 surfaces modified with a variety of organosilanes (7 specimens) using Method C, $I/I_{unreacted} = 0.47$ with a scatter of ~50%. Differently obtained but equivalent data results from Py silane-modified electrodes in which the Ti $2p_{3/2}$ band is measured, the organosilane layer removed by Ar^+ sputtering (N 1s vanishes promptly, a small residual Si 2p band remains), and the Ti band remeasured. For these $I/I_{sputtered} = 0.44 \pm 0.05$. Application of equation (5) for Ti $2p_{3/2}$

photoelectrons scattered by Py silane yields λ_{793} = 17 Å, and using this and equation (4), d ≃ 14 Å is obtained for the thickness of the Py silane layer. This result can be compared with the estimated 11 Å length of a bonded monomolecular Py silane.

3.2 *Si 2p ESCA Intensities on Chemically Modified Glassy Carbon*

The electrode substrate approach of equation (4) is not useful for chemically modified carbon electrodes due to interference from the C 1s band of the organosilane and contaminant carbon. An alternate approach involves comparison of the intensity of an elemental component of the organosilane layer with that observed for an "infinitely thick" ($d >> \lambda$) organosilane, and use of the relation [28]

$$I/I_\infty = 1 - \exp(-d/\lambda) \qquad (6)$$

This comparison has been made using the Si 2p band (unresolved doublet) of the en silane. The "thin" specimens were prepared on glassy carbon using Method A. The data obtained have a substantial scatter associated with a Si background correction amounting to ∿40% of the total intensity. (The Si blank apparently originates in an embedded residue of SiC particles from the early stages of the electrode polishing procedure which is quite difficult to remove.) The "infinitely thick" specimens of en silane were prepared by thermal polymerization of a drop of en silane reagent on a carbon electrode. The thick layer is alternatively prepared, with similar Si 2p results, by a Method A reaction deliberately contaminated with water. (Although we cannot experimentally prove that these reference layers on carbon are "infinitely thick", in identical experiments on SnO_2 electrodes the Sn 3d bands become unobservable.) The I/I_∞ data thus acquired yield d/λ values ranging from 0.4 to 0.8. From Penn's relations, the escape depth of 1152 e.v. Si 2p photoelectrons in an en silane matrix is 22 Å, from which we

estimate using equation (6), $\underline{d}$ = 9-17 Å, in the same range as results on SnO_2 and TiO_2 electrodes. (Even ignoring the Si background correction yields a worst case thickness of 31 Å).

3.3 *Measurement of Si 2p Escape Depth in Organosilanes*

The accuracy of the preceding determinations of bonded organosilane layer thicknesses depends directly on the employed value for escape depth of photoelectrons through the organosilane. To obtain experimental evidence validating the escape depths employed, we have measured the relative intensities of the Si 2p band from prepared organosilane polymers and from elemental Si°. From relations in [28], the relative escape depth of Si 2p photoelectrons in organosilane and Si° is

$$\frac{\lambda_{silane}}{\lambda_{Si^\circ}} = \frac{I_{silane} D_{Si^\circ}}{I_{Si^\circ} D_{silane}} \tag{7}$$

where D represents the Si atom density in each material. The Si° samples were 1/4" disks of pure material cleaned in an HF bath for a few seconds before the ESCA measurement. The polymers were prepared from the $\underline{PrNH_2}$ silane, $\underline{en}$ silane, and a diethylenetriamine silane ($\underline{triam}$ silane) by either thermal polymerization or by refluxing a 20% solution of silane in benzene with 10% added water overnight. The polymeric products were finely ground before the Si 2p band was measured. Elemental analysis of Si, N, C and H indicates that the polymers formed are predominantly linear. A SiO_2 disk was also measured. Results are given in Table I.

The value for the escape depth of photoelectrons through pure Si° has been measured [32] and agrees with the Penn theory [30, 31] both in absolute value and in the manner of variation with KE. The calculated λ_{Si° value for 1152 e.v. photoelectrons is 22.3 Å. This value may be taken with the results of Table I to evaluate escape depths in SiO_2 and in the organosilane polymers. Thus we

obtained a value of 15.0 Å for λ_{SiO_2} which agrees reasonably well with the value of 18.7 Å calculated from the theory. The agreement of these values with a previous experimental value [32] for λ_{SiO_2}, 25 Å, is less good.

The results of Table I for $\lambda_{silane}/\lambda_{Si^o}$ show the escape depths of 1152 e.v. photoelectrons through the various organosilanes are within experimental error about the same as through elemental Si^o. Such similarity in escape depth between Si^o and the organosilanes is predicted by equation (5), from which we calculate λ_{Si^o} = 22.3 and $\lambda_{\underline{en}\ silane}$ = 22.0 Å. The similarity in the predicted values is largely traceable to the similar valence electron densities in the two materials, which is the anticipated controlling factor in the extent of scattering in a given matrix. This agreement of theory and experiment indicates that the thickness measurement made in the preceding section for <u>en</u> silane bonded to glassy carbon is not seriously in error due to our choice of a theoretically obtained λ. Additionally, since photoelectron scattering is a function of the organosilane layer and not of the substrate atom from which the photoelectron is derived (except for the dependency on KE of equation (5)) the escape depth values employed in the thickness estimates on SnO_2 and TiO_2 electrodes are also reasonable.

Previous escape depth measurements in organic films, summarized by Powell [33], have suggested that the range of photoelectrons in such materials can be quite large (50-100 Å). The large experimental values are not anticipated by either Penn's theory [30, 31] or in earlier calculations by Powell [33]. The organic film measurements have involved oriented molecular layers of long chain molecules prepared by Langmuir trough techniques. Powell has speculated that such films could be anisotropic in photoelectron scattering properties with scattering less for photoelectrons traveling parallel to the oriented molecules. If this is true, then the much smaller escape depths determined in Table I for randomly oriented bulk organosilane polymers are less surprising. This leads to

the question of whether thin organosilane films bonded to SnO_2, TiO_2, and carbon are also randomly oriented, or have an anisotropic molecular arrangement. We have no direct experimental data on this. We have indirect evidence that, in contact with solutions, considerable disorder can exist in chain orientation. The electrochemical reactivity of bonded structures such as (2) suggests that chain flexing can occur at high frequency. The finding [27] that optical properties of a bonded chromophore are similar to those of the analogous solution chromophore also suggests the absence of a highly ordered structure.

3.4 *Measurement of Optical Absorption of a Chromophore Bonded to Glass*

Using Method B, we have bonded the $\underline{Pr}NH_2$ silane to a glass surface. A series of surface synthetic reactions was then carried out to assemble the following chromophoric system on the glass surface

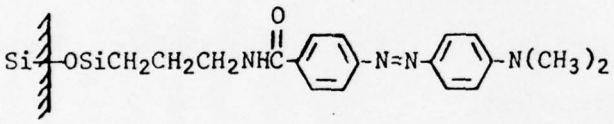

(8)

The electronic absorption spectra of this surface are quite similar to those of an analogous solution chromophore. Details of these experiments are described elsewhere [27]. Making the reasonable assumption that the molar extinction coefficients of solution and surface chromophores are the same, a molecular coverage of (8) could be calculated from the spectral data. From eight measurements $\Gamma = 1.12(\pm 0.14) \times 10^{-10}$ mole/cm^2, which corresponds to an average area per molecule of 148 Å^2. The area requirements of a model of the surface molecule, depending on the assumed orientation, range from 50-120 Å^2. The experimental coverage is thus compatible with the presumption that the prepared surface molecule is present as a monomolecular layer, or less.

In several experiments, highly colored glass surfaces were obtained, giving apparent coverages much larger than those above. It is thought that in these

experiments, adventitious water was present during the silanization step, allowing subsequent preparation of a multi-layer version of (8).

3.5 *Measurements Based on Electrochemical Reactions on Chemically Modified SnO_2 and TiO_2 Electrodes*

Electrochemically reactive groupings such as (2) prepared subsequent to the organosilane surface modification allow yet another approach to a coverage estimate. On a TiO_2 electrode surface, (2) yields an electrochemical reduction wave at the same potential (-1.35 volts vs. S.C.E., in acetonitrile solvent) as the solution methylpyridinium species [9]. Taking this plus ESCA N 1s observations as evidence that the electrochemical reduction products are the same in the two situations (e.g., $\underline{n} = 1$), the integrated charge from the electrochemical reduction wave for (2) has been used to estimate its surface population as 2.6×10^{-10} mole/cm^2. This translates to an average molecular area of 64 Å^2. The molecular area required in a model of (2) with ring parallel to the surface is ~42 Å^2.

Similar results are obtained [9] for (2) on a SnO_2 surface. The coverage estimate there is 0.8×10^{-10} mole/cm^2.

Several factors associated with the electrochemical estimate should be mentioned. First, the assumption that $\underline{n} = 1$ (one electron per molecule) may not be correct for the total surface population of (2). Secondly, in the preparation of (2), by methylation of a surface first reacted with the Py silane (Method C), the N 1s ESCA shows that roughly 50% of the originally present Py silane nitrogen does not methylate. Thus, actual coverage by Py silane could be double that indicated by the electrochemical result. We do not know the reason for the incomplete methylation. It could be explained by patches of impermeable polymer, but at this point equally plausible explanations include a surface electrostatic effect on the methylation and a base-inactivating surface side reaction we have identified for the amine organosilanes under certain conditions [34]. In any event, even an error of 2x in the coverage estimate of (2) is compatible with a

molecular monolayer or submonolayer picture. Lastly, we have not accounted for surface roughness in our calculations. This would lead to an overestimation of coverage, counterbalancing the factor discussed above.

A different set of electrochemical observations germane to the distinction between surface monolayer and polymers is based on electrochemical reactions of model solution species at organosilane-reacted SnO_2 [4] and carbon [3] electrodes. For example, on electrodes modified with $\underline{PrNH_2}$, en, or Py silanes, the electrochemical oxidation of $Fe(CN)_6^{4-}$ proceeds quite normally by cyclic voltammetric criteria. The implied accessibility of the electrode surface to a solution reactant would be unlikely on a surface coated with an organosilane polymer layer. In fact, SnO_2 and carbon electrodes modified with the highly reactive 3-chloropropylsilane reagent (Method A) gave $Fe(CN)_6^{4-}$ electrochemical data indicative of a restricted electrode area. We believe these latter electrodes, which were prepared in a period when our experiment procedures were less well developed, bore some surface polymer.

3.6 *Observations Based on Reaction Conditions*

In addition to the numerical coverage determinations discussed above, it is instructive to note certain experiences with varied reaction conditions. The most striking point is that on SnO_2, reaction Methods A-D have all been employed with the en silane at various times over a two year period with generally no more than a 2-3x variation in the absolute intensities of the Sn 3d, N 1s, and Si 2p bands observed on the modified electrodes. At least some of this variation is ascribable to variations in our electron spectrometer's sensitivity over periods of time. The reaction conditions employed vary from extremely mild (Method D) to quite forcing (Method B). It appears that the organosilane reaction, at least with the en silane, occurs extremely rapidly to cover a portion of the surface, and then more slowly, requiring more activating

conditions, to bind some further silane. Then, as long as moisture is absent, the reaction halts as the electrode's surface functional groups are exhausted.

On many occasions, some deliberate and other accidental, we have observed the effects of water and consequent polymer formation upon examining modified specimens by ESCA. The severe diminution of Sn 3d bands on SnO_2 electrodes has been the most reliable indication of this. For instance, in using the Py silane with Method A, a suspension of polymer particles sometimes forms (from adventitious water). As judged by Sn 3d ESCA, the SnO_2 electrode can sometimes be cleansed of adhering polymer by a thorough washing with benzene or methanol. On other occasions, Sn 3d intensity remains abnormally low and the electrode is discarded.

4. CONCLUSIONS

The different measurements presented above on coverage of SnO_2, TiO_2, glassy carbon, and glass surfaces by organosilane reagents under anhydrous reaction conditions are compatible with coverage predictions based on monolayer models of molecular length and area. The ESCA-based layer thickness (d) measurements fall within the extremes of 4-17 Å. Comparison of the ESCA thickness data with the mole/cm^2 coverage results of the electrochemical and optical experiments involves a mass density conversion factor. If the density of the molecular layers (2) and (8) is assumed to be unity, then d values of 4.2 Å and 3.8 Å are calculated for (2) on TiO_2 and (8) on glass, respectively. Given the diversity of the methods employed to measure coverage, the agreement between these values and the ESCA data is gratifying. Collectively, the coverage values demonstrate that the organosilane surface modification process can be largely constrained to a monomolecular layer-bonding reaction. Our data on coverage, however, are not sufficiently precise to confirm an "exact" monolayer, or to rule out the presence of some surface polymer. An average coverage of 1.5 molecular layer could be

accommodated within some of the data. A general coating of the electrode surfaces with polymer multilayers can on the other hand be ruled out. This statement only applies to reactions conducted under anhydrous conditions; our experience is that surface polymers otherwise form quite readily.

A consideration of the population of surface hydroxyl groupings available for reaction (1) on the various materials adds little to the above picture. Kirkov [35] estimates 2.23×10^{15} Sn-O sites/cm^2 on (cassiterite) SnO_2. If these are fully hydroxylated and reaction (1) forms three SnOSi linkages as shown (both being assumptions), the maximum conceivable monolayer coverage by silane would be 1.2×10^{-4} mole/cm^2. This "$\Gamma_{saturation}$" exceeds all of the experimentally measured coverages, which simply means there is no conflict between this analysis of the substrate reactivity and our view of the monolayer coverages achieved in the organosilane reaction.

ACKNOWLEDGEMENT

This research was facilitated by National Science Foundation grants MPS73-08758 and MPS75-07863 and by the U.N.C. Materials Research Center under Defense Advanced Research Projects Agency grant DAHC-15-73-G-9.

Table I

Relative Escape Depths for Si 2p Photoelectrons[a]

	Si°	SiO_2	$PrNH_2$ silane[d]	en silane[d]	triam silane[d]
D^b, g/cm^3	2.42	0.76	0.23	0.18	0.14
$I_{Si}{}^c$	2.70	0.57	0.30	0.26	0.16
$\lambda/\lambda_{Si°}$	1.00	0.67[e]	1.2[e]	1.3[e]	1.0[e]

a. 1152 e.v. kinetic energy.

b. Calculated using 2.42 and 1.1 for Si° and silane polymer densities, and analyzed % Si (Galbraith) in the silane polymers.

c. Arbitrary units of Si $2p_{1/2,3/2}$ band area.

d. In polymerized form.

e. Estimated uncertainty ±20%

REFERENCES

1. B. F. Watkins, J. R. Behling, E. Kariv, and L. L. Miller, J. Amer. Chem. Soc., 97, 3549 (1975).

2. L. L. Miller, 149th Electrochemical Society Meeting, Washington, D.C., May, 1976, Abstract 304.

3. C. M. Elliott and R. W. Murray, Anal. Chem., 48, 1247 (1976).

4. P. R. Moses, L. Wier, and R. W. Murray, Anal. Chem., 47, 1882 (1975).

5. P. R. Moses, C. M. Elliott, L. Wier, and R. W. Murray, First Chemical Congress of the North American Continent, Mexico City, December 1975.

6. N. R. Armstrong, M. E. Henne, T. Kuwana, and G. Royer, Ibid.

7. N. R. Armstrong, A. W. C. Lin, M. Fujihira, and T. Kuwana, Anal. Chem., 48, 741 (1976).

8. D. F. Untereker, R. W. Murray, P. R. Moses, L. M. Wier, and C. M. Elliott, 149th Electrochemical Society Meeting, Washington, D.C., May 1976, Abstract 349.

9. P. R. Moses and R. W. Murray, submitted for publication.

10. H. F. Walton, Anal. Chem., 48, 52R (1976).

11. E. Grushka, Ed., "Bonded Stationary Phases in Chromatography", Ann Arbor Science Pub., Ann Arbor, Michigan, 1974.

12. D. C. Locke, J. Chromatogr. Sci., 11, 120 (1973).

13. W. A. Aue and C. R. Hastings, J. Chromatogr., 42, 319 (1969).

14. C. R. Hastings, W. A. Aue, and J. M. Augl, Ibid., 53, 487 (1970).

15. C. R. Hastings, W. A. Aue and F. E. Larsen, Ibid., 60, 329 (1971).

16. J. J. Kirkland and J. J. DeStafano, J. Chromatogr. Sci., 8, 309 (1970).

17. J. J. Kirkland, Ibid., 9, 206 (1971).

18. J. J. DeStafano and J. J. Kirkland, Ibid., 12, 337 (1974).

19. R. E. Majors and M. J. Hopper, Ibid., 12, 767 (1974).

20. H. H. Weetall, Science, 160, 615 (1969).

21. H. H. Weetall and L. S. Hersh, Biochim. Biophys. Acta, 206, 54 (1970).

22. H. H. Weetall and N. B. Havewala in "Enzyme Engineering", Vol. 3, L. B. Wingard, Ed., Wiley, New York, 1972, p. 241.

23. N. B. Havewala and W. H. Pitcher, in "Enzyme Engineering", Vol. 2, E. K. Pye and L. B. Wingard, Eds., Plenum, New York, 1974, p. 315.

24. H. H. Weetall, Separation and Purification Methods, 2, 199 (1973).

25. D. M. Hercules, L. E. Cox, S. Onisick, G. D. Nichols, and J. C. Carver, Anal. Chem., 45, 1973 (1973).

26. D. E. Leyden and G. H. Luttrell, Ibid., 47, 1612 (1975).

27. L. T. Mimms, M. A. McKnight, and R. W. Murray, submitted for publication.

28. T. A. Carlson and G. E. McGuire, J. Electron Spectrosc., 1, 161 (1972/73).

29. P. W. Palmberg, Anal. Chem., 45, 549A (1973).

30. D. R. Penn, J. Vac. Sci. Technol., 13, 221 (1976).

31. D. R. Penn, private communication.

32. R. Flitsch and S. I Raider, J. Vac. Sci. Technol., 12, 305 (1975).

33. C. F. Powell, Surf. Sci., 44, 29 (1974).

34. P. R. Moses, J. Lennox, L. Wier, and R. W. Murray, unpublished results, 1975.

35. P. Kirkov, Electrochim. Acta, 17, 519 (1972).

SUPERIONIC CONDUCTORS (SOLID ELECTROLYTES): THEORETICAL STUDY

Sang-il Choi

Final Technical Report

1 June 1973 - 30 September 1976

Personnel:

J. C. Wang, Research Associate; M. Ghaffari, Research Assistant, received Ph.D., August 1975; W. M. Lee, Research Assistant, received Ph.D., September 1976; T. Takouchi, Research Assistant, received Ph.D., August 1976.

The support provided by DARPA enabled the principal investigator to initiate a new research program: THEORETICAL STUDY OF SUPERIONIC CONDUCTORS.

Our first objective was to explain observable properties (i.e. electrical conductivity, spatial distribution of carrier ions, etc.) of ion-substituted β-alumina. The variation of the potential energy of the crystal as a function of positions of a member of mobile ions was successfully used to explain ionic conductivities, mobile ion distributions and to correctly predict some vibrational frequencies observed later in other laboratories. Our theoretical success proved that the conduction mechanism in β-alumina is interstitialcy-like.

An anomally (i.e. deviation from our theory) was found for mobile ion distribution in silver β-alumina. In order to understand the anomally a quantum-mechanical calculation for electronic structure at an anti-Beevers-Ross site has been done.

Due to the existence of a large concentration of mobile ions, properties of ions adsorbed on the surface of a superionic conductor are expected to be different from those on normal ionic crystals. This was experimentally confirmed in another laboratory. As a first step in understanding the ion adsorption we have carried out quantum mechanical calculations of electronic structure of a sodium atom and a sodium ion on a site of the surface perpendicular to the ion conduction plane of β-alumina.

Since β-alumina has a very special crystal structure, a theory developed for it may not be directly applied to other superionic conductors. For this reason $RbAg_4I_5$ has been chosen as another system to be studied. Potential energy curves for a silver ion in $RbAg_4I_5$ have been calculated for various different paths. Since vibrational frequencies of a silver ion at different sites are remarkably different from each other, the influence of such differences of frequencies on the order-disorder transition theory applied to the distribution of silver ions in $RbAg_4I_5$ has been studied.

Raman spectra experimentalists identified their observed lines with the vibrational frequencies of mobile ions at the Beevers-Ross site of β-alumina. Such identification was based on our previously calculated vibrational frequencies. Since it is known that a large fraction of mobile ions occupy

mid-oxygen sites in pairs, we have decided to calculate vibrational frequencies of a super lattice with mid-oxygen site pairs regularly arranged.

Brief summaries of the specific research projects follow:

1. On the Ionic Conduction in β-Alumina: Potential Energy Curves and Conduction Mechanism [J. Chem. Phys. 63, 772 (1975); J. C. Wang, M. Ghaffair, S. Choi]. This is our first report on superionic conductors. The results of our calculation reported in this article has been extensively used by other people to explain various experimental data.

2. Vibration Effect in the Order-Disorder Transition Theory of $RbAg_4I_5$ [To be published in the Proc. of Conf. on Superionic Conductors, Plenum Publishing Co.; S. Choi and W. M. Lee]. In this article it is shown that considerable error in silver ion distribution could result if the vibrational partition function is not considered explicitly. This paper was presented at the International Conference on Superionic Conductors at Schenectady, New York in May 1976. Choi attended the conference as a theory panel member.

3. Electronic Structure at the Anti-Beevers-Ross Site in β-Alumina [Ph.D. Thesis, August 1976; T. Takeuchi]. A self-consistent multiple scattering method is applied to obtain the electronic wave functions of ion clusters representing the anti-Beevers-Ross site in sodium β-alumina. Extra stabilization of Ag^+ relative to Na^+ is found. This may be interpreted as the covalency effect.

4. Potential Energy Curves in $RbAg_4I_5$ [Ph.D. Thesis, August 1976; T. Takeuchi]. Potential energy of a silver ion along various paths in a $RbAg_4I_5$ crystal in the absence of all other silver ions have been calculated. The smallest barrier height agrees with the measured activation energy. Vibrational frequencies along the paths are in close agreement with measured Raman spectra lines.

5. Surface Adsorption Complex of β-Alumina [Ph.D. Thesis, September 1976; W. M. Lee]. Na^+ or Na adsorbed at a C_{3V} symmetry site was approximated by $NaAlO_3^=$ or $NaAlO_3^{=}$ cluster. The self-consistent multiple scattering Xα-method and the extended Hückel method both are applied. It is found that a neutral sodium ion is unstable with respect to Na^+ ion, i.e. Na atom is expected to become Na^+ on adsorption. It is also found that the electronic charge distribution of $O^=$ ions are not spherically symmetric.

Future Work:

The method we apply to study superionic conductors (solid electrolytes) has been successful so far and is unique at this time. Instead of doing a formal theory we carry out numerical computations to relate ion properties and crystal structures to the observable properties of solid electrolytes. This method could help find new solid electrolytes as well as interpret various experimental data. In future we plan to study (i) the dynamic coupling of mobile ions to the frame work ions (usually large negative ions) in various solid electrolytes, (ii) the dynamics of mobile ions on free surfaces and grain boundaries, and (iii) a general theory of ionic transport in a crystal undergoing the order-disorder transition in the presence of impurities which have strong interactions with conduction electrons.

On the ionic conduction in β-alumina: Potential energy curves and conduction mechanism*

J. C. Wang, M. Gaffari, and Sang-il Choi

Department of Physics and Astronomy, University of North Carolina, Chapel Hill, North Carolina 27514
(Received 2 April 1975)

Potential energy curves for various carrier ions in β-alumina have been calculated. All ions except the carrier ions (Li^+, Na^+, Ag^+, K^+, Rb^+, Cs^+) were assumed fixed in their equilibrium positions. These ionic positions were taken from Roth's work. In our calculation the motion of carrier ions is restricted on lines of the two dimensional hexagonal network. We show that the site energy difference between the anti-Beevers–Ross site and the Beevers–Ross site is approximately 2 eV in stoichiometric crystals. In nonstoichiometric crystals the extra carrier ions may be paired to form interstitialcy pairs. The potential energy barriers for the in-phase motion of the interstitialcy pairs are found to be comparable to the experimental activation energies. Attempt frequencies have been calculated, and a simple random walk model is used for the electrical conductivities.

I. INTRODUCTION

Solids with very high electrical conductivity are of great current interest because of their applicability as solid electrolytes. Among these solids, β-aluminas are the most widely studied. The main features of β-alumina were determined by Bragg *et al.*[1] and Beevers *et al.*,[2] who arrived at the ideal formula $Na_2O \cdot 11Al_2O_3$ and space group $P6_3/mmc$. A refinement of the structure of sodium β-alumina has been made by Peters *et al.*[3] The crystals used contained 29% excess soda relative to the ideal formula. The crystal structure of silver β-alumina has been determined by Roth[4] from the x-ray diffraction data. The structures of sodium and silver β-alumina are essentially identical. A major difference is in the position of the monovalent carrier ions as described below. According to Roth, the silver β-alumina crystal is a hexagonal layer structure with space group $P6_3/mmc$. The unit cell dimensions are given by $a = 5.595$ Å and $c = 22.488$ Å. The change of lattice constants of β-alumina produced by the ion exchange of Na^+ in β-alumina with other ions (Li^+, K^+, Ag^+, Rb^+, etc.) has been reported. There is very little change in the a axis. The c axis changes a little and expands (or shrinks) if a larger (or smaller) ion substitutes for Na^+.[5]

In each unit cell perpendicular to the c axis, there are two mirror planes containing loosely packed monovalent positive ions (such as Na^+) and O^{--} ions. These planes are separated by a spinel-like block formed by four layers of oxygen ions in cubic closest packing with aluminum ions occupying octahedral and tetrahedral interstices. Actual β-aluminas are nonstoichiometric and contain monovalent metal ions 15%–30% in excess of the stoichiometric formula. The electrical neutrality of the system is believed to be maintained by either aluminum vacancies or extra oxygen ions in the mirror planes.

Peters *et al.*[3] showed that Na^+ ions are distributed on the Beevers–Ross site and the midpoint between the B–R site and the anti B–R site. In silver β-alumina, Ag^+ ions are found to occupy the anti-Beevers–Ross site as well as the Beevers–Ross site and the midpoint (see Fig. 1).

Electrical conduction is ionic and charge carriers are monovalent metal ions. Because of the densely packed spinel-like blocks separating the conduction planes, the ionic conduction is purely two dimensional. Activation energies are approximately 0.18 eV for Ag^+ and 0.17 eV for Na^+ β-alumina. The high ionic conductivity with unusually low activation energy and unusually small frequency factor for the cation migration has attracted the interest of theorists in recent years. Kikuchi and Sato[6] applied the path probability method, and Rice and Roth[7] tried a theory similar to that of an electronic semiconductor. Whittingham and Huggins suggested the interstitialcy mechanism. It is the main objective of this paper to study an ionic conduction mechanism and support it with concrete numerical computations. Our procedure is as follows.

All ions except the monovalent metallic ions (M^+) are assumed to be fixed in their equilibrium positions reported for silver β-alumina by Roth.[4] X-ray diffraction studies of sodium and silver β-alumina suggest that the M^+ ions in the mirror plane are constrained to move along the straight lines joining the neighboring Beevers–Ross site and anti-Beevers–Ross site. These lines, then, form a hexagonal network, as shown in Fig. 2. We first assume the stoichiometric structure $M_2O \cdot 11Al_2O_3$ with M^+ ions completely occupying the Beevers–Ross sites. In this structure, the variation of the total crystal potential energy is calculated as a function of the position of one M^+ as it is moved along the straight line toward the nearest anti-Beevers–Ross site while all other ions are fixed. Such calculations show that the total potential energy increases by approximately 2 eV for all β-aluminas. This number is an order of magnitude greater than the reported activation energies of electrical conduction. Next we add one M^+ ion to an anti-Beevers–Ross site. As an M^+ ion at the B–R site nearest to the extra M^+ ion is moved along the straight line toward a nearest vacant anti-B–R site, the variation of the total crystal potential energy is calculated. In this calculation a number of other M^+ ions are allowed to adjust their positions such that the total potential energy is minimized. We find that the extra M^+ ion is not stable at the anti-Beevers–Ross site. The minimum potential energy corresponds to the pairing of the extra M^+ ion with another M^+ ion. The potential barriers for the in-phase motion of the pair are found

 Copyright © 1975 American Institute of Physics

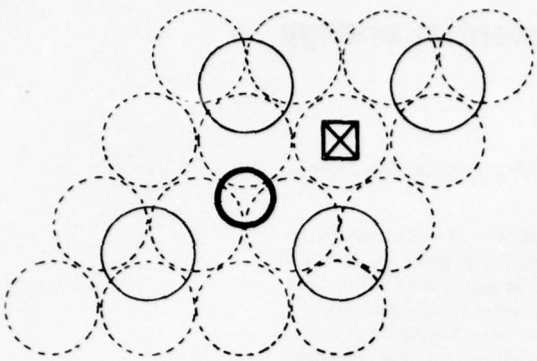

FIG. 1. Ionic arrangement in loosely packed layer of β-alumina. The small circle denotes the Beevers–Ross site, while the anti-Beevers–Ross site is where the crossed square is. The large circles with solid lines are oxygen ions in the mirror plane, and the circles with broken lines are the oxygen ions adjacent to the plane.

to be close to the conduction activation energies reported in the literature.

In Sec. II, we shall discuss the interionic potential energies considered in this work and outline the procedure used in our calculation. We shall present the results in Sec. III and show that the interstitialcy mechanism is adequate to explain observed data. Section IV will be devoted to examining the electrical conductivity and to discussion of some other consequences of the model. In Sec. V we then conclude the paper by discussing possible future developments based on the present results.

II. INTERIONIC POTENTIAL ENERGY AND CALCULATION PROCEDURE

In our model calculation, the following interionic potential energies are considered:

(a) the long range Coulomb potential energy $z_i z_j e^2/r_{ij}$, where $z_i e$ and $z_j e$ are the electric charges of ions i and j, respectively, and r_{ij} is the distance between them;

(b) the short range Born–Mayer[8] repulsive potential energy $b\epsilon_{ij}\exp[(r_i + r_j - r_{ij})/\rho]$ between ions i and j, where $b = 3.38\times 10^{-13}$ erg $= 0.211$ eV, $\rho = 1/3$ Å, and r_i and r_j are ionic radii. The parameter ϵ_{ij} is determined by[9]

$$\epsilon_{ij} = 1 + \frac{Z_i}{N_i} + \frac{Z_j}{N_j}, \tag{1}$$

where N_i is the number of electrons in the last closed shell of ion i. N_i is 2 for Li^+, 18 for Ag^+, and 8 for Na^+, K^+, Rb^+, Cs^+, O^{--}, and Al^{3+}.

(c) polarization energy $-\frac{1}{2}\alpha_i \mathbf{E}_i \cdot \mathbf{E}_i$ associated with ion i, where α_i is the ionic polarizability of the ion, and $\mathbf{E}_i$ is the resultant electric field on it. The interaction energy due to this term is calculated in a self-consistent manner.

To outline the calculation procedure, we divide the ions in the system into two groups: those allowed to move and those not allowed to move. For example, six M^+ ions are allowed to move while all other ions are fixed. The calculations are made according to the following steps:

(a) The long range Coulomb potentials for each mobile ion along its allowed path, and for each fixed ion near its fixed position due to all other ions at their ideal-structure (stoichiometric structure) positions are calculated by the Ewald method.[10] The electric fields at these points are obtained by differentiating the potentials.

(b) The initial dipole moment at each fixed ion is obtained by multiplying the polarizability of the ion with the electric field acting on it. The induced dipole moments of oxygen ions close to the mirror plane are found to be very large. For example, the oxygen ion right above an anti-Beevers–Ross site has the induced dipole moment of 1.08 eÅ (5.18 D) pointing to the mirror plane. It is necessary to include the electric fields produced by these large dipole moments at the points considered. A self-consistent calculation has been done; the resulting dipole moments are smaller than the initial values. For example, the above mentioned oxygen ion has a dipole moment of 4.10 D pointing toward the mirror plane. The electric fields produced by these final dipole moments on the allowed paths of the mobile ions are then calculated and added to those calculated in step (a).

(c) The Born–Mayer repulsive potentials for each mobile ion due to all other ions at their ideal structure positions are calculated along its allowed path.

(d) To find the total potential energy of the system at a given ion configuration, we calculate the changes of the Coulomb and repulsive potentials and the electric field at every point considered due to the deviations of the mobile ions from their ideal structure positions. The resultant field and potentials at each ion in the configuration are obtained by adding the changes to the values calculated in steps (a), (b), and (c). The total potential energy of the configuration is given by

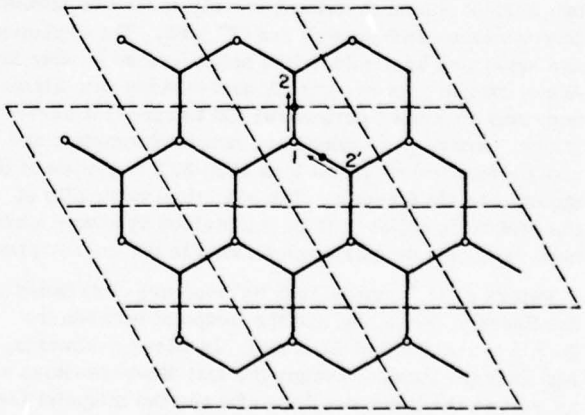

FIG. 2. The hexagonal network is made of lines joining Beevers–Ross sites and anti-Beevers–Ross sites. Vertices with open circles are Beevers–Ross sites.

TABLE I. Sources[a] and values for the ionic radii and electronic polarizabilities.

Ions	Radii (Å)	Reference	Polarizabilities (Å^3)	Reference
Li^+	0.816	T–F	0.029	TKS
Na^+	1.170	T–F	0.255	TKS
K^+	1.463	T–F	1.201	TKS
Rb^+	1.587	T–F	1.797	TKS
Cs^{+1}	1.720	T–F	3.137	TKS
Ag^+	1.26	P	1.888	PK
O^{--}	1.40	P	1.34	TKS
Al^{+++}	0.50	P	0.05	TKS

[a]T–F, Ref. 8; P, Ref. 9; TKS, Ref. 12; PK, Ref. 13.

$$E = -\frac{1}{2}\sum_i \alpha_i \mathbf{E}_i \cdot \mathbf{E}_i + \sum_i (V_{\text{rep}}^{(i)} + V_{\text{Coul}}^{(i)}) + \sum_i \sum_{j>i} [z_i z_j e^2/r_{ij} + b\epsilon_{ij} \exp(r_i + r_j - r_{ij})/\rho], \quad (2)$$

where $V_{\text{rep}}^{(i)}$ and $V_{\text{Coul}}^{(i)}$ are the repulsive and Coulomb potential energy of mobile ion i due to all fixed ions. The summation of the first term is over the mobile ions and a number of other ions near them. In most of our calculations, this number is about 200. The summations of the second and third terms are over the mobile ions only. As mentioned in Sec. I, we allow a M^+ located nearest to the added extra M^+ ion to move along the given path by successive small steps. After each step, we allow the nearby M^+ ions to adjust their positions such that the total potential energy calculated by Eq. (2) is minimum. If we plot this minimum potential energy as a function of the position of the M^+ ion, we find a minimum. The minimum corresponds to an equilibrium complex of two M^+ ions. For the extra ion to move out of one equilibrium complex to form another one at the next site, the system passes through a maximum of the potential energy. The difference between the maximum and minimum gives the potential energy barrier for the extra ion to jump from one complex to form another.

We shall now mention briefly the sources of the values used in our calculation. We assume that all β-aluminas have the same structure, with $a = 5.595$ Å and $c = 22.488$ Å, and with ions in the unit cell at the positions determined by Roth for Ag^+ β-alumina.[4]

To choose the radii and polarizabilities of the ions considered is not easy because the values variously reported in the literature do not agree. For example, the radius of Ag^+ is reported to range from 0.67 Å to 1.44 Å[9–12] and the polarizability of O^{--} ranges from 0.5 Å^3 to 3.88 Å^3.[12] This is because the radius and polarizability of an ion depend on the ion's environment and on the way they are determined.

For the ionic radii of Li^+, Na^+, K^+, Rb^+, and Cs^+, we use the values determined by Fumi and Tosi[8] because we also use their value of the parameter b used in the repulsive potential. For the radii of ions not determined by Fumi and Tosi, we use the values determined by Pauling.[9] Shannon and Prewitt[11] have made a detailed analysis of ionic radii in oxides and fluorides. They compiled a table listing several sets of values. The ionic radii chosen by us as above are consistent with one set of values given by them.

Electronic polarizabilities for all ions except Ag^+ are taken from the paper by Tessman, Kahn, and Shockley.[12] The values for O^{--} and Al^{+++} are for Al_2O_3. For Ag^+, we use the value determined by Pirenne and Karthenser.[13] A summary of the sources together with the values for the ionic radii and electronic polarizabilities is given in Table I.

III. CALCULATION OF POTENTIAL CURVES

In order to study the movements of M^+ ions along their allowed paths, we divide the line joining the neighboring Beevers–Ross site and anti-Beevers–Ross site in Fig. 1 into 20 segments with each segment of length $\Delta d = 0.1615$ Å. If, in the ideal stoichiometric structure, we move the ion on the B–R site along the path 1–2 in Fig. 3, the Coulomb potential it sees along this diagonal line is shown in Fig. 4. In the figure, the positions of the sites 1 and 2 are denoted by 0 and 20, respectively. Notice that the Coulomb potential difference between the two sites is about 2.7 eV.

Figure 4 shows the repulsive potential energies of Li^+, Na^+, K^+, Rb^+, Cs^+, and Ag^+ ions along the same path. For the smaller ions, the repulsive potentials between the B–R and anti-B–R site are essentially flat, while for the larger ions the repulsive potential energies show one minimum near the B–R site and another near the midpoint, between the B–R and anti-B–R sites.

Figure 4 also shows the polarization potential energies of Li^+ and Cs^+ ions along the same path. The results for other kinds of M^+ ions are very close to these two curves and are not shown in the figure.

Figure 5 shows the total potential energy curves of the various kinds of M^+ ions along the path 1–2. The potential energy differences between sites 1 and 2 are about 2.1–3.3 eV. This suggests that in the ideal stoichiometric structure, M^+ ions sit in deep potential wells and the ionic conduction due to these ions is very difficult in the structure.

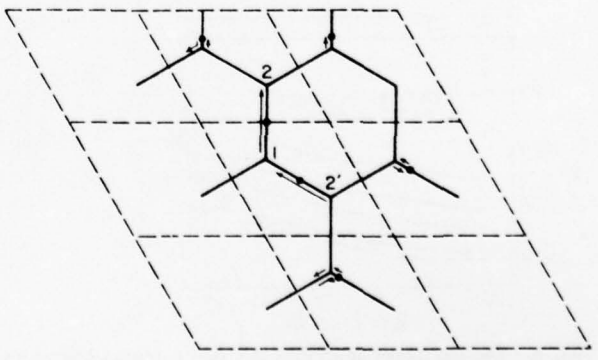

FIG. 3. The figure describes the change of configuration of metal carrier ions in response to the change of positions of the ion which occupies the site 1 (a Beevers–Ross site) in the ideal structure.

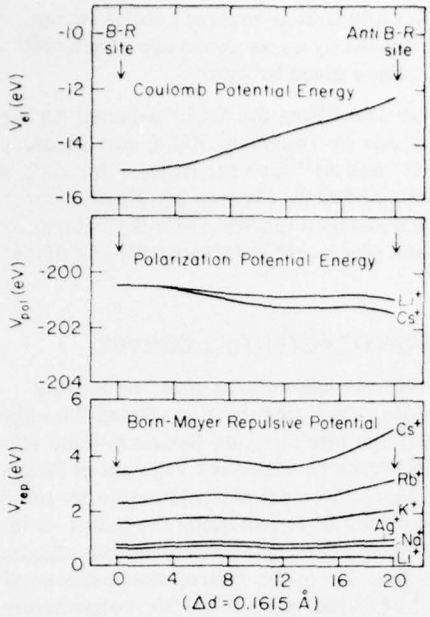

FIG. 4. Three different potential energies as functions of the position of the M^+ ion which is moved from site 1 and site 2. 0 and 20 of the abscissa denote site 1 and site 2, respectively.

Let us now consider the vacancy mechanism. Suppose in the "ideal" structure, we take an M^+ ion away from a B–R site. How difficult is it for an M^+ ion on a neighboring B–R site to move into this vacant site? Figure 5 shows the total potential energy curves of the various kinds of M^+ ions for this case. From the figure,

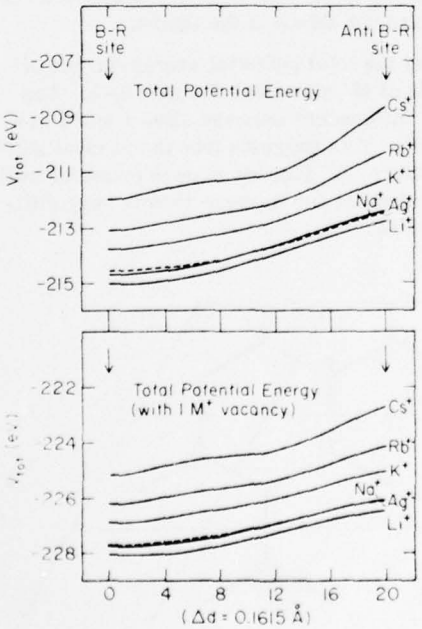

FIG. 5. The top figure describes the total potential energy variation in the stoichiometric structure. The lower figure is for the structure with a vacant Beevers–Ross site nearest in the direction of the motion of M^+ ion. The potential energy change is the potential energy barrier height for the vacancy motion.

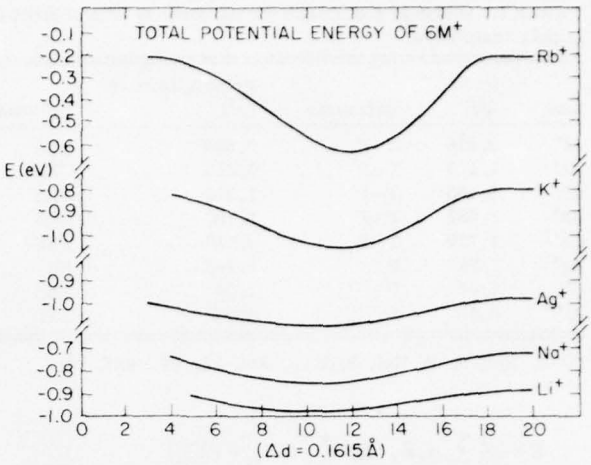

FIG. 6. Potential energy curve for six M^+ ion correlated motion. The difference between the maximum and the minimum is the potential energy barrier height for the interstitialcy-like motion.

we see that for the M^+ ions to move into the vacant B–R site, the potential barrier is of the magnitude of 1.6–2.4 eV.

Whittingham and Huggins[14] studied the transport properties of Na^+ and Ag^+ β-alumina. From the tracer diffusion coefficient D_t and the diffusion coefficient D_σ from the electrical conductivity, they calculated the ratio D_σ/D_t and found that its value is about 1.64. This suggests that the transport of M^+ ions takes place by an *interstitialcy mechanism, in which an M^+ ion residing in* an interstitial site moves into a regular M^+ lattice site, displacing the ion there to another neighboring interstitial site. We shall now show that a mechanism similar to this gives activation energies of the same order of magnitude as the experimental results.[5]

Suppose in the ideal structure we put an extra Na^+ ion on an anti-B–R site and allow only this ion and a nearby B–R site Na^+ ion to adjust their positions. As shown in Fig. 2, while the ion 1 is moved from the B–R site to site 2 (an anti-B–R site), the extra ion will move from site 2′ toward site 1. During the whole process, the system has the minimum total potential energy when they occupy the two dotted positions. This means that when an extra Na^+ ion is added to the ideal structure, it tends to move toward a B–R site and share the site with the Na^+ ion there to form a "complex" as shown by the two dotted positions in Fig. 2. For one of these two ions to move out of the complex, the system must first reach a maximum potential energy configuration with ions near site 2 and site 1, respectively. The difference between the maximum and minimum total potential energies is the potential barrier for this interstitialcy-like mechanism and is about 0.26 eV for Na^+ β-alumina in this calculation. The experimental activation energy is 0.17 eV.

To improve the calculation, we let six Na^+ ions adjust their positions to minimize the total potential energy as shown in Fig. 3. The potential energy curves are given in Fig. 6. While ion 1 is moved from site 1 to site 2, the other five ions will move as shown by the

TABLE II. Calculated potential energy barriers and experimental activation energies of β-alumina crystals in eV. $E_a(2)$ and $E_a(6)$ are calculated with 2 and 6 M^+ ions, respectively, allowed to adjust their positions.

Material	$E_a(2)$	$E_a(6)$	E_a(exptl)
Li^+-beta	0.26	0.10	0.378
Na^+-beta	0.26	0.14	0.165
Ag^+-beta	0.18	0.12	0.176
K^+-beta	0.35	0.26	0.233
Rb^+-beta	0.56	0.43	0.311
Cs^+-beta	1.19	0.84	...

arrows. During the whole process, the lowest total potential energy configuration is the one indicated by dots in Fig. 3. The calculated potential energy barrier for this case is 0.14 eV. Similar calculations are made for other β-aluminas and the results are summarized in Table II. In the table, $E(2)$ and $E(6)$ are the calculated potential energy barriers for 2 and 6 M^+ ion correlated motion, respectively. As can be seen from Table II, the calculated $E(6)$ for Li^+ is too low compared to the experimental value. This is because we assumed Li^+ ions are constrained on paths 1–2 in the mirror plane. Owing to its small size, Li^+ ions may not have a potential minima on the plane. Our calculation indeed shows that the B–R site is not the potential minimum if motion perpendicular to the plane is allowed. For the stoichiometric lithium β-alumina, Li^+ ions are not stable at the B–R site and should occupy sites away from the middle of the plane and closer to the spinel-like blocks.

To study the effect of ionic properties on the potential energy barriers, we considered the dependence on the polarizability of Ag^+ ion, the radius of Na^+ ion, and the polarizability of oxygen ion. The potential energy barrier heights increase with the Na^+ ion radius and decrease with the increasing Ag^+ ion polarizability. On the other hand, the barrier heights increase with oxygen ion polarizability. The results of our calculation are summarized in Fig. 7.

Our findings then suggest that high polarizability of the charge carrier ion is beneficial in lowering the potential energy barrier heights while a large polarizability of fixed oxygen ions is detrimental.

IV. SOME CONSEQUENCES OF THIS WORK

From our calculation discussed in Sec. III, we expect the following distribution of M^+ ions in β-alumina at low temperatures if excess M^+ concentration is small. If the density of M^+ ions is n in excess of the stoichiometric (ideal) density N, $N-n$ ions are expected to occupy the Beevers–Ross site while $2n$ ions occupy the sites midway between the Beevers–Ross site and the anti-Beevers–Ross site, i.e., sites between two loosely packed oxygen ions in the plane.

Peters *et al.*[3] reported that their crystal contained 29% excess sodium, and approximately 0.75 Na^+ were found near each B–R site while 0.52 Na^+ were found near the midpoint between the B–R site and the anti-B–R site. Our model predicts 0.71 and 0.58, respectively. For silver β-alumina with 27% excess Ag^+, Roth[4] reported 0.67 Ag^+ near each B–R site, 0.17 Ag^+ near the midpoint, and 0.43 Ag^+ near each anti-B–R site, while our model suggests 0.73 Ag^+ near each B–R site, 0.54 Ag^+ near each midpoint, and none at anti-B–R sites. This difficulty may be traced to the covalent bonding between Ag and oxygen at the anti-B–R site.

The preferred mode of M^+ ion transport is similar to the interstitialcy mechanism invoked for diffusion processes in silver halides.[14,15] In the stoichiometric structure, M^+ ion diffusion is expected to be extremely slow owing to large potential energy barriers. Even in a structure slightly deficient in M^+, M^+ ion diffusion is expected to be accompanied by high activation energies due to the high potential energy barriers for vacancy transport. Only when there are excess M^+ ions is the interstitialcy mechanism energetically favored. The potential barrier heights of the interstitialcy-like motion are an order of magnitude smaller than those of the vacancy mechanism mentioned above and become comparable to the reported experimental activation energies. At low density of excess M^+ ions, the interaction between the interstitialcy pairs may be neglected. Then the potential energy barriers we have calculated must be identified with the activation energies of diffusion or of electrical conductivity.

Our model, then, predicts that the electrical conductivity of a β-alumina crystal is proportional to the concentration of the excess M^+, n, at low values of n. As the concentration of the excess M^+ is increased, we have to consider two factors: the probability of finding a vacant site adjacent to the interstitialcy pair, and the interaction between pairs. The effect of the first factor can be made quantitative by the formula

$$\sigma = An(N-n), \tag{3}$$

where σ, n, N are the electrical conductivity, the excess M^+ ion concentration, and the number of Beevers–Ross sites per unit volume. A is a constant. Kennedy

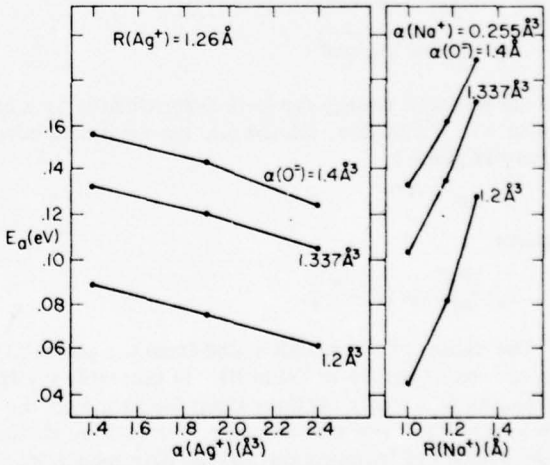

FIG. 7. Effect of polarizability of oxygen ions, polarizability of the M^+ ion, and the radius of the M^+ ion is demonstrated. The ordinate is the potential energy barrier height for the interstitialcy-like motion.

TABLE III. Calculated vibrational frequency along the trajectory.

Ion	ν_{pair} (cm^{-1}) (ν_0)	ν_{single} (cm^{-1})
Na^+	39.0	89.7
Ag^+	16.1	41.9
K^+	52.0	97.7
Rb^+	50.4	78.2

and Sammels[16] reported their findings for the relationship between the electrical conductivity and the sodium ion content for sintered sodium β-alumina containing MgO. For three different concentrations of MgO which correspond to optimum excess Na^+ concentration of $(n/N) = 0.29$, 0.41, and 0.81, they found the electrical conductivities of 3.5×10^{-3}, 8.0×10^{-3}, and 4.4×10^{-3} $\Omega^{-1}\cdot cm^{-1}$, respectively, at 25 °C. These data are in qualitative agreement with Eq. (3).

If the interaction between interstitialcy pairs is neglected, the diffusion coefficient can be calculated with the help of the random walk model.[17] Then

$$D = \tfrac{1}{2}\nu\langle l^2\rangle, \tag{4}$$

where $\langle l^2\rangle$ is the mean square of the effective jump distance and ν is the jump frequency. In our interstitialcy pair motion, $\langle l^2\rangle = a^2$, where a is the lattice constant in the mirror plane. The electrical conductivity is then obtained from the Einstein relation

$$\sigma = \frac{ne^2}{kT} D = \frac{n\nu e^2 a^2}{2kT}, \tag{5}$$

where n is the excess M^+ ion concentration.

The jump frequency is given by

$$\nu = 2\nu_0\left(1 - \frac{n}{N}\right) e^{-E_a/kT}, \tag{6}$$

where ν_0 and E_a are the oscillation frequency and the potential energy barrier, respectively, of the in-phase motion of the two particles. One finds

$$\nu_0 \cong \frac{1}{2\pi}\sqrt{3\pi^2 E_a/ma^2} \tag{7}$$

if the potential energy curve is approximated by a cosine function. From Eqs. (5) and (6), the electrical conductivity is given by

$$\sigma = \sigma_0 e^{-E_a/kT}, \tag{8}$$

where

$$\sigma_0 = \frac{e^2 a^2}{kT}\nu_0 n\left(1 - \frac{n}{N}\right). \tag{9}$$

The values of ν_0 are calculated from the potential energy curves and given in Table III. In this table the frequencies of a single particle along the path near the Beevers–Ross site also are given for various M^+ ions. The product of temperature and the preexponential factor, $T\sigma_0$, has been calculated for five different M^+ ions for 16% excess M^+ ion concentration and is listed in Table IV. The resulting values are in reasonably good agreement with experimental results for Na^+ and Ag^+.

V. DISCUSSION

In this work we assumed completely ionic bonds and included the Madelung energy, the Born–Mayer repulsion energy, and the polarization energies of ions. With excess M^+ ion concentration, electrical neutrality is expected to be maintained by aluminum vacancies or extra oxygen ions in the mirror plane. In our calculation these defects have been neglected.

Since we are interested only in the variation of the potential energy as a function of positions of M^+ ions in the mirror plane, the absolute value of the total crystal energy need not be considered.

No covalency was considered. Although covalency among fixed ions (ions in spinel blocks) may not affect our calculation to a great extent, any covalent bonding between the M^+ ion and oxygen ions in spinel blocks is expected to influence the potential energy curves. As mentioned in Sec. IV, the failure of our calculation to predict the silver ion occupation probability of the anti-Beevers–Ross site can be blamed on some covalent bonding between the Ag^+ ion and the two oxygens adjacent to the silver ions. The effect of covalency on the site energy is being investigated by the $X\alpha$ self-consistent field method.

In our calculation, all M^+ ions were constrained to the mirror plane. This restriction was imposed since Roth's x-ray work[4] indicated that Ag^+ ion motion was indeed confined to this plane. The abnormally small calculated potential barrier height for the Li^+ interstitialcy pair can be attributed to such a restriction. Because of the small size of the Li^+ ion, the Beevers–Ross site is not a position of potential minimum. Our preliminary calculation shows that the potential minima lie off the mirror plane and close to spinel blocks. Such minima are produced by the polarization energy.

Although constraining the M^+ ion motion to the mirror plane enabled us to partly avoid the polarization catastrophy, the polarization interaction energy between the two M^+ ions in the interstitialcy pair does make a difficulty in computation. This difficulty was avoided by adopting $\exp\{-(1+|R|)R/\rho\}$ in place of $\exp\{-R/\rho\}$ in the repulsive potential for $R \equiv r_- + r_+ - r > 0$, i.e., when the interionic distance is less than the sum of the ionic radii.

At present it is very difficult to see how to improve the calculation presented in this paper. Any improvement must consider the following points. In the neighborhood of any defects, the potential energy curves can

TABLE IV. Calculated and experimental values of $T\sigma_0$ for β-alumina crystals with $n = 0.16N$. The values are in units of 10^3 $(\Omega\text{-cm})^{-1}$ °K.

Material	$T\sigma_0$(calc)	$T\sigma_0$(exptl)
Li^+-beta	9.09	...
Na^+-beta	3.30	2.5
Ag^+-beta	1.57	1.6
K^+-beta	3.01	...
Rb^+-beta	2.35	...

be altered. For Li^+, one has to explore the potential energy surface off the plane. Any covalency between the M^+ ion and oxygen ions in the spinel block must be studied through a quantum mechanical calculation. Small differences in lattice dimension of various β-aluminas may change the potential energy curves.

In Table III, the vibrational frequencies along the M^+ ion trajectory are listed. We would like to point out that these frequencies do not scale with the inverse of the square root of the ion mass. According to our calculation, K^+ β-alumina has a higher frequency than Na^+ β-alumina both for pair motion and single ion motion.

Far infrared absorption has a contribution from vibrational modes other than those responsible for the ion diffusion. Although one has to consider all modes in order to explain the far infrared absorption,[18,19] the above discussion indicates the far infrared conductivity peak position may not scale with the inverse of the square root of the ion mass. Work on this problem is in progress and will be reported in the near future.

ACKNOWLEDGMENT

We are grateful to L. M. Slifkin for a critical reading of the manuscript.

*Work supported by ARPA through UNC Materials Research Center (DAHC 15 73G9) and by NSF Grant GH-37922.

[1]W. L. Bragg, G. Gottfried, and J. West, Z. Kristallogr. 77, 255 (1931).
[2]C. A. Beevers and M. A. S. Ross, Z. Kristallogr. 97, 59 (1937); C. A. Beevers and S. Brohult, Z. Kristallogr. 95, 472 (1932).
[3]C. Peters, M. Bettman, J. Moore, and M. Glick, Acta Crystallogr. B 27, 1826 (1971).
[4]W. L. Roth, J. Solid State Chem. 4, 60 (1972).
[5]J. I. Kummer, *Progress in Solid State Chemistry*, edited by H. Reiss and J. O. McCaldin (Pergamon, New York, 1972), Vol. 7, p. 141.
[6]H. Sato and R. Kikuchi, J. Chem. Phys. 55, 677, 702 (1971).
[7]M. J. Rice and W. L. Roth, J. Solid State Chem. 4, 294 (1972).
[8]M. P. Tosi and F. G. Fumi, J. Phys. Chem. Solids 25, 31, 45 (1964).
[9]L. Pauling, Z. Kristallogr. 67, 377 (1928).
[10]C. Kittel, *Introduction to Solid State Physics* (Wiley, New York, 1956).
[11]R. D. Shannon and C. T. Prewitt, Acta Crystallogr. B 25, 925 (1969).
[12]J. Tessman, K. Kahn, and W. Shockley, Phys. Rev. 92, 890 (1953).
[13]J. Pirenne and E. Kartheuser, Physica (Utr.) 30, 2005 (1964).
[14]M. S. Whittingham and R. Huggins, J. Chem. Phys. 54, 414 (1971); J. Electrochem. Soc. 118, 1 (1971).
[15]J. E. Hove, Phys. Rev. 102, 915 (1956).
[16]J. H. Kennedy and A. F. Sammels, J. Electrochem. Soc. 119, 1609 (1972).
[17]F. Reif, *Fundamentals of Statistical and Thermal Physics* (McGraw-Hill, New York, 1965), p. 486.
[18]S. J. Allen, Jr. and J. P. Remeika, Phys. Rev. Lett. 33, 1478 (1974).
[19]B. A. Huberman and P. N. Sen, Phys. Rev. Lett. 33, 1379 (1974).

VIBRATION EFFECT IN THE ORDER-DISORDER TRANSITION THEORY OF $RbAg_4I_5$ †

Sang-il Choi and W. M. Lee

Department of Physics & Astronomy
University of North Carolina
Chapel Hill, North Carolina 27514

ABSTRACT

Vibrational frequencies are expected to be quite different at different sites of the carrier ion in a superionic conductor. For a simple model of $RbAg_4I_5$, we have studied the effect of vibrational frequency differences on the equilibrium distribution of Ag^+ ions. It is found that one could introduce a considerable error by neglecting the above mentioned effect.

INTRODUCTION

In the theory of order-disorder transition it has been a common practice to neglect contribution from the vibrational motion of ions to the partition function[1,2]. This approximation is justified if the vibrational frequency distribution has a weak dependence on the spatial distribution of ions. One characteristic of superionic conductors is the availability of more than one site per carrier ion. Then it is natural to consider an order-disorder transition with respect to the arrangement of carrier ions over these sites. In applying a theory of order-disorder transition to this problem it is unlikely that one can justify neglecting the variation of vibrational frequencies over different sites. For example, previously we found that vibrational frequencies at the Beevers-Ross site of β- alumina is very different from that of the anti-Beevers-Ross site.[3]

Our objective of this study is to see the importance of the vibrational partition function (or vibrational free energy) through a relatively simple calculation. In 1969 Wiedersich and Johnston[4] reported an application of the quasichemical approximation of the theory of order-disorder transition to $RbAg_4I_5$. Their work was based on the assumption that the vibrational frequencies are independent of the distribution of Ag^+ ions. As a result of their analysis of experimental data, they deduced the site energy differences to be ~0.027 eV and ~0.042 eV. The mutual repulsion energy between two silver ions on the adjacent II-sites was found to be ~0.035 eV. In view of the existence of this interesting work, we decided to study a simplified model of $RbAg_4I_5$.

MODEL AND CALCULATION

We consider the cubic phase of $RbAg_4I_5$ of which crystal structure has been determined by Geller[5]. Iodide ions form 56 tetrahedra per unit cell which serve as sites for silver ions. The four rubidium ions are surrounded by distorted octahedra of iodide ions. The 56 sites are classified into three types: 8 of I-type, 24 each of II-type and III-type. Since there are only 16 silver ions, 3.5 sites are available for each silver ion.

We assume that all the ions except silver ions form a rigid crystal framework which produces the force field for silver ions. Then, as far as our model is concerned, the crystal is characterized by the site energy differences, the interaction energy between silver ions, and the vibrational frequencies of silver ion at the three different sites. The vibrational motion of silver ion at each site is assumed to be represented by one isotropic three dimensional harmonic oscillator. For interaction energies we consider only nearest neighbor pairs. Following Wiedersich and Johnston we assume the pair interaction energy is inversely proportional to the distance between the sites. Then our model is specified by seven parameters: 3 site energies, one pair interaction energy, and 3 vibrational frequencies. Some properties and notations of the three types of sites are listed in Table 1. The fractional occupation (i.e. number of silver ions on a given type site devided by the number of site of this type) measured at room temperature[5] is given in the seventh column. The last column contains the fraction of

Table 1

Type	Site energy	Number of sites	Frequency	Number per unit cell	Frac. occup.	Frac. ion in type
I	e_1	N_1	ω_1	8	0.111	0.055
II	e_2	$N_2 = N$	ω_2	24	0.391	0.586
III	e_3	N_3	ω_3	24	0.229	0.344

silver ions in a given type site (number of silver ions on the given type site devided by the total number of silver ions). The notations used for pairs are summarized in Table 2.

In stead of the quasichemical approximation, we resort to Bragg-Williams approximation. For our purpose this approximation is expected to be adequate. In order to find the equilibrium distribution of silver ions, the expression for free energy, $F(T, \{n_i\})$, is obtained in terms of site energies (e_i), pair interaction energies (u_i), site vibrational frequencies (ω_i), and site occupation numbers (n_i). The free energy is, then, minimized with respect to the set of occupation numbers with the constraint that total number of silver ions is constant. In Bragg-Williams method, the number of each type of site pairs is simply related to the site occupation numbers:

$$m_1 = 3n_1n_2/N_2 , \quad m_2 = n_2^2/2N_2, m_3 = m_{\bar{3}} = n_2n_3/2N_2 \quad (1)$$

The free energy of the system, then, is given by

$$F = m_1u_1 + m_2u_2 + m_3u_3 + m_{\bar{3}}u_{\bar{3}} + E_H - T[S_c(n_1,n_2,n_3) + S_H(n_1,n_2,n_3,\omega_1,\omega_2,\omega_3)] \quad (2)$$

where S_c is the configuration entropy while E_H and S_H are the energy and the entropy derived from the vibratonal partition function. The configurational entropy is given by

$$S_c = k\ell n\, W(n_1,n_2,n_3) \quad (3)$$

Table 2

Type of site pairs	Pair energy	Number of site pairs	Number of site pairs with occupation, Ag-Ag
II-I	u_1	$M_1=N$	m_1
II-II	u_2	$M_2=N/2$	m_2
$(II-III)_1$	u_3	$M_3=N$	m_3
$(II-III)_2$	u_3	$M_4=N$	m_3

where k is the Boltzman constant and W is the total number of distinguishable arrangement of silver ions for a given set of occupation numbers. In Bragg-Williams method

$$W = \frac{N_1!}{n_1!(N_1 - n_1)!} \frac{N_2!}{n_2!(N_2 - n_2)!} \frac{N_3!}{n_3!(N_3 - n_3)!} \tag{4}$$

With the help of Stirling's approximation, then,

$$S_c = k\left[\sum_{i=1}^{3} (n_i - N_i)\ell n\left(1 - \frac{n_i}{N_i}\right) - \sum_{i=1}^{3} n_i \ell n \frac{n_i}{N_i}\right] \tag{5}$$

In the high temperature approximation the partition function of a silver ion on i-site is given by

$$z_i = \left[kT/\hbar\omega_i\right]^3 \exp\left[\left(\frac{3}{2}\hbar\omega_i - e_i\right)/kT\right] \tag{6}$$

The total vibrational partition function of a given set of values of occupation numbers is

$$Z_T = \Pi_i \, z_i^{n_i} \, . \tag{7}$$

From this partition function we obtain

$$E_H = \sum_i n_i e_i + 3nkT - \frac{3}{2}\hbar \sum_i n_i \omega_i \quad , \tag{8}$$

$$S_H = 3k\left[n - \sum_i n_i \ell n\left(\hbar\omega_i/kT\right)\right] \tag{9}$$

where $n=n_1+n_2+n_3$ and is the total number of silver ion. The free energy is given by the following equation.

$$F = \frac{3n_1n_2}{N_2} U_1 + \frac{n_2^2}{2N_2} U_2 + \frac{n_2n_3}{2N_2} U_3 + \frac{n_2n_3}{2N_2} U_{\bar{3}}$$

$$+ \sum_i n_i e_i - \frac{3}{2}\hbar \sum_i n_i \omega_i \qquad (10)$$

$$-kT\left[\sum_i (n_i - N_i) \ell n \left(1 - \frac{n_i}{N_i}\right) - \sum_i n_i \ell n \frac{n_i}{N_i} - 3 \sum_i n_i \ell n \frac{\hbar\omega_i}{kT}\right]$$

The equilibrium value of occupation numbers are determined by minimizing F with respect to n_i . The two equations thus obtained are as follows.

$$- \frac{3u_1}{N_2} n_1 - \frac{(3u_1 - u_2)}{N_2} n_2 - \frac{(u_3 + u_{\bar{3}})}{2N_2} n_3 + (e_1 - e_2)$$

$$+ \frac{3}{2}\hbar(\omega_2 - \omega_1) + 3\, kT \ell n \frac{\omega_1}{\omega_2} + kT \ell n \left[\frac{n_1}{n_2} \frac{N_2 - n_2}{N_1 - n_1}\right] = 0, \qquad (11)$$

$$- \frac{3u_1}{N_2} n_1 - \frac{(2u_2 - u_3 - u_{\bar{3}})}{2N_2} n_2 - \frac{(u_3 + u_{\bar{3}})}{2N_2} n_3 + (e_3 - e_2)$$

$$+ \frac{3}{2}\hbar(\omega_2 - \omega_3) + 3\, kT \ell n \frac{\omega_3}{\omega_2} + kT \ell n \left[\frac{n_3}{n_2} \frac{N_2 - n_2}{N_3 - n_3}\right] = 0, \qquad (12)$$

Solution of these equations would yield the equilibrium silver ion distribution. Since our main objective is to see the effect of vibrational frequencies on the distribution of silver ions, we chose the parameter values determined by Wiedersich & Johnston, i.e. $e_1-e_2=0.042$ eV, $e_3-e_2=0.027$ eV, and $u_2=0.035$ eV. The values of other pair energies are also same as theirs. In order to facilitate solution of Equations (11,12) we assumed the following relationship among the frequencies.

$$\omega_1 = \omega, \quad \omega_2 = \omega(1 - \alpha), \quad \omega_3 = \omega(1 + \alpha), \tag{13}$$

where α is a parameter. At 300°K the values of $\{f_i = n_i/n\}$ are calculated for various values of α by numerical solution of Eqs. (11, 12). The results are shown in Fig. 1. The values of $\{f_i\}$ for $\alpha = 0$ agree quite well with experimental values as expected since the parameter values used were determined by Wiedersich & Johnston to reproduce the experimental values of $\{f_i\}$ when $\alpha = 0$, i.e. the vibrational effect is neglected. One must notice a large deviation from the experimental values as α is increased or decreased from 0.

The vibrational effect is demonstrated more effectively by evaluating the values of site energy differences which yield the experimental values of $\{f_i\}$. For various values of α, the site energy differences $e_1 - e_2$ and $e_3 - e_2$ are calculated and the results are shown in Figure 2. Set 2 (broken line) is for the negative values of α. $\omega = 10^{12}$ sec^{-1} is assumed.

DISCUSSION

In this study a simple theory of order-disorder transition is applied to a simplified model of $RbAg_4I_5$ crystal in order to understand the effect of vibrational motion of silver ions at different sites. This work indicates that a large error may result in the estimation of site energies and pair interaction energies through application of a theory of order-disorder transition unless the vibration effect (kinetic effect) is properly included. Figure 2 shows that e_3 could be smaller than e_2 if ω_3 were large enough compared to ω_2 even though the experimentally observed occupation number of III-site is less than that of II-site. This is due to the larger entropy for a smaller frequency compensating the larger site energy.

Better theories of superionic conductors for equilibrium and transport properties with proper incorporation of vibration effect are desired for better understanding of this interesting class of materials.

†This work was supported by ARPA through UNC materials Research Center and by the National Science Foundation.

Figure 1

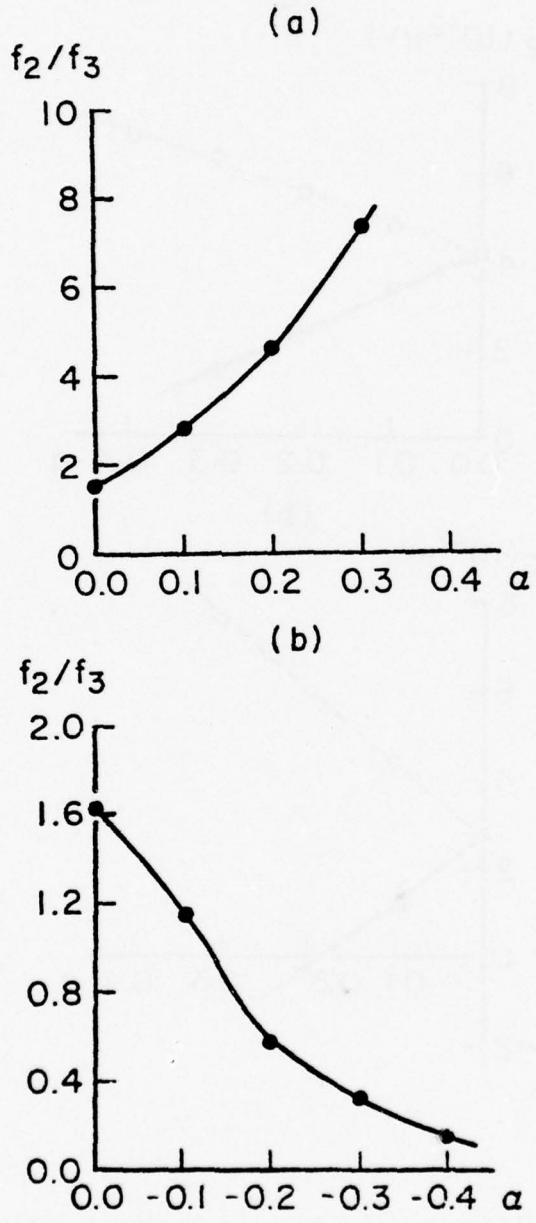

Ratio of number of silver ions in II-site and III-site.

Figure 2

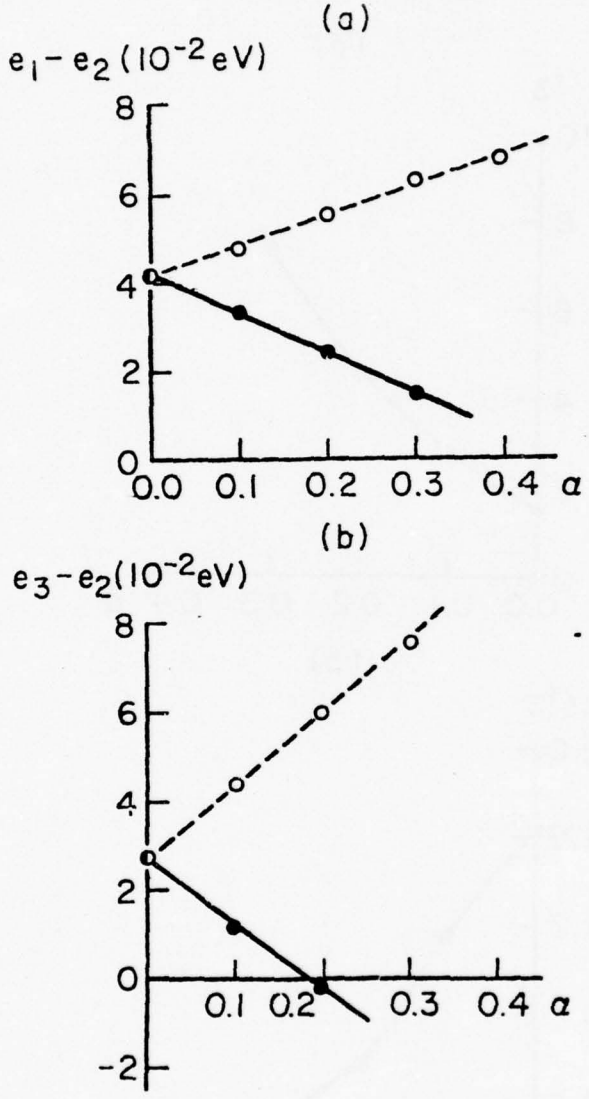

Site energy difference (a) between I-site and II-site, and (b) between III-site and II-site.

REFERENCES

1. R. H. Fowler & E. A. Guggenheim, Statistical Thermodynamics, (Cambridge University Press, 1939) p.541.

2. E. A. Guggenheim, Mixturs(Oxford Press, 1952) p.101.

3. J. C. Wang, M. Gaffari, and S. Choi, J. Chem. Phys. 63. 772 (1975).

4. H. Wiedersich and W. V. Johnston, J. Phys. Chem. Solids, 30, 475 (1969).

5. S. Geller, Science 157, 310(1967).

PRECEDING PAGE BLANK-NOT FILMED

THE CATALYSIS OF ORGANIC OXIDATION PROCESSES. FUEL CELLS.

T. J. Meyer

Final Technical Report

1 June 1973 - 30 September 1976

Personnel:

F. R. Keene, Research Associate; D. J. Salmon, Research Assistant

During the period of support from DARPA, a number of different approaches were taken to the development of catalytic systems for the oxidation of organic compounds under mild conditions in solution. Catalytic oxidations based on the redox properties of transition metal complexes were the major theme of the work where the reactions observed are chemically catalyzed, net electrochemical reactions:

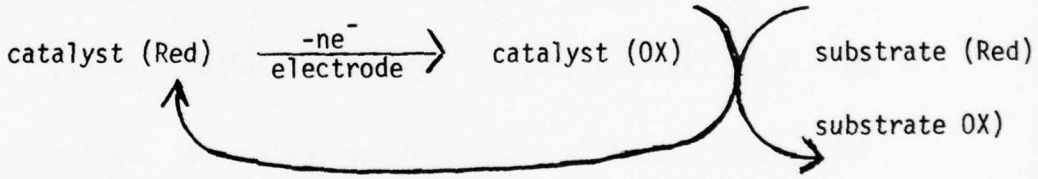

Considerable progress has been made at this level, and an important aspect of the next stage will involve attachment of catalytically useful reagents to semiconductor electrode surfaces in collaboration with the group of R. W. Murray.

1. Catalytic Oxidations Based on Ru-nitrosyl/nitrite Chemistry [Two manuscripts have been submitted to J. Amer. Chem. Soc.]. Chemical or electrochemical oxidation of Ru(II)-nitro complexes to Ru(III) occurs but the Ru(III)-nitro complexes undergo a facile disproportionation at the bound NO_2 groups (bpy is 2,2'-bipyridine; py is pyridine):

$$2[Ru^{II}(bpy)_2(NO_2)py]^+ \xrightarrow{-3e^-} [Ru^{II}(bpy)_2(NO^+)py]^{3+} + [Ru^{III}(bpy)_2(NO_3)py]^{2+}$$

In slightly basic solution the nitrosyl is converted into the nitro complex,

$$[Ru^{II}(bpy)_2(NO^{+})py]^{3+} + 2B + H_2O \longrightarrow [Ru^{II}(bpy)_2(NO_2)py]^{+} + 2BH^{+}$$

(B is 2,6-lutidine, etc.)

so that the nitrosyl complex once formed reenters the oxidation sequence and the products are $[Ru^{III}(bpy)_2(NO_3)py]^{2+}$ and BH^{+}:

$$2BH^{+} \quad \uparrow\downarrow \quad 2[Ru^{II}(bpy)_2(NO_2)py]^{+} \xrightarrow{-e^{-}} 2[Ru^{III}(bpy)_2(NO_2)py]^{2+}$$

$$2B + H_2O \quad \uparrow\downarrow \quad [Ru^{II}(bpy)_2(NO^{+})py]^{3+} \xleftarrow{-e^{-}} [Ru^{II}(bpy)_2(\dot{N}O)py]^{2+} \longrightarrow [Ru^{III}(bpy)_2(NO_3)py]^{2+}$$

In the presence of PR_3 or R_2S, the Ru(III) nitro intermediates are captured and the conversions $PR_3 \rightarrow OPR_3$ and $R_2S = O$ can be carried out <u>catalytically</u> and <u>quantitatively</u>.

$$2BH^{+} \quad \uparrow\downarrow \quad [Ru^{III}(bpy)_2(NO_2)py]^{+} \xrightarrow{-e^{-}} [Ru^{III}(bpy)_2(NO_2)py]^{2+} \quad \uparrow\downarrow \quad SR_2$$

$$2B + H_2O \quad \uparrow\downarrow \quad [Ru^{II}(bpy)_2(NO^{+})py]^{3+} \xleftarrow{-e^{-}} [Ru^{II}(bpy)_2(\dot{N}O)py]^{2+} \quad \uparrow\downarrow \quad R_2S{=}O$$

The catalytic sulfide → sulfoxide conversion has considerable promise as a commercial process. The Ru(III) nitro intermediates also show reactivity towards certain olefins, and by eliminating the competing disproportionation reaction by immobilization on a surface, we may have access to epoxides and/or diols catalytically.

2. <u>Oxidative Dehydrogenation of Alcohols and Amines</u> [J. Amer. Chem. Soc., <u>98</u>, 1884 (1976); Inorg. Chem., <u>15</u>, 190 (1976); reprints attached]. The chemical or electrochemical oxidation of coordinated amines to nitriles has been found to be a facile and quantitative process (eq. 1).

$$Ru(bpy)_2(NH_2CH_2R)_2^{2+} \xrightarrow{-8e^{-}} Ru(bpy)_2(NCR)_2^{2+} + 8H^{+} \qquad (1)$$

The reactions proceed via initial oxidation of Ru(II) to Ru(III). The disadvantages of the bpy systems (eq. 1) are that the Ru(III)/(II) reduction potentials are high, and the bound nitriles remain firmly bound in the coordination sphere of the Ru(II) product. Recent work indicates that the cluster redox couple $Ru_3O(CH_3CO_2)_6(am)_3^{+/0}$ (am = amine) may be a useful catalytic agent for the specific oxidation of amines. The +1/0 couple has a relatively low reduction potential (~0.1V vs SCE in water) and high current densities have been obtained upon electrolysis at the diffusion plateau of the $+1 \xrightarrow{+e} 0$ couple in the presence of a series of amines.

The Ru(II) and Ru(III) complexes $Ru(bpy)_2(ROH)Cl^{2+/+}$ where the alcohol is methanol or isopropanol have been generated in solution. The Ru(III) complexes undergo rapid base-catalyzed oxidation of the bound alcohol. The work here is being extended to careful kinetic and mechanistic investigations on the alcohol and related amine complexes in order to determine the factors affecting the reactivities of the bound ligands in net oxidative dehydrogenation steps,

$$R_2CHOH \xrightarrow{-2e^-} R_2C{=}O$$

$$R_2CHNH_2 \xrightarrow{-2e^-} R_2C{=}NH$$

In the future, this work will be compared with similar studies on multiple redox site systems like $(bpy)_2ClRu(III)(pyz)Ru(III)(ROH)(bpy)_2^{5+}$ (pyz is pyrazine) where multiple, intramolecular electron transfer processes may lead to facile catalytic oxidation of the bound alcohol.

Further Work:

The work described above and more recent work represent innovative attempts to solve problems of ongoing interest in chemistry using new approaches and methodology. Support from DARPA has been instrumental in the development of the work which has led to systems which have promise of commercial viability. The support of DARPA is gratefully acknowledged. However, it is unfortunate that the decision to withdraw funding comes at a time when the promise of the

science involved is rapidly expanding. That DARPA has cultivated the work to a point of tangible fruition and has then eliminated support on the basis of a change in perception of the "mission" of the DARPA agency is distressing and hopefully for the future, shortsighted.

[Reprinted from the Journal of American Chemical Society, 98, 1884 (1976).]
Copyright 1976 by the American Chemical Society and reprinted by permission of the copyright owner.

Oxidation of Primary Amines Bound to Bis(2,2′-bipyridine)ruthenium(II)

F. Richard Keene, Dennis J. Salmon, and Thomas J. Meyer*

Contribution from the W. R. Kenan, Jr., Laboratories of Chemistry, Department of Chemistry, The University of North Carolina, Chapel Hill, North Carolina 27514. *Received July 12, 1975*

Abstract: In the net sense, chemical and electrochemical oxidations of the ions $[Ru(bpy)_2(NH_2CH_2R)_2]^{2+}$ (NH_2CH_2R = allylamine, benzylamine, and *n*-butylamine) occur by dehydrogenation at the amine ligands giving the corresponding bis(nitrile) complexes, $[Ru(bpy)_2(N{\equiv}CR)_2]^{2+}$. The reactions appear to proceed by initial oxidation of Ru(II) to Ru(III), followed by a series of stepwise dehydrogenation reactions which occur via imine intermediates.

Net reactions involving the oxidative dehydrogenation of chelated amines to imines have been reported for macrocyclic amines,[1,2] and for ethylenediamine and related diamines.[3-7] For chelated amines, dehydrogenation stops at the imine stage; further oxidation gives hydroxodiimines[8] or net decomposition, rather than nitriles.[7]

There are two examples of the oxidation of monodentate primary amines to nitriles or cyanides. McWhinnie et al.[9] have reported the isolation of Ru(III) products containing the cyanide ion following the aerial oxidation of $[Ru(NH_2CH_3)_6]^{2+}$, and Diamond, Tom, and Taube[10] have shown that benzylamine bound to pentaammineruthenium(II) can be oxidized to benzonitrile.

Previous work has shown that oxidation of ligands bound to bis(2,2′-bipyridine)ruthenium(II) can be facile, and quantitative.[7,11] The reactions appear to proceed via initial oxidation of Ru(II) to Ru(III), followed by a series of rapid steps in which the net reactions involve the oxidation of a coordinated ligand.

Experimental Section

Electronic spectra were recorded on a Bausch and Lomb 210UV spectrophotometer. ^1H NMR spectra were measured on a Jeol C-60-HL spectrometer using acetone-d_6 solutions of PF_6^- salts

(Me_4Si internal reference). Ir spectra were recorded on a Perkin-Elmer 421 grating spectrophotometer using KBr disks (ca. 5 mg of complex/200 mg of KBr).

Benzylamine (Eastman), benzonitrile (MCB), allylamine (Eastman), acrylonitrile (Aldrich), *n*-butylamine (Fisher), and *n*-butyronitrile (Aldrich) were used without purification. For spectral measurements, acetonitrile (MCB, spectrograde) was used without purification and water was deionized and distilled from alkaline $KMnO_4$ before use. The complex $[Ru(bpy)_2Cl_2]\cdot 2H_2O$ was prepared as described previously,[12] and recrystallized (as the anhydrous compound) by Soxhlet extraction from methylene chloride before use. $[Ru(bpy)_2CO_3]\cdot 2H_2O$ was also prepared as described previously.[13]

Electrochemical measurements were made in acetonitrile solutions containing 0.1 M tetra-*n*-butylammonium hexafluorophosphate (TBAH) as the supporting electrolyte, or in 1.0 M HCl, vs. the saturated sodium chloride calomel electrode (SSCE) at 25 ± 2 °C, and are uncorrected for junction potentials. All potentials reported are reduction potentials vs. the SSCE. Potential control for electrochemical experiments was obtained with a Princeton Applied Research Model 173 potentiostat/galvanostat. The waveform generator for voltammetric experiments was a Princeton Applied Research Model 175 universal programmer. Voltammograms and slow scan cyclic voltammograms were recorded on a Hewlett-Packard Model 7004B x-y recorder. Fast scan cyclic voltammograms were obtained from photographs of the trace of a Tektronix Model 564B storage oscilloscope. Values of *n*, where *n* is the total number of equivalents of electrons transferred in exhaustive electrolyses at constant potentials, were calculated after measuring the total area under current vs. time curves for the complete reaction. Reactions were judged to be complete when the current had fallen below 1% of the initial value. All voltammetric measurements were carried out at platinum electrodes in solutions deaerated with a stream of dry, prepurified nitrogen.

Elemental analyses were carried out by Galbraith Laboratories Inc., Knoxville, Tenn.

Preparation of Complexes. $[Ru(bpy)_2(NH_2CH_2CH{=}CH_2)_2](PF_6)_2$. $[Ru(bpy)_2Cl_2]$ (0.46 g) was suspended in 50% aqueous MeOH (40 ml). Allylamine (5 ml) was added and the mixture kept at steam-bath temperature under N_2 for 2 h. Methanol and allylamine were evaporated off, the solution was cooled, and solid NH_4PF_6 was added slowly with stirring. The product was filtered, washed with ice-cold water and dried in vacuo, yield 0.68 g, 90%. Recrystallization was achieved by dissolution of the product in a minimum volume of CH_2Cl_2 (ca. 200 ml), filtering, and precipitating by the addition of ligroine (bp 30–60°). The red precipitate was filtered, washed with ligroine, and dried in vacuo. Anal. Calcd for $[Ru(bpy)_2(NH_2CH_2CH{=}CH_2)_2](PF_6)_2$: C, 38.2; H, 3.70; N, 10.3. Found: C, 38.0; H, 3.58; N, 10.2.

$[Ru(bpy)_2(NH_2CH_2C_6H_5)_2](ClO_4)_2$. $[Ru(bpy)_2Cl_2]$ (0.41 g) was suspended in 50% aqueous MeOH (40 ml). Benzylamine (5 ml) was added and the solution heated on a steam bath under an atmosphere of N_2 for 2 h. Methanol was evaporated off, the solution cooled, and then extracted three times with 25-ml portions of ether to remove excess benzylamine. The remaining aqueous solution was filtered, and the product precipitated by the slow addition of a filtered, saturated solution of $LiClO_4$. The red precipitate was collected, and the solid washed with ice-cold water, 2-propanol, and ether, and then dried in vacuo, yield, 0.65 g, 92%. Anal. Calcd for $[Ru(bpy)_2(NH_2CH_2C_6H_5)_2](ClO_4)_2$: C, 49.4; H, 4.15; N, 10.2. Found: C, 49.3; H, 4.09; N, 10.2.

$[Ru(bpy)_2(NH_2CH_2CH_2CH_2CH_3)_2](PF_6)_2$. $[RuB_2Cl_2]$ (0.45 g) was suspended in 50% aqueous MeOH (40 ml), *n*-butylamine (5 ml) was added, and the mixture heated on a steam bath under an N_2 atmosphere 2 h. The methanol and *n*-butylamine were evaporated off, and the last traces of the amine were removed by extraction with ether. The product was precipitated by the slow addition of solid NH_4PF_6 to a stirred solution of the complex. The solid was collected by filtration, washed with ice-cold water, and dried in vacuo. The product was recrystallized by adding a filtered CH_2Cl_2 solution to pentane, yield 0.50 g, 63%. Anal. Calcd for $[Ru(bpy)_2(NH_2CH_2CH_2CH_2CH_3)_2](PF_6)_2$: C, 39.6; H, 4.51; N, 9.9. Found: C, 39.5; H, 4.52; N, 9.7.

$[Ru(bpy)_2(N{\equiv}CR)_2](PF_6)_2$ (R is $-CH{=}CH_2$ (Acrylonitrile) and $-C_3H_7$ (*n*-Butyronitrile)). $[Ru(bpy)_2(CO_3)]\cdot 2H_2O$ (0.40 g) was suspended in acetone (15 ml) and concentrated HPF_6 (ca. 0.2 ml) added. The solution was stirred for 10 min, and anhydrous Na_2CO_3 (ca. 1 g) added. After stirring for a further 10 min the solution was filtered, the required nitrile (5 ml) added, and the mixture stirred for 2 h. The products were precipitated by adding the reaction mixtures dropwise to large volumes (300 ml) of ether, yields 0.57 g (90%) for acrylonitrile and 0.53 g (80%) for *n*-butyronitrile. Recrystallization was achieved in both cases from acetone–ether. Anal. Calcd for $[Ru(bpy)_2(N{\equiv}CCH{=}CH_2)_2](PF_6)_2$: C, 38.6; H, 2.74; N, 10.4. Found: C, 38.7; H, 2.75; N, 10.3. Calcd for $[Ru(bpy)_2(N{\equiv}CCH_2CH_2CH_3)_2](PF_6)_2$: C, 40.0; H, 3.59; N, 10.0. Found: C, 39.8; H, 3.52; N, 9.8.

$[Ru(bpy)_2(N{\equiv}CC_6H_5)_2](PF_6)_2$. The benzonitrile salt was prepared in a manner analogous to that given for the bis(benzylamine) complex, except that the complex was precipitated by the addition of NH_4PF_6 after excess benzonitrile had been removed by ether extraction. The salt was recrystallized by dissolution in CH_2Cl_2, filtering the solution, and precipitating by the addition of ligroine (bp 30–60°). The product was obtained in 71% yield. Anal. Calcd for $[Ru(bpy)_2(N{\equiv}CC_6H_5)_2](PF_6)_2$: C, 44.9; H, 2.88; N, 9.2. Found: C, 44.9; H, 2.87; N, 8.9.

Electrochemical Preparations. $[Ru(bpy)_2(N{\equiv}CC_6H_5)_2](PF_6)_2$. The salt $[Ru(bpy)_2(NH_2CH_2C_6H_5)_2](ClO_4)_2$ (120 mg) was dissolved in 1 M HCl (120 ml). The solution was electrolyzed exhaustively at 0.80 V until the current had fallen to 1% of its initial value (n = 7.9). The resulting solution was filtered and solid NH_4PF_6 added with stirring. The yellow precipitate which appeared was filtered, washed with ice-cold water, and dried in vacuo, yield 0.105 g, 87%. Recrystallization was achieved by adding ligroine (bp 30–60°) dropwise to a solution of the complex in CH_2Cl_2. Anal. Calcd for $[Ru(bpy)_2(N{\equiv}CC_6H_5)_2](PF_6)_2$: C, 44.9; H, 2.88; N, 9.2. Found: C, 44.8, H, 3.00; N, 9.2.

$[Ru(bpy)_2(NH_2CH_2C_6H_5)(N{\equiv}CC_6H_5)](PF_6)_2$. The salt $[Ru(bpy)_2(NH_2CH_2C_6H_5)_2](ClO_4)_2$ (113 mg) was dissolved in 1 M HCl (80 ml). The solution was electrolyzed exhaustively at 0.70 V until the current had fallen to 1% of its initial value (n = 3.9). The solution was filtered and solid NH_4PF_6 added slowly with stirring. The resultant precipitate was filtered, washed with ice-cold water, 2-propanol, and ether, and then air dried, yield 0.10 g, 88%. The salt was recrystallized from acetone–ether. Anal. Calcd for $[Ru(bpy)_2(NH_2CH_2C_6H_5)(N{\equiv}CC_6H_5)](PF_6)_2$: C, 44.7; H, 3.31; N, 9.2. Found: C, 44.7; H, 3.32; N, 9.2.

$[Ru(bpy)_2(NH_2CH_2R)(N{\equiv}CR)](PF_6)_2$ (R is $-CH{=}CH_2$ and $-C_3H_7$). The respective salts $[Ru(bpy)_2(NH_2CH_2CH{=}CH_2)_2](PF_6)_2$ and $[Ru(bpy)_2(NH_2CH_2CH_2CH_2CH_3)_2](PF_6)_2$ (100 mg) were dissolved in acetonitrile (30 ml; 0.1 M TBAH) and electrolyzed exhaustively at 1.10 V until the current decreased to 1% of its initial value (n = 3.8 and 3.9, respectively). The products were precipitated by filtering the solutions dropwise into stirred excesses of ether (250 ml). Recrystallization of the allylamine–(acrylonitrile) complex was achieved from CH_2Cl_2–ligroine (30–60°) (yield 0.08 g, 80%), and the *n*-butylamine–(*n*-butyronitrile) complex from acetone–ether (yield 0.03 g, 30%). Anal. Calcd for $[Ru(bpy)_2(NH_2CH_2CH{=}CH_2)(N{\equiv}CCH{=}CH_2)](PF_6)_2$: C, 38.4; H, 3.22; N, 10.3. Found: C, 38.0; H, 3.16; N, 10.2. Calcd for $[Ru(bpy)_2(NH_2CH_2CH_2CH_2CH_3)(N{\equiv}CCH_2CH_2CH_3)](PF_6)_2$: C, 39.8; H, 4.05; N, 9.9. Found: C, 39.5; H, 3.86; N, 10.0.

Results and Discussion

Electrochemical Oxidative Dehydrogenation of Bound Primary Amines. From cyclic voltammetric studies, the complexes $[Ru(bpy)_2(NH_2CH_2R)_2]^{2+}$ (R is $-Ph$, $-CH{=}CH_2$, $-CH_2CH_2CH_3$) undergo electrochemically reversible, one-electron oxidations in acetonitrile with $E_{1/2}$ = 1.03–1.04 V (Table I).[14] The electrochemical oxidations clearly involve reversible Ru(III)/Ru(II) couples; they are one-electron processes, and the $E_{1/2}$ values fall in the range found for the $[Ru(bpy)_2(NH_3)_2]^{3+/2+}$ ($E_{1/2}$ = 0.92 V) and related diamine couples.[7] However, exhaustive electrolysis on the diffusion plateaus of the oxidation waves indicated that n (the number of electrons passed per mole of complex) is greater than one, and is dependent (within certain limits) on the potential used for the electrolysis. At poten-

Table I. $E_{1/2}$ Values for Amine–Nitrile Complexes of Bis(2,2′-bipyridine)ruthenium(II) in Acetonitrile[a]

Complex	$E_{1/2}$, V (V vs. SSCE)
$[Ru(bpy)_2(NH_2CH_2Ph)_2]^{3+/2+}$	1.04
$[Ru(bpy)_2(NH_2CH_2Ph)(N{\equiv}CPh)]^{3+/2+}$	1.29
$[Ru(bipy)_2(N{\equiv}CPh)_2]^{3+/2+}$	1.52
$[Ru(bpy)_2(NH_2CH_2CH{=}CH_2)_2]^{3+/2+}$	1.04
$[Ru(bpy)_2(NH_2CH_2CH{=}CH_2)(N{\equiv}CCH{=}CH_2)]^{3+/2+}$	1.26[b]
$[Ru(bpy)_2(N{\equiv}CCH{=}CH_2)_2]^{3+/2+}$	1.53
$[Ru(bpy)_2(NH_2CH_2CH_2CH_2CH_3)_2]^{3+/2+}$	1.03
$[Ru(bpy)_2(NH_2CH_2CH_2CH_2CH_3)(N{\equiv}CCH_2CH_2CH_3)]^{3+/2+}$	1.24
$[Ru(bpy)_2(N{\equiv}CCH_2CH_2CH_3)_2]^{3+/2+}$	1.48

[a] At a Pt-bead electrode in 0.1 M TBAH–acetonitrile at 25 ± 2°. [b] Reversible only at scan speeds equal to or greater than 500 mV/s.

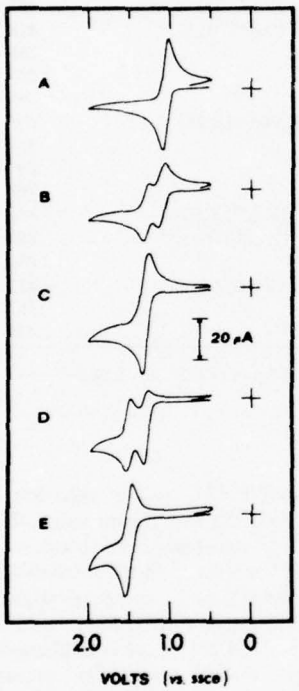

Figure 1. Cyclic voltammograms in acetonitrile of: (A) $[Ru(bpy)_2(NH_2CH_2Ph)_2]^{2+}$, (B) solution A following two-electron oxidation, (C) solution A following four-electron oxidation (giving $([Ru(bpy)_2(NH_2CH_2Ph)(N{\equiv}CPh)]^{2+}$), (D) six-electron oxidation of A, and (E) eight-electron oxidation of A (giving $[Ru(bpy)_2(N{\equiv}CPh)_2]^{2+}$). (Scan rate 200 mV/s at a Pt-bead electrode vs. the saturated sodium chloride calomel electrode at 25 ± 2°.)

tials sufficiently high on the diffusion plateau, reproducible n values of ~8.0 were obtained.

For the bis(benzylamine) complex, $[Ru(bpy)_2(NH_2CH_2Ph)_2]^{2+}$, the electrolytic oxidation was monitored in detail using cyclic voltammetry (Figure 1). Cyclic voltammograms were obtained following controlled potential electrolyses at a series of potentials. Figure 1A shows a cyclic voltammogram for the reversible $[Ru(bpy)_2(NH_2CH_2Ph)_2]^{3+/2+}$ couple. Figure 1B shows the cyclic voltammogram following electrolysis at 1.15 V until n = 2.0; there are two waves, one attributable to unreacted $[Ru(bpy)_2(NH_2CH_2Ph)_2]^{2+}$. The waves have roughly equal peak currents, indicating that there are in solution equal amounts of the starting complex, and a four-electron

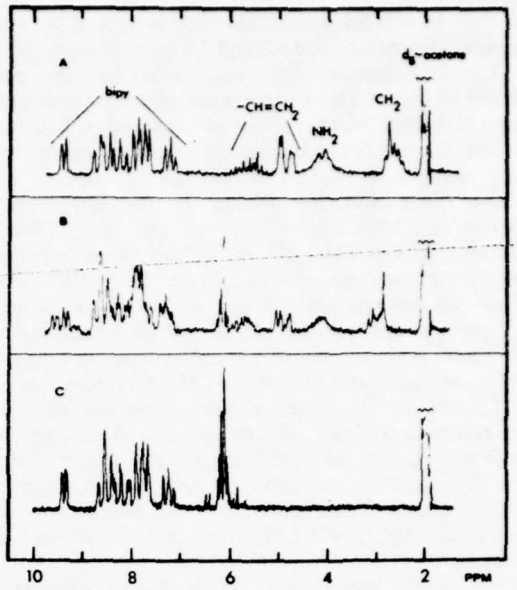

Figure 2. The 60-MHz ^1H NMR spectra in acetone d_6 of (A) $[Ru(bpy)_2(NH_2CH_2CH{=}CH_2)_2]^{2+}$, (B) four-electron oxidation product of A, and (C) eight-electron oxidation product of A ($[Ru(bpy)_2(N{\equiv}CCH{=}CH_2)_2]^{2+}$).

oxidation product with $E_{1/2}$ = 1.29 V. After complete electrolysis at 1.15 V (n = 4.0), only the four-electron oxidation product remains in solution (Figure 1C).

There are two, equally interesting, possibilities for the identity of this four-electron oxidation product. Firstly, both amine ligands might oxidize by two electrons to give the bis(monoimine) complex, $[Ru(bpy)_2(NH{=}CHPh)_2]^{2+}$ (eq 1).

$$[Ru(bpy)_2(NH_2CH_2R)_2]^{2+} \xrightarrow{-4e^-} [Ru(bpy)_2(NH{=}CHR)_2]^{2+} + 4H^+ \quad (1)$$

Reaction 1 is a likely possibility since the related four-electron oxidations of chelated diamines bound to bis(2,2′-bipyridine)ruthenium(II) have been well characterized[7] (e.g., eq 2). The second possibility is that oxidation is localized at

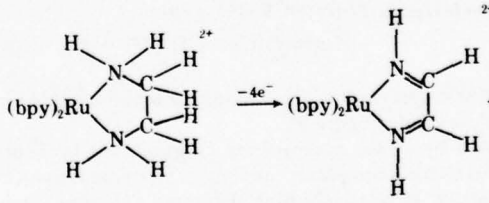

(2)

only one of the amine ligands, and the product is the amine–nitrile complex (eq 3).

$$[Ru(bpy)_2(NH_2CH_2R)_2]^{2+} \xrightarrow{-4e} [Ru(bpy)_2(NH_2CH_2R)(N{\equiv}CR)]^{2+} + 4H^+ \quad (3)$$

Predicted elemental analyses for the two possibilities are, of course, the same. However, the ^1H NMR spectrum of the complex allows a distinction to be made between them.

The effect of the four-electron oxidation on the ^1H NMR spectrum of $[Ru(bpy)_2(NH_2CH_2CH{=}CH_2)_2]^{2+}$ is shown in Figure 2. The spectrum of the bis(allylamine) complex (2A) has a typically broad and complicated region due to the 2,2′-bipyridine protons (δ 7.1–9.6 ppm, relative to Me_4Si). The $-CH{=}CH_2$ proton resonances appear at high-

er field (δ 4.7–6.1 ppm), and the $-NH_2$ and $>CH_2$ resonances are centered at δ 4.2 and 2.8 ppm, respectively.

The four-electron oxidation product has the spectrum shown in Figure 2B. An integrated spectrum indicates that the $-NH_2$ and $>CH_2$ regions are reduced to half their intensity relative to the bpy region when compared with 2A. The changes in the ^1H NMR spectra require that the four-electron oxidation product be $[Ru(bpy)_2(NH_2CH_2CH{=}CH_2)(N{\equiv}CCH{=}CH_2)]^{2+}$ and not $[Ru(bpy)_2(NH{=}CHCH{=}CH_2)_2]^{2+}$. In the latter case the imine protons would be expected to appear at lower field. Furthermore, the new resonance in the $-CH{=}CH_2$ region in 2B (δ 6.2 ppm) is an obvious characteristic of the acrylonitrile ligand, since for the bis(acrylonitrile) complex (Figure 2C) this peak constitutes the entire $-CH{=}CH_2$ resonance.

The ^1H NMR spectral changes upon oxidation for the benzylamine complex are analogous to the changes shown in Figure 2. The ^1H NMR experiment clearly shows that the four-electron oxidation product is the amine–nitrile complex, and, consequently, that the four-electron oxidation of $[Ru(bpy)_2(NH_2CH_2R)_2]^{2+}$ is described satisfactorily by eq 3.

It is worth noting that the $[Ru(bpy)_2(NH_2CH_2CH{=}CH_2)(N{\equiv}CCH{=}CH_2)]^{3+/2+}$ couple is reversible only at scan rates of > 500 mV/s. This indicates that at slower scan rates further ligand oxidation is competitive with recapture of Ru(III) at the electrode.

A further oxidation process occurs past the n = 4.0 stage. Continued electrolysis on the diffusion plateau of the $E_{1/2}$ = 1.29 V wave (at 1.35 V) gave rise to a further oxidation. If the electrolysis is stopped at n = 2.0 (n_{total} = 6.0 based on $[Ru(bpy)_2(NH_2CH_2Ph)_2]^{2+}$ as the starting complex) there are two reversible waves in the cyclic voltammogram (Figure 1D), with equal peak currents. The wave at $E_{1/2}$ = 1.29 V is clearly unreacted $[Ru(bpy)_2(NH_2CH_2Ph)(N{\equiv}CPh)]^{2+}$, and the wave at $E_{1/2}$ = 1.52 V corresponds to an n = 4.0 (n_{total} = 8.0) oxidation product. Exhaustive electrolysis on the diffusion plateau of the $E_{1/2}$ = 1.29 V wave gave n_{total} = 8.0, and the complex with $E_{1/2}$ = 1.52 V as the sole product (Figure 1E). Spectral, electrochemical, and chemical isolation studies have shown that the eight-electron product is the totally oxidized, bis(nitrile) complex, $[Ru(bpy)_2(N{\equiv}CPh)_2]^{2+}$ (eq 4).

$$[Ru(bpy)_2(NH_2CH_2R)(N{\equiv}CR)]^{2+} \xrightarrow{-4e^-} [Ru(bpy)_2(N{\equiv}CR)_2]^{2+} + 4H^+ \quad (4)$$

The ^1H NMR spectrum of the bis(acrylonitrile) complex in acetone-d_6 is shown Figure 2C.

As shown by cyclic voltammetry (Figure 1E and Table I), the bis(nitrile) complexes undergo reversible one-electron oxidations at relatively high reduction potentials. It is expected that the ruthenium(III) nitrile complexes, $[Ru(bpy)_2(N{\equiv}CR)_2]^{3+}$, should undergo rapid hydrolysis at the nitrile group to give the corresponding amides,[10,15] but these reactions have not yet been investigated.

Infrared Spectra. Infrared spectra are also informative as to the nature of the four- and eight-electron oxidation products. The four-electron products of $[Ru(bpy)_2(allylamine)_2]^{2+}$ and $[Ru(bpy)_2(benzylamine)_2]^{2+}$ have bands at 2238 and 2235 cm^{-1}, respectively, indicating the presence of nitrile ligands. Both $[Ru(bpy)_2(acrylonitrile)_2]^{2+}$ and $[Ru(bpy)_2(benzonitrile)_2]^{2+}$ have $\nu_{C{\equiv}N}$ bands at 2235 cm^{-1}.

For coordinated organonitriles where little back-bonding is expected, such as in Rh(III),[16] Ru(III),[17] and Co(III)[18] complexes, the $\nu_{C{\equiv}N}$ band is found to be 50–70 cm^{-1} higher than for the uncoordinated nitrile. In the case of $[Ru(NH_3)_5(N{\equiv}CR)]^{2+}$, $\nu_{C{\equiv}N}$ was found to decrease (0–50 cm^{-1}) from the free ligand value. The decrease has been attributed to the strong back-bonding donor ability of the $(NH_3)_5Ru^{2+}$ moiety.[17] In the nitrilebis(2,2′-bipyridine) complexes of Ru(II), $\nu_{C{\equiv}N}$ increases slightly compared to the free ligand (*n*-butyronitrile, 2271 vs. 2253 cm^{-1}; acrylonitrile, 2238 vs. 2234 cm^{-1}), or is unchanged (benzonitrile, $\nu_{C{\equiv}N}$ 2235 cm^{-1} in both cases). The increases in $\nu_{C{\equiv}N}$ are small compared with related Ru(III), Rh(III), and Co(III) cases, which is reasonable and probably means that π-back-bonding in the $Ru(bpy)_2^{2+}$ complexes is present, but to a lesser extent than in $(NH_3)_5Ru^{2+}$ type complexes. The conclusion is expected, given the strongly back-bonding acceptor nature of the 2,2′-bipyridine ligands.

Table II. Electronic Spectral Data for the Amine–Nitrile Complexes of Bis(2,2′-bipyridine)ruthenium(II) in Acetonitrile

Complex	λ_{max}, nm(ϵ)[a]
$[Ru(bpy)_2(NH_2CH_2Ph)_2]^{2+}$	491 (9 200)
	348 (7 400)
	297 (54 100)
	248 (17 500)
$[Ru(bpy)_2(NH_2CH_2Ph)(N{\equiv}CPh)]^{2+}$	449 (10 000)
	291 (61 100)
	235 (29 100)
$[Ru(bpy)_2(N{\equiv}CPh)_2]^{2+}$	414 (9 500)
	286 (57 400)
	228 (38 500)
$[Ru(bpy)_2(NH_2CH_2CH{=}CH_2)_2]^{2+}$	492 (8 800)
	349 (7 100)
	296 (56 600)
	248 (17 300)
$[Ru(bpy)_2(NH_2CH_2CH{=}CH_2)(N{\equiv}CCH{=}CH_2)]^{2+}$	446 (8 300)
	290 (57 500)
	246 (22 700)
$[Ru(bpy)_2(N{\equiv}CCH{=}CH_2)_2]^{2+}$	416 (9 300)
	286 (58 000)
	256 (17 900)
	247 (17 900)
$[Ru(bpy)_2(NH_2CH_2CH_2CH_2CH_3)_2]^{2+}$	496 (8 700)
	352 (7 300)
	297 (56 800)
	248 (17 800)
$[Ru(bpy)_2(NH_2CH_2CH_2CH_2CH_3)(N{\equiv}CCH_2CH_2CH_3)]^{2+}$	450 (7 500)
	287 (53 100)
	242 (17 600)
$[Ru(bpy)_2(N{\equiv}CCH_2CH_2CH_3)_2]^{2+}$	427 (8 500)
	287 (55 300)
	246 (17 400)

[a] λ values are ±2 nm; ϵ values are ±5%.

Electronic Spectra and Reduction Potentials. Electronic spectra (Table II) and Ru(III)/Ru(II) reduction potentials (Table I) also reflect the effects of back-bonding, but at the metal rather than at the nitrile ligand. The spectra of the bis(amine) complexes are similar to the spectrum of $[Ru(bpy)_2(NH_3)_2]^{2+}$, having two maxima in the visible region (ca. 490 and 345 nm) which have previously been assigned to $d\pi(Ru(II)) \rightarrow \pi^*(bpy)$ MLCT transitions.[19] There are also two maxima in the ultraviolet region (ca. 290 and 245 nm) which have been assigned as $\pi \rightarrow \pi^*(bpy)$ transitions for $[Ru(bpy)_2(NH_3)_2]^{2+}$.[19] Upon the replacement of an amine ligand by a nitrile group, only one $d\pi(Ru(II)) \rightarrow \pi^*(bpy)$ MLCT absorption band is found in the visible region and that band is at higher energy (450 nm). Both observations are consistent with an increase in back-bonding leading to a relative stabilization of the $d\pi$ orbitals.[7,19] This trend continues for the bis(nitrile) complexes where λ_{max}

for the single $d\pi(Ru(II)) \rightarrow \pi^*(bpy)$ band is between 414 and 427 nm (Table II). The positions of the absorbance maxima and $\nu_{C\equiv N}$ stretching frequencies for the bis(nitrile) complexes are consistent with the qualitative order of back-bonding: benzonitrile > acrylonitrile > *n*-butyronitrile.

The conclusions concerning the stabilization of $d\pi(Ru)$ levels by back-bonding are borne out by $E_{1/2}$ values for the series of Ru(III)/Ru(II) couples given in Table I. From a variety of evidence, metal → ligand back-bonding is relatively unimportant in complexes of Ru(III).[20] The effect of replacing saturated amine ligands by back-bonding ligands is to stabilize the $d\pi$ levels of Ru(II) which stabilizes the Ru(II) state. In the bis(bipyridine) complexes, the Ru(II) state is already strongly stabilized by back-bonding to the 2,2′-bipyridine ligands. However, Ru(III)/Ru(II) redox potentials remain sensitive to changes in the ligands at the fifth and sixth coordination sites.[21] This can be seen clearly in the data in Table I where the redox potentials fall into three classes: bis(amines), 1.03–1.04 V amine-nitriles, 1.24–1.29 V; bis(nitriles), 1.48–1.52 V. Changes in reduction potentials follow directly from the number of back-bonding ligands in the fifth and sixth coordination positions.

Solutions of the bis(amine) complexes in acetonitrile were found to be stable over many hours in the dark. However, in normal laboratory lighting, a clean reaction occurred which exhibited well-defined isosbestic points when monitored in the uv-visible spectral region. The photochemical reactions are apparently light-induced substitutions to give amine-acetonitrile complexes. The products had spectra which were very similar to the amine-nitrile complexes (Table II). The amine-nitrile and bis(nitrile) complexes were more stable in solution, but prolonged exposure to light caused substitution of acetonitrile into the coordination sphere. Because of the light sensitivity, much of the work reported here, including the electrochemical and spectral studies, was carried out on solutions which were protected from the light.

Oxidation by Ce(IV). Mechanism of Oxidative Dehydrogenation. The bis(amine) complexes are oxidized rapidly and quantitatively by Ce(IV) in acetonitrile. Spectrophotometric experiments have shown that upon addition of 4 mol of Ce(IV) per mole of $[Ru(bpy)_2(NH_2CH_2Ph)_2]^{2+}$, the resulting product is the amine-nitrile complex (eq 5).

$$[Ru(bpy)_2(NH_2CH_2Ph)_2]^{2+} + 4Ce(IV) \rightarrow [Ru(bpy)_2(NH_2CH_2Ph)(N{\equiv}CPh)]^{2+} + 4H^+ + 4Ce(III) \quad (5)$$

When 8 mol of Ce(IV) are added, the bis(nitrile) complex is the product (eq 6).

$$[Ru(bpy)_2(NH_2CH_2Ph)_2]^{2+} + 8Ce(IV) \rightarrow [Ru(bpy)_2(N{\equiv}CPh)_2]^{2+} + 8H^+ + 8Ce(III) \quad (6)$$

The Ce(IV) oxidations were followed stepwise by spectrophotometric titrations using a fast mixing device. The titrations were followed in two stages: 0–4 mol of added Ce(IV)/mole of complex, and 4–8 mol of added Ce(IV). In neither stage were isosbestic points observed. If clean mixtures of $[Ru(bpy)_2(NH_2CH_2Ph)_2]^{2+}$ and $[Ru(bpy)_2(NH_2CH_2Ph)(N{\equiv}CPh)]^{2+}$ (0–4 mol of Ce(IV) added) or of $[Ru(bpy)_2(NH_2CH_2Ph)(N{\equiv}CPh)]^{2+}$ and $[Ru(bpy)_2(N{\equiv}CPh)_2]^{2+}$ (4–8 mol of Ce(IV)) had been present in the solutions, isosbestic points would be expected. The absence of isosbestic points indicates the existence of intermediates in the titrations. Since the overall reactions are quantitative, the most reasonable intermediates are two-electron oxidation products containing bound imine groups: $[Ru(bpy)_2(NH_2CH_2Ph)(NH{=}CHPh)]^{2+}$ and $[Ru(bpy)_2(NH{=}CHPh)(N{\equiv}CPh)]^{2+}$. This conclusion is reasonable in light of evidence obtained recently for imine intermediates in the oxidation of amines bound to $(NH_3)_5Ru(II)$[10] and in the oxidation of coordinated diamines to α,α'-diimines.[7]

Preliminary stopped-flow kinetic studies of the oxidation reaction revealed, by direct observation of the Ru(III) species, that the Ru(II) → Ru(III) oxidation step occurs very rapidly[22] so that the ligand dehydrogenation is necessarily a subsequent process. Detailed kinetic data are not available for the dehydrogenation reactions, so that proposal of a detailed mechanism is not possible. However, assuming the intermediacy of the imine species, a series of *net* reactions can be written for the oxidation process. For example, on removal of one electron per mole of complex:

$$2[Ru(bpy)_2(NH_2CH_2Ph)_2]^{2+} \xrightarrow{-2e^-} 2[Ru(bpy)_2(NH_2CH_2Ph)_2]^{3+} \quad (7)$$

$$2[Ru(bpy)_2(NH_2CH_2Ph)_2]^{3+} \rightarrow [Ru(bpy)_2(NH_2CH_2Ph)(NH{=}CHPh)]^{2+} + [Ru(bpy)_2(NH_2CH_2Ph)_2]^{2+} + 2H^+ \quad (8)$$

The two-electron oxidation of the ligand by the one-electron oxidant (Ru(III)) requires a *net* disproportionation of the type given in eq 8; furthermore, there is direct evidence for a *net* reaction of this type in the metal-assisted oxidation of $Ru(bpy)_2(2\text{-aminomethylpyridine})^{2+}$.[7] Upon removal of a second electron, a similar sequence of *net* reactions can be written:

$$2[Ru(bpy)_2(NH_2CH_2Ph)(NH{=}CHPh)]^{2+} \xrightarrow{-2e} 2[Ru(bpy)_2(NH_2CH_2Ph)(NH{=}CHPh)]^{3+} \quad (9)$$

$$2[Ru(bpy)_2(NH_2CH_2Ph)(NH{=}CHPh)]^{3+} \rightarrow [Ru(bpy)_2(NH_2CH_2Ph)(N{\equiv}CPh)]^{2+} + [Ru(bpy)_2(NH_2CH_2Ph)(NH{=}CHPh)]^{2+} + 2H^+ \quad (10)$$

Oxidation up to the eight-electron stage (the bis(nitrile) complex) can be represented by a related series of net reactions.

It should be noted that the Ru(III) imine complex is also accessible by reactions such as that given in eq 11:

$$[Ru(bpy)_2(NH_2CH_2Ph)_2]^{3+} + [Ru(bpy)_2(NH_2CH_2Ph)(NH{=}CHPh)]^{2+} \rightarrow [Ru(bpy)_2NH_2CH_2Ph)_2]^{2+} + [Ru(bpy)_2(NH_2CH_2Ph)(NH{=}CHPh)]^{3+} \quad (11)$$

Such reactions are known to be rapid in related systems.[23] We emphasize again that detailed mechanistic information is not yet available for the individual steps and that following oxidation of Ru(II) to Ru(III) a series of interrelated reactions occurs.

In the electrochemical experiments there was no evidence for either of the imine intermediates (Figure 1). This is reasonable since electrochemical oxidation processes (eq 7 and 9) are far slower than Ce(IV) oxidations, and reactions like eq 11 allow for the conversion of the imine intermediates into the amine-nitrile and bis(nitrile) products before their concentrations become appreciable.

The ligand oxidation reactions are much more rapid in acidic aqueous solution than in acetonitrile. Cyclic voltammograms of the amine complexes in 1.0 M HCl were completely irreversible at scan rates up to 50 V/s, indicating that ligand oxidation is more rapid than recapture of Ru(III) at the electrode. Electrolysis to $n = 4.0$ at potentials more anodic than E_p for the irreversible Ru(II) → Ru(III) step, gave a mixture of 0-, 4-, and 8-electron products for R = $-CH_2CH_2CH_3$ and $-CH{=}CH_2$, and the

amine–nitrile complex was obtained cleanly only for benzylamine.

Acknowledgment is made to the Materials Research Center of the University of North Carolina under Grant No. DAHC15 73 G9 with DARPA for support of this work.

References and Notes

(1) N. F. Curtis, *Chem. Commun.*, 881 (1966); *Coord. Chem. Rev.*, **3**, 3 (1968).
(2) J. C. Dabrowiak, F. V. Lovecchio, V. L. Goedken, and D. H. Busch, *J. Am. Chem. Soc.*, **94**, 5502 (1972); V. L. Goedken and D. H. Busch, *ibid.*, **94**, 7355 (1972).
(3) H. Elsbernd and J. K Beattie, *J. Chem. Soc. A*, 2598 (1970).
(4) B. C. Lane, J. E. Lester, and F. Basolo, *Chem. Commun.*, 1618 (1971).
(5) D. F. Mahoney and J. K. Beattie, *Inorg. Chem.*, **12**, 2561 (1973).
(6) V. L. Goedken, *J. Chem. Soc., Chem. Commun.*, 207 (1972).
(7) G. M. Brown, T. R. Weaver, F. R. Keene, and T. J. Meyer, *Inorg. Chem.*, **15**, 190 (1976).
(8) H. L. Chum and P. Krumholz, *Inorg. Chem.*, **13**, 514, 519 (1974).
(9) W. R. McWhinnie, J. D. Miller, J. B. Watts, and D. Y. Wadden, *Chem. Commun.*, 629 (1971); *Inorg. Chim. Acta*, **7**, 461 (1973).
(10) S. E. Diamond, G. M. Tom, and H. Taube, *J. Amer. Chem. Soc.*, **97**, 2661 (1975).
(11) G. M. Brown, R. W. Callahan, and T. J. Meyer, *Inorg. Chem.*, **14**, 1915 (1975).
(12) J. B. Godwin and T. J. Meyer, *Inorg. Chem.*, **10**, 471 (1971).
(13) S. A. Adeyemi, Ph.D. Dissertation, University of North Carolina at Chapel Hill, 1973.
(14) Electrochemical reversibility was determined, when possible, by plots of log $(i_f - i)/i$ vs. E using stirred-solution voltammetry data. In cases where subsequent ligand reactions were too rapid, reversibility was determined using cyclic voltammetry using the ratio of anodic to cathodic peak currents (i_c/i_a), ΔE_p = 60–65 mV and the sweep rate independence of ΔE_p as criteria. The slightly greater value of ΔE_p than the theoretical value of 59 mV can be attributed to uncompensated solution resistance.
(15) A. W. Zanella and P. C. Ford, *Inorg. Chem.*, **14**, 42 (1975).
(16) R. D. Foust and P. C. Ford, *Inorg. Chem.*, **11**, 899 (1972).
(17) R. E. Clarke and P. C. Ford, *Inorg. Chem.*, **9**, 227 (1970).
(18) D. Pinnell, G. B. Wright, and R. B. Jordan, *J. Am. Chem. Soc.*, **94**, 6104 (1972); F. R. Keene and J. MacB. Harrowfield, unpublished data, Australian National University, Canberra, 1973.
(19) G. M. Bryant, J. E. Fergusson, and H. J. K. Powell, *Aust. J. Chem.*, **24**, 257 (1971).
(20) H. Taube, *Surv. Prog. Chem.*, **6**, 1 (1973).
(21) G. M. Brown, Ph.D. Dissertation, University of North Carolina, Chapel Hill, N.C., 1974.
(22) E. M. Gupton and F. R. Keene, unpublished data, University of North Carolina, Chapel Hill, 1974.
(23) J. C. Solenburger, Ph.D. Dissertation, Washington University, St. Louis, Mo., 1969; M. Chan and A. C. Wahl, 167th National Meeting of the American Chemical Society, Los Angeles, Calif., 1974, Abstract INOR 97.

[Reprinted from Inorganic Chemistry, 15, 190 (1976).]
Copyright 1976 by the American Chemical Society and reprinted by permission of the copyright owner.

Contribution from the W. R. Kenan, Jr., Laboratories, Department of Chemistry, University of North Carolina, Chapel Hill, North Carolina 27514

Oxidation of Coordinated Diamines in Bis(2,2'-bipyridine) Complexes of Ruthenium

GILBERT M. BROWN, THOMAS RAY WEAVER, F. RICHARD KEENE, and THOMAS J. MEYER*

Received May 28, 1975 AIC503632

A series of diaminebis(2,2'-bipyridine) complexes of ruthenium(II), e.g., $[Ru(bipy)_2(en)]^{2+}$, has been prepared and the spectral and redox properties were investigated. The ethylenediamine and *trans*-1,2-diaminocyclohexane complexes undergo net four-electron oxidations, either chemically or electrochemically, giving the corresponding α,α'-diimine complexes. The chemical and spectral properties of the α,α'-diimine complexes are similar to those of $[Ru(bipy)_3]^{2+}$. Complexes containing 2-(aminomethyl)pyridine and 1,2-diamino-2-methylpropane undergo net two-electron oxidations, in which the single CH_2–NH_2 linkage has undergone oxidative dehydrogenation to the imine. Electrochemical and titrimetric data (using Ce(IV)) in acetonitrile show that the diamine oxidative dehydrogenation reactions are initiated by oxidation of ruthenium(II) to ruthenium(III), and that the reactions probably occur in a stepwise manner via monoimine intermediates.

Introduction

Metal ions have been found to catalyze the oxidative dehydrogenation of coordinated amines to imines. The oxidation of macrocyclic amine complexes to imine complexes was investigated by Curtis[1] and Busch et al.,[2] and their studies have provided some insight into the mechanism of oxidative dehydrogenation. It was observed that the macrocyclic amine complexes of Ni^{2+}, Cu^{2+}, and Fe^{2+} undergo oxidative dehydrogenation whereas the complexes of Co^{3+} are resistant to oxidation. This indicated that the net reaction involved prior oxidation of the metal ion followed by oxidation of the ligand and reduction of the metal ion.

Elsbernd and Beattie[3] reported that $[Ru^{II}(en)_3]^{2+}$ (en is ethylenediamine) undergoes a net four-electron oxidation, and Lane, Lester, and Basolo[4] showed that the reaction involved oxidative dehydrogenation of ethylenediamine to give an α,α'-diimine (dim) complex of Ru(II)

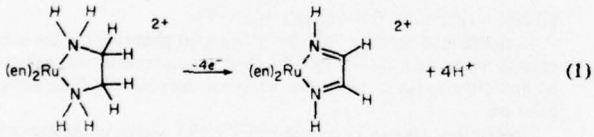

(1)

Mahoney and Beattie[5] have since reported that $[Ru(phen)_2(en)]^{2+}$ undergoes a four-electron oxidation giving $[Ru(phen)_2(dim)]^{2+}$. They also found Ru(III) intermediates in the oxidations of both $[Ru(phen)_2(en)]^{2+}$ and $[Ru(en)_3]^{2+}$. Similar oxidative dehydrogenation reactions have been observed for diamine complexes of tetracyanoferrate(II);[6] isolation of the tetracyanoethylenediamineiron(III) ion demonstrated the intermediacy of Fe(III) in the net reaction.

We have become interested in redox processes involving coordinated ligands, and in how such processes are affected by a variety of molecular features.[7-10] As part of this interest, we have studied the oxidation of a series of diaminebis(2,2'-bipyridine)ruthenium(II) complexes. In the study, evidence has been found which indicates that the oxidative dehydrogenation reactions proceed in a stepwise manner through Ru(III) intermediates.

Experimental Section

Measurements. Ultraviolet–visible spectra were obtained on Cary Model 14, Cary Model 17, or Unicam Model SP-800B spectrophotometers. Molar extinction coefficients were determined from absorbance measurements on three or more concentrations. Absorbances were checked on a Gilford Model 240 spectrometer. Infrared spectra were obtained using a Perkin-Elmer Model 421 spectrometer or a Digilab Model FTS-14 interferometer. ^1H NMR spectra were obtained on a Jeol C-60-HL spectrometer, using D_2O solutions with *t*-BuOH as an internal reference.

All electrochemical measurements were made vs. the saturated sodium chloride calomel electrode (SSCE) at 25 ± 2°C, and are uncorrected for junction potentials. All potentials reported are reduction potentials vs. the SSCE. Potential control for electrochemical experiments was obtained with a Princeton Applied Research Model 173 Potentiostat/Galvanostat. The waveform generator for voltammetric experiments was a Princeton Applied Research Model 175 Universal Programmer. Voltammograms and slow scan cyclic voltammograms were recorded on a Hewlett-Packard Model 7004B X–Y recorder. Fast scan cyclic voltammograms were obtained from photographs of the trace of a Tektronix Model 564B storage oscilloscope. Values of *n*, where *n* is the total number of equivalents of electrons transferred in exhaustive electrolyses at constant potentials, were calculated after measuring the total area under current vs. time curves for the complete reaction. Reactions were judged to be complete when the current had fallen below 1% of the initial value. All voltammetric measurements were carried out at platinum electrodes in solutions deaerated with a stream of dry, prepurified nitrogen. Platinum electrodes were cleaned by the procedure recommended by Adams.[11] Elemental analyses were carried out by Galbraith Laboratories, Inc., Knoxville, Tenn.

Materials. Tetra-*n*-butylammonium hexafluorophosphate (*TBAH*) was prepared by standard techniques,[12] recrystallized three times from hot ethanol–water mixtures, and vacuum dried at 80°C for 12 hr. Acetonitrile (MCB Spectrograde) was dried over Davison 4 Å molecular sieves for electrochemical measurements and used without drying for spectral measurements. Water was deionized and then distilled from alkaline permanganate. The ligands ethylenediamine, *trans*-1,2-diaminocyclohexane, 1,3-propylenediamine, 1,2-diamino-2-methylpropane, 2-(2'-aminoethyl)pyridine, and 2-(aminomethyl)pyridine were purchased commercially and used without further purification. (A list of the ligands used in this study, as well as their formulas and abbreviations, is given in Table I). The complexes $[Ru(bipy)_2Cl_2]\cdot 2H_2O$,[13] $[Ru(bipy)_3](ClO_4)_2$,[14] and $[Ru(bipy)_2(NH_3)_2](ClO_4)_2\cdot 3H_2O$[15] were prepared as previously described. All other chemicals were commercially available in reagent quality and were used without further purification.

$[Ru(bipy)_2(LL)](ClO_4)_2$ (LL = Ethylenediamine (en), *trans*-1,2-Diaminocyclohexane (dach), 1,2-Diamino-2-methylpropane (damp), 2-(2'-Aminoethyl)pyridine (AEPy), and 2-(Aminomethyl)pyridine (AMPy)). The diamine complexes were prepared by essentially the same procedure described for the preparation of the complexes $[Ru(bipy)_2(en)](ClO_4)_2$[15] and $[Ru(phen)_2(en)]I_2\cdot 2H_2O$.[16] The complex $[Ru(bipy)_2Cl_2]\cdot 2H_2O$ (0.50 g) was suspended in a 1:1 (by volume) water–methanol solution (30 ml) of the ligand (3 g). The mixture was heated at reflux on a steam bath for 1 hr under an atmosphere of nitrogen. The condenser was removed and the methanol was boiled off under a stream of nitrogen. The deep red solution was cooled and filtered. The filtrate was returned to the steam bath and warmed to 80–90°C. A saturated aqueous solution of $NaClO_4$ was added dropwise to the warm solution until the onset of precipitation. Slow cooling to room temperature gave deep red crystals which were collected by suction filtration, washed with small portions of ice cold water and methanol, and air dried. The products could be recrystallized from hot water containing a small amount of $NaClO_4$. Yields were 70% or greater.

Anal. Calcd for $[Ru(bipy)_2(en)](ClO_4)_2$: C, 39.3; H, 3.60; N, 12.5. Found: C, 39.3; H, 3.71; N, 12.3. Calcd for $[Ru(bipy)_2$-

* N. F. Curtis, *Chem. Commun.*, 881 (1966); *Coord. Chem. Rev.*, 3, 3 (1968).

Table I. Abbreviations and Chemical Formulas for Amine and Imine Ligands

Ligand	Formula	Abbreviation
Ethylenediamine	$H_2N-CH_2-CH_2-NH_2$	en
1,2-Diiminoethane	$HN=CH-CH=NH$	dim
trans-1,2-Diaminocyclohexane	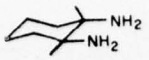	dach
1,2-Diiminocyclohexane	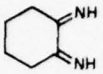	dich
1,2-Diamino-2-methylpropane	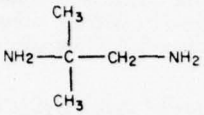	damp
2-Amino-2-methylpropanalimine	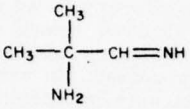	iamp
1,3-Propylenediamine (trimethylenediamine)	$NH_2-CH_2-CH_2-CH_2-NH_2$	tn
2-(Aminomethyl)pyridine	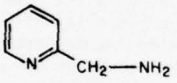	AMPy
2-(Iminomethyl)pyridine	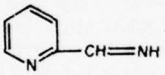	IMPy
2-(2'-Aminoethyl)pyridine	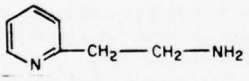	AEPy
Glyoxalbismethylimine	$CH_3N=CH-CH=NCH_3$	GMI

(dach)](ClO4)2: C, 43.0; H, 4.16; N, 11.6. Found: C, 43.0; H, 4.00; N, 11.4. Calcd for [Ru(bipy)2(damp)](ClO4)2: C, 41.2; H, 4.03; N, 12.0. Found: C, 41.0; H, 3.95; N, 11.9. Calcd for [Ru(bipy)2(AEPy)](ClO4)2: C, 44.2; H, 3.57; N, 11.4. Found: C, 43.9; H, 3.45; N, 10.8. Calcd for [Ru(bipy)2(AMPy)](ClO4)2: C, 43.3; H, 3.36; N, 11.7. Found: C, 43.5, H, 3.28; N, 11.5.

[Ru(bipy)2(tn)](PF6)2·2H2O (tn = 1,3-Propylenediamine). The complex was prepared as described above. The salt was precipitated by the addition of a filtered aqueous solution of NH_4PF_6 to a filtered, aqueous solution of the complex. The product was purified by reprecipitation from acetone–ether and vacuum dried overnight.

Anal. Calcd for [Ru(bipy)2(tn)](PF6)2·2H2O: C, 34.0; H, 3.72; N, 10.3. Found: C, 33.1; H, 3.06; N, 10.6.

[Ru(bipy)2(LL)](PF6)2 (LL = 1,2-Ethylenediimine (dim), 1,2-Diiminocyclohexane (dich), 2-(Iminomethyl)pyridine (IMPy)). The corresponding diaminebis(bipyridine)ruthenium(II) complex (100 mg) was dissolved in 1.0 *M* aqueous HCl (30 ml). The solution was oxidized by exhaustive electrolysis at constant potential which was anodic of $E_{1/2}$. It is essential that the potentials not be made so anodic that the desired diimine products are oxidized. Electrolysis was continued until the current had fallen to about 1% of the initial current. The product was precipitated from solution by the addition of a filtered, saturated, aqueous solution of NH_4PF_6 (2 ml). The product was purified by reprecipitation from acetone–ether.

Anal. Calcd for [Ru(bipy)2(dim)](PF6)2: C, 34.8; H, 2.65; N, 11.1; F, 30.0. Found: C, 34.7; H, 2.75; N, 10.9; F, 29.8. Calcd for [Ru(bipy)2(dich)](PF6)2·2H2O: C, 36.8; H, 3.56; N, 9.9; F, 26.8. Found: C, 36.9; H, 3.26; N, 9.9; F, 26.6. Calcd for [Ru(bipy)2(IMPy)](PF6)2: C, 38.6; H, 2.75; N, 10.4; F, 28.2. Found: C, 38.3; H, 2.68; N, 10.3; F, 28.0.

[Ru(bipy)2(iamp)]2+ (iamp = 2-Amino-2-methylpropanalimine). This complex was prepared in situ and not isolated. Attempts to isolate salts of the complex failed to give a pure material. Solutions of the complex were prepared from solutions of $[Ru(bipy)_2(damp)]^{2+}$ in 0.1 *M* TBAH–CH_3CN by exhaustive electrolysis at the $E_{1/2}$ of the $[Ru(bipy)_2(damp)]^{3+/2+}$ couple (0.99 V).

Conversion of perchlorate or hexafluorophosphate salts of the above cations to the chloride salt for ^1H NMR measurements was achieved by precipitation (using tetra-*n*-butylammonium chloride) from acetone solution.

Spectrophotometric Titrations with Ce(IV). Some of the oxidative dehydrogenation reactions were studied by spectrophotometric titrations in 0.1 *M* aqueous $HClO_4$ and acetonitrile solutions, using Ce(IV) as oxidant. The concentration of Ce(IV) was determined spectrophotometrically,[17] and the solutions were used immediately and protected from the light. Titrations were carried out by adding aliquots of oxidant to solutions of the complex, and monitoring the changes in absorbance in the range 600–320 nm. Some of the reactions studied required rapid mixing of the ruthenium and Ce(IV) solutions, which was accomplished by using a hand-driven device patterned after a stopped-flow syringe drive train.

Table II. Half-Wave Potentials and Electronic Spectra for Diaminebis(2,2'-bipyridine)ruthenium(II) Complexes in Acetonitrile

Compd	$E_{1/2}$, V[a]	λ_{max}, nm (ϵ)[b]
$Ru(bipy)_2(NH_3)_2^{2+}$	0.92	490 (9300) 345 (7600) 290 (54000) 243 (20000)
$Ru(bipy)_2(en)^{2+}$	0.96	485 (9900) 344 (7600) 291 (60000) 243 (21000)
$Ru(bipy)_2(dach)^{2+}$	0.96	488 (9900) 344 (7600) 292 (58000) 244 (21000)
$Ru(bipy)_2(damp)^{2+}$	0.99	487 (10000) 345 (7600) 292 (58000) 244 (21000)
$Ru(bipy)_2(tn)^{2+}$	~0.98	492 (8500) 348 (6600) 292 (52000) 244 (18000)
$Ru(bipy)_2(AMPy)^{2+}$	1.12	471 (10000) 422 (sh) (6300) 339 (11000) 298 (55000) 244 (23000)
$Ru(bipy)_2(AEPy)^{2+}$	1.12	471 (9000) 425 (sh) (5600) 338 (9700) 289 (54000) 243 (23000)

[a] $E_{1/2}$ values vs. the saturated sodium chloride calomel electrode (SSCE) in 0.1 *M* $N(n\text{-}C_4H_9)_4PF_6$ at 25 ± 2°C. [b] λ_{max} values ± 2 nm; ϵ values ±5%.

Results and Discussion

Net Electrochemical Oxidation of Bound Diamine Ligands. The complex $[Ru(bipy)_2(NH_3)_2]^{2+}$ undergoes an electrochemically reversible one-electron oxidation at a platinum electrode in acetonitrile, as shown by the cyclic voltammogram in Figure 1A. Under the same experimental conditions, the complex $[Ru(bipy)_2(en)]^{2+}$ also undergoes an electrochemically reversible one-electron oxidation on the cyclic voltammetry time scale (Figure 1B).[18] The similarity in reduction potentials for the series of diamine complex 3+/2+ couples studied and that for the $[Ru(bipy)_2(NH_3)_2]^{3+/2+}$ (Table II) indicates that this oxidation occurs in all cases at the ruthenium.

Exhaustive electrolysis of acetonitrile solutions of $[Ru(bipy)_2(en)]^{2+}$ at a constant potential (1.15 V) on the diffusion plateau for the voltammetric wave gave a coulometric *n* value of 3.82. The product of the electrolytic oxidation was identified by spectral and electrochemical measurements (see below) as the α,α'-diimine complex, $[Ru(bipy)_2(dim)]^{2+}$. The net

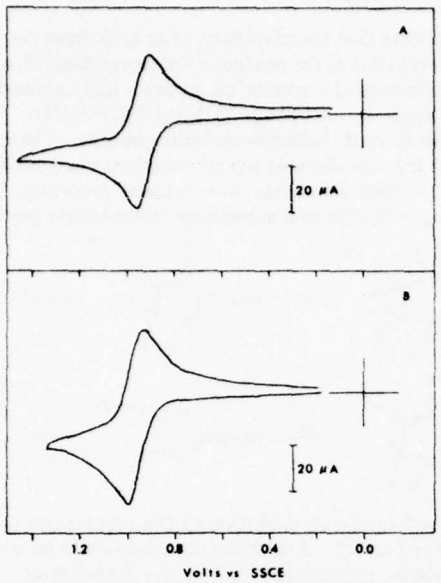

Figure 1. Cyclic voltammograms (200 mV/sec) of (A) $[Ru(bipy)_2(NH_3)_2]^{2+}$ (1.0×10^{-3} *M*), and (B) $[Ru(bipy)_2(en)]^{2+}$ (1.2×10^{-3} *M*) in acetonitrile solution (0.1 *M* TBAH).

stoichiometry of the oxidation is given by eq 2.

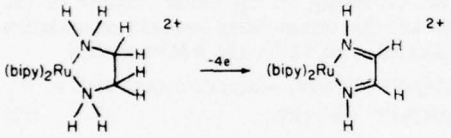

(2)

The oxidation process thus consists of two parts: initial oxidation of the metal to Ru(III)

$$[Ru(bipy)_2(en)]^{2+} \xrightarrow{-e^-} [Ru(bipy)_2(en)]^{3+} \quad (3)$$

followed by oxidation of the coordinated ligand

$$[Ru(bipy)_2(en)]^{3+} \xrightarrow{-3e^-} [Ru(bipy)_2(dim)]^{2+} + 4H^+ \quad (4)$$

In acetonitrile, for $[Ru(bipy)_2(en)]^{2+}$, and also for $[Ru(bipy)_2(dach)]^{2+}$, the initial one-electron oxidation is faster than the subsequent oxidation of the ligand. At slow voltammetry scan rates (0.2 V/sec), recapture of $[Ru(bipy)_2(en)]^{3+}$ by reduction at the electrode is more rapid than ligand oxidation, and the voltammetric waves are reversible.

In aqueous solution (1.0 *M* HCl or 1.0 *M* NaCl), electrochemical oxidation of $[Ru(bipy)_2(en)]^{2+}$ (or $[Ru(bipy)_2(dach)]^{2+}$) at a Pt electrode was irreversible, even by fast cyclic voltammetry (100 V/sec). Exhaustive electrolysis at 0.80 V (vs. SSCE) in 1.0 *M* HCl gave the corresponding α,α'-diimine complexes quantitatively and provided a convenient synthetic route to these complexes.

The ligand 2-(aminomethyl)pyridine (AMPy) contains one imine (pyridine) and one amine nitrogen atom, so that the α,α'-diimine linkage is half present initially. Exhaustive electrolysis of $[Ru(bipy)_2(AMPy)]^{2+}$ in acetonitrile at a potential on the diffusion plateau for oxidation (1.20 V) gave a coulometric *n* value of 1.96 and the α,α'-diimine complex as the sole product:

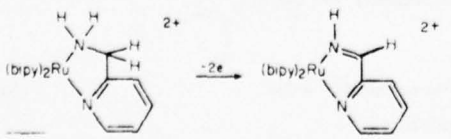

(5)

Cyclic voltammetry of $[Ru(bipy)_2(AMPy)]^{2+}$ at slow scan rates was irreversible, but at faster scan rates (≥5 V/sec) the cyclic voltammetric data were consistent with a reversible one-electron oxidation. Since the $[Ru(bipy)_2(AMPy)]^{3+/2+}$ potential (1.12 V) is higher than the potentials of the diamine complexes, the Ru(III) complex would be more strongly oxidizing and a higher rate of ligand oxidation (e.g., eq 4) is not unexpected.

Table III. Half-Wave Potentials and Electronic Spectra of Diiminebis(2,2'-bipyridine)ruthenium(II) Complexes in Acetonitrile

Compd	$E_{1/2}$, V[a]	λ_{max}, nm (ϵ)[b]
$Ru(bipy)_3^{2+}$	1.29	450 (14000) 283 (80000) 242 (25000)
$Ru(bipy)_2(dim)^{2+}$	1.33	454 (14000) 280 (46000) 242 (17000)
$Ru(bipy)_2(dich)^{2+}$	1.20	472 (16000) 285 (48000) 242 (18000)
$Ru(bipy)_2(iamp)^{2+}$	1.06	475 (9000) 335 (9100)
$Ru(bipy)_2(IMPy)^{2+}$	1.27	470 (13000) 430 (sh) 345 (sh) 315 (sh) 286 (51000) 245 (18000) 242 (20000)

[a] Vs. the SSCE in 0.1 *M* $N(n\text{-}C_4H_9)_4PF_6$ at 25 ± 2°C. [b] λ_{max} values are ±2 nm; ϵ values ±5%.

The ligand 1,2-diamino-2-methylpropane (damp) has a skeletal framework similar to ethylenediamine, but oxidative dehydrogenation can only occur at one $-CH_2-NH_2$ group, leading to a coordinated monoimine. Cyclic voltammetry in acetonitrile solution shows that $[Ru(bipy)_2(damp)]^{2+}$ undergoes an electrochemically reversible one-electron oxidation. Exhaustive electrolysis at $E_{1/2}$ gave an *n* value of 1.76 and near-quantitative conversion to a single product whose redox and spectral properties are consistent with a monoimine complex.

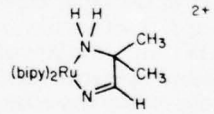

When electrolysis was carried out at potentials more anodic than $E_{1/2}$, further oxidation processes, involving the ion $[Ru(bipy)_2(iamp)]^{2+}$, occurred. The electrochemical oxidation of $[Ru(bipy)_2(damp)]^{2+}$ in aqueous solution was completely irreversible, and attempts to prepare the monoimine complex $[Ru(bipy)_2(iamp)]^{2+}$ by exhaustive electrolysis were frustrated by competitive processes involving oxidation of bound iamp. In both these cases, it is apparent that both $[Ru(bipy)_2(damp)]^{2+}$ and $[Ru(bipy)(iamp)]^{2+}$ are oxidizable, and that the oxidation rates are comparable. Because of the further ligand oxidation, a possible complicating reaction here, and in related systems, is bimolecular electron transfer giving the Ru(III) form of the ligand-oxidized complex,

$$[Ru(bipy)_2(damp)]^{3+} + [Ru(bipy)_2(iamp)]^{2+} \rightleftharpoons [Ru(bipy)_2(damp)]^{2+} + [Ru(bipy)_2(iamp)]^{3+} \quad (6)$$

Equation 6 is an equilibrium in which the forward reaction is slightly disfavored thermodynamically (using $E_{1/2}$ data in Tables II and III). From rate data on other bis(2,2'-bipyridine)ruthenium(III)–(II) electron transfer reactions,[20] the forward reaction should still be rapid, and if followed by rapid Ru(III) ligand oxidation accounts for such phenomena as the dependence of products on rates of mixing with chemical oxidants and our inability to prepare imine complexes in such systems.

The ligands 1,3-propylenediamine (tn) and 2-(2'-aminoethyl)pyridine (AEPy) contain one methylene group more than ethylenediamine and 2-(aminomethyl)pyridine, respectively, and hence cannot give conjugated α,α'-diimines upon oxidation. The complexes $[Ru(bipy)_2(tn)]^{2+}$ and $[Ru(bipy)_2(AEPy)]^{2+}$ undergo electrochemically reversible one-electron oxidations in acetonitrile solutions, as determined by cyclic voltammetry. Exhaustive electrolyses on the diffusion plateaus of the oxidation waves gave high n values and a variety of products (as shown by cyclic voltammetry), consistent with oxidation past the imine stage.

Oxidations by Ce(IV). Spectrophotometric Titrations. The oxidative dehydrogenation reactions could also be carried out chemically using Ce(IV). The Ce(IV) oxidations were studied by spectrophotometric titrations.

The spectrophotometric titration of $[Ru(bipy)_2(AMPy)]^{2+}$ with Ce(IV) in either acetonitrile or 0.1 *M* aqueous $HClO_4$ gave a smooth conversion to $[Ru(bipy)_2(IMPy)]^{2+}$ (isosbestic points at 388 and 513 nm) with the stoichiometry given in eq 7. The addition of more than 2 equiv of Ce(IV) per mole of

$$[Ru(bipy)_2(AMPy)]^{2+} + 2Ce(IV) \rightarrow [Ru(bipy)_2(IMPy)]^{2+} + 2Ce(III) + 2H^+ \quad (7)$$

ruthenium did not give a smooth conversion to the imine product. It appears that further oxidation of the ligand occurs, giving products which we have not characterized.

The oxidation of $[Ru(bipy)_2(damp)]^{2+}$ with Ce(IV) in acetonitrile led to the formation of $[Ru(bipy)_2(iamp)]^{2+}$, with the stoichiometry given in eq 8. The reactions were clean only

$$[Ru(bipy)_2(damp)]^{2+} + 2Ce(IV) \rightarrow [Ru(bipy)_2(iamp)]^{2+} + 2Ce(III) + 2H^+ \quad (8)$$

if the Ce(IV) and ruthenium solutions were mixed rapidly and 1 mol or less of Ce(IV) was added per mole of ruthenium. If these conditions were met, isosbestic points were observed at 477, 379, and 360 nm, and the observed spectra were consistent with the sums of the spectra of $[Ru(bipy)_2(damp)]^{2+}$ and $[Ru(bipy)_2(iamp)]^{2+}$ in the ratios expected from the stoichiometry given in eq 8. These results are understandable if the reaction of Ce(IV) with $[Ru(bipy)_2(damp)]^{2+}$ is faster than the oxidative dehydrogenation reaction, and the rate of further ligand oxidation of $[Ru(bipy)_2(iamp)]^{2+}$ is competitive with the initial oxidative dehydrogenation. The Ce(IV) oxidation of bis(2,2'-bipyridine)ruthenium(II) complexes is known to be very rapid.[20]

Titration of $[Ru(bipy)_2(dach)]^{2+}$ with Ce(IV) indicated a 4:1 stoichiometry with the formation of $[Ru(bipy)_2(dich)]^{2+}$, eq 9. Addition of 4 mol of Ce(IV) per mole of ruthenium

$$[Ru(bipy)_2(dach)]^{2+} + 4Ce(IV) \rightarrow [Ru(bipy)_2(dich)]^{2+} + 4Ce(III) + 4H^+ \quad (9)$$

gave a spectrum identical with that of an analyzed sample of $[Ru(bipy)_2(dich)]^{2+}$ prepared electrochemically. An isosbestic point occurred at 380 nm for all additions up to 4 mol of Ce(IV) per mole of ruthenium. However, the lack of an isosbestic point in the region of the 472-nm absorbance of $[Ru(bipy)_2(dich)]^{2+}$ and the 488-nm absorbance of $[Ru(bipy)_2(dach)]^{2+}$ indicated interference in this region from a third species. The likely explanation of this combination of observations is that an intermediate exists which contains one imine and one amine linkage. The addition of more than 4 mol of Ce(IV) per mole of ruthenium leads to complicated product spectra, probably due to the further oxidation of the α,α'-diimine ligand. The data indicate that the oxidative dehydrogenation leading to $[Ru(bipy)_2(dich)]^{2+}$ is faster than further oxidation of the coordinated dich ligand.

Spectrophotometric titrations of the complex $[Ru(bipy)_2(en)]^{2+}$ with Ce(IV) were extremely complicated. The data indicate that complications arise both from competitive further oxidation of the product, $[Ru(bipy)_2(dim)]^{2+}$, and from the interference of a species containing a half-oxidized ligand, with a single imine linkage ($HN{=}CHCH_2NH_2$).

Mechanism of Oxidative Dehydrogenation. These studies indicate that the diamine ligand oxidation, reaction 4, can be further broken down into two stepwise processes, the first involving oxidation to a monoimine intermediate (eq 10), and

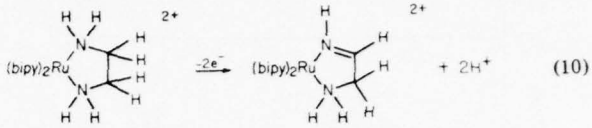

(10)

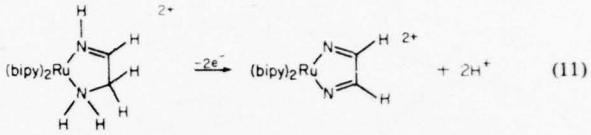

(11)

the second involving oxidation of the monoimine to the α,α'-diimine (eq 11). Analogous equations could be written for the oxidative dehydrogenation of the dach ligand.

For the complexes $[Ru(bipy)_2(AMPy)]^{2+}$ and $[Ru(bipy)_2(damp)]^{2+}$, only one of these two-electron steps is possible. On addition of a 1:1 stoichiometric quantity of Ce(IV) to a solution of either of these complexes, a clean oxidation occurs producing an equimolar mixture of the starting complex and the corresponding two-electron oxidation product, as indicated in eq 12 for the AMPy species:

$$2[Ru(bipy)_2(AMPy)]^{2+} + 2Ce(IV) \rightarrow [Ru(bipy)_2(AMPy)]^{2+} + [Ru(bipy)_2(IMPy)]^{2+} + 2Ce(III) \quad (12)$$

From the instantaneous color changes observed on the addition of Ce(IV) to solutions of the diamine complexes (spectrophotometric titrations), preliminary kinetic studies on the Ce(IV) oxidation of $[Ru(bipy)_2(en)]^{2+}$ and $[Ru(bipy)_2(AMPy)]^{2+}$,[20] and the electrochemical results, the initial step in the oxidation process involves oxidation of ruthenium(II) to ruthenium(III). Furthermore, in the Ce(IV) titration of $[Ru(bipy)_2(dach)]^{2+}$ there is clear evidence for an intermediate of a monoimine type. Detailed mechanistic information about the oxidative dehydrogenation step is not available. However, under conditions where stoichiometric amounts of oxidant are added, an overall pattern of *net* reactions can be written, and this is illustrated for $[Ru(bipy)_2(en)]^{2+}$ below:

$$2[Ru(bipy)_2(en)]^{2+} \xrightarrow{-2e^-} 2[Ru(bipy)_2(en)]^{3+} \quad (13)$$

$$2[Ru(bipy)_2(en)]^{3+} \rightarrow$$

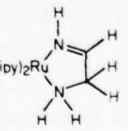

$$+ [Ru(bipy)_2(en)]^{2+} + 2H^+ \quad (14)$$

$$2[Ru(bipy)_2(monoimine)]^{2+} \xrightarrow{-2e^-} 2[Ru(bipy)_2(monoimine)]^{3+} \quad (15)$$

$$2[Ru(bipy)_2(monoimine)]^{3+} \rightarrow$$

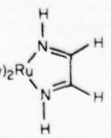

$$+ [Ru(bipy)_2(monoimine)]^{2+} + 2H^+ \quad (16)$$

On further oxidation,

$$[Ru(bipy)_2(dim)]^{2+} \xrightarrow{-e^-} [Ru(bipy)_2(dim)]^{3+} \quad (17)$$

$$[Ru(bipy)_2(dim)]^{3+} \rightarrow \text{further ligand oxidation} \quad (18)$$

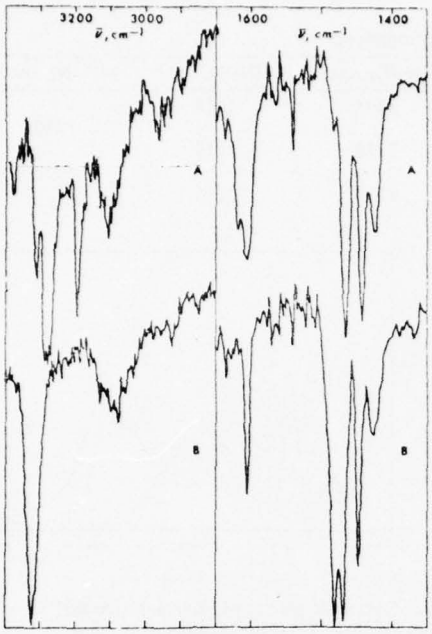

Figure 2. Infrared spectra (KBr pellets) of (A) $[Ru(bipy)_2(en)](ClO_4)_2$ and (B) $[Ru(bipy)_2(dim)](PF_6)_2$ in the regions 3400–2800 and 1650–1350 cm^{-1}.

In cases where eq 18 is sufficiently rapid, electron transfer as in eq 6 can occur giving a pathway for the depletion of the imine complexes by further ligand oxidation.

Electrochemical and Chemical Behavior of the Imine Complexes. The ruthenium(II) complexes of the α,α'-diimines reported here are stable for several hours in aqueous 1.0 *M* acid and in 0.1 *M* base solution. In neutral solution, the complexes showed little (if any) decomposition after several days. In acetonitrile solution, the complexes were also found to be unchanged after several days, even when unprotected from light.

The redox properties of the α,α'-diimine complexes were investigated by electrochemical techniques, both in aqueous solution and in acetonitrile. In aqueous solution, using 0.5 *M* *p*-toluenesulfonic acid (HTos) as the supporting electrolyte, cyclic voltammetry experiments show that the α,α'-diimine complexes $[Ru(bipy)_2(dim)]^{2+}$, $[Ru(bipy)_2(dich)]^{2+}$, and $[Ru(bipy)_2(IMPy)]^{2+}$, undergo electrochemically irreversible oxidations at a Pt electrode. However, in 0.1 *M* TBAH–CH_3CN, the complexes each undergo a reversible, or nearly reversible, one-electron oxidation at Pt, apparently involving the oxidation of Ru(II) to Ru(III).

$$[Ru^{II}(bipy)_2(\alpha,\alpha'\text{diimine})]^{2+} \xrightarrow{-e} [Ru^{III}(bipy)_2(\alpha,\alpha'\text{-diimine})]^{3+}$$

At slow scan rates (0.2 V/sec), the ratio of the cathodic to anodic peak currents (i_c/i_a) is less than one in all cases. However, at faster scan rates (10 V/sec) the ratio of i_c/i_a is one and no additional waves appeared in the cyclic voltammograms, indicating that decomposition had not occurred. Exhaustive electrolysis at controlled potentials more positive than $E_{1/2}$ gave large *n* values; the products were not characterized. Apparently, the further oxidations result in the oxidation of the α,α'-diimine ligands.

Cyclic voltammetry of the α,α'-diimine complexes in 0.1 *M* TBAH–CH_3CN also shows an electrochemically irreversible reduction in addition to the usual 2,2'-bipyridine reductions which occur at more cathodic potentials.[21] The products of the reduction waves are apparently bound, reduced radical anions in which the reduction is localized mainly on an imine linkage. Reduction of $[Ru(bipy)_2(dim)]^{2+}$ by exhaustive electrolysis gave a variety of products, as shown by cyclic voltammetry, and was not pursued further. Sodium borohydride reacts slowly with the α,α'-diimine complexes in either water or acetonitrile, but does not give well-defined products.

The α,α'-diimine complexes $[Ru(bipy)_2(dim)]^{2+}$, $[Ru(bipy)_2(dich)]^{2+}$, and $[Ru(bipy)_2(IMPy)]^{2+}$ have stability and chemical and physical properties reminiscent of $[Ru(bipy)_3]^{2+}$. On the cyclic voltammetry time scale the ruthenium(III) complexes $[Ru(bipy)_2(\alpha,\alpha'\text{-diimine})]^{3+}$ are stable (the $[Ru(bipy)_2(\alpha,\alpha'\text{-diimine})]^{3+/2+}$ couples are electrochemically reversible, or nearly reversible). However, on longer time scales, the ruthenium(III) complexes are unstable, apparently because of further oxidation processes involving the coordinated ligands. We have not investigated the subsequent reactions in detail. Chum and Krumholz[22] have investigated ligand oxidation reactions in iron(II) α,α'-diimine complexes like $[Fe(GMI)]^{2+}$ (GMI is $CH_3{-}N{=}CH{-}CH{=}N{-}CH_3$) and have found reactions such as,

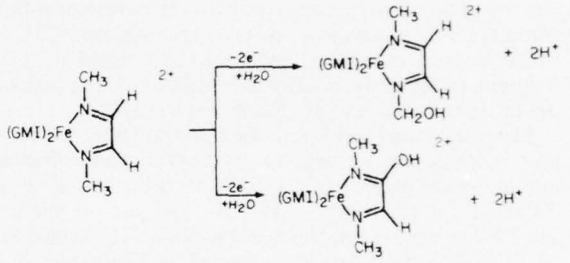

The reactions of the α,α'-diimine ligands in the coordination sphere of the ruthenium complexes may be similar.

The subsequent α,α'-diimine oxidation presents a synthetic difficulty in the conversion of diamines into α,α'-diimines. It is essential that controlled-potential electrolysis methods be used to avoid oxidation of the α,α'-diimine complexes once formed. The reaction potentials for the α,α'-diimine (1.20 to 1.33 V, Table III) and diamine couples (0.96 to 0.99 V, Table II) are sufficiently different so that electrolyses can be carried out cleanly on the diffusion plateau of the $[Ru(bipy)_2(diamine)]^{3+/2+}$ wave.

Infrared Spectra. Infrared spectra were helpful in the characterization of the α,α'-diimine complexes.

The infrared spectra of the complexes $[Ru(bipy)_2(en)](ClO_4)_2$ and $[Ru(bipy)_2(dim)](PF_6)_2$ in the regions 3400–2800 and 1650–1350 cm^{-1} are illustrated in Figure 2. For the complex $[Ru(bipy)_2(en)]^{2+}$, the absorptions at 3315, 3280, and 3195 cm^{-1} can be assigned as N–H stretching vibrations (ν_{N-H}). The absorption at 1618 cm^{-1} can be assigned as an N–H deformation (δ_{N-H}). Upon oxidation to $[Ru(bipy)_2(dim)]^{2+}$, the N–H stretching region simplifies to one absorption at 3325 cm^{-1}, as expected for an imine complex. Also as expected, the N–H deformation near 1600 cm^{-1} disappears for the imine complexes. A new absorption appears at 1480 cm^{-1} for the salt $[Ru(bipy)_2(dim)](ClO_4)_2$. A pure –C=N– stretching vibration would be expected to appear around 1600 cm^{-1}.[23,24] Nakamoto has carried out a normal coordinate analysis of the ion $[Fe(GMI)_3]^{2+}$, and has identified a band at 1530 cm^{-1} as a combination mode, which is made up predominantly of a –C=N– stretching vibration.[25] The band at 1480 cm^{-1} for $[Ru(bipy)_2(dim)](ClO_4)_2$ can reasonably be assigned to a combination mode consisting largely of the conjugated –C=N– stretch of the α,α'-diimine ligand ($\nu_{C=N}$). The characteristic ν_{N-H}, $\delta_{N=H}$, and $\nu_{C=N}$ bands for some of the ruthenium(II) amine and α,α'-diimine complexes studied are summarized in Table IV. The C=N stretching mode could not be found for the complex $[Ru(bipy)_2(IMPy)]^{2+}$. There are many strong absorptions due to the bipyridine ligands in this region, and the band of interest may well be

Table IV. Infrared Spectra of Bis(2,2'-bipyridine)ruthenium(II) Amine and Imine Complexes

Complex	ν(N-H)$_{as}$, cm^{-1}	ν(N-H)$_s$, cm^{-1}	δ(N-H), cm^{-1}	ν(C=N), cm^{-1}
[Ru(bipy)$_2$(en)](ClO$_4$)$_2$	3315 3280	3195	1618	
[Ru(bipy)$_2$(dim)](PF$_6$)$_2$	3325			1480
[Ru(bipy)$_2$(dach)](ClO$_4$)$_2$	3280 3252	3178	1615	
[Ru(bipy)$_2$(dich)](PF$_6$)$_2$	3300			1450
[Ru(bipy)$_2$(AMPy)](ClO$_4$)$_2$	3300 3267	3185	1615	
[Ru(bipy)$_2$(IMPy)](PF$_6$)$_2$	3322			

hidden. Also the intensity of the band may be diminished due to poor conjugation of the –C=N– group with the pyridine group. King and Douglas[23] observed that the –C=N– vibration was very weak in the monoalkylimine complex ((CH$_3$)$_2$C=NH)Cr(CO)$_5$.

^{1}H NMR Spectra. The ^{1}H NMR spectra of the imine complexes in D$_2$O solution were of limited use for characterization since the –N=CH resonance was hidden by the very complicated resonances due to the bipyridine ligands (δ = 7.0–9.0 ppm). The spectra were however consistent with the compiex formulations given above; for example, the >CH$_2$ and –NH$_2$ resonances in [Ru(bipy)$_2$(en)]$^{2+}$ (centered at 2.8 and 3.5 ppm, respectively, relative to *t*-BuOH at 1.23 ppm) were absent in the spectrum of [Ru(bipy)$_2$(dim)]$^{2+}$.

Electrochemical and Electronic Spectral Data. Electronic spectra (absorption maxima and molar extinction coefficients) and half-wave potentials in acetonitrile solution are given in Table II for [Ru(bipy)$_2$(NH$_3$)$_2$]$^{2+}$ and for the diamine-bis(2,2'-bipyridine) complexes of ruthenium(II) studied here. In Table III, similar data are presented for [Ru(bipy)$_3$]$^{2+}$ and for the various imine complexes considered in this work.

Ruthenium(III)/ruthenium(II) reduction potentials are known to be dependent upon the presence of back-bonding ligands in the coordination sphere,[26–28] the potential increasing as the number of back-bonding ligands is increased. Qualitatively, this change in potential can be attributed to a stabilization of the ruthenium(II) oxidation state by increased back-bonding: back-bonding is thought to be insignificant between ruthenium(III) and pyridine-type ligands.[26] Such a trend is evident from the data in Table II: the $E_{1/2}$ values for the chelated diamine couples [Ru(bipy)$_2$(en)]$^{3+/2+}$, [Ru(bipy)$_2$(dach)]$^{3+/2+}$, [Ru(bipy)$_2$(damp)]$^{3+/2+}$, and [Ru(bipy)$_2$(tn)]$^{3+/2+}$ are close to that for [Ru(bipy)$_2$(NH$_3$)$_2$]$^{3+/2+}$, whereas the $E_{1/2}$ values for the pyridine–amine couples [Ru(bipy)$_2$(AMPy)]$^{3+/2+}$ and [Ru(bipy)$_2$(AEPy)]$^{3+/2+}$ are at considerably more anodic potentials.

If the back-bonding argument is correct, the data in Table III indicate that imine ligands undergo appreciable back-bonding with ruthenium(II) in bis(2,2'-bipyridine) complexes. The Ru(III)/Ru(II) potentials for [Ru(bipy)$_2$(dim)]$^{2+}$ and [Ru(bipy)$_2$(dich)]$^{2+}$ are at considerably higher potentials than the corresponding diamine complexes, and the potentials for all three α,α'-diimine complexes fall in the same range (1.20–1.33 V) as the potential for the [Ru(bipy)$_3$]$^{3+/2+}$ couple. The ligands 2,2'-bipyridine and 1,10-phenanthroline are high in the spectrochemical series and capable of strong back-bonding,[29] and it has been suggested[30] that it is the α,α'-diimine linkage

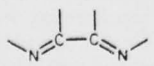

which is the important bonding feature responsible for the back-bonding. The similarities in properties between [Ru(bipy)$_3$]$^{2+}$ and the α,α'-diimine complexes reported here are consistent with this suggestion. However, it is not clear that *linked* imine systems are necessary to explain the effects observed. The linked imine system benefits from the chelate effect, and the chemical link may be the origin of the unusual chemical stability of the α,α'-diimine complexes. However, the spectral and redox properties of [Ru(bipy)$_2$(py)$_2$]$^{2+}$ are essentially identical with those for [Ru(bipy)$_3$]$^{2+}$.[14] The electronic effects of the α,α'-diimine ligand, particularly with regard to back-bonding, may originate primarily from the two imine linkages, irrespective of a chemical link between them.

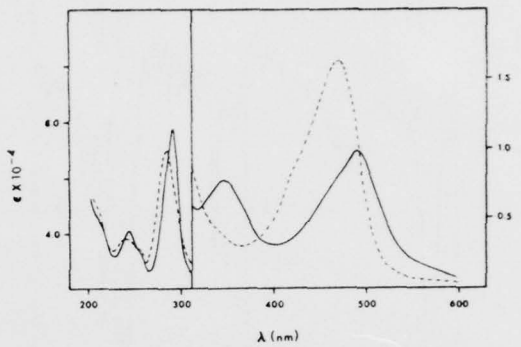

Figure 3. Electronic spectra of [Ru(bipy)$_2$(dach)]$^{2+}$ (—) and [Ru(bipy)$_2$(dich)]$^{2+}$ (- - -) in acetonitrile solution.

The reduction potential for the monoimine couple [Ru(bipy)$_2$(iamp)]$^{3+/2+}$ is higher than that for its precursor diamine couple [Ru(bipy)$_2$(damp)]$^{3+/2+}$, but is similar to that for the pyridine–amine couple [Ru(bipy)$_2$(AMPy)]$^{3+/2+}$. The similarity indicates the monoimine linkage may be similar to a pyridine group in back-bonding ability.

The electronic spectra of *cis*-bis(2,2'-bipyridine)ruthenium(II) complexes are also sensitive to the presence of back-bonding ligands in the two remaining coordination positions.[15,28] The spectrum of [Ru(bipy)$_2$(NH$_3$)$_2$]$^{2+}$ has two broad maxima in the visible region, which have previously been assigned as d(Ru(II)) → π^*(bipy) MLCT transitions.[15] There are also two maxima in the uv region, which have been assigned as 2,2'-bipyridine $\pi \rightarrow \pi^*$ transitions.[15] From the data in Table II it can be seen that the electronic spectra of the diamine complexes of bis(2,2'-bipyridine)ruthenium(II) are all very similar to the spectrum of [Ru(bipy)$_2$(NH$_3$)$_2$]$^{2+}$. The spectrum of the complex [Ru(bipy)$_2$(dach)]$^{2+}$ is shown in Figure 3.

The spectra of the complexes [Ru(bipy)$_2$(AMPy)]$^{2+}$ and [Ru(bipy)$_2$(AEPy)]$^{2+}$ differ slightly from the spectra of the diamine complexes, there being additional transitions at 422 and 425 nm, respectively. An assignment of these bands as d(Ru(II)) → π^*(py) MLCT transitions is reasonable since similar transitions are known for related complexes.

As the number of back-bonding ligands in bis(2,2'-bipyridine)ruthenium(II) complexes increases, the energy of the bands in the visible region increases and for complexes with back-bonding ligands in both sites there is typically only one d(Ru(II)) → π^*(bipy) MLCT transition.[31] Distinct shoulders are also sometimes observed since the broad absorption bands are clearly a composite of allowed transitions.[15] The energy of the first d → π^* transition is observed to increase from [Ru(bipy)$_2$(NH$_3$)$_2$]$^{2+}$ (490 nm) to [Ru(bipy)$_3$]$^{2+}$ (450 nm), and those for the α,α'-diimine complexes occur between 454 and 472 nm, which again indicates considerable back-bonding from the metal to the α,α'-diimine ligand. The spectrum of [Ru(bipy)$_2$(dich)]$^{2+}$ is shown in Figure 3.

The electronic spectrum of the monoimine complex [Ru(bipy)$_2$(iamp)]$^{2+}$ is quite similar to the visible spectrum of the

pyridine–amine complex $[Ru(bipy)_2(AMPy)]^{2+}$, but lacks the d(Ru) → π*(pyridine) MLCT band at 422 nm as expected. The complex $[Ru(bipy)_2(IMPy)]^{2+}$ has a very complicated electronic spectrum, but this is expected since transitions in the MLCT region are expected to appear due to d(Ru) → π*(L) transitions, where L = 2,2'-bipyridine, pyridine, and the imine group.

The effects of back-bonding in the α,α'-diimine complexes are felt both at the metal (redox and spectral properties) and also at the ligand. For example, simple organic imines are known to be unstable with respect to hydrolysis,[32] yet coordinated α,α'-diimine ligands are remarkably stable in aqueous solution.

The complexes $[Ru(bipy)_2(AEPy)]^{2+}$ and $[Ru(bipy)_2(tn)]^{2+}$ do not have stable imine oxidation products. Because of the structures of the ligands, the imine oxidation products cannot be α,α'-diimines. It is probable that oxidation of these ligands gives first an imine intermediate, e.g.,

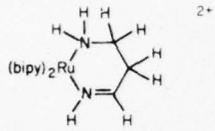

which is unstable with respect to further oxidation at the imine site. The instability of nondelocalized imines appears to be further evidence for the unusual stability of the α,α'-diimine linkage.

Acknowledgment. Acknowledgments are made to the Materials Research Center of the University of North Carolina under Grant DAHC15 73 G 9 with DARPA for support of this research.

Registry No. $[Ru(bipy)_2Cl_2]$, 19542-80-4; $[Ru(bipy)_3](ClO_4)_2$, 15635-95-7; $[Ru(bipy)_2(NH_3)_2](ClO_4)_2$, 56993-99-8; $[Ru(bipy)_2(en)](ClO_4)_2$, 31659-06-0; $[Ru(bipy)_2(dach)](ClO_4)_2$, 56889-66-8; $[Ru(bipy)_2(damp)](ClO_4)_2$, 56889-68-0; $[Ru(bipy)_2(AEPy)](ClO_4)_2$, 56889-70-4; $[Ru(bipy)_2(AMPy)](ClO_4)_2$, 56889-72-6; $[Ru(bipy)_2(tn)](PF_6)_2$, 56889-74-8; $[Ru(bipy)_2(dim)](PF_6)_2$, 56889-76-0; $[Ru(bipy)_2(dich)](PF_6)_2$, 56889-78-2; $[Ru(bipy)_2(IMPy)](PF_6)_2$, 56889-80-6; $[Ru(bipy)_2(iamp)]^{2+}$, 56889-81-7; Ce(IV), 16065-90-0.

References and Notes

(1) N. F. Curtis, *Chem. Commun.*, 881 (1966); *Coord. Chem. Rev.*, **3**, 3 (1968).
(2) J. C. Dabrowiak, F. V. Lovecchio, V. L. Goedken, and D. H. Busch, *J. Am. Chem. Soc.*, **94**, 5502 (1972); V. L. Goedken and D. H. Busch, *ibid.*, **94**, 7355 (1972).
(3) H. Elsbernd and J. K. Beattie, *J. Chem. Soc. A*, 2598 (1970).
(4) B. C. Lane, J. E. Lester, and F. Basolo, *Chem. Commun.*, 1618 (1971).
(5) D. F. Mahoney and J. K. Beattie, *Inorg. Chem.*, **12**, 2561 (1973).
(6) V. L. Goedken, *J. Chem. Soc., Chem. Commun.*, 207 (1972).
(7) J. A. Ferguson, T. J. Meyer, and D. G. Whitten, *Inorg. Chem.*, **11**, 2767 (1972).
(8) G. M. Brown, F. R. Hopf, J. A. Ferguson, T. J. Meyer, and D. G. Whitten, *J. Am. Chem. Soc.*, **95**, 5939 (1973).
(9) G. M. Brown, R. W. Callahan, and T. J. Meyer, *J. Am. Chem. Soc.*, **96**, 7829 (1974).
(10) R. W. Callahan, G. M. Brown, and T. J. Meyer, 168th National Meeting of the American Chemical Society, Atlantic City, N.J., September 1974, Abstract No. INOR 121.
(11) R. N. Adams, "Electrochemistry at Solid Electrodes", Marcel Dekker, New York, N.Y., 1969, p 206.
(12) J. A. Ferguson, Ph.D. Dissertation, University of North Carolina at Chapel Hill, 1971.
(13) J. B. Godwin and T. J. Meyer, *Inorg. Chem.*, **10**, 471 (1971).
(14) J. N. Braddock and T. J. Meyer, *J. Am. Chem. Soc.*, **95**, 3158 (1973).
(15) G. M. Bryant, J. E. Fergusson, and H. K. J. Powell, *Aust. J. Chem.*, **24**, 257 (1971).
(16) F. P. Dwyer, H. A. Goodwin, and E. C. Gyarfas, *Aust. J. Chem.*, **16**, 544 (1963).
(17) R. W. Callahan, G. M. Brown, and T. J. Meyer, *Inorg. Chem.*, **14**, 1443 (1975).
(18) Electrochemical reversibility was determined, where possible, from plots of log $([i_l - i]/i)$ vs. E from stirred solution voltammetry data. For cases where subsequent ligand oxidation was too rapid, reversibility was determined by cyclic voltammetry. In such experiments, reversibility was based on the ratio of anodic to cathodic peak currents (i_c/i_a) and the potential separation of the peaks (ΔE_p). At fast scan rates, ΔE_p was greater than the theoretical value of 59 mV which was probably due to uncompensated resistance between the working electrode and the reference electrode tip. For such cases, ΔE_p for the electrode reaction of interest was compared with ΔE_p for the couple $[Ru(bipy)_2(NH_3)_2]^{3+/2+}$, which is reversible. The half-wave potentials, $E_{1/2}$, reported here differ from formal reduction potentials by a usually small term involving differences in diffusion coefficients,[19] and refer to reactions such as $[Ru(bipy)_2(en)]^{3+} + e \rightarrow [Ru(bipy)_2(en)]^{2+}$.
(19) R. W. Murray and C. N. Reilley, "Electroanalytical Principles", Interscience, New York, N.Y., 1963, p 2175.
(20) J. N. Braddock, J. L. Cramer, E. M. Gupton, and F. R. Keene, unpublished results, University of North Carolina, 1974.
(21) N. E. Tokel-Takvoryan, R. E. Hemingway, and A. J. Bard, *J. Am. Chem. Soc.*, **95**, 6582 (1973).
(22) H. L. Chum and P. Krumholz, *Inorg. Chem.*, **13**, 514, 519 (1974).
(23) R. B. King and W. M. Douglas, *J. Am. Chem. Soc.*, **95**, 7528 (1973).
(24) S. Patai, Ed., "The Chemistry of the Carbon-Nitrogen Double Bond", Interscience, London, 1970.
(25) K. Nakamoto, "Advances in the Chemistry of Coordination Compounds", Wiley, New York, N.Y., 1963.
(26) H. Taube, *Surv. Prog. Chem.*, **6**, 1 (1973).
(27) D. A. Buckingham and A. M. Sargeson, "Chelating Agents and Metal Chelates", F. P. Dwyer and D. P. Mellor, Ed., Academic Press, New York, N.Y., 1964, p 269.
(28) G. M. Brown, R. W. Callahan, M. Cooke, E. C. Johnson, T. J. Meyer, and T. R. Weaver, manuscript in preparation; J. L. Cramer, unpublished results, University of North Carolina, 1974.
(29) F. A. Cotton and G. Wilkinson, "Advanced Inorganic Chemistry", 3rd ed, Interscience, New York, N.Y., 1972, p 577.
(30) P. Krumholz, *Struct. Bonding (Berlin)*, **9**, 139 (1971).
(31) S. A. Adeyemi, Ph.D. Dissertation, University of North Carolina at Chapel Hill, 1973.
(32) J. March, "Advanced Organic Chemistry", McGraw-Hill, New York, N.Y., 1968, p 656.

APPLICATIONS OF PATTERN RECOGNITION IN CHEMISTRY

T. L. Isenhour

Final Technical Report

1 June 1973 - 30 September 1976

Personnel:

J. de Haseth, Research Assistant.

The support provided the Principal Investigator during the above period has allowed further development of the exciting new area of Pattern Recognition applied to chemistry. Data evaluation tasks normally considered to require human intelligence can be performed by computers programmed to pattern recognition functions. In conjunction with computer information handling systems which automatically perform routine duties, such intelligent machines can materially aid in dealing with the tremendous quantities of information produced by sophisticated scientific instrumentation.

Thus far our research has made fundamental contributions to interpretation of infrared and mass spectral data as well as the development of pattern recognition and search and retrieval methods. Furthermore, we have begun studies on the application of machine decisions to failure analysis.

Brief summaries of research progress on DARPA-supported research follow:

1. Relationship Between Mutual Information and Classification [Anal. Chem., 48, 1027 (1976); G. L. Ritter, S. R. Lowry, H. B. Woodruff, and T. L. Isenhour, reprints attached]. Mutual information is an information theory term, which describes the amount of information to distinguish among members of different classes. This concept is demonstrated for describing the classification ability of a maximum likelihood classifier. In an artificially generated problem, the recognition ability and the square root of mutual information are seen to be linearly related. The linear correlation drops to 0.83 for a series of infrared questions where the statistical independence assumption is not strictly valid.

2. Density Estimations and the Characterization of Binary Infrared Spectra [Tech., 17, 455 (1975); H. B. Woodruff, G. L. Ritter, S. R. Lowry, and T. L. Isenhour, reprints attached]. A truncated orthogonal expansion has been used to represent binary data taken from a multidimensional file of infrared data. The expansion represents an approximation for the true class conditional probability density functions (pdf's). As a first approximation, statistical independence is assumed and the only terms necessary are the estimated class conditional probabilities for each peak. A more accurate estimation of the pdf is attained when a second term, a correlation term, is included in the expansion.

The data set consists of 2600 spectra in thirteen mutually exclusive classes with each spectrum represented by 139 dimensions. Results are obtained for a maximum discriminant function case, as well as for pairwise discrimination among the classes. For the thirteen class problem, correct classification occurs 67.2% of the time by the class conditional probabilities and 87.3% of the time when the correlation terms are included. For pairwise discrimination, the results are 92.9% and 98.1%, respectively.

3. Feasibility of a One-Dimensional Search System [submitted to Computers and Chemistry; G. L. Ritter and T. L. Isenhour, preprint attached]. There has been frequent interest in the chemical literature describing methods for the rapid search of large data collections. Since these collections may contain 10^4 to 10^5 entries, any similarity search is difficult. However if one number is assigned to each entry and that number retains all similarity information, then a simple binary search can produce the data collection entries that are most similar to an unknown. This approach is investigated for a file of gas chromatographic liquid phases and for a large set of mass spectra. Obvious limitations occur when the data is multi-dimensional. However indications of multi-dimensional similarity are retained even in the difficult mass spectral example.

Further Work:

The thrust of this project is the application of machine decisions to failure analysis. The specific work proposed for the period between June, 1975 and June, 1976, is the development of information retrieval systems for application to centralized data banks to allow comparison of current conditions to previous events thereby allowing on-site diagnosis to predict impending failures.

During this period particular emphasis has been placed in developing text search methods for retrieving archival information. High speed, digital computers now allow storage and retrieval of large blocks of information quickly. A generalized text processor has been developed which allows retrieval of bibliographic and other archival information based on Boolean algebraic entries.

This system has first been applied to Chemical Abstracts Service Chemical Condensates and allows complex literature profiles to be rapidly searched against weekly bibliographic data sets. The system is rapid and general and can treat any text data.

The system has further been tested against the ASTM infrared data file of 91,875 infrared spectra. The text method can perform the same type of search as conventional arithmetic methods but has additional capabilities to handle items such as name fragment.

Of particular interest is the capability of this system to do error detection. Contradictory logical entries can be successfully used to detect errors in the data bank itself. The work is being further developed.

The system is being applied to a specific naval problem. Mr. John Patton, Project Engineer, NOS Louisville, has provided us with a set of analysis data on hydraulic fluid maintenance for the 5"-38 gun mount. The remainder of the project will be applied to investigating text search methods on the hydraulic fluid data. It is expected to be shown that queries relative to in-field problems can be used to search the data base and retrieve comparable past conditions. It is hoped that this will lead toward more efficient mechanisms for predicting and preventing failures.

Density Estimations and the Characterization of Binary Infrared Spectra

H. B. Woodruff, G. L. Ritter, S. R. Lowry and T. L. Isenhour

Department of Chemistry
University of North Carolina
Chapel Hill, North Carolina 27514

A truncated orthogonal expansion has been used to represent binary data taken from a multidimensional file of infrared data. The expansion represents an approximation for the true class conditional probability density functions (pdf's). As a first approximation, statistical independence is assumed and the only terms necessary are the estimated class conditional probabilities for each peak. A more accurate estimation of the pdf is attained when a second term, a correlation term, is included in the expansion.

The data set consists of 2600 spectra in thirteen mutually exclusive classes with each spectrum represented by 139 dimensions. Results are obtained for a maximum discriminant function case, as well as for pairwise discrimination among the classes. For the thirteen class problem, correct classification occurs 67.2% of the time by the class conditional probabilities and 87.3% of the time when the correlation terms are included. For pairwise discrimination, the results are 92.9% and 98.1%, respectively.

KEY WORDS

Infrared Spectroscopy
Density Estimation
Bahadur-Lazarsfeld Expansion

1. INTRODUCTION

Improved instrumentation has resulted in large compilations of chemical data. Some compilations contain so many spectra that, if the files are to remain manageable, some form of data compression is essential. For example, the ASTM file of over 90,000 infrared (IR) spectra is represented in a peak/no peak format. This means a spectrum is represented solely by a bit string and contains no intensity information. If a peak maximum occurs within a particular 0.1 μm interval, the corresponding bit is turned on. Otherwise, the bit remains off. For the IR region from 2.0 to 15.9 μm, a spectrum is represented by a series of 139 ones and zeros.

The reason for compiling large quantities of data is to aid the chemist in rapidly identifying a spectrum measured in the laboratory. Conceptually, the simplest approach is to search the file, comparing each spectrum with the unknown and reporting any match. In this case, if the unknown is in the file, the recognition approaches an optimum. Should the unknown spectrum not be in the file, the best result that could be hoped for would be a similar compound. Several search systems utilizing binary IR data have been reported [1, 5]. Unfortunately, unless special techniques, such as the use of inverted files [10] or hash coding [8], are applicable, search time increases linearly with the size of the file and often becomes prohibitively long.

An alternative approach is to utilize pattern recognition techniques in order to classify the unknown spectrum [6]. An estimate of the true class probability density functions (pdf's) may be determined. As more terms are included in the pdf estimates the recognition improves. Also, however, the time of investigation increases, and the technique more closely parallels a search.

The present example involves characterizing structural features in a randomly chosen file of IR spectra using the pdf estimation approach. Absorptions of IR radiation are indicative of molecular vibrational transitions. The transitions occur at well-defined frequencies for molecular functional groups. Thus, the presence of given absorptions (peaks) in the IR spectrum is reason to suspect the existence of certain functional groups.

As was mentioned, the spectra are coded as a multivariate set of binary variables. The data file is divided into thirteen mutually exclusive classes, each delineated by some functional group (Table 1). Pairwise discrimination is attempted, where the spectrum is known to belong to one of the classes. The principal test of recognition is the selection of the best of the thirteen discriminators. These results indicate how well each functional group is characterized relative to all others. This is a point of

Received July 1974; revised May 1975

departure from the branching tree method previously reported in the chemical literature [6].

Several methods have been suggested for treating a problem involving Bernoulli variables [4, 7]. One treatment presupposes the statistical independence of the variables comprising the observation. Chow has shown that this approximation for the pdf may be put into the form of a linear discriminant of the conditional probabilities for the class [3]. Bahadur has shown that the statistical independence estimate is but a first approximation to an orthogonal expansion for the true pdf's [2, 9]. The introduction of correlations and higher terms leads to the truer measure. Thus, a second order approximation considers the estimated prior probabilities and the correlations, while omitting all higher order terms.

This paper reports the results obtained when classifying binary infrared data by using first the statistical independence assumption, and then by adding the correlation terms. Finally, results are reported and discussed for classification using only the correlation terms.

2. Theory

Let each observation be represented by an ordered vector $\mathbf{x}$ composed of a set of experimental measurements $(x_1, x_2, \cdots, x_d)$. The problem is to decide which pre-selected class, ω_i, best describes the set of measurements. To minimize the probability of error a Bayesian decision rule is employed; *i.e.*, choose class ω_k, if $P(\omega_k \mid \mathbf{x}) = \max \{P(\omega_i \mid \mathbf{x})\}$. $P(\omega_i \mid \mathbf{x})$ is the *a posteriori* probability of ω_i occurring. Thus, the best decision is made by selecting the class which appears most frequently for $\mathbf{x}$.

Appealing to Bayes' rule, an equivalent relation may be derived from

$$P(\omega_i \mid \mathbf{x}) = \frac{P(\mathbf{x} \mid \omega_i)P(\omega_i)}{\sum_i P(\mathbf{x} \mid \omega_i)P(\omega_i)}. \tag{1}$$

$P(\mathbf{x} \mid \omega_i)$ is the i-class conditional probability density for $\mathbf{x}$ and $P(\omega_i)$ is the *a priori* probability of class ω_i. The decision rule now becomes choose ω_k, if

$$[P(\mathbf{x} \mid \omega_k)P(\omega_k)] = \max_i \{P(\mathbf{x} \mid \omega_i)P(\omega_i)\}.$$

If the measurements comprising $\mathbf{x}$ are assumed to be statistically independent, then

$$P(\mathbf{x} \mid \omega_i) = P(x_1, x_2, \cdots, x_d \mid \omega_i) = \prod_{j=1}^{d} P(x_j \mid \omega_i). \tag{2}$$

$P(x_j \mid \omega_i)$ becomes the i-class conditional probability of variable x_j.

When x_j is a binary variable, the expectation value of x_j, $E(x_j)$, for class ω_i is simply

$$E(x_j) = P(x_j = 1 \mid \omega_i) = \alpha_{ji}. \tag{3a}$$

Likewise

$$P(x_j = 0 \mid \omega_i) = 1 - \alpha_{ji}. \tag{3b}$$

These may be combined into one term of the form: [3]

$$P(x_j \mid \omega_i) = \alpha_{ji}^{x_j}(1 - \alpha_{ji})^{1-x_j}. \tag{3c}$$

Taking the logarithm of both sides leaves the following expression:

$$\log P(x_j \mid \omega_i) = x_j \log \frac{\alpha_{ji}}{1 - \alpha_{ji}} + \log (1 - \alpha_{ji}). \tag{3d}$$

The monotonic nature of the logarithm function and the assumption of statistical independence imply that maximizing $P(\mathbf{x} \mid \omega_i)\ P(\omega_i)$ is equivalent to maximizing

$$\sum_{j=1}^{d} \left[x_j \log \left(\frac{\alpha_{ji}}{1 - \alpha_{ji}} \right) + \log (1 - \alpha_{ji}) \right] + \log P(\omega_i). \tag{4}$$

By inspection this equation is linear in x_j, or denoting the function by S_i gives

$$S_i(\mathbf{x}) = \sum_{j=1}^{d} w_{ji}x_j + w_{0i} \tag{5}$$

where

$$w_{ji} = \log \left(\frac{\alpha_{ji}}{1 - \alpha_{ji}} \right)$$

and

$$w_{0i} = \sum_{j=1}^{d} \log (1 - \alpha_{ji}) + \log P(\omega_i).$$

The discriminator is now in a form where all weighting information is contained in the prior probabilities of ω_i and the class conditional probabilities for parameters x_j. Greater value is added to the discriminator when x_j equals one and there is a high likelihood or expectation of ones in the prior data.

Statistical independence is unlikely, and thus some correction in the estimate of class conditional probabilities is necessary. For example, assume a high positive correlation between x_r and x_j in class ω_k. An unknown should be classified into class ω_k more favorably when $x_r = x_j$ (than when $x_r \neq x_j$). Thus, correction factors should include a consideration of correlation.

For a class ω_i, a transformation of parameter x_j into z_j may be made.

$$z_j = (x_j - \alpha_{ji})[\alpha_{ji}(1 - \alpha_{ji})]^{-\frac{1}{2}} \tag{6}$$

(The parameter z_i assures a zero mean and unit variance in ω_i.) The multinomial class conditional probabilities may be expressed in terms of the transformed variables.

$$P(\mathbf{x}) = P_w(\mathbf{x})[1 + \sum_{i<k} E(z_i z_k) z_i z_k + \sum_{i<k<l} E(z_i z_k z_l) z_i z_k z_l + \cdots + E(z_1 z_2 \cdots z_d) z_1 z_2 \cdots z_d] \quad (7)$$

Here the $P_w(\mathbf{x})$ is the same as the term given in (3c). This reparameterization and expansion describing the class pdf is due to Bahadur and Lazarsfeld [4].

A natural first approximation is to include only the first term in the sum. $P_1(\mathbf{x}) = P_w(\mathbf{x})$. When the logarithm is taken, this approximation is the same as the statistically independent criterion considered earlier.

Similarly, a reasonable second approximation is

$$P_2(\mathbf{x}) = P_w(\mathbf{x})[1 + \sum_{i<j} E(z_i z_j) z_i z_j]. \quad (8)$$

If the logarithm is taken, the second order result is simply found by adding a correction term to the first approximation. The coefficients, the expectation values of quadratic products, take the form of correlation terms. Thus, the correlation argument made earlier has been justified.

Since complete knowledge of the probabilities and correlations is nearly impossible in a real problem, they may only be estimated from a known training set. The training set estimates are entered into the pdf approximations. When these values are entered into the approximation, $P_2(\mathbf{x})$ may become negative. In this case, the second order estimate insufficiently describes the pdf. When this occurs, $P_2(\mathbf{x})$ is set to 10^{-5}, as has been recommended by Moore [11].

3. Data Set

The data for this study were obtained from the file of 91,875 binary infrared spectra assembled by the American Society for Testing and Materials and made accessible at the Triangle Universities Computation Center (TUCC), by the North Carolina Educational Computing Service, and the R. J. Reynolds Tobacco Company. Thirteen mutually exclusive classes (see Table 1) were selected. Compounds containing C, H, O, and N atoms exclusively and with a carbon content ranging from 1–15 carbon atoms were the only ones used in this study. From those spectra belonging strictly to one of the thirteen classes, 200 were randomly selected, resulting in a data set of 2600 spectra. The range from 2.0 to 15.9 μm was divided into 139 intervals of 0.1 μm each. Computations were done on the TUCC IBM 370/165 teleprocessing with the University of North Carolina Computation Center IBM 360/75 using FORTRAN IV computer programs.

TABLE 1—*Chemical Classes Used in the Study*

Class No.		Chemical Functionality
1	Carboxylic Acid	
2	Ester	
3	Ketone	
4	Alcohol	ROH
5	Aldehyde	
6	1° Amine	RNH_2
7	2° Amine	
8	3° Amine	
9	Amide	
10	Urea and derivatives	
11	Ether and acetal	ROR',
12	Nitro and nitroso	RNO_2, RN=O
13	Nitrile and isonitrile	RCN, RNC

4. Results and Discussion

The results presented in Table 2 are for the case where: 1) statistical independence is assumed and 2) the largest of the discriminators is selected. The column headings refer to the discriminant functions (the i values in equation 5), while the row headings correspond to the class to which the spectrum actually belongs. By summing column 1, for example, it is determined that $S_1(\mathbf{x})$ is the largest discriminant a total of 191 times. The compound is actually a carboxylic acid (class 1) 154 times, a value of 80.6% recognition for discriminant $S_i(\mathbf{x})$. Every row sums to 200, since each class contains that number of spectra. Thus 154/200 or 77% of the carboxylic acids are correctly recognized. Clearly, the most desirable situation would be to have large numbers on the diagonal of Table 2 and small numbers elsewhere.

The major interferences are predicted easily from elementary chemical considerations. For example, the greatest problem is class 3 (ketones) interfering with class 2 (esters). As mentioned previously, infrared absorptions are indicative of molecular vibrational transitions. The major characteristic in

IR spectra of both ketones and esters is a peak in the 5.5–6.5 μm region due to carbonyl stretching. Thus, some incorrect recognition is expected.

The nitrile (class 13) discriminant function results in a correct prediction 80% of the time. Much poorer results (48%) are obtained with the amide (class 9) discriminant function. Again chemical considerations are responsible for these facts. The presence of a peak in the 4.4–4.6 μm region is highly characteristic of the triple bond stretching between carbon and nitrogen. This peak is usually present in nitriles and isonitriles and nearly always absent in spectra of the other twelve classes. Therefore, the strong showing of class 13 is not surprising. On the other hand, amides contain a carbonyl group (C = O), as do classes 1, 2, 3, 5, 10 and also a nitrogen atom, as do classes 6, 7, 8, 10, 12, 13. Many of these classes interfere with class 9. Class 10 interferes the most, as expected, since amides and urea derivatives are quite similar in structure.

Table 3 presents the results obtained from pairwise discrimination of the classes, still assuming statistical independence. Each entry in the table indicates the percentage of the time that the two appropriate

TABLE 2—*Maximum Discriminant Case when Statistical Independence Assumed*

Class	Maximum Discriminant Function												
	1	2	3	4	5	6	7	8	9	10	11	12	13
1	154	5	7	0	2	1	0	2	12	10	1	1	5
2	4	171	7	0	2	0	0	1	3	1	8	2	1
3	8	34	105	2	5	3	2	3	11	7	11	5	4
4	0	0	2	160	1	7	9	1	9	3	5	1	2
5	6	4	15	0	144	3	1	5	6	5	3	4	4
6	1	0	1	5	0	133	10	1	25	14	2	6	2
7	1	1	4	9	7	16	105	22	10	5	7	12	1
8	1	10	6	7	5	4	15	115	8	1	18	5	5
9	6	9	9	1	3	10	7	3	113	28	9	1	1
10	5	3	2	0	6	8	3	3	26	134	2	7	1
11	0	5	6	28	6	6	9	9	5	0	119	7	0
12	4	2	3	0	0	5	6	4	8	15	7	134	12
13	1	3	2	3	3	0	2	2	2	13	0	8	161

Overall % = 67.2

TABLE 3—*Pairwise Discrimination Case When Statistical Independence Assumed (in %)*

Class i	Class j												
	1	2	3	4	5	6	7	8	9	10	11	12	13
1													
2	94.8												
3	89.5	86.5											
4	96.5	99.8	96.2										
5	92.8	95.2	89.0	98.8									
6	97.2	99.0	95.8	93.2	97.2								
7	95.8	95.8	93.8	87.8	93.5	88.0							
8	95.0	93.5	90.0	90.2	92.2	93.0	84.5						
9	90.0	93.0	85.8	93.5	92.5	86.2	88.2	89.5					
10	91.8	97.0	92.0	95.0	92.0	89.0	92.0	93.2	79.5				
11	97.2	91.8	89.0	87.0	91.5	95.5	89.0	83.8	90.5	94.5			
12	94.0	96.8	92.8	95.0	95.2	93.0	90.5	94.2	92.8	91.0	93.8		
13	97.2	97.0	95.2	95.5	96.2	97.2	94.5	94.0	96.0	94.0	97.0	91.7	
Overall	94.3	95.0	91.3	94.0	93.8	93.7	91.1	91.1	89.8	91.7	91.7	93.4	95.5

Overall % = 92.9

classes are distinguishable, that is, when the correct discriminant function is maximum. For example, classes 1 and 2 are distinguished 94.8% of the time, while for classes 1 and 3, the technique is 89.5% successful. Once again, the similarity between amides and urea derivatives is manifested by the poor results for distinguishing between classes 9 and 10. Class 13 gives the best results when the overall percentage is calculated (95.5%), while class 9 does the poorest (89.8%).

When the correlation term in the Bahadur-Lazarsfeld expansion is retained, the results improve substantially, but computation time increases fifteenfold. Tables 4 and 5 present the results for the

TABLE 4—*Maximum Discriminant Case When Correlation Term Included*

Class	Maximum Discriminant Function												
	1	2	3	4	5	6	7	8	9	10	11	12	13
1	178	2	3	0	1	0	0	1	5	8	1	0	1
2	3	191	1	0	1	0	0	0	2	0	1	1	0
3	3	14	162	1	3	0	1	1	3	4	2	3	3
4	2	0	0	185	0	3	3	2	2	0	1	2	0
5	1	1	6	0	183	0	0	0	1	3	0	3	2
6	0	0	0	2	0	176	5	0	6	6	2	2	1
7	1	2	0	2	4	7	164	9	6	0	1	4	0
8	0	4	3	4	1	1	10	163	2	3	6	3	0
9	3	5	6	1	2	2	2	3	154	17	5	0	0
10	3	3	1	0	1	3	1	0	2	182	1	3	0
11	0	3	1	12	1	1	5	6	2	0	166	2	1
12	1	1	0	0	0	4	3	1	1	4	1	178	6
13	0	1	0	0	3	0	1	0	2	3	0	1	189

Overall % = 87.3

TABLE 5—*Pairwise Discrimination Case When Correlation Term Included (in %)*

Class i	Class j												
	1	2	3	4	5	6	7	8	9	10	11	12	13
1													
2	97.8												
3	97.2	95.2											
4	99.2	100.0	99.0										
5	98.2	98.8	96.8	99.8									
6	98.5	99.5	98.8	97.5	99.8								
7	99.5	98.8	98.8	96.5	98.8	96.2							
8	99.0	98.0	98.0	97.5	99.0	98.5	94.8						
9	96.8	97.8	96.2	98.0	97.8	97.8	96.5	97.0					
10	96.5	99.2	98.0	99.5	99.0	97.5	98.5	98.8	95.0				
11	99.2	99.0	98.0	95.0	99.0	98.8	97.2	96.2	97.2	98.5			
12	99.5	99.2	98.0	98.8	98.8	97.5	98.0	98.8	99.2	97.5	99.0		
13	99.2	99.2	98.8	99.5	98.5	99.0	99.2	99.8	98.5	99.0	98.5	97.5	
Overall	98.4	98.5	97.7	98.4	98.7	98.3	97.7	98.0	97.3	98.1	98.0	98.5	98.9

Overall % = 98.1

maximum discriminator case and the pairwise discrimination case, respectively. The major interferences are still between similar compounds (esters and ketones, alcohols and ethers, secondary and tertiary amines, amides and ureas), although interferences have decreased.

The retention of the correlation term in the expansion results in the addition of $n(n-1)/2$ extra terms to the statistically independent case (where n is the number of dimensions). Assuming an information contribution from each of these terms, the recognition ability will increase. The addition of extra terms suggests the possibility of overdetermining the data. To determine how well the extra terms represent the data set, the same recognition procedures are performed, using exclusively the correlation term. The results from this test are presented in Tables 6 and 7. Despite the many extra terms involved with the correlations, the results are only slightly better than the one

TABLE 6—*Maximum Discriminant Case for Correlation Term Only*

Actual Class	Predicted Class 1	2	3	4	5	6	7	8	9	10	11	12	13
1	137	7	0	11	4	5	6	2	1	5	0	18	4
2	0	154	4	1	2	3	14	5	5	2	4	0	6
3	1	5	146	12	5	2	8	4	1	2	2	6	6
4	0	2	2	158	2	5	4	2	0	9	2	8	6
5	1	1	1	3	165	8	10	0	0	1	2	6	2
6	1	31	4	5	14	123	2	5	0	1	2	7	5
7	3	13	2	7	12	3	152	1	0	2	0	1	4
8	0	1	4	3	2	9	3	160	0	2	4	7	5
9	1	18	17	19	19	3	2	4	95	3	2	10	7
10	5	11	6	14	7	1	1	4	0	120	2	26	3
11	0	10	0	5	6	0	1	0	0	9	158	3	8
12	2	15	3	23	5	1	2	0	0	2	0	144	3
13	0	10	4	7	7	8	2	2	1	4	1	8	146

Overall % = 71.5

TABLE 7—*Pairwise Discrimination Case for Correlation Term Only (in %)*

Class i \ Class j	1	2	3	4	5	6	7	8	9	10	11	12	13
1													
2	97.2												
3	98.0	97.0											
4	95.8	98.5	95.2										
5	97.8	97.8	97.8	98.0									
6	95.8	90.5	95.5	93.5	94.0								
7	96.8	90.2	95.0	94.0	93.2	97.5							
8	99.0	96.5	97.0	98.0	97.8	94.8	97.8						
9	96.0	91.2	91.5	91.8	92.0	97.8	98.8	95.0					
10	91.5	94.2	92.5	89.8	95.2	97.8	97.0	95.2	94.8				
11	98.5	95.5	98.8	97.5	97.0	98.5	98.2	97.5	96.5	92.2			
12	92.5	93.5	96.0	89.2	95.0	95.8	98.5	97.0	95.0	89.2	99.0		
13	98.0	94.5	95.8	96.2	96.8	95.2	97.2	96.8	96.0	94.2	96.5	96.0	
overall	96.4	94.7	95.8	95.6	96.0	95.6	96.2	96.9	94.7	94.5	97.1	94.7	96.1

overall % = 95.5

term statistical independence approximation. The fact that correlations do well can be predicted since procedures exist which depend primarily on correlation effects [12].

Very little work has been reported using pattern recognition to classify binary infrared data. Three other discrimination procedures using the same data set have been employed in our laboratory. For the first technique, an average spectrum is obtained for each of the thirteen classes by summing each 0.1 μm interval over all 200 class members. Classification of one of the data set members requires that the distance from it to each of the average spectra be measured (14). The class with the average spectrum nearest to the unknown is the class to which the unknown is predicted to belong. Tables 8 and 9 show the distance measurement results for the maximum discriminant case (59%) and the pairwise discriminant case (89.5%), respectively.

The other two techniques are similarity measures. Each of the data set members is taken in turn as the unknown and compared to the remaining members. The unknown is predicted to belong to the same class as the most similar spectrum in the data set. The two similarity measures employed are the Hamming distance and the Tanimoto similarity (13). The results from these predictions for the maximum discriminant case are shown in Table 8. A disadvantage in the similarity measures is that they require the comparison of an unknown with every spectrum in the file. This is a time consuming procedure for the maximum discriminant case. For the pairwise discriminant case, the seventy-eight pairwise predictions take too long to calculate.

5. Summary

A truncated orthogonal expansion has been used to represent binary data taken from a multidimensional file of infrared spectra. Twenty-six hundred spectra in thirteen mutually exclusive classes comprise the 139-dimensional data set.

The expansion represents an approximation for the true class conditional probability density functions. The only terms that are needed for a first approximation are the class conditional probabilities for each peak. Introducing correlations allows a second, more accurate, estimate of the pdf.

The thirteen class problem results in 67.2% correct classification by the class conditional probabilities (the statistical independence assumption). This compares quite favorably with the values of 49%, 54% and 59% obtained from the other three techniques discussed. (Random guessing would result in less than 8% correct classification.) Since the classes chosen are mutually exclusive, the optimal probability of misclassification is zero. However, as discussed previously, chemical considerations quickly show why the optimal probability is not achieved. The classes are not truly independent. For example, classes 1, 2, 3, 5, 9, 10 all contain a carbonyl group and, therefore, all should contain a peak in the carbonyl stretching region. As a result, some incorrect classification is expected.

The thirteen class case is a more difficult problem than one generally hopes to solve by any technique. A more practical situation is to make a prediction as to which of two or three possible classes an unknown might belong. So the results for the pair-

Table 8—*Comparison of Maximum Discriminant Case Results*

	pdf Approx.		Distance	Similarity	
Class	1st Order	2nd Order	from Means	Distance	Tanimoto
1	81	91	67	61	58
2	69	84	62	66	72
3	62	89	56	40	42
4	74	89	59	56	60
5	78	92	73	56	67
6	69	89	63	52	52
7	62	84	43	40	52
8	67	88	60	46	55
9	48	82	43	22	33
10	58	79	50	48	48
11	62	89	54	34	46
12	69	88	59	58	59
13	80	93	76	63	55
Overall	67	87	59	49	54

TABLE 9—*Comparison of Pairwise Discriminant Case Results*

	pdf Approx. 1st Order	pdf Approx. 2nd Order	Distance from Mean
% correct	92.9	98.1	89.5

wise discrimination case of 92.9% when statistical independence is assumed and 98.1% when it is not assumed are very satisfactory.

In addition, work is in progress in this laboratory to determine the effect of feature reduction (selecting a much smaller set of variables) on the classification results obtained. Should the results compare favorably with those from this work, then one would have an extremely useful classification tool, as the time required for classification would be greatly reduced.

Selection of the best classification technique for a particular problem is dependent upon the situation. If the unknown spectrum happens to be included in an accessible file, then a search system is one of the best approaches. For some situations where the unknown is not in the file, the techniques described in this paper might be superior to a search. With statistically independent data, the first order approximation is a rapid and accurate means of classification. When the correlation terms are included, the time required for classification is similar to that for a search, but the results obtained are different. The second order approximation of the pdf's results in a functional group categorization, whereas, a search results in a general similarity measure. The choice of the better approach is clearly a function of the problem to be solved.

6. Acknowledgment

This work was supported by the Materials Research Center, University of North Carolina under contract number DAHC-15-73-69 with the Advanced Research Projects Agency. The financial support of the National Science Foundation is gratefully acknowledged. The authors wish to express their gratitude to the Associate Editor for the constructive suggestions which led to an improvement of this paper.

References

[1] Anderson, D. H. and Covert, G. L., (1967). "Computer Search and Retrieval System for Infrared Data", *Anal. Chem., 39,* 1288–1293.

[2] Bahadur, R. R., (1961). "A Representation of the Joint Distribution of Responses to *n* Dichotomous Items", *Studies in Item Analysis and Prediction* (ed. H. Solomon), 158–68, Stanford University Press, Stanford.

[3] Chow, C. K., (1965). "Statistical Independence and Threshold Functions", *IEEE Trans. on Electronic Computers, EC-14,* 66–68.

[4] Duda, R. O. and Hart, P. E., (1973). *Pattern Classification and Scene Analysis,* Wiley-Interscience, New York.

[5] Erley, D. S., (1968). "Fast Searching System for the ASTM Infrared Data File", *Anal. Chem., 40,* 894–898.

[6] Isenhour, T. L. and Jurs, P. C., (1971). "Some Chemical Applications of Machine Intelligence", *Anal. Chem., 43,* 20A–35A.

[7] Ito, T., (1968). "A Note on a General Expansion of Functions of Binary Variables", *Information and Control, 12,* 206–211.

[8] Jurs, P. C., (1971). "Near Optimum Computer Searching of Information Files Using Hash Coding", *Anal. Chem., 43,* 364–367.

[9] Lord, F. M., (1962). "Review of *Studies in Item Analysis and Prediction*", *Psychometrika, 27,* 207–213.

[10] Lytle, F. E., (1970). "Computerized Searching of Inverted Files", *Anal. Chem., 42,* 355–357.

[11] Moore, D. H., II, (1973). "Evaluation of Five Discrimination Procedures for Binary Variables", *J. Amer. Statist. Assoc., 68,* 399–404.

[12] Otsu, N., (1972). "An Optimal Nonlinear Transformation Based on Variance Criterion for Pattern Recognition I. Its Derivation", *Bul. Electrotech. Lab., 36,* 815–830.

[13] Rogers, D. J. and Tanimoto, T. T. (1960). "A Computer Program for Classifying Plants", *Science, 132,* 1115–1118.

[14] Woodruff, H. B., Lowry, S. R., and Isenhour, T. L. (1975). "A Comparison of Two Discriminant Functions for Classifying Binary Infrared Data", *Appl. Spectrosc., 29,* 226.

Reprinted from **ANALYTICAL CHEMISTRY**, Vol. 48, Page 1027, June 1976
Copyright 1976 by the American Chemical Society and reprinted by permission of the copyright owner

Relationship between Mutual Information and Classification

G. L. Ritter, S. R. Lowry, H. B. Woodruff, and T. L. Isenhour*

Department of Chemistry, University of North Carolina, Chapel Hill, N.C. 27514

Mutual information is an information theory term, which describes the amount of information to distinguish among members of different classes. This concept is demonstrated for describing the classification ability of a maximum likelihood classifier. In an artificially generated problem, the recognition ability and the square root of mutual information are seen to be linearly related. The linear correlation drops to 0.83 for a series of infrared questions where the statistical independence assumption is not strictly valid.

In most chemical problems, the goal is to find some transformation of measured experimental properties that reveals another more obscure chemical or physical property. Recently there has been interest in applying the principles of information theory to such chemical systems (cf. *1–3*).

Modern information theory is largely a result of work done by Claude Shannon in the 1940's (*4*). Shannon was investigating communication systems where a message is transferred from a transmitter to a receiver. In this work, he assumed that the source of the message was stochastic, and he wished to exactly or approximately reproduce the message at the receiver. The solution to the problem required a definition of an uncertainty or "entropy" in the message at the receiver.

In chemical systems, the format of the information theory problem is usually similar. First, an experimenter measures an event, X, which may take on any of several states, x_i. The outcome of X must fall into one of the states; call it x_k. The fraction of the time that x_k occurs denotes a probability for the state, p_k. Given this stochastic form for X, information theory defines information or entropy as a measure of the uncertainty in predicting the state of X. Shannon suggested the following as a measure of the uncertainty for a system of n possible states.

$$H = -\sum_{i=1}^{n} p_i \log_2 p_i \qquad (1)$$

Some other event, Y may occur in conjunction with X. A complete description of this system requires not only a probability scheme for the states of X, but also a probability scheme for Y and a set of conditional probabilities. The conditional probability, denoted $P_{k|j}$, indicates the probability of state x_k arising when Y is in steady y_j. From the complete set of probabilities and conditional probabilities, the mutual information may be found. The mutual information is the amount of information in the event X to determine the state of Y (*5*). These definitions suggest the application of information theory to chemical classification problems.

In the classification problem, we wish to distinguish or discriminate an obscure chemical or physical property by use of a mathematical transformation of the measured experimental quantities. This property classifier is normally designed to minimize the number of incorrect categorizations in a collection of known data. If the classifier is to do well, then there must be information in the experimental data to determine the unknown property. To test the relationship between classification or discrimination and mutual information, we wish to choose a classifier that is stochastic and attempts to minimize the number of errors. This classifier is a maximum likelihood estimator.

The spectroscopic data that we use to test the relationship are a series of substructure questions using infrared spectra. The spectra are coded in an intensity eliminated or peak/no peak form. From the experimentally measured binary infrared spectra, we attempt to estimate the amount of information to determine the various chemical substructures. In the classification decision, the category or substructure that is most likely to give the infrared spectrum of the unknown is selected. If the mutual information content is high, then the recognition ability should also be high.

DATA

The data for this study have been taken from the American Society for Testing and Materials file of 91 875 binary infrared spectra. Thirteen mutually exclusive classes were chosen as the criterion for selecting spectra (Table I) (*6*). Of the spectra belonging exclusively to each of the classes, 200 were randomly chosen and placed into the data set. The resulting 2600 compounds each contain fewer than sixteen carbons and contain only hydrogen, oxygen, and nitrogen otherwise. Each compound is represented by a peak/no peak spectrum in the range 2.0 to 15.9 μm. This range is divided into 139 equal-sized intervals, each describing whether a peak maximum occurs in the corresponding interval. For convenience, therefore, each spectrum is given as a 139-dimensional binary vector **x** such that

Table I. Chemical Classes Used in the Study

Class No.	Chemical functionality	
1	Carboxylic acid	RCOH
2	Ester	RCOR′
3	Ketone	RCR′
4	Alcohol	ROH
5	Aldehyde	RCH
6	1° Amine	RNH
7	2° Amine	RNR′
8	3° Amine	RNR″
9	Amide	RCN(R′)R″
10	Urea and derivatives	R′R″NCNRR‴
11	Ether and acetal	ROR′, RCH(OR′)OR″
12	Nitro and nitroso	RNO$_2$, RN=O
13	Nitrile and isonitrile	RCN, RNC

$$\mathbf{x} = (x_1, x_2, x_3, \ldots x_i, \ldots x_{139})$$

and

$$x_i = \begin{cases} 1, \text{ if a peak maximum occurs in the 0.1-}\mu\text{m interval} \\ \text{preceding } (2.0 + 0.1\,i)\mu\text{m} \\ 0, \text{ otherwise} \end{cases}$$

This type of problem is motivated by the increasing size of many data files. In order to store the file easily, an intensity eliminated format may be used. Thus, special interest is needed in solving problems with binary data.

THEORY

The classification methods used in this paper have been described extensively elsewhere and therefore will be reviewed only briefly.

Recognition (7, 8). The classification algorithm assumes that all of the descriptive parameters, the infrared peak positions, are statistically independent. The classification scheme is illustrated in the following example. Suppose that an investigator decides that a classification decision may be made on the basis of one spectral interval (denoted by x_1). From the information in this interval, the compound is to be classified into one of two classes, c_1 or c_2. The statistical maximum likelihood classifier requires the knowledge of four conditional probabilities, 1) the probability of a peak maximum in x_1 for members of c_1, 2) the probability of no peak maximum in x_1 for c_1, 3) the probability of a peak maximum in x_1 for c_2, and 4) the probability of no peak maximum in x_1 for c_2. These four probabilities are designated $P(x_1 = 1 \mid c_1)$, $P(x_1 = 0 \mid c_1)$, $P(x_1 = 1 \mid c_2)$ and $P(x_1 = 0 \mid c_2)$. Since a peak maximum must either occur or not occur in a given interval only two of these probabilities are independent, i.e., since $P(x_1 = 1 \mid c_j) + P(x_1 = 0 \mid c_j) = 1$, only $P(x_1 = 1 \mid c_j)$ is needed to describe c_j. An example of these probabilities is shown in Table II. The value for $P(x_1 = 1 \mid c_1)$ implies that ¼ of all class 1 spectra have a peak maximum in x_1. Similarly ½ of all class 2 spectra have $x_1 = 1$. The maximum likelihood decision then chooses the class which is most likely to have that response. Thus, if an unknown is found to have a peak maximum in x_1 (i.e., $x_1 = 1$), the decision will be class 2. Class 2 is chosen since ½ of c_2 have $x_1 = 1$ and only ¼ of c_1 have $x_1 = 1$.

Table II. Example Probabilities for One Spectral Interval

$P(x_1 = \delta_1 \mid c_j)$	$j = 1$	$j = 2$
$\delta_1 = 1$	¼	½
$\delta_1 = 0$	¾	½

Table III. Example Probabilities for Two Spectral Intervals

	$P(x_i = \delta_i \mid c_j)$	$j = 1$	$j = 2$	$P(x_i = \delta_i)$
$i = 1$	$\delta_1 = 1$	¼	½	⅜
	$\delta_1 = 0$	¾	½	⅝
$i = 2$	$\delta_2 = 1$	⅓	⅜	17/48
	$\delta_2 = 0$	⅔	⅝	31/48

Table IV. Joint Probabilities if Statistical Independence is Valid

$P(\delta_1, \delta_2 \mid c_j)$	$j = 1$	$j = 2$
$\delta_1 = 1, \delta_2 = 1$	1/12	3/16*
$\delta_1 = 1, \delta_2 = 0$	1/6	5/16
$\delta_1 = 0, \delta_2 = 1$	¼*	3/16*
$\delta_1 = 0, \delta_2 = 0$	½*	5/16

At this point, the investigator may decide that a more accurate decision may be made if a second spectral interval, x_2 is added. The probabilities for x_2 are included in Table III. Then, if the unknown is found to have no peak maximum in x_2, which classification decision should be made? Or, which is larger $P(1,0 \mid c_1)$ or $P(1,0 \mid c_2)$? If the intervals are assumed to be statistically independent, then $P(1,0 \mid c_j)$ will be the product of $P(x_1 = 1 \mid c_j)$ and $P(x_2 = 0 \mid c_j)$.

$$\begin{aligned} P(1,0 \mid c_1) &= P(x_1 = 1 \mid c_1) \cdot P(x_2 = 0 \mid c_1) \\ &= (\tfrac{1}{4}) \cdot (\tfrac{2}{3}) \\ &= \tfrac{1}{6} \end{aligned} \qquad (2)$$

$$\begin{aligned} P(1,0 \mid c_2) &= P(x_1 = 1 \mid c_2) \cdot P(x_1 = 0 \mid c_2) \\ &= (\tfrac{1}{2}) \cdot (\tfrac{5}{8}) \\ &= \tfrac{5}{16} \end{aligned}$$

Since 5/16 of all c_2 spectra have a (1,0) spectrum and ⅙ of c_1 spectra have (1,0) spectrum, the decision is still class 2.

Table IV presents the joint probabilities for each possible spectrum in both classes. The starred values indicate the maximum likelihood estimates.

This concept is extended to three, four, or more spectral intervals in the obvious way. In turn, each probability is multiplied and the overall products are compared to make the classification decision.

$$\begin{aligned} P(x \mid c_j) &= P(\delta_1, \delta_2 \ldots, \delta_d \mid c_j) \\ &= \prod_{i=1}^{d} P(x_i = \delta_i \mid c_j) \end{aligned} \qquad (3)$$

Equation 3 may be written in a linear form when the following steps are taken. First the notation is changed so that $p_{i|j} = P(x_i = 1 \mid c_j)$ and then Equation 3 is rewritten

$$P(x \mid c_j) = \prod_{i=1}^{d} (p_{i|j})^{1-\delta_i}(1 - p_{i|j})^{1-\delta_i} \quad (4)$$

This is equivalent to Equation 1 since if $\delta_i = 1$, only $p_{i|j}$ is included in the product and if $\delta_i = 0$, only $(1 - p_{i|j})$ is included in the product.

If the logarithm of both sides is taken, then the class is chosen such that the following term is maximized

$$\log P(x \mid c_j) = \sum_{i=1}^{d} \delta_i \log \frac{p_{i|j}}{(1 - p_{i|j})} + \sum_{i=1}^{d} \log (1 - p_{i|j}) \quad (5)$$

Information Theory and Mutual Information (9). The mutual information is the average amount of information to distinguish members of class 1 from members of class 2. This is best explained and calculated as the difference between the total average entropy of the spectra and the average conditional entropy of the spectra.

The total average entropy, $H(x)$, is the average amount of information to distinguish among the spectra. In other words $H(x)$ is the average amount of information to distinguish 1) among members of class 1, 2) among members of class 2, and 3) among members of class 1 and class 2. If all of the spectra have some interval in which no peak maximum occurs, then p_k (the probability of a peak occurring in interval k regardless of class) is zero. Then, in this spectral interval, there is no information to distinguish a spectrum from any of the others, or $H(x_1)$ should be zero. However, if, in the spectral interval, a maximum does occur in some of the spectra, then there should be some information present to discriminate among spectra and $H(x_1)$ should not be zero. The value of $H(x_1)$ when two responses are possible is given by

$$H(x_1) = -p_1 \log p_1 - (1 - p_1) \log (1 - p_1) \quad (6)$$

Normally, the logarithms are taken to the base 2 and the units of the result are "bits". According to this formula, the maximum information occurs when $dH/dp_1 = 0$; this occurs if $p_1 = \frac{1}{2}$. The total average entropy when $p_1 = \frac{1}{2}$ is

$$H(x_1) = -\tfrac{1}{2} \log \tfrac{1}{2} - \tfrac{1}{2} \log \tfrac{1}{2} = 1 \text{ bit} \quad (6a)$$

If the measurements are statistically independent, the total average entropy for x is the sum of the entropies for each parameter.

$$H(x) = \sum_{i=1}^{d} H(x_i) \quad (7)$$

$$= -\sum_{i=1}^{d} [p_i \log p_i + (1 - p_i) \log (1 - p_i)]$$

In the example given in Table III, the last column indicates p_i if the classes are assumed to be the same size. The total average entropy is calculated below.

$$H(x) = -\tfrac{7}{8} \log \tfrac{7}{8} - \tfrac{5}{8} \log \tfrac{5}{8} - \tfrac{17}{48} \log \tfrac{17}{48} - \tfrac{31}{48} \log \tfrac{31}{48} = 1.89 \text{ bits} \quad (8)$$

Therefore, there is an average of 1.89 bits to distinguish the spectra.

The average conditional entropy, $H(x \mid c)$, measures the average information to distinguish among members of the same class. The conditional entropy for c_1 is calculated as shown below where the conditional probabilities are used in the calculation.

$$H(x \mid c_1) = -\sum_{i=1}^{d} [p_{i|1} \log p_{i|1} + (1 - p_{i|1}) \log (1 - p_{i|1})] \quad (9)$$

The conditional entropies are summed for both classes to give $H(x \mid c)$. Each term in the sum is weighted by the relative class size. If $P(c_j)$ is the probability that class j occurs, then

$$H(x \mid c) = \sum_{j=1}^{2} P(c_j) H(x \mid c_j) \quad (10)$$

$$= \sum_{j=1}^{2} P(c_j) \sum_{i=1}^{d} [p_{i|j} \log p_{i|j} + (1 - p_{i|j}) \log (1 - p_{i|j})$$

The class probabilities must be consistent with the maximum likelihood classifier that is used earlier. In this classifier, each class is assumed to be equally probable, or $P(c_1) = P(c_2) = \frac{1}{2}$. Using this, $H(x \mid c)$ is calculated below.

$$H(x \mid c) = -\tfrac{1}{2}[\tfrac{1}{4} \log \tfrac{1}{4} + \tfrac{3}{4} \log \tfrac{3}{4} + \tfrac{1}{3} \log \tfrac{1}{3} + \tfrac{2}{3} \log \tfrac{2}{3}] - \tfrac{1}{2}[\tfrac{1}{2} \log \tfrac{1}{2} + \tfrac{1}{2} \log \tfrac{1}{2} + \tfrac{3}{8} \log \tfrac{3}{8} + \tfrac{5}{8} \log \tfrac{5}{8}] = 1.84 \text{ bits} \quad (11)$$

Thus, there are 1.84 bits of information to distinguish among members of the same class.

The difference between the total average entropy and the average conditional entropy is the average information to distinguish among members of class 1 and class 2. This is the mutual information (M.I.).

$$\text{M.I.} = H(x) - H(x \mid c) \quad (12)$$

In the example the mutual information is

$$\text{M.I.} = 1.89 - 1.84 = 0.05 \text{ bit} \quad (13)$$

Then only 0.05 bit of information is available to distinguish among the members of the two classes. This is the basis for the expected parallel between recognition ability and mutual information.

RESULTS

In the example problem, the mutual information is 0.05 bit and the recognition ability is still unknown. This recognition may be estimated if the independence assumption is true. In this case, the probability for each possible two-dimensional spectrum for each class is collected in Table IV. Given a maximum likelihood decision, if an unknown spectrum is (1,1), it will be placed into class 2. However, this forces the $\frac{1}{12}$ of all class 1 spectra which are represented by (1,1) to be incorrectly classified. Since the classes are assumed to be equiprobable, $\frac{1}{24}$ of all possible spectra are misclassified if the spectrum is (1,1). Similarly $\frac{1}{8}$ of the class 1 spectra (or $\frac{1}{12}$ of all the spectra) are misclassified if the spectrum is (1,0). The total proportion misclassified then is

$$\text{error rate} = \frac{1}{24} + \frac{1}{12} + \frac{3}{24} + \frac{5}{32} = \frac{3}{8} \quad (14)$$

Then three out of every eight spectra are misclassified given this set of probabilities and the expected recognition is 62.5% for this problem.

The relationship between M.I. and recognition is first tested by randomly generating a set of tables similar to Table II. Once the values of $P(x_1 = 1 \mid c_1)$, $P(x_2 = 1 \mid c_1)$, $P(x_1 = 1 \mid c_2)$ and $P(x_2 = 1 \mid c_2)$ have been generated, the M.I. and expected recognition are calculated as shown above. A plot of M.I. vs. recognition is shown in Figure 1 for 100 randomly drawn probability sets. In Figure 2, the recognition is plotted vs. the square root of the M.I. This plot appears linear and has linear correlation of 0.98. The relationship between recognition and mutual information appears unmistakable for the artificial problem. Difficulties with the probabilities not strictly obeying the independence assumption are investigated in the infrared application.

The seventy-eight pairwise questions generated from the thirteen classes of infrared spectra are used as an empirical

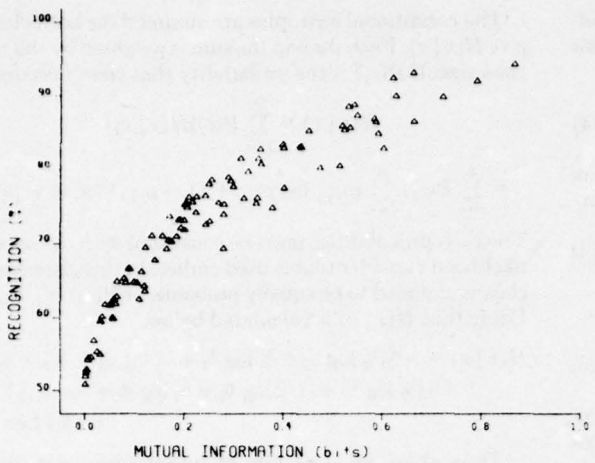

Figure 1. Plot of recognition vs. mutual information for a set of randomly selected two-dimensional classifiers

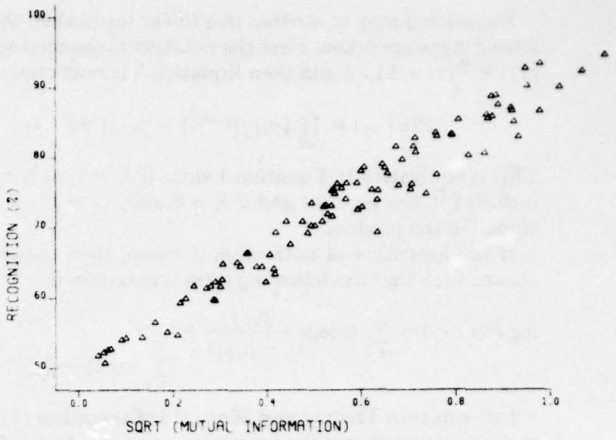

Figure 2. Plot of the data in Figure 1, recognition vs. square root of mutual information

Table VA. Recognition Results for Two Class Problems (in %)

	1	2	3	4	5	6	7	8	9	10	11	12	13
1													
2	94.8												
3	89.5	86.5											
4	96.5	99.8	96.2										
5	92.8	95.2	89.0	98.8									
6	97.2	99.0	95.8	93.2	97.2								
7	95.8	95.8	93.8	87.8	93.5	88.0							
8	95.0	93.5	90.0	90.2	92.2	93.0	84.5						
9	90.0	93.0	85.8	93.5	92.5	86.2	88.2	89.5					
10	91.8	97.0	92.0	95.0	92.0	89.0	92.0	93.2	79.5				
11	97.2	91.8	89.0	87.0	91.5	95.5	89.0	83.8	90.5	94.5			
12	94.0	96.8	92.8	95.0	95.2	93.0	90.5	94.2	92.8	91.0	93.8		
13	97.2	97.0	95.2	95.5	96.2	97.2	94.5	94.0	96.0	94.0	97.0	91.7	

Table VB. Mutual Information for Two Class Problems (in bits)

	1	2	3	4	5	6	7	8	9	10	11	12	13
1													
2	2.17												
3	1.11	1.01											
4	2.55	1.71	1.48										
5	1.67	1.63	1.28	2.05									
6	2.57	2.61	1.89	1.38	2.36								
7	1.98	2.13	1.40	1.15	1.86	0.98							
8	1.96	1.61	1.32	1.37	1.55	1.74	0.72						
9	1.45	2.24	1.22	1.81	1.95	1.14	1.20	1.65					
10	1.78	2.56	1.55	2.22	1.85	1.25	1.60	2.10	0.74				
11	2.00	1.34	1.07	1.19	1.86	1.55	0.91	0.80	1.52	2.30			
12	2.10	2.52	1.88	2.40	2.44	1.55	1.38	1.65	1.37	1.74	1.47		
13	1.89	2.29	1.74	2.08	1.79	1.97	1.73	2.00	1.82	1.82	1.91	1.61	

test of the relationship between M.I. and recognition. In the training step, the data set is used to estimate the class conditional probabilities. The members of the training set are then classified in the recognition step.

The recognition results for the 78 questions have been computed and are tabulated in Table VA. The entry in row i and column j indicates the percentage of (the 400) spectra in classes i and j that are correctly classified. The recognition results lie in the range [79.5–99.8%] which indicates that the classification algorithm is quite successful. Table VB presents the amount of M.I. (in bits) calculated for each question. The general format of the table is the same as in Table VA. Again, if the M.I. is related to the recognition ability, a high correlation is expected between the corresponding elements of the two tables.

The linear correlation between the recognition and the square root of M.I. is calculated to be 0.83. For random, unrelated variables the probability of a correlation this high is $\ll 0.001$. In this real problem, M.I. and recognition are positively correlated. In more quantitative terms when the M.I. is less than 1.3 bits, the recognition rate is below 90%. Similarly when the M.I. is at least 2.0 bits, the recognition is greater than or equal to 93%. In fourteen of the 20 cases where M.I. is ≥ 2.0 bits, the recognition is at least 95%.

There are some inconsistencies in the comparison. A notable example is the ester (class 2)-alcohol (class 4) question. Despite the very high recognition (399 of 400 are correctly classified), M.I. is only moderately high, 1.71 bits. The inconsistency results from two factors: 1) the invalidity of the statistical independence approximation for the infrared spectral intervals and 2) the scatter in the plot of recognition vs. the square root of M.I. when statistical independence is true. The first factor may be illustrated by the dependence of the C=O and O—H stretches in carboxylic acids. The second factor is seen in Figure 2.

Thus far, we have no clue to the amount of mutual information that is necessary to absolutely determine the correct class if the statistical independence assumption is valid. When there is complete inter-class information (i.e., no two samples in different classes have the same spectrum), the M.I. is given by

$$\text{M.I. (indep)} = -\sum_j P(c_j) \log P(c_j) \qquad (15)$$

[$P(c_j)$ again is the probability of occurrence of class j.] For the two class equiprobable case, $P(c_1) = P(c_2) = \frac{1}{2}$ and M.I. (indep.) is 1.0 bit. This implies that 1 bit of mutual information is necessary to distinguish separable, equi-probable classes. A value of M.I. greater than 1.0 bit implies that there is redundant information in the data. This, however, is consistent with the statistical dependence of the data.

If the mutual information is to adequately rate a classifier, then the degree of statistical independence must be similar for each question (this is factor 1 above). Since a high correlation is found in the infrared problem, this is a good supposition and M.I. does act as a guide to the predictive ability of the maximum likelihood estimator.

CONCLUSION

The mutual information is shown to be directly related to the classification ability of a maximum likelihood classifier. First, the relationship is demonstrated on an artificially generated set of probability schemes. In this problem, the linear correlation between recognition and the square root of M.I. is given to be 0.98. This high degree of correlation is further tested on a collection of binary infrared spectra. In this case, the linear correlation between recognition and M.I.$^{1/2}$ is 0.83. The decrease in the degree of correlation is caused by the invalidity of the statistical independence assumption for the infrared spectral intervals. The order of magnitude of the mutual information for the infrared problems is a direct function of the probability scheme and the degree of statistical independence. Since the magnitude of the latter component cannot be estimated beforehand, M.I. serves best as a comparative measure of recognition ability. This best describes the role of information theory for predicting classification results.

LITERATURE CITED

(1) R. D. Levino and R. Kosloff, *Chem. Phys. Lett.*, **28**, 300 (1974).
(2) H. P. Yockey, *J. Theor. Biol.*, **46**, 369 (1974).
(3) A. Eskes, F. Dupuis, A. Dijkstra, H. DeClerq, and D. L. Massart, *Anal. Chem.*, **47**, 2168 (1975).
(4) C. E. Shannon, *Bell Syst. Tech. J.*, **27**, 379 (1948).
(5) H. C. Andrews, "Mathematical Techniques in Pattern Recognition", Wiley-Interscience, New York, 1972.
(6) H. B. Woodruff, S. R. Lowry and T. L. Isenhour, *Anal. Chem.* **46**, 2150 (1974).
(7) C. K. Chow, *IEEE Trans. Electron. Comput.*, **EC-14**, 66 (1965).
(8) H. B. Woodruff, G. L. Ritter, S. R. Lowry, and T. L. Isenhour, *Technometrics*, **17**, 455 (1975).
(9) F. M. Reza, "An Introduction to Information Theory", McGraw-Hill, New York, N.Y., 1961.

RECEIVED for review September 8, 1975. Accepted March 15, 1976. This work was supported by the Materials Research Center, University of North Carolina under contract number DAHC-15-73-69 with the Advanced Research Projects Agency. The financial support of the National Science Foundation is also appreciated.

FEASIBILITY OF A ONE-DIMENSIONAL SEARCH SYSTEM

G. L. Ritter and T. L. Isenhour

The University of North Carolina
Department of Chemistry
Chapel Hill, North Carolina

The financial support of the National Science Foundation (Grant GP-43720) and the Materials Research Center, University of North Carolina (Contract Number DAHC-15-73-69) with the Advanced Research Projects Agency is gratefully acknowledged.

Abstract

There has been frequent interest in the chemical literature describing methods for the rapid search of large data collections. Since these collections may contain 10^4 to 10^5 entries, any similarity search is difficult. However if one number is assigned to each entry and that number retains all similarity information, then a simple binary search can produce the data collection entries that are most similar to an unknown. This approach is investigated for a file of gas chromatographic liquid phases and for a large set of mass spectra. Obvious limitations occur when the data is multi-dimensional. However indications of multi-dimensional similarity are retained even in the difficult mass spectral example.

Three methods have been applied to the interpretation of spectral data. These methods fall into the general categories of file searching, pattern recognition and artificial intelligence.[1]

Artificial intelligence is an attempt to encode the rules that are used to interpret the spectrum. This system is the most theoretical method since the spectra of no known compounds are used in the interpretation.[2] Pattern recognition is a more empirical technique. Known compounds are used to determine effective classifiers of molecular substructures. The classifiers provide only structural information and, in general, no absolute identification.[3]

File search methods have received considerable attention in identifying data library members.[4-7] The first step in the search procedure is the coding of a library of known compounds. Frequently the code for a compound is some subset of the complete spectrum. This is adequate since, for example, the information in a mass spectrum is overdetermined. Much of the information can be deleted without giving up the possibility of analytical reliability.

The unknown is coded in the same way and then compared to the members of the library. The unknown may be compared to all members of the library or to some selected subset (for example, in hash coding[8] or inverted files[9]). Those members of the file that are most similar to the unknown are reported. The efficacy of the file search algorithm is determined by the data collection, the coding method and the similarity measure.

This work investigates the feasibility of a one-dimensional search system. In this system each library member is coded into one number.

Ideally very similar compounds will be assigned numbers that are nearly the same.

Setting up a one-dimensional search. A search strategy depends on a measure of similarity between two entities. When an appropriate similarity measure is accepted, the searcher is interested in finding the library members that are most similar to his unknown. A proper choice of similarity means that the file members that are reported are structurally like the unknown.

In the search algorithm the information that is coded represents several measurements on an entity. Suppose, for example, that two measurements have been made on each of nine entities. A plot of the measurement values is shown in Figure 1. Let entity A be most similar to entity B since they are spatially close, i.e. B is nearest to A. Similarly A and C are most similar to B. When each entity is projected onto the 45° line (Figure 2(a)), the representation is modified to Figure 2(b). However B is still most similar to A and all other spatial similarities are also maintained. In the projection only one number is used to describe each point, A through I. If this set is reasonably complete, there is a high probability that some arbitrary unknown is in the set, or at least that a very similar compound is in the set. The unknown is projected onto the 45° line and compared to the one-dimensional projections of the library members. In this example the low dimensionality form is very successful.

Figure 3 illustrates an example where a 1-dimensional scheme is less impressive. Again B is most similar to A and all of the near neighbor information is contained in Table 1. Each point is projected onto a

45° line and the result is shown in Figure 4. In this form C, G and H are nearer to A than is B. The last column in Table 1 indicates the one-dimensional near neighbor rankings for the sample points. In this problem to be certain that the most similar compound appears in a list, six entities must be reported in the 1-dimensional solution.

The general problem involves finding a transformation of the multi-dimensional data so that for entity A as many of its n most similar entities appear in the m most similar entities in the 1-dimensional representation ($m \geq n$). If k measurements have been made for entity A, then $A = (a_1, a_2, \ldots, a_k)$ where a_i is the value for measurement i. The 1-dimensional form is a linear combination of the measured values. The number, N which describes A depends on the measurements and a set of weights $\{c_i, i = 1, k\}$.

$$N_A = \sum_{i=1}^{k} c_i a_i \qquad (1)$$

As the number of measurements increases, the difficulty in finding an effective 1-dimensional search should also increase.

A one-dimensional search in gas chromatographic analysis. The search strategy is best illustrated in a real example. The example described in this section uses the gas chromatographic retention data collected by McReynolds.[10] McReynolds tabulated quantitative retention data on 226 stationary (liquid) phases. Each liquid phase was described by its behavior in retaining ten test solutes. The test solutes were defined to cover the range of separations normally attempted by GC (see Table 2). In this illustration the liquid phases are ordered so that each phase remains close to other phases that are similar to it. The

subsequent discussion will consider the development and application of this search system.

The first consideration is the type of similarity measure that will be used. According to work by Leary, et al.,[11] one method of denoting the similarity between phases A and B is as a simple Euclidean distance between A and B.

The distance between A and B, d_{AB} is calculated by

$$d_{AB} = \left[\sum_{i=1}^{10} (\Delta I_{iA} - \Delta I_{iB})^2 \right]^{1/2} \qquad (2)$$

where ΔI_{iA} is the reported retention value for standard solute i on phase A. In the one-dimensional form

$$d_{AB}^{N} = |N_A - N_B|. \qquad (3)$$

The next problem is determining the values for the ten constants c_i. These values must be chosen so that the n most similar phases to A appear among the m most similar phases in a one-dimensional form.

The gas chromatographic data has been analyzed by McCloskey and Hawkes[12] in a principal component analysis. They found that nearly all of the variance in the data could be described in one factor. In chromatographic terms separations are done almost exclusively on the basis of polarity. Graphically the one factor is illustrated in the plot of retention results on nitropropane and pyridine (Figure 5). The ten values reported by McCloskey are given in Table 3 (the values are modified to remove the effect of autoscaling in McCloskey's work). Since very little other variance appears in the data, the values for c_i are taken to be equal to the first principal component terms.

Using the c_i values, each liquid phase is given *one* numerical value, so that 226 values now describe the 226 stationary phases. These 226 numbers (and the corresponding phases) are placed into ascending numerical order. The phases are now set up for a binary search. The binary search depends upon an ordered list of $2^n - 1$ entities. If there are t entities, then n is chosen so that

$$2^{n-1} - 1 < t \leq 2^n - 1. \tag{4}$$

Using the ordered phases, the remaining $2^n - t - 1$ spaces are filled with large values. In the GC liquid phase example t = 226, n = 8 and the remaining $2^8 - 226 - 1 = 29$ search spaces are filled by large numbers. The first 226 spaces have been filled with the ordered list of numbers for the chromatographic phases.

For the sake of the following argument suppose that only 14 phases exist in the data set, or more appropriately, suppose that an unknown stationary phase is most likely to be very similar (or identical) to one of 14 particular liquid phases. When these phases, denoted A through N, are projected into one value using eq. (1), the values in column 2 of Table 4 are found. In columns 4 and 5 the phases are reordered in numerical order. Value 0 is added to complete the table. An unknown is introduced which is found to have value 121. The value for the unknown is first compared to the $2^{n-1} = 2^3 = 8$th phase. The value 121 is greater than 103 and therefore the unknown must lie between phases 8 and 15. The next entity checked is number $2^3 + 2^2 = 12$. (Had the unknown value been less than 103, then the next entity would be $2^3 - 2^2 = 4$.) Value 121 is less than 127 and now the unknown is trapped between phases 8 and 12. Next entity $2^3 + 2^2 - 2^1 = 10$ is

checked. Since 121 is greater than 115, the unknown lies between phases 10 and 12. Finally the $2^3 + 2^2 - 2^1 + 2^0$ (= 11th) entity is tested to find that the unknown falls between knowns 11 and 12. The unknown is then most similar to phases J and A. The most similar is J since

$$d^N_{JU} = |118 - 121| = 3 < d^N_{AU} = |127 - 121| = 6 \qquad (5)$$

In n (= 4) lookups in the ordered table the unknown is trapped between two entities.

The ability of the one-dimensional search to maintain the similarity in the multi-dimensional data was measured by another experiment. The three phases most similar to each of the 226 library entities were computed using all ten standard solutes (according to eq. (2)). For liquid phase A the three nearest phases are denoted A_1, A_2 and A_3, respectively. Using the one-dimensional values, the number of phases that are nearer to A than is A_1 are counted and that number is called P_1. Similarly P_2 and P_3 are enumerated. Figure 6(a) is the distribution of the P_1 values for all liquid phases. For 30% of the phases the most similar phase in ten dimensions is also the most similar phase in one dimension. If five phases are reported, then the actual most similar phase is included for 70% of the liquid phases. Figure 6(b) shows the distribution of all the values for P_1, P_2 and P_3. A total of 62% of these 678 true neighbors appear in the five most similar transformed phases. Figure 6(c) presents the distribution of P where $P = \min \{P_1, P_2, P_3\}$. Thus when five neighbors are reported, at least one of the actual three most similar phases will be present for 85% of the phases.

The one-dimensional strategy therefore is successful in this example where nearly all variance lies along one direction. However search systems have usually been designed for large data collections and the large multi-dimensional files introduce several new problems into the analysis. These problems will become more apparent in the mass spectral search that is discussed in the subsequent sections.

The one-dimensional mass spectral search system. The one-dimensional search technique has been investigated using a large file of mass spectra. The specific problem is reproducing the similarity in a set of 1827 sulfur containing compounds taken from McLafferty's low resolution mass spectral data file.[13] The spectra are chosen so that the highest 1% fragment does not exceed 400 amu. and such that only the elements C, H, N, O, S, Cl, Br, F, I, and P occur in the compounds. Since only the integral mass positions are included, each compound is represented by a string of 400 numbers, x_i, the intensities at the 400 mass positions.

The difficulty in reproducing intensities from instrument to instrument has led to a reduced intensity format for the search. If the maximum intensity has been set to 99 and y_i indicates the reduced intensity for m/e = i, then

$$\begin{aligned} &\text{i)} \quad y_i = 0, \text{ if } x_i < 1, \\ &\text{ii)} \quad y_i = 1, \text{ if } 1 \le x_i < 10, \\ &\text{iii)} \quad y_i = 2, \text{ if } 10 \le x_i < 99, \\ &\text{iv)} \quad y_i = 3, \text{ if } x_i = 99. \end{aligned} \tag{6}$$

Now each compound is represented by the 400 numbers, y_i.

The Euclidean distance is again used to measure the similarity. The distance between compounds A and B is calculated as

$$d_{AB} = \{ \sum_{i=1}^{400} [y_i(A) - y_i(B)]^2 \}^{1/2} \quad (7)$$

Finding the set of coefficients to define the one dimension. Again the objective of this section is to find a set of c_i so that a one dimensional form

$$Z(A) = \sum_{i=1}^{400} c_i y_i(A) \quad (8)$$

which preserves similarity in the mass spectra is calculated. The approach used in the liquid phase example is appropriate as a starting step. Therefore a 400 x 400 principal component analysis needs to be done. (The principal component problem or eigen problem is discussed in the appendix.) Machine limitations make this analysis very difficult and an alternative scheme is preferred.

Hites and Biemann[14] describe a search which divides the spectrum into consecutive regions of 14 mass units. They choose the 14 mass unit interval because it indicates the $-CH_2-$ link in a homologous series of ions. Employing this guideline, 14 smaller principal component problems can be solved. The first subproblem uses the mass units 1, 15, 29, 43, ..., 14 n + 1, ..., 393. The characteristic set of eigenvectors and eigenvalues is found. The second subproblem uses mass units 2, 16, 30, 44, ..., 14 n + 2, ..., 394 and gives a set of eigenvectors and eigenvalues. This continues until the fourteen sub-analyses are finished. In the end there are 400 eigenvalues and eigenvectors.

The eigenvalues are placed in descending order. The partial sums are plotted in Figure 7 and it is found that 166 eigenvalues account for more than 90% of the total variance.

If the 166 eigenvectors are applied to each compound, then the 400 dimensional spectra are reduced to 166 dimensions at the loss of less than 10% of the total variance. These 166 features are divided into four subproblems for eigenanalyses. Two of the analyses result in 42 eigenvectors and eigenvalues and the others result in 41 vectors and values. The partial sums for this step are plotted as a solid line in Figure 8. (The dotted line is a reproduction of part of Fig. 7.) Seventy-two features now contain more than 73% of the total variance.

If the 72 eigenvectors are applied to the 166 dimensional transformed values, the spectra have been reduced from 400 to 72 dimensions at the cost of less than 30% of the total variance. Finally the 72 x 72 eigenanalysis is done. Table 5 records the eigenvalues and weighted cumulated sums from this analysis. More than half of the total variance is found in the first ten eigenvectors. This implies that it is possible to define ten values related to the mass spectra of the sulfur containing compounds so that half of the total possible variation is present. To accumulate another ten percent of the variation it takes thirteen additional features. Table 6 collects the mass intervals which have the largest absolute magnitudes in c_i when the results of the three sets of eigenanalyses are combined.

In the gas chromatographic analysis the values for the coefficients in the one-dimensional search are the weights from the first eigenvector. Since in that example nearly all of the variation occurs in that direction, the choice was obvious. In the mass spectral problem the first eigenvector accounts for only about 31% of the total variation. To find the best set of search coefficients, the measured parameters must be combined to maintain similarity or near neighbor information. Since the

first ten eigenvectors contain a majority of the variation the following approximation will be made:

Instead of finding c_i which satisfies

$$Z(A) = \sum_{i=1}^{400} c_i y_i(A) \tag{8}$$

for each compound (spectrum) A, find c_i'

$$Z'(A) = \sum_{i=1}^{10} c_i' f_i(y(A)) \tag{9}$$

where

$$f_i(y(A)) = \sum_{j=1}^{400} C_{ji} y_j(A)$$

with C_{ji} representing the coefficients for each mass position j for eigenvector i.

When the analysis is complete a 400 dimensional form is reproduced according to

$$Z'(A) = \sum_{i=1}^{10} c_i' \sum_{j=1}^{400} C_{ji} y_j(A)$$

$$= \sum_{j=1}^{400} \left(\sum_{i=1}^{10} c_i' C_{ji} y_j(A) \right) . \tag{10}$$

In the description that follows the goal is to force as many of the five most similar compounds in 400 dimensions into the most similar compounds in 1-dimension. To accomplish this the 5 most similar compounds to each library member must be found. This is nearly impossible to do within a practical computer time limit. The difficulty is overcome by choosing prototype spectra in the data file and finding only the most similar compounds for the prototypes.

A weighting scheme is rated by using the following criterion: For a given weighting scheme c_i' there is a one-dimensional representation for each of the 1827 sulfur containing compounds.

i) Set up a total counter, T which indicates the effectiveness of the weights. Initialize T = 0

ii) For each prototype spectrum, A, consider each of the five most similar compounds, A_1, A_2, A_3, A_4 and A_5. Find the number of compounds whose 1-dimensional value is closer to the prototype than is the particular neighbor, A_i, and denote that number as p_i

iii) Add $\sum p_i$ to the total counter ($T = T + p_1 + p_2 + p_3 + p_4 + p_5$)

iv) When all prototype spectra have contributed to the total, the criterion for the weighting scheme is complete.

The minimum possible value for $\sum p_i$ for five near neighbors is 15. For s prototype compounds the minimum sum is $T_{min} = 15s$. The larger the value for T the less desirable is the weighting scheme. The goal is to find the weighting scheme for which T is minimized.

Determining the prototype compounds. To find the most similar to each of the 1827 compounds is very costly in terms of computer time. An alternative is to look at some subset of the total library. The subset should be typical of the entire data set; that is, the subset should contain cluster centers. For example suppose that projections of the data appear as in Figure 9 and three compounds were to be chosen as prototypes. Compounds B, F and L represent more typical points than do the set E, F, G.

One hundred prototypes were to be drawn from the 1827 sulfur containing compounds. The algorithm that was chosen iteratively selects spectra that are nearer to several other library spectra than are any of the other prototypes. To further conserve computer time the problem is divided into four identical subsections. For each subsection one quarter of the sulfur containing compounds are taken. From each quarter, twenty-five typical spectra are selected at random. The distance from each member of the quarter library to each of the 25 typical spectra is found. Then the number of times that each typical compound is closest to a member of the quarter library is counted. If all of the typical compounds are nearest to at least k of the quarter library set, then the typical points are prototypes. In the discussion for the mass spectral search k is taken to be four. (Since there are ~ 450 spectra per subset, the maximum value of k is 450/25 = 18.) If at least one cluster or typical spectrum has fewer than k neighbors, new typical points are defined. These are the set of spectra that are nearest to each existing cluster center. The method continues until a set of prototypes is found.

The result of this stage of the procedure is 100 prototype compounds and spectra. These compounds are used to determine the best coefficients, c_i' for the 1-dimensional search.

The near optimum 1-dimensional search coefficients. The problem of finding the best coefficients has been expressed as an optimization problem--among all possible values for $(c_1', c_2', \ldots, c_{10}')$, find the set which minimizes T. The sequential simplex search method is used as the optimization scheme.

The initial vertices for the simplex are taken from the eigenvector projections. Using the ten eigenvectors with largest eigenvalues, each spectrum is reduced from 400 to ten dimensions. The initial values for the ten weighting schemes on the ten reduced dimensions are shown in Table 7. The sign of each weighting term is determined randomly.

The sequential simplex algorithm allows the weighting coefficients to approach a local optimum. Five different combinations of signs in Table 7 have been run. The best coefficients and values for the response, T, are given in Table 8. The eigenvector corresponding to the largest eigenvalue gives a response equal to 193,262. After the simplex algorithm is applied T varies from 120,580 to 121,542. The improvement allowed by the simplex method is unmistakable, however T is much larger than T_{min} (T_{min} = 1500). The ten values for c_i' can be used to define the 400 c_i values for the untransformed mass positions. Table 9 gives the mass positions which have large absolute coefficients.

Discussing the results. The best coefficients have been indicated in Tables 8 and 9. The value of T implies that for 500 neighbors the average is about 240 places. This result is much less desirable than the results that were found for GC liquid phases. The distribution of the 500 p_i values is shown in Figure 10. Each interval represents five places. If twenty compounds from the one-dimensional search are reported, 55/500 or 11% of the five nearest neighbors are included. For 50 compounds, 98/500 or ~ 20% of the neighbors are shown.

Perhaps a more reasonable expectation is that at least one of the five most similar compounds appears in the first *m* compounds given by the 1-dimensional form. Figure 11 shows a histogram for the 100 minimum p_i values. Again each interval represents five places. If *m* equals

10, then 64/100 or 64% of the prototypes have one neighbor included. This much weaker condition can be attained more easily.

The search results for the complex multi-dimensional data then are less notable than for a low dimensional problem. Nonetheless if a weak condition, at least one of n near neighbors in the m most similar compounds in 1-dimension, is imposed, the algorithm is more acceptable.

Appendix: Principal component analysis. Principal component (PC) analysis is the name that is used to indicate the eigen treatment given the covariance or correlation matrix of a data set. The analysis starts with a library of n entities or compounds, $\{X_i\}$. Each individual compound is described by k measurements, so that for compound j,

$$X_j = \{x_{1j}, x_{2j}, \ldots, x_{kj}\} . \tag{11}$$

All of the compound and measurement data can be written as a k x n matrix (k rows and n columns). Each column is the complete description of a single compound.

$$X = \begin{bmatrix} x_{11} & x_{12} & \cdots & x_{1n} \\ x_{21} & & & \vdots \\ \vdots & & & \\ x_{k1} & \cdots & & x_{kn} \end{bmatrix} \tag{12}$$

Each variable x_{rs} is translated and scaled before the next step of the analysis is done. The new variable y_{rs} is given by

$$y_{rs} = (x_{rs} - t_s)/c_s. \tag{13}$$

This describes a new data matrix $Y = [y_{rs}]$.

The k x n rectangular Y matrix is postmultiplied by its n x k transpose and the result is a k x k co-variation matrix, A.

$$A = Y Y^T \tag{14}$$

If t_s is the mean value for all measurements for compound s and c_s the standard deviation in the measurements for compound s, then $\mathbf{A}$ is a statistical correlation matrix. This is the approach taken by McCloskey and Hawkes[16] in their gas chromatographic liquid phase work. Other analyses indicated by Rozett and Petersen[17] are shown in Table 10. The specific analysis used for the mass spectral system assumes $t_s = 0$ and $c_s = 1$. Thus it is a covariance analysis about a zero mean.

The k x k co-variation matrix, $\mathbf{A}$, is used in the eigenanalysis. In the eigenvalue problem the set of vectors z_r is sought so that

$$\mathbf{A}\, z_r = \lambda_r z_r \tag{15}$$

where λ_r is a number that is the eigenvalue for eigenvector z_r. In general there will be k orthogonal eigenvectors for the k nondegenerate eigenvalues. These may be collected in a k x k eigenvector matrix $\mathbf{Z}$ (each column represents a k dimensional eigenvector) and an eigenvalue matrix $\boldsymbol{\lambda}$.

$$\mathbf{A}\, \mathbf{Z} = \boldsymbol{\lambda}\, \mathbf{Z} \tag{16}$$

Under unitary transformation, such as $\mathbf{Z}$, the trace or character of the matrix is invariant. The sum of the eigenvalues λ_r, equals the sum of the variations for the untransformed variables, or

$$\sum_{r=1}^{k} \lambda_r = \sum_{r=1}^{k} \left(\sum_{s=1}^{n} y_{rs}^{\,2} \right). \tag{17}$$

In the case of a covariance matrix, the variance remains constant during transformation although it is redistributed. The value of λ_r that is largest indicates the linear transformation of the data for which the

largest variance occurs. The second largest value of λ_r indicates the linear transformation of the data that is orthogonal to the first transformation *and* has largest remaining variance. If the eigenvalues (and eigenvectors) are placed in descending order, then the transformations describe the optimum method of packing the total variance into the fewest terms.

The co-variation matrix can be reproduced from the eigenvalues and eigenvectors according to

$$A = \sum_{r=1}^{k} \lambda_r z_r z_r^T . \tag{18}$$

If nearly all of the variation can be described by $k'(< k)$ terms, then A is approximately represented by

$$A \doteq \sum_{r=1}^{k'} \lambda_r z_r z_r^T . \tag{19}$$

This provides the justification for using only k' terms to describe the data. Since only differences or variations in the compounds are necessary to distinguish among them, k' terms are used rather than k terms per compound.

Finally the form of each individual k' term must be described. This amounts to asking how the data is transformed to give variables with variation λ_r. From eq. (A-5),

$$z_r^T A \; z_r = \lambda_r z_r^T z_r = \lambda_r . \tag{20}$$

Since $A = Y Y^T$,

$$(Y^T z_r)^T \; (Y^T z_r) = \lambda_r \tag{21}$$

and the transformation which produces a variation of λ_r is given by $\gamma^T z_r$. Each compound should be described by

$$y'_{rs} = \sum_{i=1}^{k} z_{ri} y_{is}. \tag{22}$$

Captions

Figure 1. Nine two-dimensional points for a 1-dimensional search.

Figure 2. Points are projected onto the line.
(a) project points onto line
(b) 1-dimensional representation

Figure 3. Data for a less impressive one-dimensional search.

Figure 4. Projection onto 45° line.

Figure 5. Retention results for nitropropane and pyridine.

Figure 6. Results of a 1-dimensional search on GC liquid phase data.
(a) distribution of p_1 values
(b) sum distribution for p_1, p_2 and p_3
(c) distribution for min $\{p_1, p_2, p_3\}$

Figure 7. Partial sum of piecewise eigenvalues.

Figure 8. Partial sum for second set of eigenvalues.

Figure 9. Choosing prototypes.

Figure 10. Distribution of 500 p_i values for a 1-dimensional mass spectral search.

Figure 11. Histogram for 100 p values.

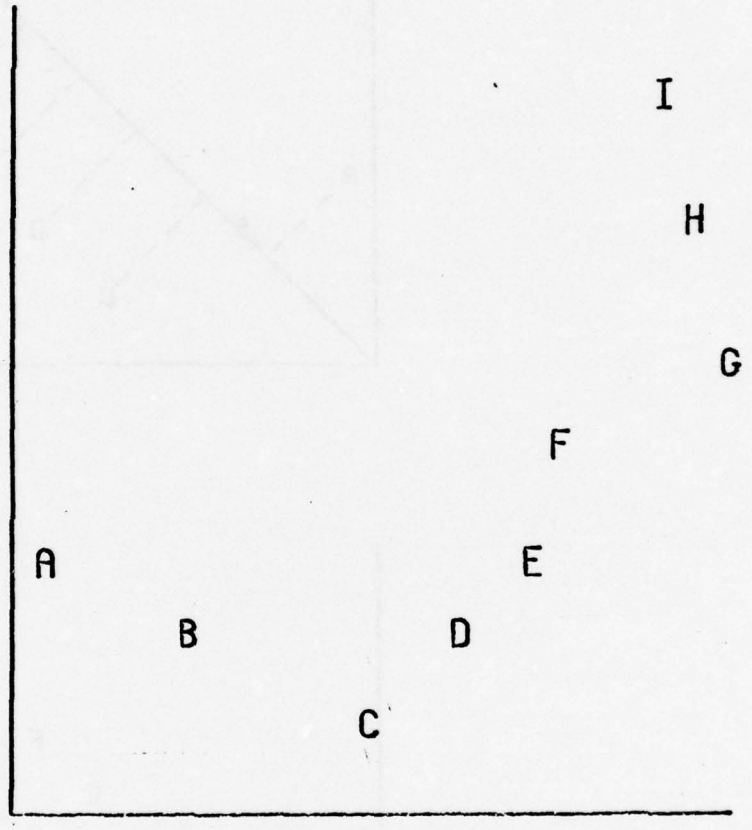
I
H
G
F
A
E
B
D
C

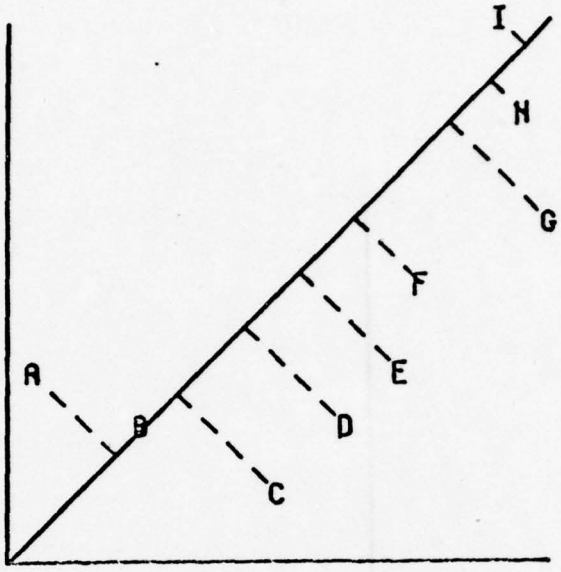
I
H
G
F
E
D
C
B
A

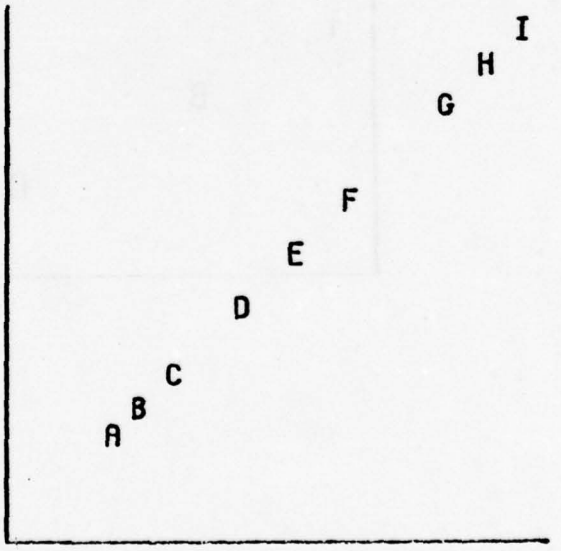
I
H
G
F
E
D
C
B
A

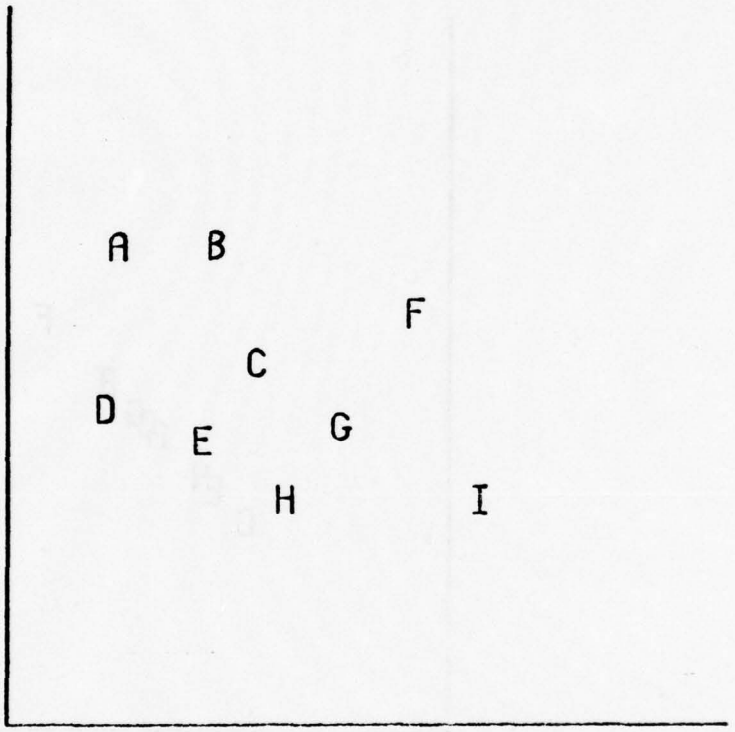
A
B
F
C
D
E
G
H
I

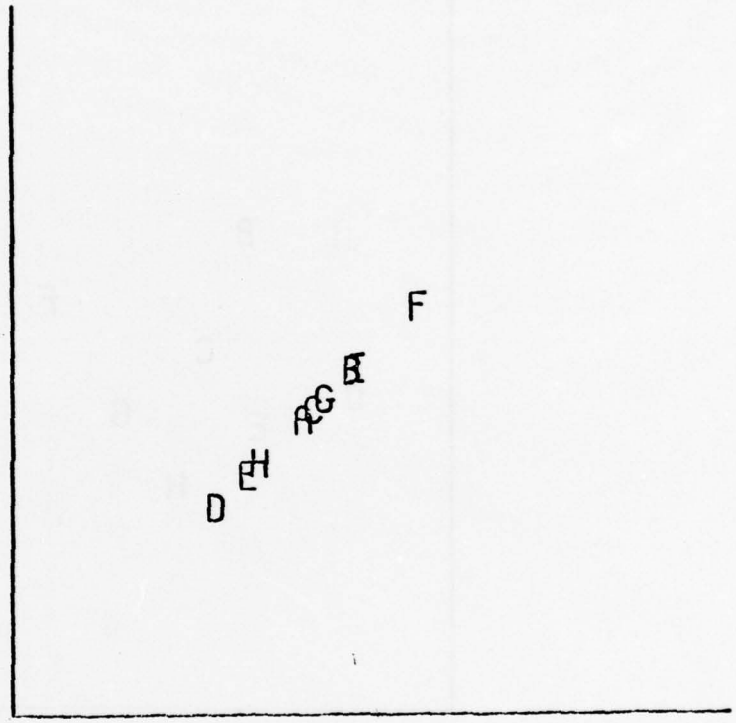
F
B
A
G
D
E
H

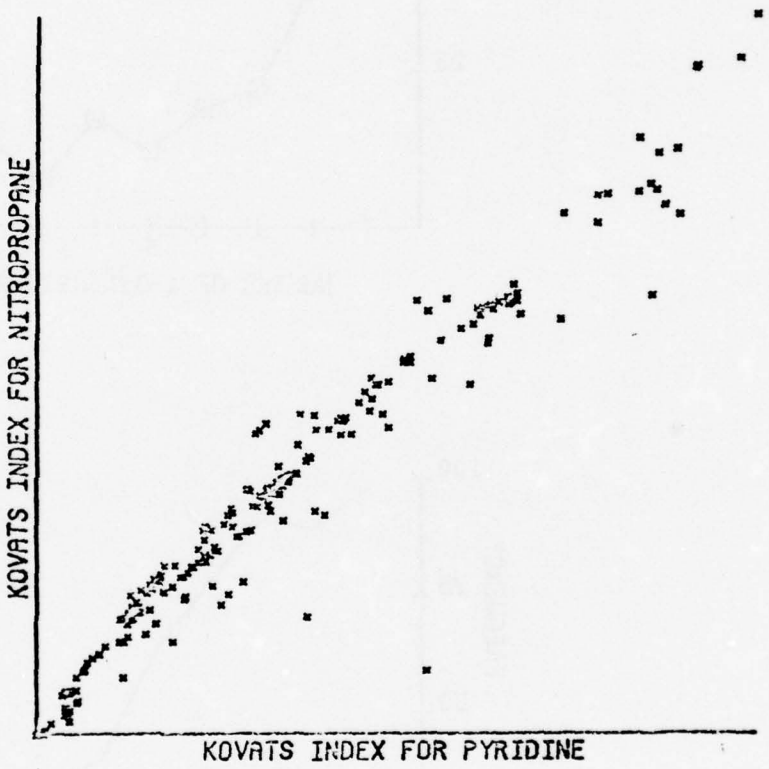
KOVATS INDEX FOR NITROPROPANE
KOVATS INDEX FOR PYRIDINE

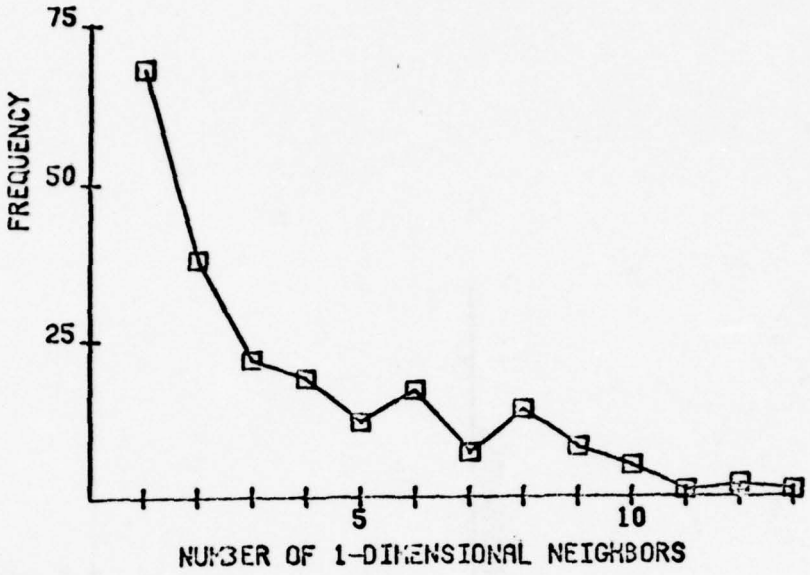
75
50
25
FREQUENCY
5
10
NUMBER OF 1-DIMENSIONAL NEIGHBORS

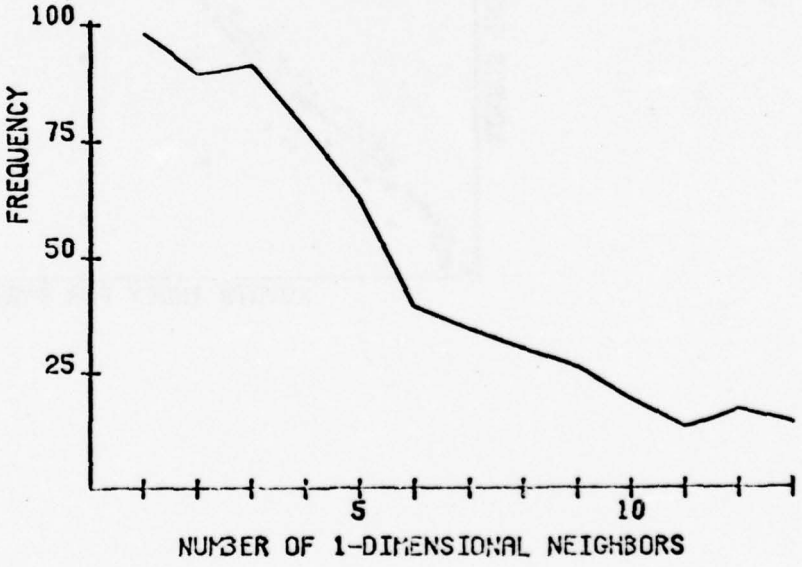
100
75
50
25
FREQUENCY
5
10
NUMBER OF 1-DIMENSIONAL NEIGHBORS

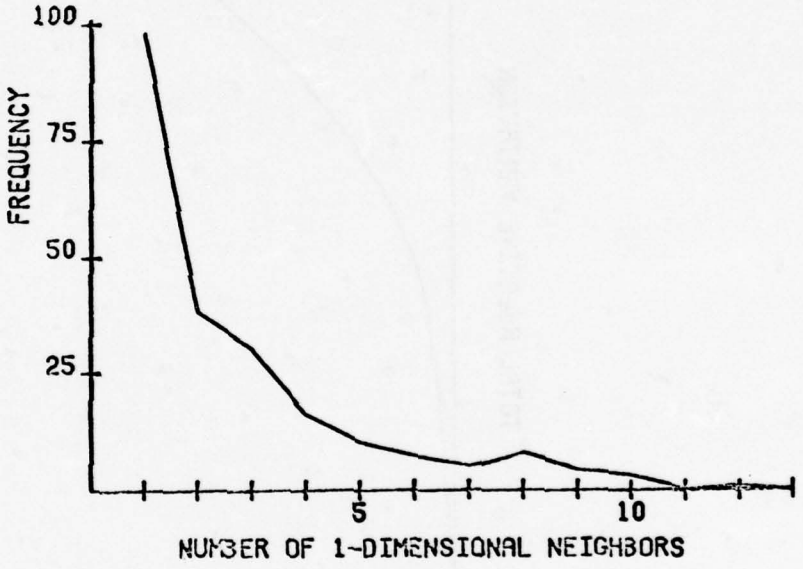
100
75
50
25
FREQUENCY
5
10
NUMBER OF 1-DIMENSIONAL NEIGHBORS

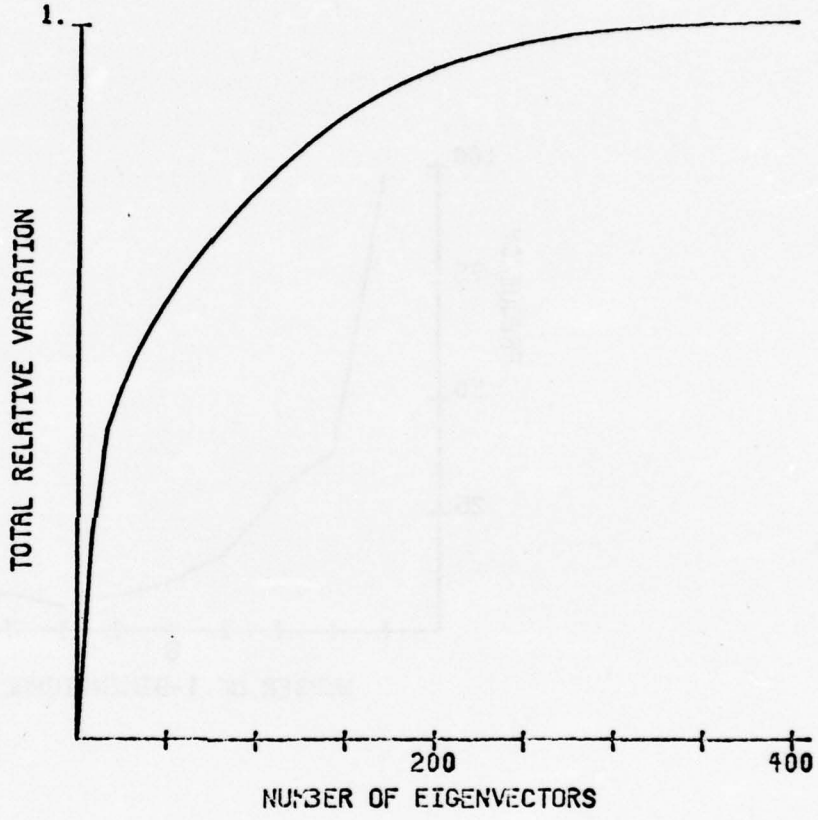
1.
TOTAL RELATIVE VARIATION
200
400
NUMBER OF EIGENVECTORS

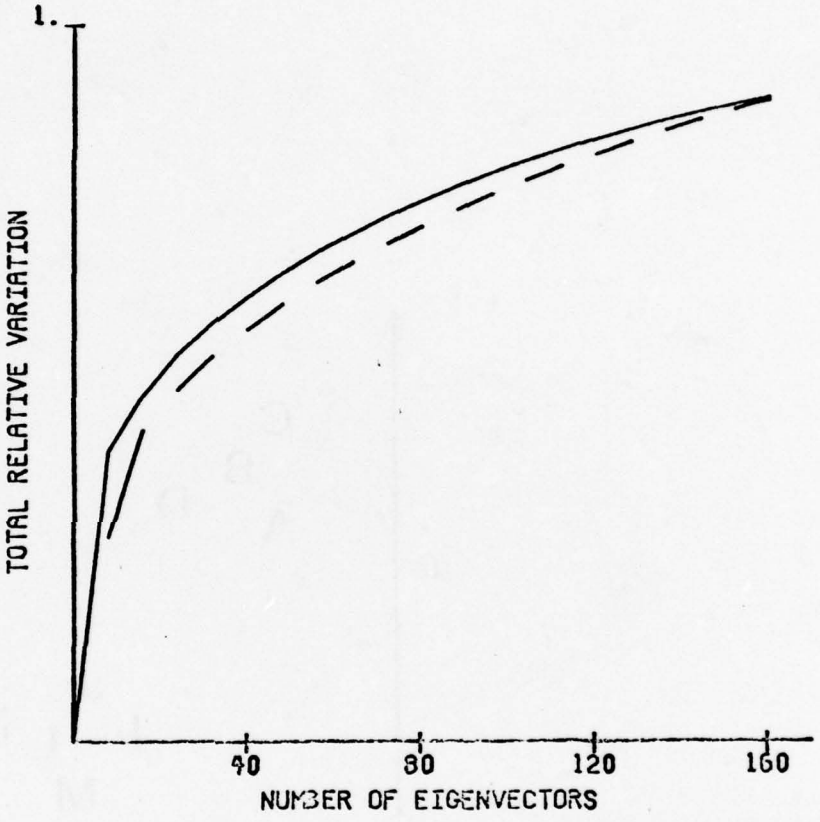
1.
TOTAL RELATIVE VARIATION
40
80
120
160
NUMBER OF EIGENVECTORS

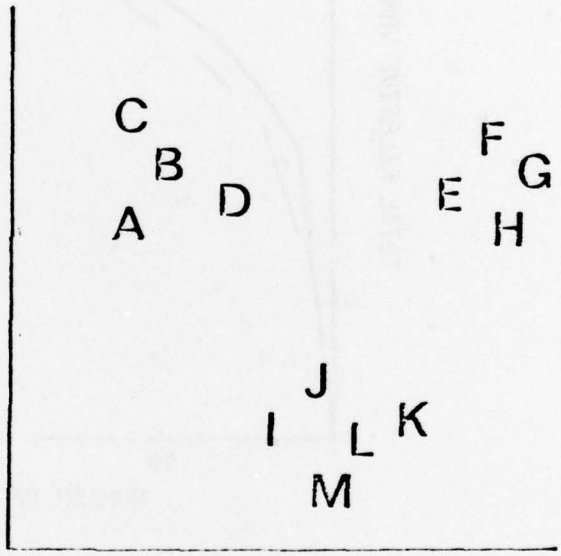
C
B
D
A
F
G
E
H
J
I
L
K
M

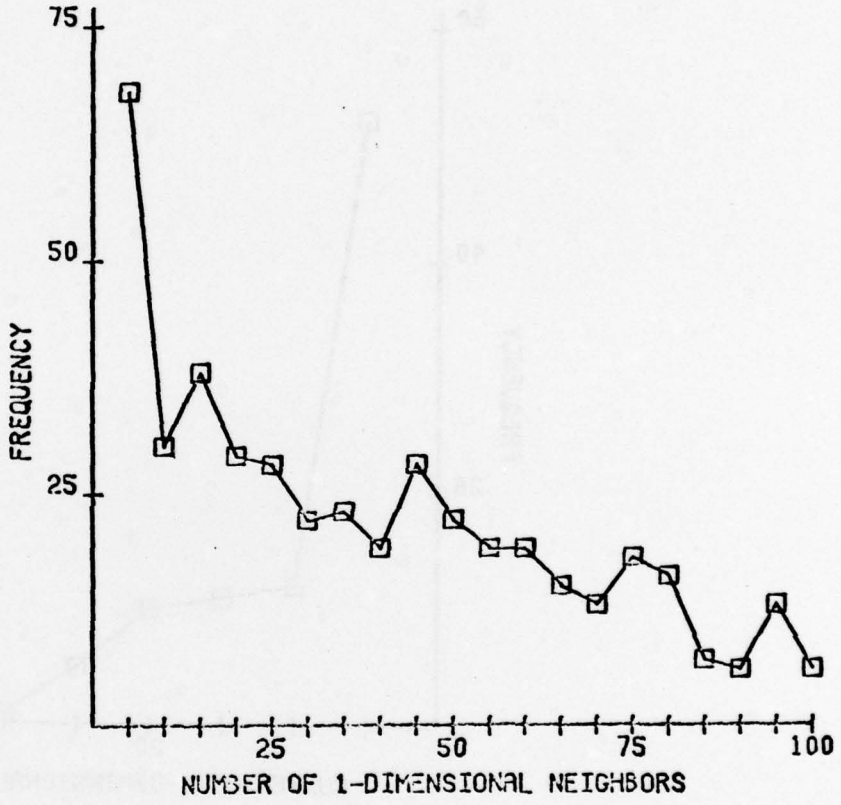
75
50
25
FREQUENCY
25
50
75
100
NUMBER OF 1-DIMENSIONAL NEIGHBORS

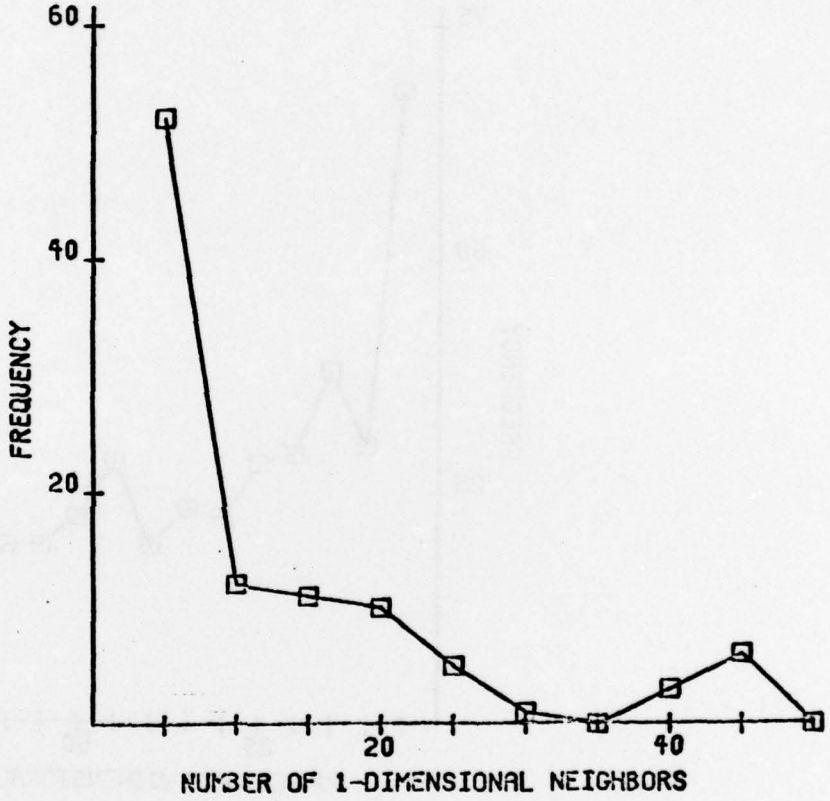
60
40
20
FREQUENCY
20
40
NUMBER OF 1-DIMENSIONAL NEIGHBORS

Table 1. Two-dimensional nearest neighbor information

entity	near neighbors 1	2	3	1-dim order
A	B	D	C	C,G,H,B,I
B	A	C	E	I,G,C,A,F
C	E	G	B	A,G,B,I,H,E
D	E	C	A	E,H,A,C,G
E	C	H	D	H,D,A,C,G
F	G	C	I	I,B,G,C,A
G	H	C	F	C,A,B,I,H
H	G	E	C	E,A,D,C,G
I	G	H	F	B,G,C,A,F

Table 2. Ten standard probes described by McReynolds

Probe	Structure
benzene	
1-butanol	$CH_3CH_2CH_2CH_2OH$
2-Pentanone	$CH_3CH_2CH_2\overset{\overset{O}{\|\|}}{C}CH_3$
1-nitropropane	$CH_3CH_2CH_2NO_2$
pyridine	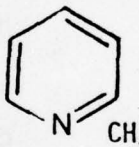
2-methyl-2-pentanol	$CH_3CH_2CH_2\overset{\overset{CH_3}{\|}}{\underset{\underset{OH}{\|}}{C}}CH_3$
1-iodobutane	$CH_3CH_2CH_2CH_2I$
2-octyne	$CH_3\text{-}(CH_2)_5\text{-}C{\equiv}CH$
1,4-dioxane	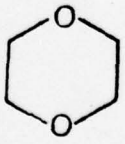
cis-hydrindane	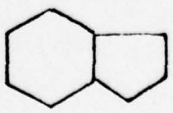

Table 3. Weighting constants given by McCloskey and Hawkes

test solute	weight term
benzene	0.2959
1-butanol	0.1896
2-pentanone	0.2428
nitropropane	0.1771
pyridine	0.1779
2-methyl-2-pentanol	0.2416
1-iodobutane	0.3428
2-octyne	0.4564
1,4-dioxane	0.2047
cis-hydrindane	0.5732

Table 4. Example of a binary search

phase	value	#	ordered phase	value	inclusive range 1	2	3	4
A	127	1	C	49				
B	84	2	F	60				
C	49	3	E	63				
D	136	4	H	77				
E	63	5	B	84				
F	60	6	I	88				
G	115	7	N	92				
H	77	8	K	103	↓	↓		
I	88	9	M	109				
J	118	10	G	115			↓	
K	103	11	J	118				↓
L	137	12	A	127		↑	↑	↑
M	109	13	D	136				
N	92	14	L	137				
		15	O	1000	↑			
			U	121				

Table 5. Eigenvalues and weighted cumulated sums from the final eigenanalysis

number	eigenvalue	weighted sum
1	25.30	30.9
2	4.85	36.9
3	2.77	40.3
4	2.12	42.8
5	1.42	44.6
6	1.23	46.1
7	1.13	47.5
8	1.05	48.8
9	0.99	49.9
10	0.85	51.0
11	0.80	52.0
12	0.76	52.9
13	0.71	53.8
14	0.69	54.6
15	0.63	55.4

Table 6. Mass intervals with large coefficients in eigenanalysis

eigenvector	m/e	coeff.	eigenvector	m/e	coeff.
1	45	1.000	4	39	1.000
	41	0.913		65	0.814
	39	0.841		117	- 0.694
	43	0.743		27	0.682
	57	0.666	5	29	1.000
	55	0.642		51	- 0.837
	69	0.629		43	0.807
	59	0.623	6	91	1.000
	47	0.600		55	0.815
	42	0.595		28	- 0.719
	58	0.594	7	51	1.000
	77	0.593		39	0.905
2	27	1.000		50	0.818
	77	- 0.977	8	29	1.000
	29	0.946		27	0.942
	43	0.893		43	- 0.782
	65	- 0.867	9	69	1.000
	41	0.848		45	0.884
3	77	1.000		92	- 0.728
	75	0.992	10	45	1.000
	97	- 0.852		91	0.921
	76	0.815		59	0.631

Table 7. Initial weighting schemes or vertices of the sequential simplex

Vector	c'_1	c'_2	c'_3	c'_4	c'_5	c'_6	c'_7	c'_8	c'_9	c'_{10}
1	1	0	0	0	0	0	0	0	0	0
2	1	$\pm$ 1	0	0	0	0	0	0	0	0
3	1	0	$\pm$ 1	0	0	0	0	0	0	0
4	1	0	0	$\pm$ 1	0	0	0	0	0	0
5	1	0	0	0	$\pm$ 1	0	0	0	0	0
6	1	0	0	0	0	$\pm$ 1	0	0	0	0
7	1	0	0	0	0	0	$\pm$ 1	0	0	0
8	1	0	0	0	0	0	0	$\pm$ 1	0	0
9	1	0	0	0	0	0	0	0	$\pm$ 1	0
10	1	0	0	0	0	0	0	0	0	$\pm$ 1

Table 8. Best linear combinations and response values

Response	c_1'	c_2'	c_3'	c_4'	c_5'	c_6'	c_7'	c_8'	c_9'	c_{10}'
193262	1.000	0.000	0.000	0.000	0.000	0.000	0.000	0.000	0.000	0.000
121542	1.000	- 5.464	1.274	- 4.241	0.673	0.610	- 0.078	2.205	2.928	1.042
121054	1.000	- 5.294	1.239	- 4.195	0.514	0.666	0.067	2.370	2.786	1.475
121016	1.000	- 6.814	1.771	- 5.367	1.559	0.462	0.823	2.772	3.627	1.652
120778	1.000	- 4.970	1.296	- 3.697	0.832	0.413	0.540	1.909	2.492	1.448
120580	1.000	- 6.159	1.416	- 4.520	1.432	0.392	1.138	2.058	3.223	1.660

Table 9. Mass positions with large coefficients

T = 121542

m/e	coeff.
41	1.000
135	- 0.892
43	0.822
165	- 0.810
121	- 0.715
136	- 0.705

T = 121054

m/e	coeff.
41	1.000
43	0.841
135	- 0.803
165	- 0.713
121	- 0.667
57	0.647

T = 120580

m/e	coeff.
41	1.000
43	0.889
135	- 0.757
121	- 0.682
57	0.681
165	- 0.678
55	0.641
42	0.613
134	- 0.613
136	- 0.582
149	- 0.548
166	- 0.540

T = 121016

m/e	coeff.
41	1.000
135	- 0.907
43	0.864
165	- 0.818
121	- 0.754
134	- 0.726

T = 120778

m/e	coeff.
41	1.000
43	0.875
135	- 0.741
57	0.681
165	- 0.659
121	- 0.642

Table 10. Co-variation analyses

$t_s \rightarrow$ / $\downarrow c_s$	t_s = *mean*	$t_s = 0$
c_s = std. dev.	correlation about the mean	correlation about zero
$c_s = 1$	covariance about the mean	covariance about zero

References

1. Lederberg, J., G. L. Sutherland, B. G. Buchanan, E. A. Feigenbaum, A. V. Robertson, A. M. Duffield and C. Djerassi, J. Amer. Chem. Soc., 91, 2973 (1969).

2. Isenhour, T. L., B. R. Kowalski and P. C. Jurs, CRC Reviews Anal. Chem., 4, 1 (1974).

3. Abrahamsson, S., S. Stallberg-Stenhagen and E. Stenhagen, Biochem. J., 92, 2 (1964).

4. Hites, R. A. and K. Biemann, Adv. Mass Spectrom., 4, 37 (1968).

5. Grotch, S. L., Anal. Chem., 45, 2 (1973).

6. Kwok, K.-S., R. Venkataraghavan and F. W. McLafferty, J. Amer. Chem. Soc., 95, 4185 (1973).

7. Jurs, P. C., Anal. Chem., 43, 364 (1971).

8. Lytle, F. E., Anal. Chem., 42, 355 (1970).

9. McReynolds, W. O., J. Chromatog. Sci., 8, 685 (1970).

10. Leary, J. J., J. B. Justice, S. Tsuge, S. R. Lowry and T. L. Isenhour, J. Chromatog. Sci., 11, 201 (1973).

11. McCloskey, D. H. and S. J. Hawkes, J. Chromatog. Sci., 13, 1 (1975).

12. Stenhagen, E., S. Abrahamsson and F. W. McLafferty, Registry of Mass Spectral Data, Wiley-Interscience, New York, N. Y., 1974.

13. Hites and Biemann.

14. Ritter, G. L., S. R. Lowry, C. L. Wilkins and T. L. Isenhour, Anal. Chem., 47, 1951 (1975).

15. McCloskey and Hawkes.

16. Rozett, R. and E. M. Petersen, Anal. Chem., 47, 1301 (1975).